UNIVERSITY OF Southampton

University of Southampton Research Repository

Copyright © and Moral Rights for this thesis and, where applicable, any accompanying data are retained by the author and/or other copyright owners. A copy can be downloaded for personal non-commercial research or study, without prior permission or charge. This thesis and the accompanying data cannot be reproduced or quoted extensively from without first obtaining permission in writing from the copyright holder/s. The content of the thesis and accompanying research data (where applicable) must not be changed in any way or sold commercially in any format or medium without the formal permission of the copyright holder/s.

When referring to this thesis and any accompanying data, full bibliographic details must be given, e.g.

Thesis: Author (Year of Submission) "Full thesis title", University of Southampton, name of the University Faculty or School or Department, PhD Thesis, pagination.

Data: Author (Year) Title. URI [dataset]

UNIVERSITY OF SOUTHAMPTON

Properties of Organosiloxane Liquid Crystals for Dye Guest Host Ferroelectric Display Devices

DEAN EDWARD SHOOSMITH

A thesis submitted for the degree of Doctor of Philosophy
Department of Physics and Astronomy
Faculty of Science
November 2001

UNIVERSITY OF SOUTHAMPTON

ABSTRACT

FACULTY OF SCIENCE
DEPARTMENT OF PHYSICS AND ASTRONOMY

Doctor of Philosophy

PROPERTIES OF ORGANOSILOXANE LIQUID CRYSTALS FOR DYE GUEST HOST FERROELECTRIC DISPLAY DEVICES

Dean Edward Shoosmith

The purpose of this thesis is to investigate a new series of organosiloxane liquid crystals and the effects of dye addition by mixing and synthetic addition. The organosiloxane compounds are the result of a building block process that seeks to combine the high tilt and wide phase range properties of laterally substituted biphenyl benzoate mesogens with the polymer ruggedness of siloxane head groups. Initially the biphenyl benzoate mesogenic precursors are investigated with bromine, chlorine and fluorine substituents. The materials yield 20-45° tilt angles with 70-130 $nCcm^{-2}$ spontaneous polarisation. When combined with a siloxane head group, the only liquid crystal phase seen is a 50°C wide SmC* phase in each of the three compounds. The siloxane moieties micro-segregate and form a virtual backbone. As a consequence of the new molecular arrangement, temperature independent, near 45° or 45° tilt angles are measured for all three compounds. Switching time measurements reveal sub-millisecond switching down to 40°C below the I→SmC* transition. The attachment of a biphenyl benzoate molecule at either end of the siloxane core results in a series of bi-mesogenic compounds. These compounds yield 60°C wide antiferroelectric SmC^*_A phases. The antiferroelectric nature is proposed to arise due to a bent conformation of the bi-mesogenic molecules. The spontaneous polarisation is further enhanced to 100-140 $nCcm^{-2}$ whilst the other electro-optic properties broadly follow similar trends to the mono-siloxane compounds.

The synthesis of 45° tilt ferroelectric compounds opens up the possibility of many new device applications. The feasibility of transferring the benefits offered by ferroelectrics to the field of dyed and single polariser devices is investigated. Three commercial dyes are mixed with the laterally halogen substituted mono-mesogenic organosiloxanes. The phase sequence of the host is maintained along with the near 45° tilt angles of the host material. The magnitude of the spontaneous polarisation is reduced in line with the dilution effect of the non-liquid crystalline dye compounds. The switching times, although marginally increased with dye addition, still remained in the hundred microsecond regime demonstrated by the hosts. With the addition of one of the commercial dyes to an antiferroelectric host, three optically distinct states can be observed in a suitably oriented cell. This single polariser tri-state dye guest host device is only made possible by the near 45° tilt angle of the bi-mesogenic organosiloxane compounds.

In order to introduce more dye into the organosiloxane hosts, a nitrostilbene dye molecule is grafted onto a siloxane core via an eleven carbon length alkyl chain. Following the pattern of the host organosiloxanes, monomeric and dimeric nitrostilbene compounds are studied, and the effect that grafting has on the dye's absorption properties is examined. This attempt to mimic the host structure proved highly successful, with the resultant organosiloxane dyes exhibiting liquid crystalline phases and showing complete miscibility with the organosiloxane hosts over the entire concentration range. Of particular note is the presence of antiferroelectricity in a mono-mesogenic ferroelectric host on addition of a dimeric non-ferroelectric dye. The results of this work show that the virtual backbone effect in low molar mass organosiloxane liquid crystals can be used to increase the solubility of a dye guest moiety and influence the stability and form of the mesophases. The ferroelectric / antiferroelectric characteristics of the liquid-crystal host can be retained and room temperature ferroelectric phases are created with broad temperature invariant properties. In this thesis, as well as the study of the physical and chemical properties of these new materials, some of the potential devices that now become possible are considered.

To Mum, Dad and Deb, with love always.

CONTENTS

DECLARATION

This thesis is the result of work done by the author whilst in registered postgraduate candidature at the University of Southampton. The work is entirely original except where due reference is made and no portion of the work referred to in this thesis has been submitted in support of an application for another degree or qualification at this or any other university or institute of learning. Results obtained in collaboration with others are clearly indicated and may be submitted by them for another degree.

ACKNOWLEDGEMENTS

There are many people without whom this thesis would not have been possible. Particular thanks to:

Harry, for bringing me down south, providing a great lab, fun people to work with, a free hand to experiment and for keeping enthusiastic throughout.

Professor G. W. Gray and Professor L. Komitov, my two examiners, for taking the time and having the patience to wade through this lengthy tome, and making my viva interesting and enjoyable!

Phil for the early days, when labs were dark and mysterious and the best explanation was in Klingon.

Wendy, for a guiding hand and answering so many early questions, particularly with the initial organosiloxane work.

Il Professore Carboni, for strong coffee and long chats, for giving me the enthusiasm to keep going through all the nitrostilbene batch mixtures and a constantly enquiring mind and the illumination of so many paths.

Marcus, for keeping the Manchester spirit alive, believing like me that the best way to fix something is to take it to pieces and keep reformatting it until it gives in, ensuring that someone's milk and coffee was always available, and teaching me that the DSC could be my friend.

Petra II, for providing long complicated chemical explanations in a mist of smoke and mirrors.

Steve, for explaining to an A-Level chemistry student what was really going on and understanding that a request for 'a lot' of a sample meant more than two cells worth!

Seb, for keeping me sane and for all his assistance, particularly with the optical apparatus, and providing PTFE alignment cells.

Bronje, for so many things. Leading the way and showing how it should be done, moreover showing that it could be done. Constant encouragement, particularly whilst writing up, and of course more strong coffee. Finally, for being a great friend and always having faith.

Chris, for providing a finely tuned rotating analyser rig and the technical expertise to encourage it to produce results. Many squash tutorials and stress relief in the gym. For being a true friend and always listening.

All the other group members for their patience and friendship, not forgetting Colin, Vince, Tom and Eric - thanks for the added colour!

All my housemates over the years, especially Ben and Flipper for keeping me swimming and playing water polo, Michelle and all my other friends for encouragement and understanding.

My family: Mum and Dad for believing in me. For nurturing an enquiring mind, with the principle that anything is possible if you want it enough and never give in. Glenn, for never asking if the thesis was finished and being a good friend. My extended family, Dick, Elaine and Doreen for providing encouragement and support. Lastly and most importantly Deb, without whom none of this would have happened, no words can express the debt I owe you.

If we knew what it was we were doing, it wouldn't be called research, would it?

Albert Einstein 1879-1955

Chapter One

An Introduction to Liquid Crystals

"Would you tell me, please, which way I ought to go from here?"
"That depends a good deal on where you want to get to", said the Cat.
"I don't much care where ... ", said Alice.
"Then it doesn't matter which way you go", said the Cat.
"So long as I get somewhere", Alice added as an explanation.
"Oh, you're sure to do that", said the Cat, "If you only walk long enough."

Alice's Adventures in Wonderland, Lewis Carroll 1832-1898

1.1 INTRODUCTION AND OVERVIEW

This thesis concentrates chiefly on the ability of new liquid crystal materials to modulate light, with a view to their final application in the displays market place. Already a multi-billion dollar industry, the current generation of displays, although radically improved from five years ago, still have many inherent drawbacks. New standards of refresh rates require even faster switching displays, and the constant drive for miniaturisation is hampered by the high power consumption demands of backlighting. Such issues are the motivation for the work in this thesis.

In a wider context, when discussing liquid crystals, most people think of their applications in flat panel digital displays, watches and computer screens. It is important to note that the market for electro-optic devices is not limited to flat panel displays. New devices are being widely sought in the communications industry as the optical revolution has created a market for fast response modulators and optical data storage devices; these are just some examples of fields where liquid crystals can be useful. Obviously, display applications represent only the tip of the iceberg. Indeed, liquid crystals are found throughout nature and are studied across the scientific disciplines by biologists, chemists, physicists and mathematicians.

The first three chapters form the foundation of the thesis. The theory and vast range of equipment necessary for this work are examined in some depth, before leading onto the results and conclusions. This chapter introduces the broad family of liquid crystals and their discovery. As the name suggests, the liquid crystalline state lies between an ordered crystalline solid and a fluid isotropic liquid. The purpose of this thesis is to investigate the new series of organosiloxane liquid crystals and the effects of dye addition by mixing and synthetic addition. To accomplish this, the work is set in the context of the wider field of liquid crystals and the basic thermotropic calamitic families. An order parameter is introduced to help describe the phases, then taken further by considering Landau theory, which is utilised in understanding some of the dependencies of the physical parameters of a phase and to help describe phase transitions.

Chapter two outlines the theories directly applicable to this work. The concept of ferroelectricity is introduced along with the symmetry requirements and the cell geometries used in electro-optic work. Switching and measurement theory is discussed and the possibility of tri-stable switching with antiferroelectrics introduced. Particular attention is paid to the dynamics of director motion and the equations that can be derived. In order to assess the suitability of compounds and different techniques for display applications, several fundamental parameters such as tilt angle, switching time and spontaneous polarisation are studied. In the third chapter the process of measurement is outlined, from cell fabrication and testing, through to liquid crystal parameter determination and analysis.

In chapter three, the first of the results chapters, the low molar mass organosiloxane system that is the mainstay of the work in this thesis is investigated. These compounds are synthesised in-house and are the result of a building block process where it is hoped to combine the high tilt and wide phase range properties of laterally substituted biphenyl benzoate mesogens with the polymer ruggedness of siloxane head groups. In order to test this theory, initially the biphenyl benzoate mesogenic precursors are investigated with bromine, chlorine and fluorine substituents. The attachment of a biphenyl benzoate moiety at one or both ends of a siloxane core results in the series of mono and bi-mesogenic organosiloxane compounds. An examination of the viscosities of the switching process allows a study of the activation energy of the switch. The parameters of tilt angle, spontaneous polarisation and switching time are measured in ferroelectric and antiferroelectric samples.

The synthesis of 45° tilt compounds opens up the possibility of many new device applications. Chapter four focuses on the dye guest host effect. Although a well established field, until now only commercial nematic devices have been developed. An inability to compete as successfully in the market-place as the twisted-nematic mode has stalled widespread investigation in this area. The possibility of transferring the benefits offered by ferroelectrics to the field of dyed and single polariser devices is investigated. Three commercial dyes are used to establish the feasibility of a single polariser device. The dyes are added to the three laterally halogen substituted mono-mesogenic organosiloxanes already investigated in the previous chapter. Electro-optic parameters are studied to measure the effect of the dye addition. The limitations of contrast ratio and brightness are considered. The potential advantages and inherent drawbacks of dye-guest host media are discussed, and the results of the current work demonstrated. In the final part of the dye guest host work, the possibility of a tri-state device is investigated. With the addition of one of the commercial dyes to an antiferroelectric host, three distinct states can be observed in a suitably oriented cell. This single polariser tri-state dye guest host device is only made possible by the near 45° tilt angle of the bi-mesogenic organosiloxane compounds.

In order to introduce more dye into the organosiloxane hosts and thereby improve the optical contrast, chapter six advances the dye guest host work with the investigation of devices containing dyed liquid crystalline molecules. In order to mimic the organosiloxane host as closely as possible, the dye molecule, in this case a nitrostilbene, is grafted onto a siloxane core via an eleven length alkyl chain. Following the pattern of the host organosiloxanes, monomeric and dimeric nitrostilbene compounds are studied, and the effect that grafting has on the dye's absorption properties is examined. In order to assess the possibilities of these dye compounds for a dye guest host device, a wide range of mixtures are made, with the two dyes individually mixed with a ferroelectric then an antiferroelectric material from the first results chapter. The phase ranges are studies and the exciting possibilities for controllable temperature and optical parameters are introduced. Once again, the electro-optic parameters of tilt angle, spontaneous polarisation and switching time are assessed.

The thesis is concluded in chapter seven with a summary and discussion of the work presented and a look to the future. The ongoing work includes some initial results showing the effects of fluorination chemistry on the organosiloxane molecules synthesised for this work and the potential use of fluorescent and optically active dyes.

1.2 Liquid Crystal History and Grouping

All systems exhibit differing degrees of order, as conditions, such as temperature are varied. Such variations can result in phase changes, commonly grouped into the three basic states of matter: solid, liquid or gas. In the solid state, the molecules possess orientational and positional order. The only motions the molecules can undergo are small vibrations at their lattice sites. These limitations give solids many of their characteristics; chiefly their shape and resistance to deformation. If a solid is heated it can melt into a liquid state. The increased thermal energy allows the molecules to lose their positional and orientational ordering, giving the system very different characteristics; it can flow and is deformed easily. Finally, if further heated, the molecules can break away from each other entirely and form a gaseous state. This brief description is an oversimplification. The melting process for an anisotropic molecule can be more complex. If the molecular interactions are also anisotropic, lateral forces across molecules can be greater than the longitudinal forces between their ends. The breakdown in order from solid to liquid can involve many steps and it is here that the liquid crystalline phase exists.

Many of the concepts utilised in this thesis rely on relatively recent work, often in the last forty years. However, the existence of the thermotropic liquid crystal state has been known for over a century. Their original discovery is credited to Friedrich Reinitzer, an Austrian botanist studying cholesterol derivatives in plants. In 1888 when observing the properties of cholesteryl benzoate, he noted that it showed two distinct melting points[1]. On heating, the solid turned initially to a cloudy liquid then finally became clear. Otto Lehmann, a German physicist, studied the intermediate cloudy phase and concluded that although liquid-like in nature, it had a crystal-like structure and termed the phase, liquid crystal[2]. This label has stuck and is used to describe the two broad families of liquid crystals; lyotropics and thermotropics.

1.2.1 Lyotropics

Lyotropics are the most commonly found liquid crystals, studied in biology and chemistry; they are widely seen in nature. The mesophase structures they exhibit are mainly due to their concentration in a solvent, often simply water. Examples can be found throughout the human body and animal kingdom, including the mechanics of the DNA double helix[3] and the formation of cell membranes by the interaction of phospholipids in water. Although numerous natural examples exist, the most

commercially active areas of research are in the surfactants and soap industries[4]. The detergent industry has the largest turnover of any commercial liquid crystal activity, although surprisingly this is not commonly seen as a liquid crystal industry. The lyotropic family of liquid crystals lies outside the subject area of this thesis.

1.2.2 Thermotropics

As the name suggests, the thermotropic class of liquid crystals has properties that rely on temperature. These liquid crystals form the basis of most display applications. In a digital display, it is mainly the electro-optic switching properties of liquid crystals, rather than their thermotropic properties that are utilised. Thermal properties become more useful in applications such as the colour change thermometers often seen on fish tanks, and other applications where a material property changes observably with temperature. The liquid crystals studied in this thesis are all members of this group.

1.3 Liquid Crystal Phases

One of the main requirements for a molecule to exhibit a liquid crystal phase is shape anisotropy. This requires at least one of its physical dimensions to differ from the rest. The two main types are calamitics (rod shaped) and discotics (disk like), although more exotic configurations such as bowl and plank shaped liquid crystal molecules also exist. The molecules studied in this thesis are designed to be calamitic; discotics are more complex and rarely seen as active elements in display devices. Figure 1.1 shows the structure of one of the most famous liquid crystals, a cyanobiphenyl whose chemical name is 5CB. This compound was one of the first liquid crystals developed specifically for display purposes and was synthesised by a team led by G.W.Gray[5]. The rod-like shape anisotropy can be clearly seen along with the rigid core and flexible end chain common to basic calamitics.

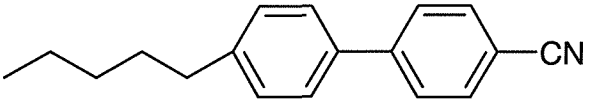

Figure 1.1 The structure of the cyanobiphenyl nematic liquid crystal 5CB.

A fully liquid state has no positional or orientational order and is termed isotropic (I). In contrast, a crystalline solid (Cr) possesses positional and orientational order. The order of a crystal can be lost in one jump if it melts straight to an isotropic liquid. Alternatively, the order can decrease in steps, leading to a variety of subphases or mesophases, which are reproducible and stable. A molecule that exhibits several mesophases is termed polymorphic. Normally, mesophase-to-mesophase transitions

are reversible, although a little hysteresis can occur. A degree of supercooling is often observed with mesophase to crystalline transitions. Consequently more mesophases can sometimes be seen on cooling than on heating. Those occurring below the melting point on supercooling are metastable and termed monotropic. Generally mesophases that occur above the melting point are stable and are termed enantiotropic. All liquid crystal phases possess some degree of orientational order, whereas the positional order can almost disappear. This requires molecules to be held together by highly anisotropic van der Waals forces. The following classes of nematic and smectic mesophases apply chiefly to the thermotropic rod-like liquid crystals studied in this work, although there are analogies in many other systems.

1.3.1 The Nematic Mesophase

With the exception of the exotic blue phases[6], the nematic mesophase is the least ordered mesophase. If exhibited by a sample, it is the first phase seen on cooling from an isotropic liquid. The molecules have no positional order and it is only the dynamic long-range orientational order that distinguishes this phase from the isotropic fluid. The molecules are in a constant state of thermal motion and are free to rotate and translate, resulting in a random distribution of their centres of mass. However, they favour an orientation with the long axis lying on average, parallel to a common axis. This directional axis is described by a unit vector, **n**, called the director. A schematic representation is shown in Figure 1.2. There is complete rotational symmetry about the director axis; therefore macroscopically the mesophase is non-polar. Although an individual molecule may distinguish head from tail, there is an equal probability of finding it pointing up or down, thus the system is invariant under the transformation **n** to **-n**. Thus the phase is centrosymmetric, and typically it is optically uniaxial[7] with the optic axis lying along the director. As the temperature is lowered, the order in the phase increases and the individual molecules become more parallel to the director.

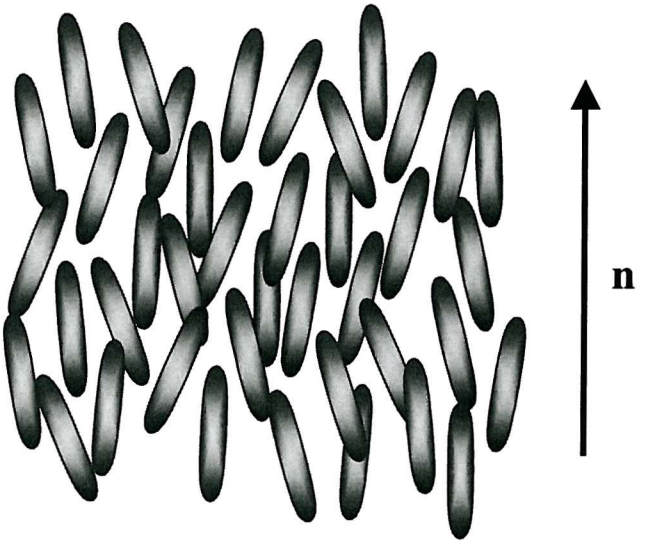

Figure 1.2 A schematic representation of the nematic mesophase and director.

Small domains form within the bulk material, each with a different preferred orientation of the director. The discontinuity of the director at the domain boundaries and thermally induced fluctuations give the bulk phase a turbid appearance as transmitted light is intensely scattered. As the phase is heated to an isotropic liquid this turbidity disappears; thus this transition is often called the clearing point. When sandwiched between glass plates and viewed through crossed polarisers, this phase is characterised by a "schlieren texture" of thread-like defects. It is this texture that gives the phase its name, nematic, from the Greek for thread, and is commonly denoted N.

1.3.1.1 Chiral Nematic Mesophase

When the molecules are chiral, the least ordered mesophase is called the chiral nematic phase. The presence of one or more chiral centres prevents a molecule being superimposed on its mirror image, giving it a unique handedness. The phase is often historically termed cholesteric, as it was first seen by Friedrich Reinitzer in derivatives of cholesterol. In the bulk, the molecules' chirality induces a helical twist in the alignment and thus the director rotates, forming a helical axis. Two enantiomeric chiral forms (left and right handed) give the two possible twist directions for the helix. The pitch length is defined as the distance over which the director rotates through 360°. As with an achiral nematic, the phase is non-polar and thus **n** is indistinguishable from **-n**. Therefore, the helical period is actually half the pitch length and is often a few microns. The twist gives the phase slightly more long-range orientational order than a conventional nematic, although both phases have similar symmetry, possess uniform density and are thermodynamically similar. Chiral liquid crystal phases are given the superscript *, hence the chiral nematic phase is commonly denoted N*. A schematic representation of the molecular orientation is shown in Figure 1.3. The director is shown rotating through 180° over half the pitch length and the twist has been highly exaggerated to emphasise the helical nature of the phase.

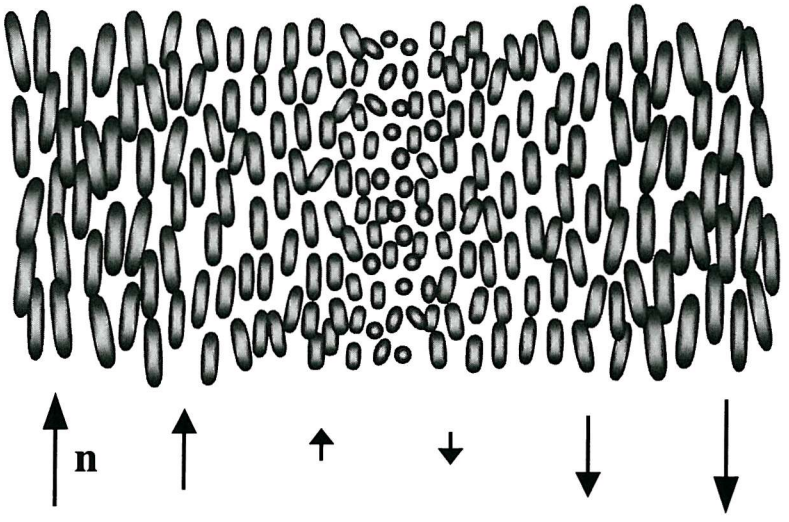

Figure 1.3 A schematic representation of the chiral nematic mesophase and director.

The pitch length can be as short as 100nm but is often comparable to optical wavelengths and Bragg scattering of incident light can occur[8]. Consequently the structure can selectively reflect appropriately polarised light. Variations in temperature cause the pitch length to change and this characteristic is utilised in many thermometry applications. Chiral nematics can also be seen in the natural environment and are responsible for many of the vivid colours of butterflies and beetles. The presence of the helix gives the phase an unusually high optical rotary power, often greater than 10^4 °/cm. This rotary power is significantly higher than is found in optically active solids and isotropic liquids, which normally lie in the region 10^{-1} - 10^3 °/cm. An example is the liquid crystal CE6. In the isotropic phase this has a specific rotation of 3 °/cm, whilst an aligned film in the N* phase[9] gives $\approx 10^4$ °/cm. If the propagation direction of a beam of plane-polarised light, of wavelength less than the helical pitch length is parallel to the helical axis, the plane of polarisation will rotate with the helix. This guiding ability is used particularly effectively in many display applications resulting in the utilisation of chiral nematics for a number of years in electro-optic devices. More recently, new applications have been found which utilise the flexoelectro-optic effect[10]. This process offers an alternative to the normal use and geometries of the N* phase and, although in its infancy, has many exciting possibilities. For a detailed explanation the reader is directed to the thesis of B. Musgrave[11].

Although chirality can be a fundamental property of the molecules, the N* phase can be imposed in an achiral system with the addition of a chiral dopant[12]. This allows the pitch length to be easily controlled. Conversely, a mixture of chiral molecules in which equal amounts of each enantiomer are present, known as a racemic mixture, gives rise to an infinite pitch length and so acts like an achiral nematic. In this way, any nematic can be thought of as a chiral nematic with infinite pitch. In some cases, highly chiral materials can exhibit the exotic blue phases. These are seen between the isotropic and chiral nematic phases and typically exist over only a few degrees centigrade. The full structure is highly complex and, although not fully understood, is thought to be due to the propagation of a helical structure along multiple axes[13].

1.3.2 The Smectic Phases

The smectic phases are more ordered than the nematic phases and possess orientational and positional order. They are typically found at lower temperatures than the nematic phases although some re-entrant phases have been reported[14]. Unlike the uniform density of both nematic phases, there is some correlation between the smectic molecules' centres of mass, resulting in a layered structure. To describe smectics we assign a layer normal, **k**, perpendicular to the average layer plane. These layers are not discrete but diffuse. The molecules' positions can be described by a probability density wave[15] represented by a sinusoidal-like wave of the centre of mass distribution $\rho(z)$ in the direction of **k**:

$$\rho(z) = \bar{\rho}\left(1 + \xi\cos\left[\frac{2\pi z}{d}\right]\right), \qquad 1.1$$

where $\overline{\rho}$ is the average phase density, d the layer spacing and ξ is the order parameter, typically complex. Additional harmonics can be added but do not contribute significantly. For a typical smectic, a simple sinusoidal description is sufficient. Layer to layer forces are weak compared with the lateral molecular forces, thus, the layers are not fixed and are free to move over one another. Although this gives the phase some fluid properties, smectics are as a rule more viscous than nematics.

There are many different types of smectic phase and they are characterised by the orientation of the director with respect to the layer normal and the degree of molecular ordering within the layers. The many smectic types are classified alphabetically as they were discovered, from the notation suggested by Sackmann and Demus[16]. The differences between smectic phases, which are often subtle, can make classification by optical texture alone very difficult. Techniques such as x-ray diffraction are often needed for more accurate identification. The name smectic (derived from the Greek word for soap) was coined by Friedel[17] who noticed that the phase possesses mechanical properties reminiscent of soaps. Similar to the nematic phase, systems containing chiral molecules are denoted * and the general class labelled Sm.

1.3.2.1 Smectic A Phase

The smectic A phase is the least ordered of the smectic phases and if present is seen first on cooling from a nematic or isotropic phase. Within the layers, the molecules are oriented similar to a nematic possessing only one-dimensional positional order and can be considered as a two-dimensional liquid. Once again, the molecules are relatively free to wobble, but point on average in a common direction, **n** (see Figure 1.4). The director, **n**, lies along the layer normal, **k**, and like a nematic, the phase is centrosymmetric and optically uniaxial. Following the labelling convention, this is denoted SmA.

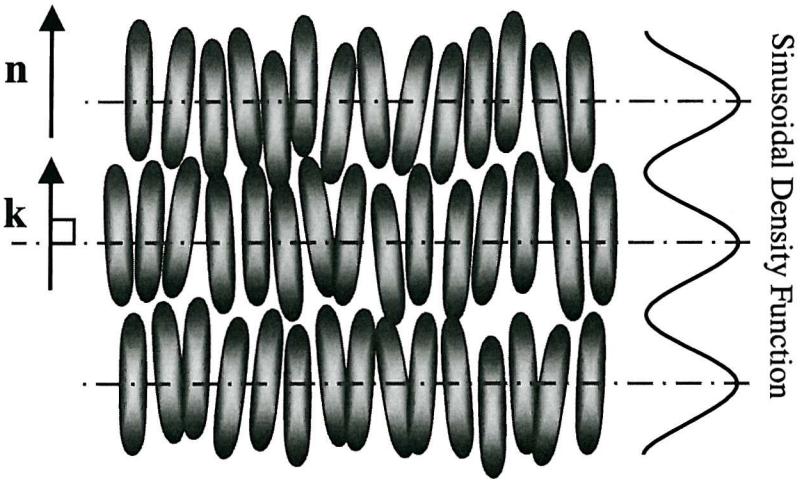

Figure 1.4 A schematic representation of the smectic A mesophase.

The layer spacing is approximately equal to the molecular length with thermal fluctuations causing this to vary slightly. However, in special cases the layer spacing can be as small as 0.8 or as large as 1.4 times the molecular length. Layer compression is accounted for largely by molecular deformations since most molecules exhibiting a SmA phase have flexible end groups and are slightly randomly tilted[18]. Layer expansion can be far more complex, involving interdigitated bilayer structures[19]. Systems comprising exclusively monolayer or bilayer structures are known as commensurate, whereas complex systems comprising both, are known as mixed layer or incommensurate systems.

A SmA phase can be formed by chiral molecules. The requirement of a layer structure and the condition of rotational symmetry about the director prevent the formation of a helix. However, the macroscopic properties can be very different and therefore the phase is distinguished as SmA*. In 1988, Renn and Lubensky suggested that if the chiral forces are sufficiently great, an N* phase cooled into a SmA* phase can form a twist grain boundary state[20]. The high molecular chirality results in grain boundaries of screw dislocations that twist blocks of layers with respect to each other. Soon this separate phase was confirmed by x-ray and also seen in materials exhibiting direct isotropic to smectic transitions[21].

1.3.2.2 Smectic C Phase

Essentially similar to a SmA phase, the smectic C phase (SmC) is the tilted analogue, shown schematically in Figure 1.5. The molecules are on average tilted in their layers, so now the director, **n**, lies at an angle, θ, dependent on temperature, to the layer normal, **k**. The tilt directions in adjacent layers are coupled and thus orientation is preserved over long distances leading to an overall uniform tilt.

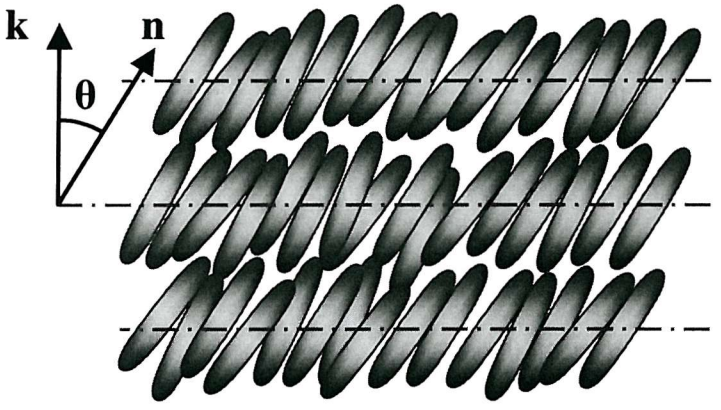

Figure 1.5 A schematic representation of the smectic C mesophase.

If the molecules are chiral or a dopant is added, the mirror symmetry is lost. Microscopically, the phase is polar and helical. The tilt angle, θ, is the same but the azimuthal direction of tilt traces a

helix as shown in Figure 1.6. The pitch is typically longer than seen in chiral nematics, but still in the order of microns. As with chiral nematics, the phase is capable of Bragg reflection if the pitch is of the order of visible light. In comparison with the SmA phase, different molecular properties yield differing layer geometries, including once more a chiral twist grain boundary phase[22].

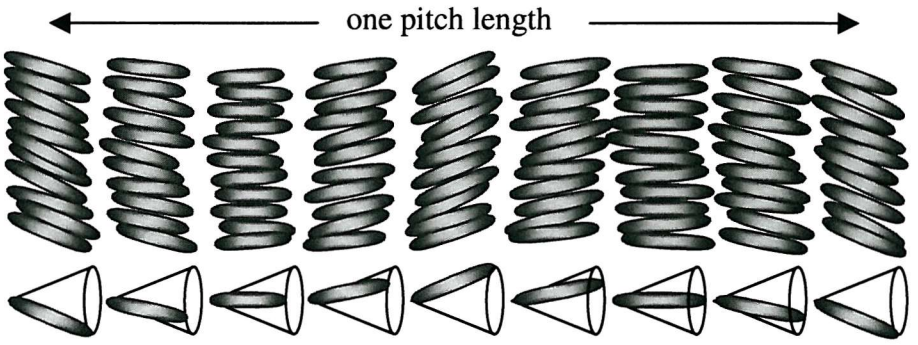

Figure 1.6 A schematic representation of the chiral smectic C mesophase.*

The SmC* phase has attracted much interest in recent years. Suitably surface stabilised it is able to exhibit ferroelectricity and its molecules can be rapidly switched by an electric field. This phase thus has great potential in display devices and is the focus of much of the work in this thesis. The physical nature and properties of the phase are explored in the following theory chapter.

1.3.2.3 Higher Order Smectics

As the level of order nears the crystalline state, higher order phases can arise from greater positional ordering within the layers. Most relevant to this work are the SmI and SmF phases. If either phase is seen, it is typically on cooling from a SmC. Like the SmC, the molecular long axis and hence the director are tilted at a temperature dependent angle. The layers exhibit pseudo-hexagonal molecular packing with respect to the director and this positional ordering extends around 150-600 Å [23]. This structure is only seen locally as defects prevent its uniform growth throughout the system. Although the tilt direction is roughly preserved between layers, similar to a SmC the layers are not fixed; they have little layer correlation, making these phases true smectics.

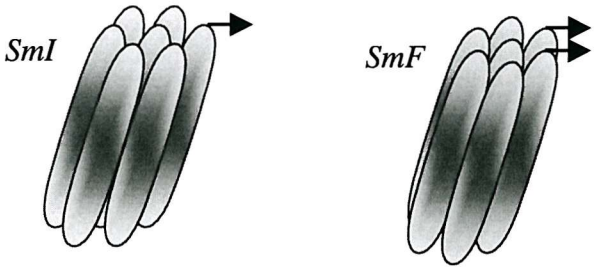

Figure 1.7 A schematic representation of the hexatic SmI and SmF mesophases.

The tilt orientations of the SmI and SmF phases differ with respect to their packing net. As shown in Figure 1.7, the molecules of a SmI phase tilt towards the apex of the hexagon whilst the SmF molecules tilt to the side[24]. If chiral, many tilted phases can exhibit ferroelectricity, although most relevant to SmC* in this work, it also applies to SmI* and SmF*. Both possess a macroscopic helix; the tilt and the hexagonal close packing net spiral orthogonal to the layer plane.

Further ordering gives rise to the crystalline analogues of SmI and SmF, denoted J and G respectively. The molecules are close packed but the layers are well correlated, giving a three dimensional structure that can be considered crystalline[25]. These are members of the family known as orientationally disordered solids, anisotropic plastic liquid crystals, or sometimes soft crystals, hence the prefix Sm is dropped. These possess the same three-dimensional order as a crystalline solid but have a reduced orientational order. This decrease in orientational order can allow the molecules at different lattice sites to adopt a number of different configurations with the molecules still free to revolve around their long axis. Other examples are H and K phases, which possess a high degree of in-plane ordering with a herringbone molecular packing arrangement and long-range interlayer correlation. The chiral forms G*, H*, J* and K* are soft smectic crystals, however, due to the long-range positional order of their molecules, the helical ordering can be completely suppressed. The hexatic B phase is a non-tilted analogue of the SmI and SmF phases and is thus essentially a hexatically ordered SmA.

The crystal phases are more viscous than the true smectics, but have sharper thresholds and suitably oriented can exhibit improved bistability; this gives them potential in optical storage media[26]. The SmA and SmC phases are the least viscous and therefore have the greatest potential in electro-optic shutters. For further reading on the subject of smectic phases, the reader is directed to the book dedicated to the subject by Gray and Goodby[27].

1.4 The Nematic Order Parameter

Previously the director, **n**, was introduced to describe the average orientational direction of the molecular long axis in a nematic and then used to help describe smectics. It does not say anything about the degree of orientation in the system, only its preferred direction. As previously mentioned, the molecules in a liquid crystal phase are not fixed. Thermal energy gives rise to constant fluctuations and interactions between the molecules. It is therefore desirable to obtain a measure of the order present in a phase. This becomes increasingly important as a system undergoes a transition between phases; it is the order parameter that delineates this change.

If the nematic phase is considered initially, it is obvious that the order present is related to the director and the angle that individual molecules make to it. One approach is to describe an alignment function

that gives the probability of finding the molecules within a small solid angle. To simplify the equations, certain assumptions are made. The phase is considered to consist of solid rods whose long axis is represented by a vector, **l**. This is represented in Figure 1.8, where θ is the angle between **l** and the director, **n**.

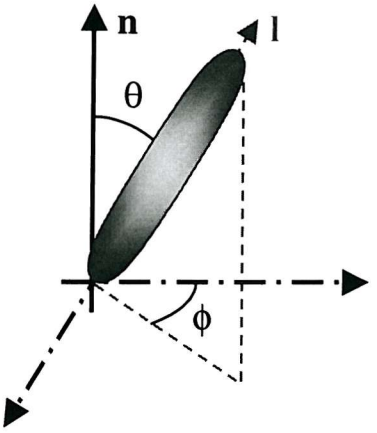

Figure 1.8 A schematic showing the angles and vectors used in establishing an order parameter.

The rods are assumed to have a cylindrically symmetric distribution about the director, **n**, and thus no azimuthal, ϕ, dependence is required. Hence the alignment of the rods can be described solely by an angular distribution function of θ. This is obtained from a power expansion of the Legendre polynomials of cosθ. The molecules in a mesophase can be in constant motion, so the thermal average is used, this is denoted by the brackets. The simplest function is $\langle \cos\theta \rangle$, however, this function equates to zero under the nematic precondition that **n** = -**n**, therefore, a more complex non-zero function is required. The next Legendre polynomial is the P_2 quadrupole moment in $\langle \cos^2\theta \rangle$, or:

$$S = \frac{1}{2}\langle 3\cos^2\theta - 1 \rangle . \qquad 1.2$$

This is the order parameter S, first introduced by Zwetkoff[28]. In a totally random system $\langle \cos^2\theta \rangle$ averages to ⅓, but if the system has perfect parallel alignment it equals 1. Hence P_2 varies from 0 in the isotropic to 1 in a perfect crystal, allowing the state of alignment to be approximated by a simple number rather than a complex function. Typically, values of S range from ~0.3 up to ~0.8 in nematics. This basic description can also be applied to smectics, where values as high as 0.9 can be seen, an indication of the greater ordering in these systems. The additional translational order due to the layer structure can be allowed for with an extension of the basic nematic order parameter, but this is unnecessary for most practical purposes.

The order parameter definition is deliberately over simplistic. A more thorough function would include higher order Legendre polynomial terms, P_4, and so on. These terms are commonly ignored, as specialist techniques such as Nuclear Magnetic Resonance and Polarised Raman Spectroscopy are required to show up the small differences these terms would cause[7]. Raman spectroscopy[7, 29] has shown that different parts of a molecule respond differently in an electric field, thus a full description would require order parameters for each part of the molecule. The rigid rods can be replaced by more accurate molecular dimensions, but this creates an unwieldy, complex equation. Although it is important to understand the limitations this imposes, the simple definition can be used to predict many liquid crystalline properties. Another approach is to consider the problem from a macroscopic viewpoint. This has the advantage of not necessitating large simplifications of the molecules themselves. For a full definition the reader is directed to de Gennes and Prost[30].

1.5 THERMODYNAMIC PROPERTIES

Now that an order parameter has been established, the Landau theory of phase transitions is discussed. This has been developed by de Gennes into one of the most successful phenomenological theories of liquid crystal phase transitions. Many of the models for the SmC* phase are derived from dynamical and statistical descriptions of uniaxial nematics, and this is no exception. Landau theory makes use of any order parameter, ξ, of a system to describe the phase as it goes from an ordered state with a non-zero order parameter to a less ordered state with a zero order parameter. The ξ chosen can differ from system to system. The orientation distribution parameter, S, described earlier is applicable for transitions to the isotropic. More relevant to the current work, for a transition such as SmC to SmA, the molecular tilt angle can be used.

1.5.1 Landau – de Gennes Theory of Phase Transitions

The fundamental assumption of Landau theory is that F, the free energy per unit volume, can be written as an expansion of an order parameter; for liquid crystals this is a function of the temperature, T. A further assumption is made that the phases have a centre of inversion symmetry, this means we can replace ξ by $-\xi$ without changing the equation. Thus the expansion is in even powers only:

$$F\{\xi,T\} = g_0\{T\} + \tfrac{1}{2}g_2\{T\}\xi^2 + \tfrac{1}{4}g_4\{T\}\xi^4 + \tfrac{1}{6}g_6\{T\}\xi^6 + ... \qquad 1.3$$

The values of the coefficients g_0, g_2, g_4 and so on, can be determined by experiment or theory in a given system. These determine the temperature dependence of F.

The simplest method of modelling a phase transition is to change the sign of the g_2 coefficient at the transition temperature T_0. However, if g_2 is positive on one side of the transition and negative on the other it must vanish at T_0. Therefore, in a small temperature range close to the transition, it is reasonable to say

$$g_2\{T\} = \alpha(T - T_0), \qquad 1.4$$

where α is a positive constant.

The thermodynamically stable phase of any system is the one possessing the lowest free energy. Therefore Equation 1.3 is differentiated and set to zero:

$$\left.\frac{\partial F}{\partial \xi}\right|_T = 0 = g_2\xi + g_4\xi^3 + g_6\xi^5 + ... \qquad 1.5$$

1.5.1.1 Second Order Transitions

If g_4 is considered positive, higher terms in Equation 1.5 can be ignored as they do not contribute significantly to the understanding of phase behaviour. Thus the stable phase is given by

$$\left.\frac{\partial F}{\partial \xi}\right|_T = \alpha(T - T_0)\xi + g_4\xi^3 = 0 \qquad 1.6$$

which has two solutions; $\xi = 0$ and $\xi^2 = (T - T_0)\left(\frac{\alpha}{g_4}\right)$.

As a result, the order parameter goes to zero at a temperature T_0 and hence this is the phase transition temperature, T_c. The thermodynamically stable states indicated by the free energy minima exist above T_0 with an order parameter of zero and below T_0 where the order parameter is non-zero. As the temperature, T_0, is approached from below, the order parameter gradually decreases to zero, thus the transition is smooth. Differentiation of Equation 1.3, the free energy expression, with respect to temperature yields the entropy of the system. This is continuous so the transition would not be expected to show a heat of transition. Further differentiating with respect to temperature yields the specific heat. This is discontinuous, therefore this behaviour is termed second order.

The dependence of ξ on $T^{1/2}$ can be seen in many places, one instance is the SmC to SmA transition. Here the order parameter is the tilt angle, θ, from the layer normal. The theory successfully predicts the tilt angle dependency as zero in the SmA phase at temperatures above T_c. A more useful

consequence is the prediction of behaviour in the SmC phase, below T_c. Here the root relationship yields an equation for the tilt angle;

$$\theta\{T\} = \theta_0\left(\frac{T - T_c}{T_c}\right)^{\frac{1}{2}}. \qquad 1.7$$

The addition of a T_c denominator is simply to give the constant of proportionality, the dimensions of tilt. Although not perfect, good experimental agreement can be seen with this and other physical parameters.

1.5.1.2 First Order Transitions

If g_4 is now considered negative, the higher order term, g_6, is significant when considered positive. Now the stable phase is given by

$$\left.\frac{\partial F}{\partial \xi}\right|_T = \alpha(T - T_0)\xi - |g_4(T)|\xi^3 + g_6\xi^5 = 0 \qquad 1.8$$

which has two solutions; $\xi = 0$ and $\alpha(T - T_0) - |g_4(T)|\xi^2 + g_6\xi^4 = 0$.

The phase transition occurs at the critical temperature, T_c, when the order parameter goes to zero. Here this no longer has to occur at T_0 and this accounts for supercooling and superheating, not seen in first order transitions.

The temperature dependence of the resultant free energy equation means that above T_c only one minimum exists with an order parameter of zero. Below T_c, there is a solution with a non-zero order parameter. At the critical temperature, there are two solutions, one equalling zero and one non-zero. This corresponds to a discontinuous change in ξ and in the first temperature derivative of the free energy; hence this describes first order behaviour.

The discontinuity in the first derivative corresponds to entropy, which manifests itself as latent heat. This is in contrast to the second order transition that has no enthalpy change through a transition. An example of first order behaviour is the transition from isotropic to SmC, again using tilt as the order parameter. At temperatures above T_c, the tilt is zero but a measurable angle appears spontaneously as the transition is passed. It should be noted that the order parameter, in this example the tilt, no longer follows a $T^{½}$ relationship. Another important consequence of the first order discontinuity is that the phases above and below the transition can coexist in equilibrium.

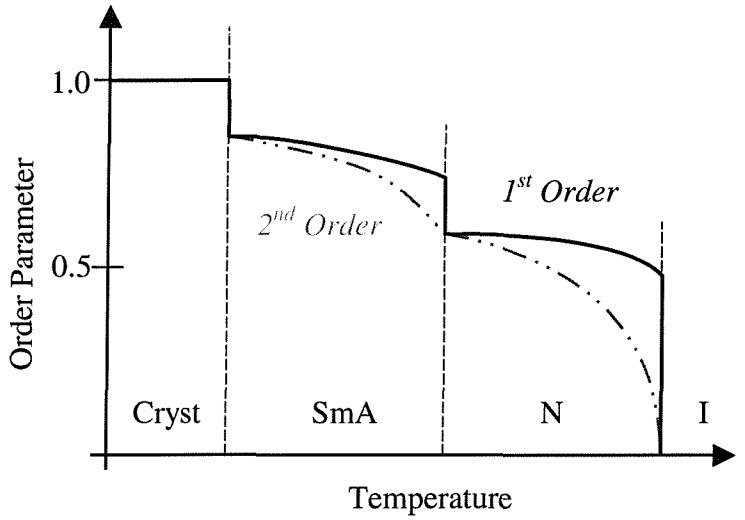

Figure 1.9 A graph showing the hypothetical variations of an order parameter undergoing 1st and 2nd order phase transitions.

Parameters that have a functional dependence on ξ will also show similar behaviour. Hence in first order transitions there will be a discontinuity and in second order transitions they will be continuous. Figure 1.9 demonstrates how the behavioural changes might look if a transition was hypothetically purely first or second order. Thus, simple Landau theory can be used to model the temperature and field dependencies of many physical parameters.

1.5.2 Actual Phase Transitions

Transitions seen in actual liquid crystal samples tend not to be purely first or second order as shown in Figure 1.9, but a combination of both. For a given transition, the size of the discontinuity and any pre-transitional effects will determine whether it can be considered strongly or weakly first order. For example, on heating a SmC there are three likely transitions; SmC → I, SmC → N and SmC → SmA. In the first two instances, more than one degree of order vanishes, for example, both the layer structure and molecular tilt disappear. Generally these are first order transitions, but the order parameter and related properties often show a pre-transitional fall, smoothing the expected discontinuity. The SmC to SmA transition is more complex and is similar to a second order, but a small amount of latent heat is often seen. The majority of SmC to SmA transitions are actually mean-field[31]. Ordering effects from a nematic or smectic phase can be maintained several degrees into the isotropic over small distances, these are known as nematic and smectic swarms.

First order transitions are often characterised by superheating and supercooling. If on cooling there are no nucleation points present to seed the start of crystallisation, a phase can exist well below its expected transition, this is the phenomenon of supercooling. Similarly, the lack of disruptions in a

material can allow a phase to last longer on heating, known as superheating. Examples include monotropic and glass phases. These phenomena highlight the effects of purity and cell conditions such as heating and cooling rates.

If a solid sample has a clearing temperature above that required by its inherent liquid crystal phase, it will melt directly to an isotropic liquid. However, on cooling, if conditions are right and insufficient nucleation points exist, the crystallisation process is hindered and the liquid crystal mesophase can form. These monotropic phases are metastable and are highly dependent on the cooling conditions and storage environment. Glass phases are an extreme example of supercooling. Under the right conditions, a sample may be cooled to a temperature where the viscosity is so great that although true crystallisation has not occurred, the samples structure is frozen. Although such a glass phase is very similar to a crystal in that the molecules are almost fixed in place, the phase lacks the regular crystal lattice. Once again, the formation and stability of the phase is dependent on cooling rates and conditions.

1.6 SUMMARY

This chapter has given a brief overview of the very broad family of liquid crystals. This breadth has been continued with a look at a nematic order parameter used to describe molecular order. Basic Landau – de Gennes theory has been used to explain the basis for many of the relationships seen in liquid crystals and particularly the transition between phases. Although many of the ideas introduced apply elsewhere in liquid crystals, the focus has been on the thermotropic calamitic phases. Thus far, the phases have been considered in a broad sense; now some of the theories behind them are introduced. In particular, the focus of the following chapter is on the concept of ferroelectricity.

1.7 REFERENCES

[1] F. Reinitzer, *Monatsch. Chem.*, **9**, 421 (1888).
[2] O. Lehmann, *Z. Phys. Chem. (Leipzig)*, **4**, 462 (1889).
[3] H.H.Strey, J.Wang, R.Podgornik, A.Rupprecht, L.Yu, V.A.Parsegian, E.B.Sirota, *Phys. Rev. Lett.*, **84**(14), 3105 (2000); A.Leforestier, F.Livolant, *J. Phys. II France*, **2**, 1853 (1992).
[4] F.B.Rosevear, *J. Am. Oil Chem. Soc.*, **31**, 628 (1954).
[5] G.W.Gray, K.J.Harrison, J.A.Nash, *Electron. Lett.*, **9**(6), 131 (1973); E.Merck KGaA, Frankfurter Str. 250, D-64271, Darmstadt, Germany. http://www.merck.de
[6] H.Stegemeyer, TH.Blümel, K.Hiltrop, H.Onusseit, F.Porsch, *Liq. Cryst.*, **1**(1), 3 (1986).
[7] S.Jen, N.A.Clark, P.S.Pershan, E.B.Priestly, *J. Chem. Phys.* **66**(10), 4635 (1977).
[8] P.J.Collins, M.Hird, *Introduction to Liquid Crystals,* Chpt **1**, (Taylor & Francis, London, 1998).
[9] D.A.Dunmur, *The Optics of Thermotropic Liquid Crystals*, (ed. Steve Elston, Roy Sambles), Chpt. **2**, (Taylor & Francis, London, 1998).
[10] J.S.Patel, R.B.Meyer, *Phys. Rev. Lett.*, **58**(15), 1538 (1987).
[11] B.Musgrave, *Ph.D. thesis,* Univ. Southampton, U.K., (2000).
[12] L.N.Lisetski, A.V.Tolmachev, *Liq. Cryst.*, **5**(3), 877 (1989);
[13] P.P.Crooker; *Liq. Cryst.*, **5**(3), 751 (1989); R.Miller, *Liq. Cryst. Today,* **9**(3/4), 7 (Dec, 1999).
[14] P.E.Cladis, *Mol. Cryst. Liq. Cryst.*, **165**, 85 (1988);
[15] R.Schaetzing, J.D.Litster, *Advances in Liquid Crystals*, ed. G.H.Brown, (Academic Press, 1979), **4**, 147.
[16] H.Sackmann, D.Demus, *Mol. Cryst.*, **2**, 81 (1966); *Mol. Cryst. Liq. Cryst.*, **21**, 239 (1973).
[17] G.Friedel *Ann. Phys. (Paris),* **18**, 273 (1922).
[18] J.W.Goodby, *Handbook of Liquid Crystals – Low Molecular Weight Liquid Crystals I,* (ed D.Demus, J.Goodby, G.W.Gray, H.-W.Spiess, V.Vill) Vol.**2A**,Chpt.**1-§2** (Wiley-VCH, Germany, 1998).
[19] A.J.Leadbetter, J.L.A.Durrant, M.Rugman, *Mol. Cryst. Liq. Cryst. Lett.*, **34**, 231 (1977); A.J.Leadbetter, J.C.Frost, J.P.Gaughan, G.W.Gray, A.Mosley, *J. Phys. (Paris)*, **40**, 375 (1979)
[20] S.R.Renn, T.C.Lubensky, *Phys. Rev. A*, **38**(4), 2132 (1988).
[21] J.W.Goodby, M.A.Waugh, S.M.Stein, E.Chin, R.Pindak, J.S.Patel, *Nature*, **337**, (Feb 1989); *J. Am. Chem. Soc.*, **111** 8119 (1989).
[22] S.R.Renn, T.C.Lubensky, *Mol. Cryst. Liq. Cryst.* **209**, 349 (1991); H.T.Nguyen, A.Bouchta, L.Navailles, P.Barois, N.Isaert, R.J.Twieg, A.Maaroufi, C.Destrade, *J. Phys. II France*, **2**, 1889 (1992).
[23] J.W.Goodby, *Handbook of Liquid Crystals – Fundamentals* (ed D.Demus, J.Goodby, G.W.Gray, H.-W.Spiess, V.Vill) Vol.**1**,Chpt.**5-§4.2** (Wiley-VCH, Germany, 1998).
[24] P.A.C.Gane, A.J.Leadbetter, P.G.Wrighton, *Mol. Cryst. Liq. Cryst.*, **66**, 247 (1981).
[25] D.R.Nelson, B.I.Halperin, *Phys. Rev. B*, **21**(11), 5312 (1980).
[26] J.W.Goodby, J.S.Patel, T.M.Leslie, *Ferroelectrics,* **59**, 121 (1984).
[27] G.W.Gray, J.W.G.Goodby, *Smectic Liquid Crystals: Textures and Structures*, (Leonard Hill, 1984).
[28] W. Zwetkoff, *Acta Phys. (URSS)*, **16**(3), 132 (1942).
[29] K.M.Booth, H.J.Coles., *Liq. Cryst.*, **13**(5), 677 (1993).
[30] P.G.deGennes, J.Prost, *The Physics of Liquid Crystals (2nd Ed.),* Chpt. **2**, (Clarendon Press, 1995).
[31] R.J.Birgeneau, C.W.Garland, A.R.Kortan, J.D.Lister, M.Meichle, B.M.Ocke, C.Rosenblatt, L.J.Yu, J.Goodby, *Phys. Rev. A,* **27**(2), 1251 (1983); M.Meichle, C.W.Garland, *ibid,* **27**(2), 2624 (1983).

Chapter Two

Ferroelectricity, Switching and Physical Parameters

There is a theory which states that if ever anyone discovers exactly what the Universe is for and why it is here, it will instantly disappear and be replaced by something even more bizarre and inexplicable.
There is another which states that this has already happened.

The Restaurant at the End of the Universe, Douglas Adams 1952-2001

2.1 INTRODUCTION

Now that the concept of liquid crystallinity has been introduced, the physical properties of specific mesophases are examined. The focus of this chapter is the SmC* phase and the concept of ferroelectricity. With the introduction of its use in the surface stabilised cell geometry, the study of the electro-optic properties of the SmC* phase forms the backbone of much of the work in this thesis. The ideas and theoretical concepts behind some of the physical parameters of ferroelectric liquid crystals are examined. The concept of antiferroelectricity is introduced. Finally, some of the molecular requirements for liquid crystallinity are discussed.

2.2 FERROELECTRICITY AND MOLECULAR PROPERTIES

In some cases, dielectrics can exhibit a permanent and finite value of electric polarisation, known as spontaneous polarisation. This polarisation exists in the absence of an applied field or mechanical stress. If the direction of the spontaneous polarisation can be changed by an applied field, these polar-materials are known as "ferroelectrics". The first evidence of ferroelectricity was seen in the solid state by Joseph Valasek in 1921[1] when, studying Rochelle salt, he observed two states of permanent electric polarisation that decreased with increasing temperature. He saw parallels between this and ferromagnetic materials, which possess domains, exhibit hysteresis loops and show Curie-Weiss behaviour near their phase transition temperatures. Thus he named the new phenomenon "ferroelectricity" and called the temperature at which the polarisation vanished the "Curie temperature".

In the mid 1970s, Meyer used a symmetry argument to suggest that any tilted chiral smectic phase could be ferroelectric. This work led his collaborators to the specific design of a liquid crystal, with the hope of demonstrating ferroelectricity properties in a chiral smectic[2]. In 1980, Clark and Lagerwall outlined the physical application of a ferroelectric device as an electro-optic modulator[3]. The molecules in the phase each possess a small transverse dipole. Interactions between neighbouring molecules hinder rotation and the dipoles line up within the smectic layers. Recalling the schematic idea of the SmC* phase from chapter 1, the molecules twist around a helix. This also causes the aligned dipoles to adopt a screw twist as shown in Figure 2.1.

If the helical twist can be unwound, all these layer dipoles can combine to form a macroscopic spontaneous polarisation. This macroscopic polarisation is responsible for many of the SmC* phase electro-optic properties. To understand the polarisation and ferroelectricity, it is important to explain the concepts behind Meyer's arguments. Although these arguments can explain the phenomenon of ferroelectricity in certain phases, they can also be used to exclude it in others.

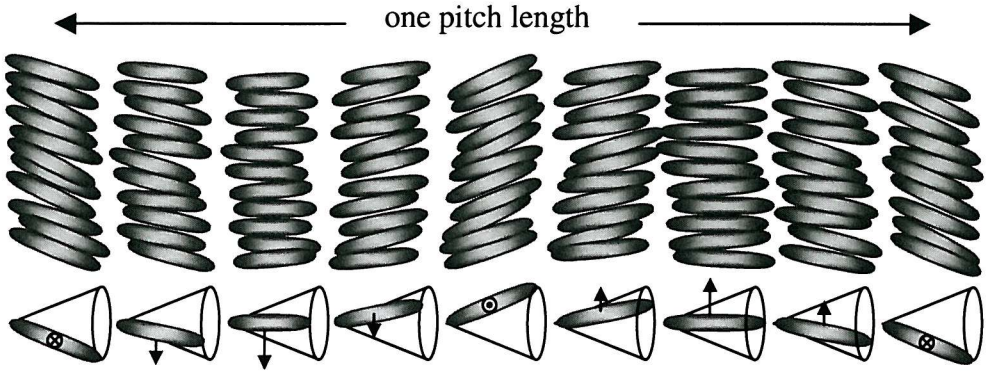

Figure 2.1 A representation of the SmC phase with molecular dipoles.*

2.2.1 Symmetry Requirements

The important characteristic of a ferroelectric is its ability to exhibit spontaneous polarisation (P_s). Symmetry considerations alone are sufficient to judge if a liquid crystal phase can exhibit ferroelectricity and this requirement can be summarised by Franz Neumann's principle[4], which states that, "*The symmetry elements of any physical property of a crystal must include the symmetry elements of the point group of the crystal*". The point group of a crystal is the group of macroscopic symmetry elements that its structure possesses. Thus any symmetry operation that leaves the medium unchanged must also leave the macroscopic physical properties, such as P_s, unchanged for the phase to show ferroelectricity.

The macroscopic spontaneous polarisation is due to the addition of the molecular polarisation dipoles. It is therefore easy to understand that in a normal, randomly ordered isotropic fluid these molecular dipoles do not reinforce one another to give a macroscopic P_s. The argument is complicated if the fluid is composed of chiral molecules. This is best demonstrated by considering the polarisation, **P**, of the liquid. **P** is a vector quantity and as such can be expressed as components along three mutually orthogonal axes:

$$\mathbf{P} = (\mathbf{P}_x, \mathbf{P}_y, \mathbf{P}_z). \qquad 2.1$$

Following Neumann's principal, for a spontaneous polarisation to exist in a phase, **P** must be invariant under all symmetry operations that leave the phase invariant. In an isotropic fluid, any polarisation direction can be arbitrarily chosen. A 180° rotation around the y-axis for example, does not alter the phase and therefore must not alter **P**. Thus,

$$(\mathbf{P}_x, \mathbf{P}_y, \mathbf{P}_z) = (-\mathbf{P}_x, \mathbf{P}_y, -\mathbf{P}_z). \qquad 2.2$$

For this expression to hold, polarisation can only exist in the y-direction. A further 90° rotation around the z-axis gives the following equation:

$$(0,\mathbf{P}_y,0)=(\mathbf{P}_x,0,0). \qquad 2.3$$

This leads to the conclusion that polarisation cannot exist in any direction and hence isotropic fluids cannot be ferroelectric.

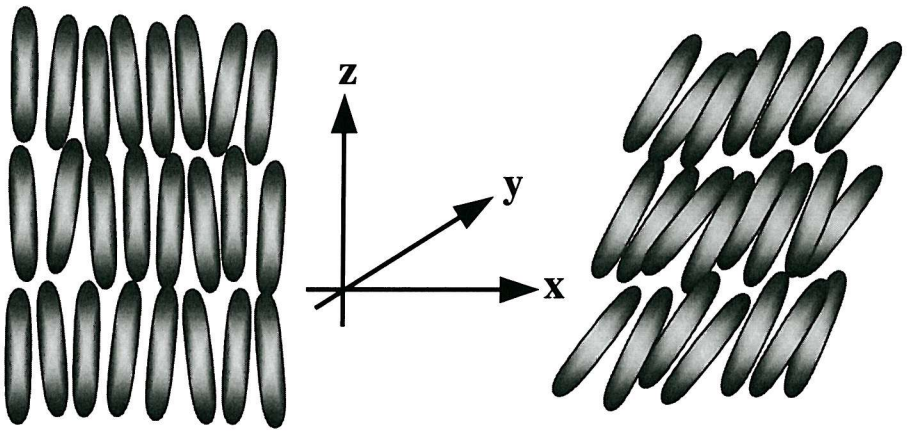

Figure 2.2 A schematic showing the SmA and SmC phases with a co-ordinate system to explain the arguments behind ferroelectricity.

The same argument of rotational symmetry can be applied to exclude ferroelectricity in the N, N* and SmA phases[5]. As the co-ordinate system shown in Figure 2.2 demonstrates, the two rotations described previously are still symmetry transformations, despite the extra order shown by the phases. Finally, consideration is given to the presence or absence of ferroelectricity in the SmC and SmC* phases. The presence of chirality in the SmC* phase giving rise to the helicoidal structure was discussed in the previous chapter. The complication this adds is avoided by considering only a few layers. This treatment is valid because the precession of the tilt is slow at a molecular level with the pitch typically of the order of a thousand times larger than the inter-layer spacing, producing global not local changes in the symmetry.

The invariance of the director means that a 180° rotation about the y-axis shown in Figure 2.2 is still a valid symmetry operation. Therefore, as before, polarisation can only exist along the y-axis and

$$\mathbf{P}=(0,\mathbf{P}_y,0). \qquad 2.4$$

Rotations around the z-axis are no longer symmetry operations; however, the SmC phase has a mirror plane in the x-z plane that can transform the polarisation director giving

$$(0,\mathbf{P}_y,0)=(0,-\mathbf{P}_y,0). \qquad 2.5$$

These symmetry operations are known as C_{2h} and these arguments preclude the presence of ferroelectricity in the SmC phase.

The principles presented for the SmC phase are not fully applicable in the case of the SmC* phase. The component of polarisation $\mathbf{P}_y$ does not have to vanish, as the x-z plane is not a mirror symmetry plane for chiral molecules, consequently the phase has a reduced C_2 symmetry. This can result in a polarisation in the smectic layer plane in a direction orthogonal to the tilt plane. It is the absence of this mirror plane that allows ferroelectricity to exist. This argument can be extended to other chiral tilted smectic phases.

No consideration has yet been given to the effect of molecular rotation around the long molecular axis. In a SmC* phase, such behaviour would result in a random azimuthal distribution of the molecular dipoles, and the macroscopic polarisation would average to zero. In practice, the interaction between neighbouring molecules results in a chiral molecule's rotation being hindered. The slightest asymmetry about the long axis is sufficient to ensure that the polarisation is finite.

In the above arguments several layers have been considered, assuming local global symmetry. However, the chirality of the SmC* phase causes a helical rotation of the director, (this has led the SmC*, SmF* and SmI* phases to be termed helielectrical). The rotation of the director results in a similar rotation of the local layer polarisation. Thus the macroscopic polarisation of the bulk material averages to zero, and the phase does not exhibit a spontaneous polarisation. For ferroelectricity to be useful in many devices, the helix must be unwound. As mentioned in the previous chapter, in some very highly ordered chiral smectic crystal phases, the helical order can disappear because of strong interlayer forces. This allows some phases to exhibit true ferroelectricity[6], but their highly ordered structure is not conducive to fast electro-optic switching.

2.2.2 $\mathbf{P_s}$ Convention

One of the consequences of the arguments describing ferroelectricity in the SmC* phase is that the spontaneous polarisation vector, **P,** must lie within the layer plane. Utilising the definition of **k** as a vector along the layer normal and **n** as a vector along the molecular long axis, the polarisation is defined as

$$\mathbf{P} = P_0 \mathbf{k} \wedge \mathbf{n}. \qquad 2.6$$

The cross product allows a sign convention to be assigned to **P**. Figure 2.3 demonstrates two possible stable states in the presence of an electric field. On the left, the molecular polarisation is pointing into the page, aligned parallel to an applied field into the page. The molecular long axis is tilted at an angle θ. The field couples to the P_s dipole giving a polarisation torque. Thus when the field is reversed, the polarisation realigns with the field to point out of the paper and the molecule is forced to switch and tilt at an angle of $-\theta$. Normally the tilt has no sign convention; the negative sign is only used to highlight the switch that has occurred. It follows that the functional dependence of the spontaneous polarisation should be closely related to θ.

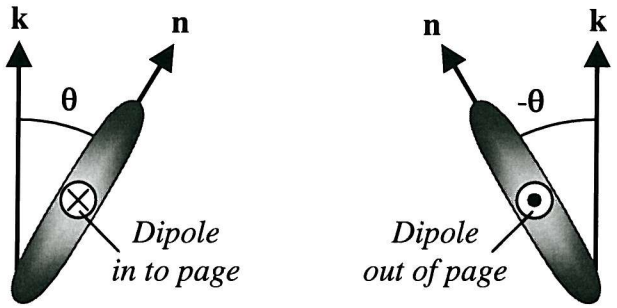

Figure 2.3 A schematic showing the P_s convention with tilt.

It is worth noting that although molecules are often drawn schematically rotating about one end, in a true picture the switch may be closer to the centre of mass. The full picture, however, is complicated by layer interdigitations and packing forces.

2.2.3 Soft Mode and Goldstone Modes

The fundamental order parameter of the SmC* phase is the tilt angle. When the tilt forms, there is not always a restriction on the plane in which this must occur: the azimuthal angle, ϕ, is not constrained by free energy considerations. To consider both tilt components, a simplified argument considers the order parameter as a complex quantity, i.e.

$$\xi = \theta e^{i\phi}, \qquad 2.7$$

where θ is the tilt angle and ϕ is the azimuthal angle of the director as shown in Figure 2.4. In the SmC* phase, variations in θ cause a compression or dilation of the layers. θ is therefore considered to be a hard variable, as variations from its thermodynamically predetermined value require considerable elastic energy. The azimuthal angle, ϕ, is not fixed thermodynamically and is considered to be a gauge variable. Only spatial changes or gradients in ϕ affect the free energy of the system.

Having established that an appropriate field can switch SmC* molecules between two states, the nature of the switch is examined. The switching process can occur in two distinct ways, namely the soft mode and the Goldstone mode. The most direct method of switching is for molecules to remain in the layer plane and vary the tilt angle, θ, as shown in Figure 2.4. However, this alteration of the layer spacing is very energetically expensive. This is known as the soft mode[7], and despite the unfavourable energy conditions, does occur in some systems. One example is the SmA* phase where it is the only allowed tilt motion and is specifically termed electroclinic switching.

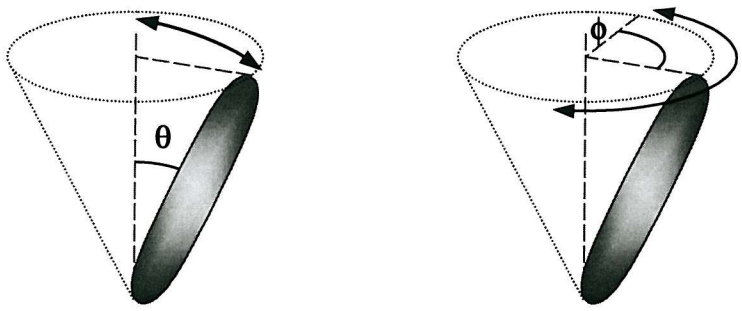

Figure 2.4 The switching motions comprising the soft and Goldstone modes.

An alternative method is for the molecules to rotate around the cone defined by 2θ, maintaining the tilt and the layer spacing. Such changes in orientation are easily excited and the effect is called the Goldstone mode[8]. The value of the azimuthal angle, ϕ, can be easily varied since it is not fixed thermodynamically; hence a SmC* molecule is easily switched in this mode by an external electric field.

2.2.3.1 Electroclinic Effect

In the SmC* phase the Goldstone mode dominates. The soft mode is mainly observed in the SmA* phase with an underlying SmC*, where it is known as electroclinic switching[9]. As the SmC*→ SmA* transition is approached, the soft mode becomes easier to excite due to the lower symmetry of the SmA* phase. The application of a field normal to the director induces a field-dependent molecular tilt, a phenomenon which has been explained by using a symmetry argument similar to that given above for ferroelectricity in the SmC* phase[9]. An applied field biases the free rotation of the molecules, resulting in a transverse polarisation in the field direction and in turn causes a tilt of the molecular long axis.

At low fields, away from the SmA*→ SmC* transition, the induced tilt is linear in applied field and increases with decreasing temperature. Thus the electroclinic effect has no threshold field or bistability. The response time is field independent and can be sub-microsecond, typically 10-100 times faster than a typical Goldstone switch [7,10]. However, at high fields and near the transition, the induced tilt follows an $E^{1/3}$ trend[11]. One disadvantage of electroclinic switching is the strong temperature dependence. Although the induced tilt angles are typically less than 10°, in exceptional cases they can reach as high as 20°, especially in the few degrees near a transition[12]. The fast response and linearity to the applied field give the electroclinic mode potential for optical modulation[13] and grey scaling[14]. One drawback of this type of application is the lack of a bistable mode, thus necessitating active matrix addressing which can complicate manufacture.

The characteristic features of the electroclinic effect may be deduced from a simple phenomenological description[15]. The field induced tilt is linear under certain conditions, such that,

$$\theta_{ec} = e_{ec}E \quad \text{where} \quad e_{ec} = \frac{s_{ec}}{\alpha\left(T - T_c\right)}, \tag{2.8}$$

where E is the field strength and e_{ec} is an electroclinic coefficient that diverges as $T \rightarrow T_c$. The constant α is a coefficient of the Landau free energy expression, and s_{ec} is a structure coefficient. A consequence of this is a field independent electroclinic response time,

$$\tau = \frac{\gamma_{ec}}{\alpha\left(T - T_c\right)}. \tag{2.9}$$

Here, γ_{ec} is the electroclinic viscosity. Once more, the temperature dependent properties are clearly seen. It may seem unusual to have a response time independent of field, but this can be rationalised by considering an increase in field. Doubling the applied field may double the angular response speed but the induced tilt will also double and the total time for a saturated switch will remain the same. Finally, it is worth noting that the induced tilt breaks the degeneracy around the layer normal and leads to an induced polarisation, which follows the simple relation

$$P = s_{ec}\theta. \tag{2.10}$$

On cooling through the SmA*→SmC* transition, the SmC* tilt and polarisation form, analogous to the Curie point in a classical ferroelectric or ferromagnetic. At the transition a combined tilt is observed, as shown in Figure 2.5. Measurements of tilt angles across the transition temperature range are affected by electroclinic switching initially and then by the Goldstone mode in the SmC* phase. Garoff and Meyer[9] concluded that the phase change is driven by the intermolecular forces acting to form the SmC* phase, and not the spontaneous polarisation which merely provides a perturbation. Thus, they saw the electroclinic effect as a measure of the critical behaviour near the transition, instead of a measure of dipole-dipole interactions.

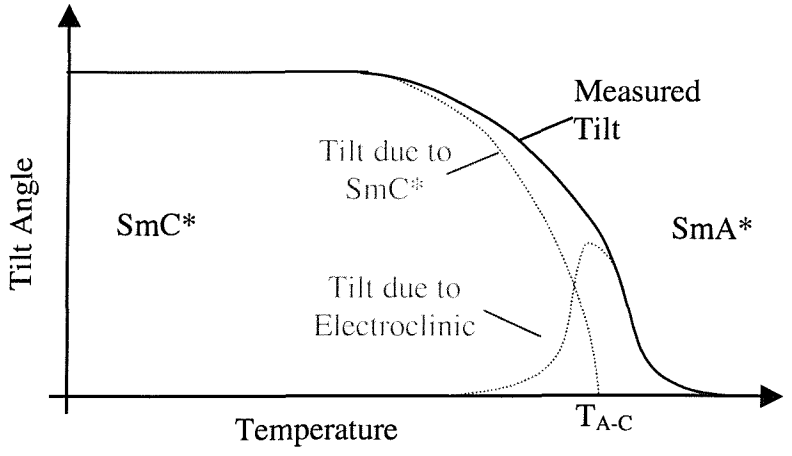

Figure 2.5 The effect of Goldstone and electroclinic tilt near the SmC - SmA* transition.*

Electroclinic switching is not confined to the SmA* phase and it has also been seen in the N* phase. Observation of the phenomenon is dependent on partial helix unwinding. Thus it has been observed close to the N*→SmA* transition[16] and in the vicinity of a twist inversion[17], however the associated angles can be very small (<0.1°).

2.2.4 Helix Unwinding

In order to demonstrate ferroelectric behaviour, the helix of the helielectrical SmC* phase must be suppressed[3]. One method for unwinding this helix is to apply an electric field in the direction of the layer plane. At sufficient strength, this causes the polarisation dipoles within the layers to align with the field. The competing helical molecular alignment forces result in a threshold or critical field for helix unwinding. This requires a complex consideration of frequency and dielectric forces[18]; however, to a reasonable approximation the critical field, E_c, is given by[2,19],

$$E_c = \frac{\pi^4 K}{4LP}, \qquad 2.11$$

where K is a torsional elastic constant, L is the length of the helix pitch and P is the polarisation density. Typical values for the critical field[19] are less than 0.1 $V\mu m^{-1}$ and this effect is exploited in devices to switch between scattering and transmitting states[20]. The unwound helix is unstable and reforms upon removal of the field. A more permanent method of unwinding the helix is to use an alignment layer, by sandwiching the sample between appropriately treated glass plates for example. A fully unwound helix is essential for comparative studies.

2.2.5 Anisotropic Properties

As a consequence of their molecular shape anisotropy, most liquid crystals are anisotropic in other material parameters. Microscopic anisotropy combined with orientational order leads to bulk anisotropy, which is seen in the response of liquid crystal materials to electric and magnetic fields and also mechanical stress. Thus a measured material property depends on both the orientation of the molecules and of the sample.

2.2.5.1 Optical Anisotropy

An optically anisotropic material has more than one refractive index. Incident light can be resolved into two components, the ordinary and extraordinary waves. These are polarised orthogonal to each other and experience different refractive indices as they propagate within a "birefringent" material. A uniaxial birefringent system has two principal refractive indices. The ordinary component, n_o, is independent of the path taken by the light, and the extraordinary component, n_e, contains the angular dependence of the refractive index. The birefringence results in a phase difference, and thus the total birefringence is the difference in the effect of these two indices, i.e.

$$\Delta n = n_e - n_o . \qquad 2.12$$

Principal liquid crystal indices are typically in the range of 1.4 to 1.9. A uniaxial system has one symmetry axis, known as the optic axis. Two orthogonal polarisations propagating along a direction parallel to the optic axis experience the same refractive index, hence no phase mismatch occurs and the material responds as an isotropic medium. A biaxial system is more complex, possessing three different refractive indices and two optic axes. However, in liquid crystals, one index is often far greater than the other two and the biaxiality is small. Many nematic and SmA systems are uniaxial with the optic axis lying along the director. This means that with reference to the molecular long axis, $n_e \equiv n_\parallel$ and $n_o \equiv n_\perp$, hence Equation 2.12 becomes

$$\Delta n = n_\parallel - n_\perp . \qquad 2.13$$

At optical wavelengths, smectics can also be considered to be broadly uniaxial, although strictly they are in fact weakly biaxial[21]. Smectic liquid crystals typically have positive birefringence; $n_\parallel > n_\perp$ and Δn varies from $\sim +0.4 \rightarrow +0.02$. Equation 2.13 represents idealised behaviour; in reality the statistical nature of a liquid crystal phase reduces the actual birefringence of the phase by a factor equal to the order parameter.

2.2.5.2 Dielectric Anisotropy

When an electric field is applied to an FLC cell, there will be a dielectric torque in addition to the ferroelectric one. The response of a uniaxial system to an electric field depends on the strength of its two dielectric constants. The dielectric constant or relative permittivity of a material comes from two contributions. The first is an induced electronic polarisation; this occurs in all dielectrics and is due to the relative displacement of the electronic and atomic densities. The second is an orientational polarisation, which occurs in polar materials because of the permanent molecular dipole's tendency to align with a field. The dielectric anisotropy is derived from the two orthogonal permittivities (dielectric constants) parallel and perpendicular to the director, $\varepsilon_\parallel$ and $\varepsilon_\perp$, and is simply defined as

$$\Delta\varepsilon = \varepsilon_\parallel - \varepsilon_\perp . \qquad 2.14$$

The value of $\Delta\varepsilon$ can be positive or negative depending on the magnitude and orientation of the polarisation contributions. Although Equation 2.14 is true for D.C. and A.C. fields, the dielectric constants can be frequency dependent. This frequency dependence appears because the dipole moments take a finite time to reorient in an electric field[22]. A fundamental frequency exists for each reorientation; below this frequency the dipole can follow the field, above it a phase lag occurs until eventually at high enough frequencies the dielectric constant associated with the dipole moment is lost (Debye relaxation). The response of a biaxial system, such as a SmC* phase, is complicated by its three competing dielectric constants. In a ferroelectric system, the coupling of the polarisation

with the field to give a ferroelectric torque is significantly greater than the field-induced dielectric torque.

2.2.5.3 Conductivity

Liquid crystals have an intrinsic electrical conductivity, σ. This property is mainly due to ionic impurities and typically[22] has values from around 10^{-8} to 10^{-12} $\Omega^{-1}cm^{-1}$. The determination of conductivity due to additional dopants is difficult to achieve. The conductivity measured in liquid crystals is dependent upon the movement of ionic impurities rather than the motion of electrons as in conductive solids. The temperature dependence is governed by that of the ion mobilities and ionisation-recombination constants, and will generally follow an Arrhenius behaviour with a corresponding activation energy.

The presence of ions within a device can affect the switching as they interact with the spontaneous polarisation dipoles. Ions will drift to stabilize a dipole field making it difficult to switch states; this leads to the phenomenon of sticky pixels. In the presence of a field, the ions will drift in opposition to the field. Upon removal of the field, a bounce back to the opposite state can occur[23]. In a smectic mesophase, it is easier for ionic impurities to move along the layer plane than to move parallel to the director. In the SmA phase this has important consequences for the electrohydrodynamic motion of the molecules.

2.2.6 Field Effects in the SmA Mesophase

In order to establish a well ordered ferroelectric phase, it is desirable to establish a well aligned layer structure. This can be achieved more easily if a lower ordered SmA phase is exhibited previously on cooling. This section looks at some of the effects of an applied field in the SmA phase, and the structures produced. Two types of field induced behaviour have been seen in smectic A materials; effects directly due to the flow of current are known as electrohydrodynamic (EHD) and those due to coupling of the field and liquid crystal molecules result in dielectric reorientation. The SmA phase is utilised chiefly for alignment purposes in this work and a rigorous theoretical investigation is not required. The theories referenced in this section give a fuller picture that is extended from elasticity and dynamical equations of the nematic phases.

2.2.6.1 Electrohydrodynamic Instabilities

The formation of strong electrohydrodynamic instabilities requires firstly a strongly conducting sample. Conduction is achieved by an adequate ionic content and can occur naturally due to impurities or be controlled with an ionic dopant. Secondly a negative conductivity anisotropy is

typical, this means that conduction perpendicular to the molecules must be greater than that parallel to them. This is favoured by the smectic layer geometry encouraging ionic material to move in the layer planes. If a sufficiently large low frequency or D.C. field is applied to a SmA, a liquid flow pattern can develop in the cell.

With the field applied, an electrohydrodynamic instability is seen in homeotropically aligned samples with positive dielectric anisotropy; this develops a scattering texture similar to dynamic scattering seen in nematics which can spread throughout the cell, and causes a marked drop in the transmitted intensity that can persist after field removal[24]. Local disruption in the smectic layers causes the onset of this complex mechanism. A non-perfect parallel alignment of the smectic layers is thus required to provide centres for the scattering to develop, and this can be affected by such things as surface imperfections resulting in a lower threshold voltage and higher critical frequency. After field removal, the optical pattern based on small focal conics causes a long relaxation time, sometimes measured in years. This effect can be erased by dielectric reorientation in a high frequency field as described in the following section, allowing two stable states to be addressed. These states can form the basis of a scattering display; changing the frequency from 10^3 to 10^2 Hz can allow a reversible transition from clear to scattering with response times of approximately 10ms. The electrohydrodynamic process was modelled by Geurst and Goossens[25] who extended the Carr-Helfrich[26] nematic model of dynamic scattering in nematics. Some electrohydrodynamic effects can also be seen in planar aligned samples with negative dielectric anisotropy. This causes domain instabilities and is thought to occur due to destabilisation of the thin layers adjacent to the electrodes[27].

2.2.6.2 Dielectric Reorientation

Compounds with a positive dielectric anisotropy under the influence of high fields will want to orient with the director parallel to the field. A high quality planar alignment will form a quasi-homeotropic state via intermediate structural defects, the strong surface alignment preventing a full homeotropic structure[28]. The threshold field is proportional to the square root of the sample thickness. For this to occur, the field induced torque must overcome the elastic stabilising forces. With initial focal conic alignment, a switch to homeotropic alignment can occur at voltages less than those of dynamic scattering[29]. Below a critical voltage no effect is seen, but above it disclination lines appear on the edges of the focal conic domains which reorder into a homeotropic state, reversing the action of the electrohydrodynamic instabilities described above. Once again, after the removal of the field relaxation can be a long process. The theory behind this transition has been generalised for the SmA phase by de Gennes[30] based on a model by Helfrich and Hurault[31] for a similar effect in the N* phase.

2.3 THE SURFACE STABILISED GEOMETRY

In 1977, Meyer suggested that a thin sample of SmC* material could support a stable unwound structure due to surface interactions[19]. This surface stabilised ferroelectric liquid crystal (SSFLC) structure was demonstrated in 1980 by Clark and Largerwall[3] and uses sample thickness, layer direction and boundary conditions to suppress the helical structure. The inner surfaces of two glass plates are treated with an alignment layer. This layer encourages a planar (homogeneous) alignment of the director; the liquid crystal molecules lie parallel to the glass plates. In order for the alignment forces to overcome the helical winding forces, the internal thickness must be much less than about one quarter of the pitch length[32], which is typically between 1-100 microns. The tilt, θ, is a very strong thermodynamic property and the molecules are still constrained on a cone, but the weaker azimuthal angle allows the molecules to adjust to the surface conditions. The surface breaks the energetic degeneracy of the switching cone, creating two energy wells. The molecules in contact with the alignment layer are prevented from rotating around the cone. Thus the intersection of the cone with the alignment layer plane results in two possible states. These thermodynamically stable states can propagate across the cell if the gap is sufficiently small. This surface stabilised geometry leads to a threshold for switching. Although the application of a small field may lift the molecules slightly around the cone, when the field is removed, the molecules will want to return to the surface orientation. If the field is sufficient to lift the molecules to the mid-point of the cone, they can proceed spontaneously to the other switched state; thus the surface stabilised cell is bistable as shown schematically in Figure 2.6.

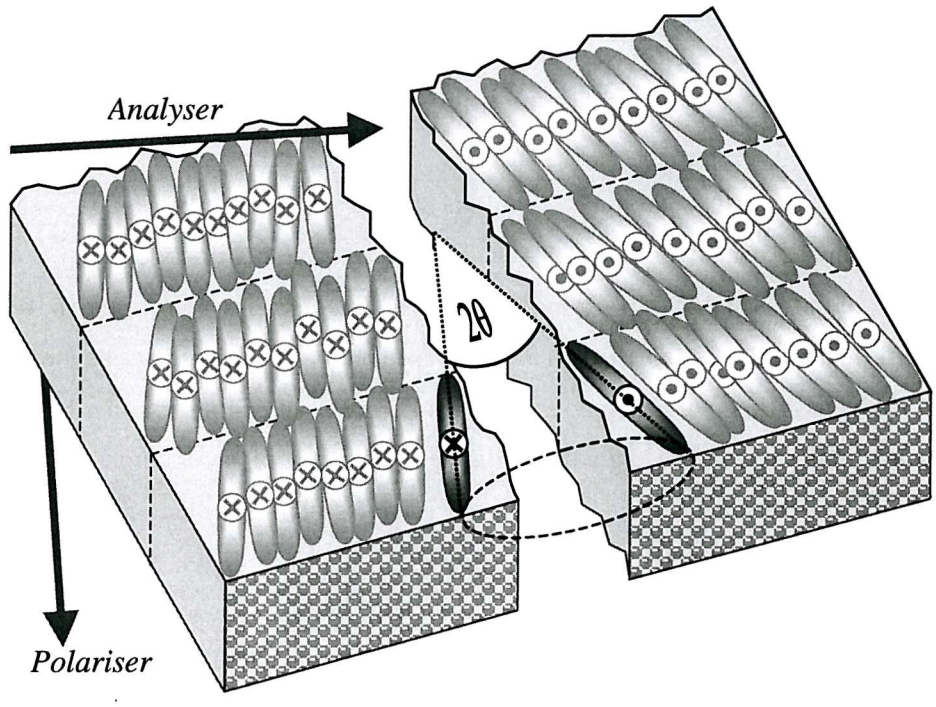

Figure 2.6 A schematic representation of the two bistable states of the surface stabilised ferroelectric liquid crystal cell geometry.

Once the helix is suppressed by surface forces, the device can exhibit true ferroelectric characteristics such as spontaneous polarisation, bistability, domains and hysteresis. The coupling of the applied field and molecular dipole allow fast switching times. These can be ~10μs for a good SSFLC device in comparison with ~10ms for some nematic devices. The SSFLC device would therefore seem to be ideal for use in display applications, however, some of the greatest problems hampering SSFLC device development are that of alignment and maintaining a uniform cell gap.

2.3.1 Molecular Geometry

As the SmC* phase is composed of chiral molecules, the two bistable positions in the SSFLC may have slightly different energies. Polar interactions at the liquid crystal/glass interface affect the direction of the molecular dipole. If equivalent states are to form at both surfaces, the molecules must rotate through the azimuthal angle of 180° and this causes a splay across part of the sample. This splay deformation has consequences for the switching dynamics of the mode and can result in states that do not show extinction and are highly coloured, particularly at low voltages. The elastic deformations allow light to leak through in the "off state" and this impairs the efficiency of the device as an optical switch. The phase geometry is further complicated by the competing forces that occur in layer formation.

2.3.1.1 Layer Formation

There are four basic models of the smectic layer arrangement within a typical SSFLC cell; these are the bookshelf, tilted layer, symmetric chevron and asymmetric chevron geometries. The bookshelf geometry, shown in Figure 2.7, is the classic alignment, and is so-called because the layer planes are flat and upright, stacking like books on a shelf. This simple model describes the layer structure in the smectic A phase.

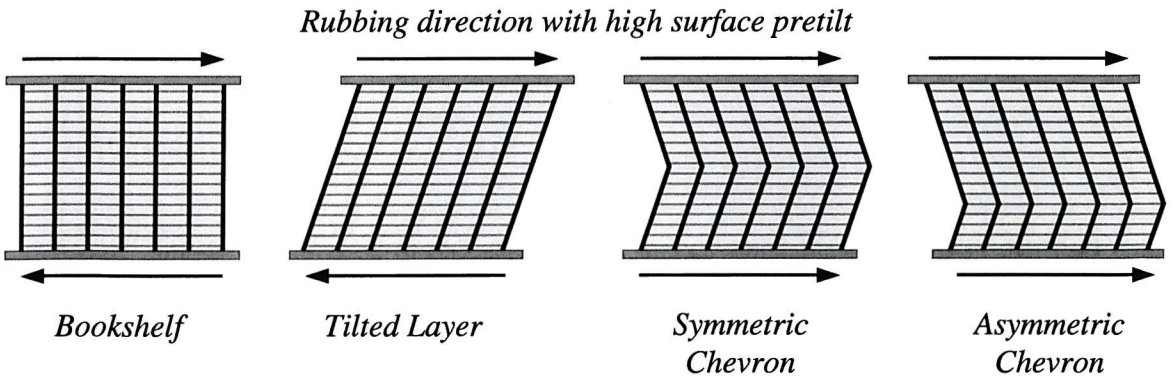

Figure 2.7 Different smectic layer geometries in a surface stabilised device.

If a SmC* phase forms from the SmA* phase, the layer planes are already present. The presence of a tilt angle at the transition causes the layer spacing to shrink and buckle. If the phase forms from an N* or isotropic, the layer planes are not already present, but if the tilt in the SmC* phase shows temperature dependence, cooling down from the transition can also cause a change in the layer planes. The surface molecules are pinned by alignment forces, so one solution that allows the layers to remain unbroken is for them to tilt over; this creates the parallel tilted structure illustrated in Figure 2.7. A simpler transition is for the layers to buckle. It can be shown that if the bend energy is minimised across the sandwich, the most energetically favourable solution results in a chevron structure[33]. The existence of a chevron structure has been corroborated by x-ray studies[34]. The formation of the chevron plane is not constrained to occur symmetrically; an asymmetric chevron geometry can form where the chevron plane formed by the meeting of the smectic layer planes is parallel to the substrate planes but does not lie in the centre of the cell gap.

The smectic layers can bend parallel or anti-parallel to the alignment rubbing direction, allowing two types of chevron to form. Domain wall defects occur where the two forms meet. These are represented symbolically as >>*<< where the chevrons point together and <<*>> where they point apart. When viewed between crossed polarisers this gives rise to broad disclinations at >>*<< running parallel to the smectic layers and narrow disclinations at <<*>> running approximately normal to the layers. These often form hairpin and lightning zigzag defects, seen as light leaks through the device[35]. An example in the ferroelectric mixture SCE13 [36] is shown in Figure 2.8. On the left, the thin and broad walls can be clearly seen, and on the right, the deterioration of the dark state due to light leakage is demonstrated.

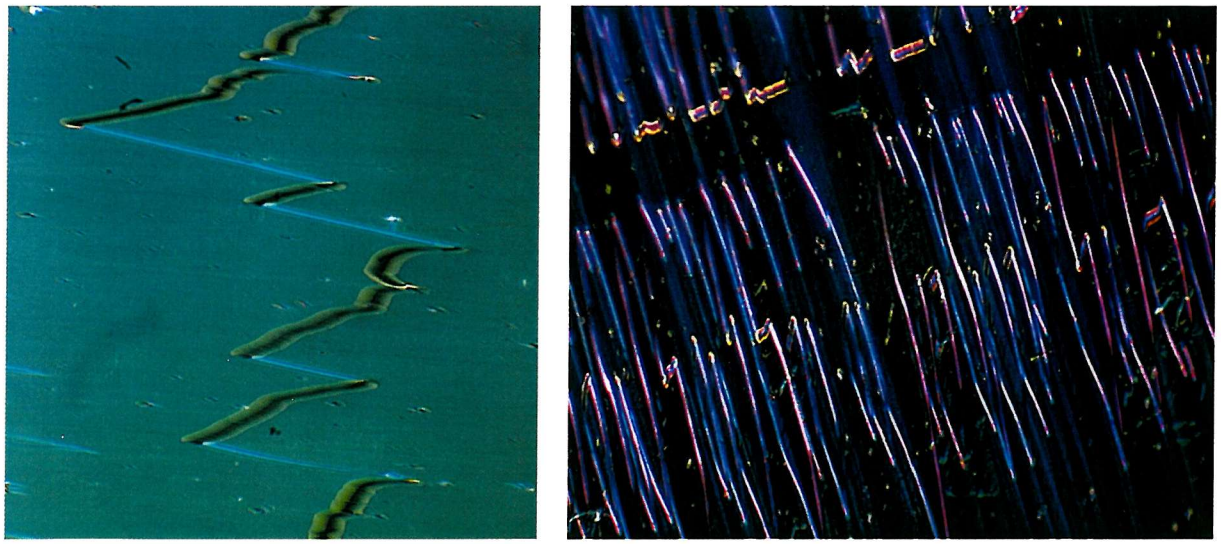

Figure 2.8 Photomicrographs at 50x magnification of SCE13 in the SmC phase showing lightning defects as a consequence of competing chevron geometries.*

2.3.1.2 Alignment Layer Effects

The bookshelf and chevron geometries are affected by the alignment layer. To induce a parallel alignment, the alignment layers are deposited or rubbed in one direction. The interaction of the smectic layers with the unidirectional alignment layer results in a small "pre-tilt" angle between the surface liquid crystal molecules and the substrate. The size of the angle depends on the particular liquid crystal and alignment characteristics, and can be used to control chevron formation. If the rubbing directions on the internal cell walls are parallel, with high pretilt, one chevron will require slightly less energy to form and will dominate, reducing the number of disclination defects, (see Figure 2.7). Anti-parallel rubbing directions favour the bookshelf geometry and are used in all the experiments in this thesis, unless specified otherwise.

The alignment pretilt affects the switching cone of the surface molecules. If no pretilt exists, the alignment layer will bisect the switching cone, giving two bistable states with a full switch of 2θ. The presence of pretilt reduces the intersection of the alignment plane and smectic cone, and this reduces the angle between the two bistable states[37].

2.3.2 Cell Operation

Internal electrodes are needed to apply electric fields across the SSFLC cells. A thin, transparent layer of indium tin oxide is patterned on to the glass substrates before the alignment layer is deposited. A sufficiently large electric field will cause the LC molecules to align their transverse dipoles in the direction of the field. In an SSFLC cell, the field direction is parallel to the layer planes. If the polarity of the field is reversed, the molecules will want to reorient. The threshold field required to overcome the elastic forces and reorient the molecules is small, typically less than 1 V/μm, however, the field required to reorient well anchored surface molecules can be significantly greater. The effect of surface anchoring results in three field regimes. Very low fields can cause some switching throughout the sample except at the boundaries, which may reorient slowly via surface defects. Higher fields are sufficient to drive the entire sample. Very high fields can produce soliton motion through the sample. Ions can be pulled from the substrates and dielectric breakdown can occur usually resulting in a dramatic short. The work in this thesis is carried out with the appropriate medium strength fields for the particular sample.

In highly chiral compounds or when using large cell gaps, the alignment forces can be insufficient to propagate the layer structure across the cell. A partial helix may remain in the bulk of the sample. Although surface pinning can complicate the process[38], increasing the applied field should continuously increase the helical pitch until a sufficient field will totally unwind the helix to give a saturated state. Once more it is essential that alignment forces or field strengths are sufficient to ensure a fully unwound helix for efficient cell operation and comparative studies.

2.3.2.1 Birefringence

Typically, the cell is operated in the birefringent mode where it is placed between crossed polarisers. In this configuration, the cell can be considered to act like a slab of uniaxial crystalline material with an optic axis along the director. The optical transmission of such a cell in its switched states is given by

$$I = I_0 \sin^2(2\alpha)\sin^2\left(\frac{\Delta n d\pi}{\lambda}\right), \qquad 2.15$$

where I_0 is the light intensity passed by the first polariser, α is the angle between the optic axis and one of the polarisation axes, Δn is the birefringence, d the cell thickness and λ the wavelength of the incident light. This assumes that the glass substrates, ITO electrodes, alignment layers and polarisers are all perfect. Clearly, the transmitted intensity will be at a maximum when both sine-squared terms equal one, and at a minimum when either sine-squared term equals zero. For the first term this means that for zero transmission, α must equal 0, $\frac{\pi}{2}$, π ... Thus if the cell is oriented so that the molecules lie on one of the polarisation planes, the transmitted intensity will be zero. Maximum transmission will occur when $\alpha = \frac{\pi}{4}$; this can be achieved by rotating the cell or, more usefully, by rotating the LC molecules. Since the molecules switch through twice the tilt angle, α=20, the ideal tilt angle for a device in this mode is θ=22.5°. The second term in Equation 2.15 corresponds to the phase delay produced between the extraordinary and ordinary rays, and this is maximised by matching the values of Δn and d at appropriate visible wavelengths. With typical values of Δn around 0.15, and visible light, the value of d, the cell thickness, is in the range 1.5-2 μm. These conditions allow a properly oriented cell in ideal conditions to act as a ½ wave plate and be switched from zero to maximum transmission. In reality the birefringent mode is not truly bistable; a significant reduction in transmission can occur upon field removal due to surface pre-tilt conditions and chevron formation[39].

At a particular wavelength, a contrast ratio (CR) can be defined utilising the maximum and minimum intensities, I_{light} and I_{dark} respectively, as shown:

$$CR = \frac{I_{light}}{I_{dark}}. \qquad 2.16$$

This ratio is a very useful measure of optical performance for a commercial application as it gives an idea of how well neighbouring pixels in a display can be differentiated. An ideal display will have an I_{dark} of zero and thus an infinite contrast ratio. In practice, the many defects in the cell, the thermal fluctuation of the molecules and director, and the non-ideal polarisers give a finite dark intensity.

2.4 DYNAMICS OF DIRECTOR MOTION

So far only the approximate nature of the switching in a SmC* phase has been considered. It is highly desirable to have an idea of the viscous forces acting in the switching mechanism. An elastic continuum theory by Leslie et al.[40] sets out the framework for a thorough study of the phase rheology; this involves in excess of 20 elastic constants and is too complex for use in this work. Instead, the problem is approached by using a model proposed by Escher et al.[41]. This model is based on the dynamics of polarisation reversal and lends itself well to the experimental technique used in this thesis. It also allows a study of some of the viscous forces acting in the switching process. In order to understand the equations utilised in both methods, the dynamics of director motion must be studied. The actual experimental method measures the charge produced when the molecular dipoles reorient under an applied field. Known as the current pulse technique, this is explained fully in the following experimental chapter.

The geometry of director motion is shown in Figure 2.9. The z-axis is orthogonal to the layer planes and the principal axis of the molecule lies along the director, **n**. The vector **c** represents the projection of the director onto the smectic plane. The assumptions are made that the smectic layers and tilt angle do not vary significantly with the application of an electric field, and that the molecules exhibit negligible biaxiality.

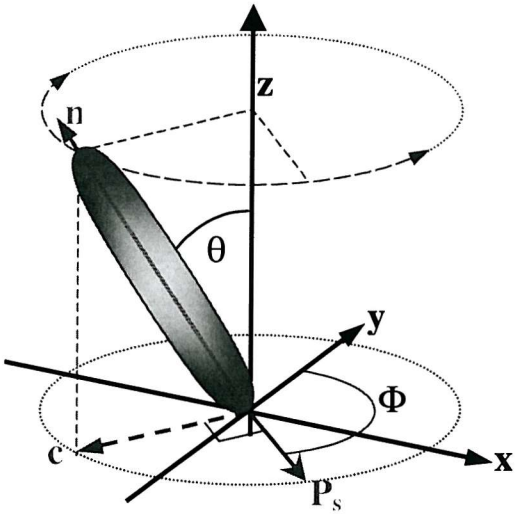

Figure 2.9 The co-ordinates for the dynamics of director motion.

The applied electric field acting along the y-axis will exert a torque on the liquid crystal molecule. In this snapshot view, the molecules will be planar aligned such that the **c** director will lie on the x-axis in either of its two switched states. Here, Φ will equal 0 or π and the electric field torque is zero. In order for the torque to have an effect, the molecule must be perturbed from the y-axis. In reality this occurs as a consequence of thermal fluctuations or the chiral tendency to form a twisted state, and so is not a problem[42]. This gives an equation of rotational motion:

$$\dot{\mathbf{L}} + \gamma_\varphi \dot{\Phi} + \mathbf{P}_{Tot} \wedge \mathbf{E} = 0, \qquad 2.17$$

where **L** is the molecular moment of inertia and γ_φ is the azimuthal rotational viscosity of the **c** director. The parameter γ_φ is related to the rotational viscosity, γ, of the director, **n**, by $\gamma_\varphi = \gamma \sin^2 \theta$. Φ is the azimuthal angle of the spontaneous polarisation with the y-axis and **E** is the applied field. The total polarisation, $\mathbf{P}_{Tot}$, takes account of the inherent ferroelectric polarisation, $\mathbf{P}_s$, plus a field-induced component, $\mathbf{P}_{ind}$;

$$\mathbf{P}_{ind} = \varepsilon_0 \Delta\varepsilon(\mathbf{n} \bullet \mathbf{E})\mathbf{n} + (\varepsilon_\perp - 1)\varepsilon_0 \mathbf{E}, \qquad 2.18$$

which is expressed in terms of the dielectric anisotropy $\Delta\varepsilon = \varepsilon_\parallel - \varepsilon_\perp$. Since the second term in Equation 2.18 is in the direction of the applied field, it will not contribute to the torque and can be neglected. In real applications, the contribution of the moment of inertia is so small it can also be ignored. The dynamical Equation 2.17 becomes

$$\gamma_\varphi \dot{\Phi} = -\mathbf{P}_s \wedge \mathbf{E} - \varepsilon_0 \Delta\varepsilon(\mathbf{n} \bullet \mathbf{E})\mathbf{n} \wedge \mathbf{E}. \qquad 2.19$$

In liquid crystal applications, the contribution of the dielectric term is sufficiently small in comparison to the P_s term to be neglected. The equation of motion of the dipole is therefore reduced to

$$\dot{\Phi} = -\frac{P_s E}{\gamma \sin^2 \theta} \sin \Phi. \qquad 2.20$$

2.4.1 Resistance and Capacitance

A liquid crystal cell can be thought of as a resistor and capacitor connected in parallel. When a varying voltage, V, is applied, the total current induced has three main components: these are contributions from ion flow, charge accumulation in the cell, and polarisation realignment. These parameters are combined respectively to give

$$I = \frac{V}{R} + C\dot{V} + \int j dA, \qquad 2.21$$

where C is the capacitance of the liquid crystal layer, R is its resistance and j is the effective current density, due to the reorientation of the spontaneous polarisation, integrated over the electrode area, A. If a triangular waveform is used, the resistive current is linear in the applied field. The capacitance contribution is seen as a small jump in the measured current when the field reverses. The final term, the polarisation realignment peak is therefore easily subtracted. The polarisation current density is

$$j_p = -P_s \dot{\Phi} \sin \Phi. \qquad 2.22$$

2.4.2 Spontaneous Polarisation

The size of the spontaneous polarisation is predicted by integrating the polarisation current density, j_p, over a full reorientation of the cell under the applied field. This results in a total charge, Q, such that

$$Q = \int\left(\int j_p dt\right)dA = -AP_s\int\dot{\Phi}\sin\Phi\,dt = -AP_s\int_0^{\Phi=\pi}\sin\Phi\,d\Phi = -2AP_s. \qquad 2.23$$

Neglecting the sign convention, Equation 2.23 yields

$$P_s = \frac{Q}{2A}. \qquad 2.24$$

The cell area, A, is known and the size of the charge, Q, can be measured, as will be described in the following chapter.

2.4.3 Rotational Viscosity

The value of the rotational viscosity, γ, can be derived from the same data used to calculate the spontaneous polarisation. Substituting the equation of motion of the dipole (Equation 2.20) into the current density formula (Equation 2.22) yields

$$j_p = \frac{P_s^2 E\sin^2\Phi}{\gamma\sin^2\theta}. \qquad 2.25$$

The most easily measured variable is the maximum current; therefore, j_p is differentiated with respect to time and set to zero:

$$j_p(\max) = \frac{dj_p}{dt} = \frac{P_s^2}{\gamma\sin^2\theta}\left(\dot{E}\sin^2\Phi + 2E\dot{\Phi}\sin\Phi\cos\Phi\right) = 0. \qquad 2.26$$

Substituting once more for $\dot{\Phi}$ from Equation 2.20 and attaching m to signify the use of maximum values gives

$$j_p^m = \frac{P_s^2 E_m}{\gamma\sin^2\theta}\left(1 - \left(\frac{\gamma\sin^2\theta\dot{E}_m}{2P_sE_m^2}\right)^2\right). \qquad 2.27$$

In a typical cell used in this work, the second term in parenthesis is $\approx 10^{-16}$ and can be ignored. The maximum polarisation current through the sample, I_p^m, can be directly determined experimentally and if this value is substituted for $j_p^m A$, the rotational viscosity of the phase is obtained:

$$\gamma = \frac{AP_s^2 E_m}{I_p^m\sin^2\theta}. \qquad 2.28$$

2.5 TEMPERATURE DEPENDENCIES

The physical parameter arguments thus far have all assumed constant temperature. Although some approximations are made, these parameters often demonstrate simple temperature dependencies.

2.5.1 Viscosity

Viscosity can also be described by the Eyring theory, which is concerned with the molecular nature of a liquid, and takes into account that for a liquid to flow, molecules must alter their position. The positional change involves a potential energy barrier due to intermolecular forces. This theory yields a velocity equation:

$$\eta = \frac{h}{v_m}\exp\left(\frac{\varepsilon_A}{k_B T}\right), \qquad 2.29$$

where h is Planck's constant, k_B is Boltzmann's constant, ε_A is the rotational activation energy required for motion, T is the temperature in Kelvin and v_m is the effective molecular volume. Utilising Equation 2.28 to measure the viscosity from experimentally determined variables, Equation 2.29 can give an idea of the activation energy required for the switching mechanism. This is more simply approximated by the Arrhenius behaviour:

$$\gamma = \gamma_h \exp\left(-\frac{\varepsilon_A}{k_B T}\right), \qquad 2.30$$

where the factor γ_h represents a measure of the rotational hindrance with the units of viscosity.

2.5.2 Response Time

The viscosity arguments give a time constant, τ, for dipole reorientation:

$$\tau = \tau_0 \exp\left(\frac{\varepsilon_A}{k_B T}\right), \qquad 2.31$$

where τ_0 is a temperature independent constant. Due to the field dependence of the realignment torque it is also worth noting that

$$\tau_\varphi = \frac{\gamma_\varphi}{P_s E}. \qquad 2.32$$

2.5.3 Tilt Angle

The molecular tilt angle is considered to be the primary order parameter associated with the SmA*-SmC* transition. Recalling the Landau free energy expansion minimisation with respect to θ and P_s from the previous chapter, indicates the form of the temperature dependence of these parameters. If a material exhibits the second order transition SmC*-SmA* at a temperature T_c, the theoretical dependence of θ can be described as[43]

$$\theta = \theta_0 \left(\frac{T_c - T}{T_c} \right)^{\beta}, \qquad 2.33$$

where θ_0 is a constant with units of degrees and β is the critical exponent. The Landau minimisation arguments from chapter 1 give $\beta = 0.5$. Further work by de Gennes[44] utilising analogous arguments yield a lower value of $\beta \approx 0.35$. Accurate determination of the exponent in the SmC* phase requires extremely sensitive equipment. The accurate determination of β is further complicated by the reality that the SmC*-SmA* transition is not wholly second order. In fact, a mean field to tricritical crossover behaviour is displayed as the transition is approached[45]. Experimentally the value $\beta = 0.5$ compares well with the value determined theoretically. In practical applications the tilt is often strongly temperature dependent up to 10°C below the critical temperature of the phase transition. Thereafter the dependence becomes weaker as the temperature of the phase is decreased. For a first order transition, from the isotropic directly to a SmC* phase, the tilt is no longer a thermodynamic variable and can often be constant with temperature[46].

2.5.4 Spontaneous Polarisation in the SmC* Mesophase

Although the polarisation is the natural primary order parameter in solid ferroelectrics, it is important to emphasise that the spontaneous polarisation is not a primary order parameter of the SmC* phase, since it cannot completely describe the thermodynamic nature of the phase[47]. Spontaneous polarisation is termed a secondary order parameter because it is coupled to the tilt, the primary order parameter of the phase[48]. Field reversal in an SSFLC device causes fast switching between the two tilted states via rapid motion of the director around the switching cone. As might be expected, the size of the spontaneous polarisation is a critical factor determining the speed of the switch and thus an important fundamental measurement. A typical FLC can have P_s values of 1-100 nC cm^{-2}, several orders of magnitude lower than the values of 1-100 $\mu C\,cm^{-2}$ seen in a conventional ferroelectric crystal. The magnitude of the spontaneous polarisation depends on four main factors; the magnitude of the molecular dipole moment, rotational hindrance about the chiral centre, the influence of the core structure, and sample temperature; this is discussed further in §2.7.1.3.

As described earlier in §2.2.2, a consequence of the sign convention of P_s and tilt means that when the direction of the P_s vector is reversed, so is the tilt. To a first approximation P_s must be linear in θ. The temperature dependence of θ has already been discussed as a consequence of Landau theory (shown in Equation 2.33). This linear P_s-θ coupling means that the polarisation will also follow Curie type behaviour below a second order transition,

$$P_s = P_o\left(\frac{T_c - T}{T_c}\right)^{\beta}, \qquad 2.34$$

where T is the temperature, T_c is the transition temperature, P_0 is a constant with units $nCcm^{-2}$ and β is the critical exponent equal to ½ in mean field theory. This expression is a simplification since the assumption of linearity between P_s and θ is only an approximation. A more complex argument is possible, but because Equation 2.34 provides a good fit for much of the data, it is assumed to be accurate enough for the purposes of this explanation. For a first order transition from the isotropic to SmC* phase, the tilt is no longer a thermodynamic variable and can often be constant with temperature. Since the spontaneous polarisation is a secondary order parameter, it must follow the tilt or some other primary parameter.

2.6 ANTIFERROELECTRICITY

Antiferroelectricity is the most recent of the discoveries covered in this chapter and was first seen in 1987. Publications by Chandani et al[49] and Furukawa[50] outlined observations of tristable switching and other anomalous results in apparent ferroelectric switching of a SmC* phase. Work by Chandani et al[51] in 1989 attributed these effects to a new phenomenon of antiferroelectricity and denoted it SmC^*_A. The unwound herringbone structure proposed for the phase is shown schematically in Figure 2.10.

Figure 2.10 Schematic of the antiferroelectric SmC^*_A phase.

The structure was confirmed with x-ray work by Galerne and Liebert[52] and reflectance studies by Takanishi et al.[53] In comparison to the SmC* phase the molecules have the same average tilt from the layer normal, but the interaction between molecules in adjacent layers favours an anticlinic

arrangement. Thus each layer is rotated 180° with respect to the next; therefore, the tilt direction and molecular dipole alternate between layers. This results in the structure possessing no net polarisation regardless of whether or not the structure is helicoidal. The presence of chirality causes the tilt direction to precess as in a SmC* phase with similar pitch lengths but opposite handedness. As with the SmC*, the pitch length, P, is far longer than d, the interlayer spacing, typically $P/d \approx 1000$, thus on a local level the herringbone structure is a good approximation. Non-chiral forms have also been shown to exist[54] although this relies on unique molecular geometry instead of layer interactions. In the bulk the antiferroelectric system can be thought of as two intertwined helices 180° out of phase. One consequence of the structure is that the average optic axis will lie on the layer normal, unlike in a ferroelectric phase where it more closely follows the director at the tilt angle, θ. This in turn affects the birefringence, which is smaller than in a ferroelectric phase, decreasing further as the layer tilt increases.

2.6.1 Layer Structure

It is assumed that the molecular tilt in a SmC* phase is correlated over large distances, however, the antiferroelectric herringbone structure is incompatible with the typical SmC* layer density-wave model. It is not clear in the SmC^*_A phase which of the two possible directions the molecules will take in the minimum density regions. Consequently the SmC^*_A phase has a more defined layer structure and this is confirmed in the x-ray studies[55]. One consequence of this is increased ruggedness. Unlike a SmC* where deformations can permanently damage the layer structure, the SmC^*_A phase has been shown to recover well[56].

2.6.2 Switching and Hysteresis

If an antiferroelectric material is aligned in a surface stabilised geometry, the helix can be unwound as with a normal ferroelectric. The layers adopt the herringbone structure shown in Figure 2.10. The application of a transverse field will cause dipole alignment. This results in a rotation of half of the layers to adopt a ferroelectric alignment. If a negative field is applied, the opposite rotation will occur giving three distinct states; a relaxed antiferroelectric state and two driven ferroelectric states. This behaviour gives rise to tristable switching, as shown in Figure 2.11.

It is the application of a triangle or sine wave that highlights the true nature of the antiferroelectric phase. When examining the intensity of light transmitted by a switching sample between crossed polarisers a characteristic double hysteresis loop is seen, shown in Figure 2.12a. The shape is frequency dependent and the loop is symmetric, indicating that the two switched states are identical. With small fields well below the switching threshold there is a non-hysteric electroclinic-like response, where the transmitted intensity follows the field. Large fields above the switching threshold

result in a fully switched state that is unchanged with further increases. Between these two regions, hysteresis occurs because the field does work on re-aligning the dipoles. If the frequency of the applied field is increased sufficiently, the antiferroelectric phase has no time to form, and as with a square wave, the sample is driven between its two ferro states. The hysteresis changes to look more like the single loop characteristic of ferroelectrics[57], shown in Figure 2.12b.

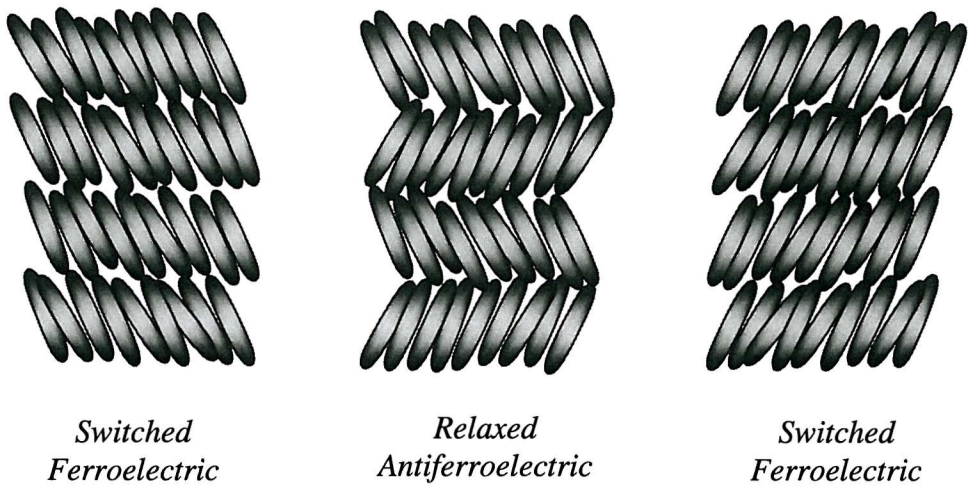

Figure 2.11 The relaxed antiferro and two switched ferro states of tristable switching.

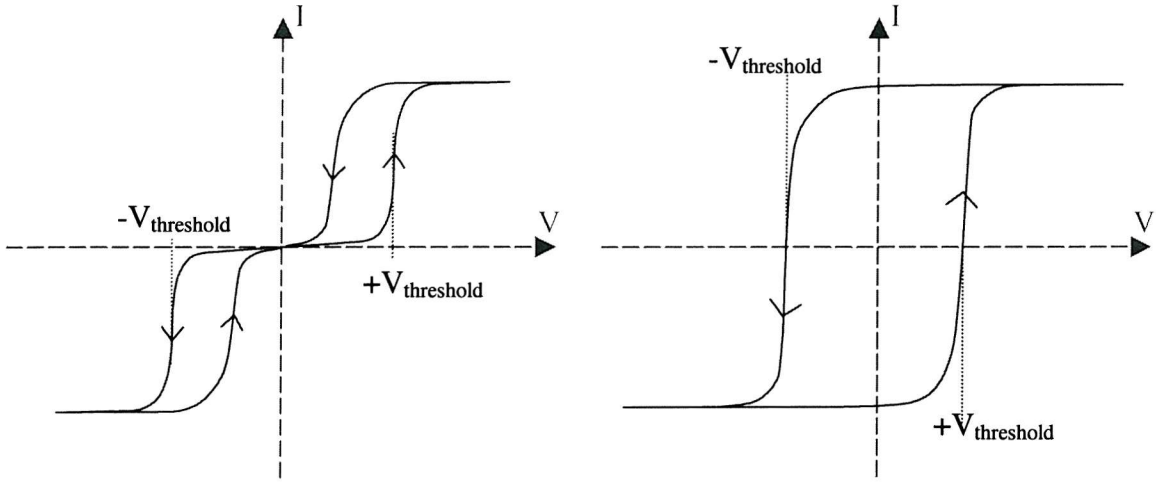

a) Antiferroelectric Hysteresis b) Ferroelectric Hysteresis

Figure 2.12 Hysteresis curves for antiferroelectric and ferroelectric switching.

Interestingly x-ray diffraction studies of antiferroelectric materials have shown that tristable switching can also be accompanied by a reversible switch from chevron to bookshelf geometries[58]. The antiferroelectric phase has great potential for use in electro-optic devices. Another of its switching features is the ability to provide grey scale[59], achieved by using pulse height modulation of the antiferroelectric – ferroelectric state.

2.6.3 Subphases and Ferrielectricity

For a complete picture, it is worth noting the discovery of two subphases that can be seen in some compounds of high optical purity exhibiting antiferroelectricity. These were first observed by Fukui in 1989 through careful calorimetry measurements[60]. The subphases occurred each side of the SmC* phase and were denoted SmC^*_α at higher temperatures and SmC^*_γ at lower temperatures. The enthalpies involved are very small, typically ~0.01 Jg^{-1}, making detection very difficult. The SmC^*_α is an unwound antiferroelectric phase and the SmC^*_γ is ferrielectric (explained below). The molecular interactions responsible for the stabilisation of the SmC* and SmC^*_A phases are complex and not understood in the same depth as the N, N* and SmA phases. The formation of subphases is the result of competition between the packing entropy of the SmC* phase and the pairing entropy of the transverse dipoles of the SmC^*_A phase [55].

2.6.3.1 Ferrielectricity

Ferrielectric phases can exist between the SmC* and SmC^*_A phase. They consist of a number of layers of antiferroelectric material separated by ferroelectric material[61], and are characterised by the ratio of these two configurations. The optic axis lies between the layer normal of antiferroelectrics and the optical tilt angle of ferroelectrics. One example, the SmC^*_γ phase, often has a P_s and tilt angle approximately equal to one third of the comparable ferroelectric state. This can be explained by a 2:1 layer orientation of ferroelectric to antiferroelectric material to give a triple layer structure[61]. Many other ferrielectric phases are seen with different layer ratios that can vary from fully ferroelectric to fully antiferroelectric. Transition temperatures can show considerable hysteresis and the complex multi-layer nature of the phase can allow multi-mode switching[62]. A field driven switch from a ferrielectric to a fully ferroelectric state occurs through many intermediate states. Variation of the applied field or the sample temperature changes the layer ratios, which can be described by a Devil's staircase[63].

2.7 STRUCTURE

This chapter is brought to a close with a consideration of some of the general shape and molecular requirements desirable to form the liquid crystalline phases discussed. Shape anisotropy is a crucial property of all thermotropic liquid crystals, as it ensures that above a critical density it is energetically favourable for the molecules to lie side by side rather than be randomly ordered. Aside from the oblate calamitic structure, other broad families of thermotropic liquid crystals exist. In the prolate discotic phases[64], as the name suggests, molecules are disc shaped and have one symmetry axis. Structurally, they fall into two broad categories: the discotic nematic phases and the columnar phases.

The discotic nematic phases, like the calamitic nematic phases, are the most fluid-like with only some orientational order. In the columnar phases the molecules pack into columns, described analogously as a stack of pennies. First seen by Chandrasekhar et al.[65] these columnar phases have two degrees of translational order. The individual discotic columnar phases are characterised by the type of 2D lattice formed by the column and their degree of molecular order or tilt.

Although less common, more exotic phases associated with unusual molecular structures exist. Some molecules have characteristics of both disc and calamitic molecules and are able to exhibit both types of phase; these are known as phasmidic due to their shape. A combination of disc and spherical molecular shape can yield bowlic or pyramidal phases[66], whose packing arrangements can be similar to those of discotics. A final shape is the Sanidic[67]; these are board-like molecules and again are a mixed type that is sterically biaxial. The phases formed by such molecules are not as widely documented, often because their very high viscosities make electro-optic modulation difficult.

2.7.1 Comments on Calamitic Phases

Classically, the calamitic liquid crystal is thought of as a rigid core with flexible alkyl chains connected to it. Typically the length to width ratio is in excess of 1.4:1, which gives the structure the necessary anisotropic shape, with higher ratios more likely to yield increased order parameters. The rigid core is essential in maintaining this anisotropy in order to favour intermolecular alignments. Variation of the length and composition of the terminal alkyl chains lead to many different effects. One example is the odd-even effect, where the physical parameters of the phase can zigzag up and down with varying terminal chain length. Liquid crystal phases can form in materials containing molecules with no tails or twin swallow bifurcated tails[54,68]. However, it is generally the case that long terminal chains are required to form the smectic phases.

2.7.1.1 Tilt Formation

In order to explain the formation of molecular tilt as a sample cools from the SmA phase to the SmC phase, two basic models exist: dipolar and steric. One example of a dipolar theory is McMillan's model[69]. The SmA phase is considered to be well ordered with only in-plane translation and rotation about the molecular long axis permitted. The rotation is considered to freeze on transition to the SmC phase, as it does so the influence of dipole forces align the molecules. The dipoles' alignment results in a torque that tilts the molecules in the direction of polarisation. Wulf's model[70] is an example of steric theory. The model does not consider the molecular dipolar properties and instead uses a zigzag packing configuration to explain the tilt. Studies have shown that neither model fully explains the formation of tilted phases and that both dipolar and steric forces have a part to play[71]. Thus the best explanation of molecular tilt is a combination of both models.

2.7.1.2 SmC Formation

The following conditions are not hard and fast rules, but give an idea of the molecular properties that are often associated with the formation of the SmC phase. Molecules that form the SmC phase usually possess flexible terminal alkyl chains connected to a rigid aromatic core. The rigid part is typically composed of aromatic cyclic structures. These rings are rigidly linked, typically by double or triply bonded moieties such as an ester (CO_2) or an azo (N≡N) group. The rigid core forms the molecular long axis and provides an easy route for charge transfer. Tilting is favoured by branching in the terminal chains[71], however branched alkyl chains at each end of the core can affect the thermal stability[72]. Work on esters by Coates has identified other general trends[72]:

- Lateral substitution in the aromatic core reduces the occurrence of higher order phases;
- A lateral group is most efficient for SmC production when pointing away from the aromatic core;
- Small lateral polar groups such as fluorine are sometimes better than hydrogen for SmC phase production.

2.7.1.3 SmC Formation*

For SmC* phases the previous generalisations can apply, but tilting can occur with shorter chain lengths because of the higher branching of many chiral systems. Vital for a SmC* system is the presence of a large, local, transverse polarisation; hence large transverse dipoles are incorporated into the molecular structure. It is worth noting, however, that the thermally driven oscillation of the molecules, and the flexibility and rotational freedom of the terminal chains, significantly reduces the dipole's effectiveness. The spontaneous polarisation measured in liquid crystals is typically 100-1000 times lower than in solid ferroelectrics due to these molecular rotations.

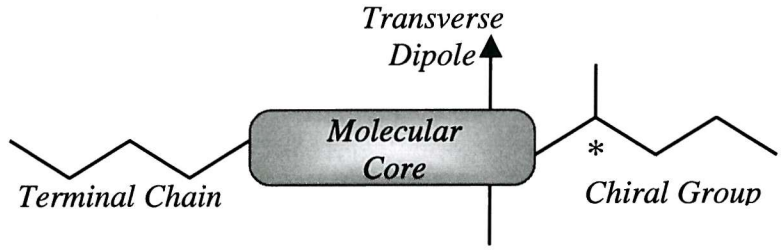

Figure 2.13. A schematic of a typical calamitic SmC structure.*

A typical calamitic SmC* molecule has a structure similar to that shown in Figure 2.13. Generally the effective dipole can be maximised by steric hindrance. Steric hindrance occurs by virtue of the chiral substituent's size or by placing the chiral centre close to the aromatic core. This proximity can

allow the motion of the functional group to couple to the motion of the core and can hinder the molecular rotation. This is essential in forming a macroscopic polarisation as discussed in §2.2.1. If the chiral centre also confers the lateral dipole, the greater the electronegativity of the substituent attached to the chiral carbon the better.

2.8 SUMMARY

This chapter has sought to introduce the main concepts and mathematical conclusions used throughout this work. In summary, it has been shown that:

- Any tilted phase can be ferroelectric;
- Switching occurs in the SmC* phase by two different methods, soft mode (in plane) and Goldstone mode (azimuthal);
- A helical phase can be unwound in a surface stabilised geometry;
- This yields a bistable optical switch with an ideal tilt angle of θ=22.5°;
- As a consequence of director dynamics, equations can be derived to allow the measurement of several physical parameters for the Goldstone mode with an idea of their temperature dependence;
- Tilt, $\theta = \theta_0\left(\frac{T_c - T}{T_c}\right)^{\beta}$;
- Spontaneous Polarisation, $P_s = \frac{Q}{2A}$, $P_s = P_0\left(\frac{T_c - T}{T_c}\right)^{\beta}$;
- Response time, $\tau_\varphi = \frac{\gamma_\varphi}{P_s E}$, $\tau = \tau_0 \exp\left(\frac{\varepsilon_A}{k_B T}\right)$;
- Viscosity, $\gamma = \frac{A P_s^{\,2} E_m}{I_p^m \sin^2\theta}$, $\gamma = \gamma_h \exp\left(-\frac{\varepsilon_A}{k_B T}\right)$.

The next chapter describes the experimental techniques used to measure these key parameters.

2.9 REFERENCES

[1] J.Valasek, *Phys. Rev.,* **17**(4), 475 (1921).
[2] R.B.Meyer, L.Liébert, L.Strzelecki, P.Keller. *J. Phys. Lett. (Paris),* **36**, L69 (1975).
[3] N.A.Clark, S.T.Lagerwall, *Appl. Phys. Lett.*, **36**(11), 899 (1980).
[4] J.F.Nye, *Physical Properties of Crystals,* Chpt.1-§5 (Oxford University Press, 1964).
[5] S.T.Lagerwall, I.Dahl, *Mol. Cryst. Liq. Cryst.*, **114**, 151 (1984).
[6] H.R.Brand, P.E.Cladis, *Mol. Cryst. Liq. Cryst.,* **114**, 207 (1984).
[7] I.Abdulhalim, G.Moddel, *Liq. Cryst.,* **9**(4), 493 (1991).
[8] A.Schönfeld, F.Kremer, R.Zentel, *Liq. Cryst.,* **13**(3), 403 (1993).
[9] S.Garoff, R.B.Meyer, *Phys. Rev. Lett.,* **38**(15), 848 (1977); *Phys. Rev. A,* **19**(1), 338 (1979).
[10] G.Andersson, I.Dahl, P.Keller, W.Kuczyński, S.T.Lagerwall, K.Sharp, B.Stebler, *Appl. Phys. Lett.,* **51**(9), 640 (1987).
[11] Sin-Doo Lee, J.S.Patel, *Appl. Phys. Lett.,* **54**(17), 1653 (1989).
[12] M.Redmond, H.J.Coles, E.Wischerhoff, R.Zentel, *Ferroelectrics,* **148**, 323 (1993).
[13] CH.Bahr, G.Heppke, *Liq. Cryst.,* **2**(6), 825 (1987).
[14] I.Abdulhalim, G.Moddel, K.M.Johnson, *Appl. Phys. Lett.,* **55**(16), 1603 (1989).
[15] G.Andersson, I.Dahl, W.Kuczyński, S.T.Lagerwall, K.Sharp, B.Stebler, *Ferroelectrics.,* **84**, 285 (1988).
[16] Z.Li, R.G.Petschek, C.Rosenblatt, *Phys. Rev. Lett.*, **62**(7), 796 (1989).
[17] I.Dierking, P.Rudquist, L.Komitov, S.T.Lagerwall, B.Stebler, *Mol. Cryst. Liq. Cryst.*, **304**, 389 (1997).
[18] Ph.Martinot-Lagarde, *Mol. Cryst. Liq. Cryst.,* **66**, 61 (1981).
[19] R.B.Meyer, *Mol. Cryst. Liq. Cryst.,* **40**, 33 (1977).
[20] J.Fünfschilling, M.Schadt, *J. Appl. Phys.* **66**(8), 3877 1989.
[21] T.E.Lockhart, D.W.Allender, E.Gelerinter, D.L.Johnson, *Phys. Rev. A,* **20**(4), 1655 (1979); T.E.Lockhart, E.Gelerinter, M.E.Neubert, *ibid.* **25**(), 2262 (1985).
[22] L.M.Blinov, V.G.Chigrinov, *Electrooptic Effects in Liquid Crystal Materials,* Chpt. 2, (Springer-Verlag, 1994).
[23] D.C.Ulrich, S.J.Elston, *Liq. Cryst.,* **18**(3), 511 (1995).
[24] C.Tani, *Appl. Phys. Lett.,* **19**(7), 241 (1971).
[25] J.Geurst, W.Goossens, *Phys. Lett.,* **41**(4), 369 (1972).
[26] W.Helfrich, *J. Chem. Phys.,* **51**(9), 4092 (1969);
[27] L.M.Blinov, V.G.Chigrinov, *Electrooptic Effects in Liquid Crystal Materials,* Chpt. 6, (Springer-Verlag, 1994).
[28] M.Hareng, S.LeBerre, J.J.Metzger, *Appl. Phys. Lett.,* **27**(11), 575 (1975).
[29] M.Hareng, S.LeBerre, L.Thirant, *Appl. Phys. Lett.,* **25**(12), 683 (1974).
[30] P.G.deGennes, J.Prost, *The Physics of Liquid Crystals,* (2nd Ed. Clarendon Press, 1995).
[31] W.Helfrich, *Appl. Phys. Lett.,* **17**(12), 531 (1970).; J.P.Hurault, *J. Chem. Phys.,* **59**(4), 2068 (1973).
[32] J.S.Patel, J.W.Goodby, *Opt. Eng.,* **26**(5), 373 (1987).
[33] T.P.Rieker, N.A.Clark, G.S.Smith, D.S.Parmar, E.B.Sirota, C.R.Safinya, *Phys. Rev. Lett.*, **59**(23), 2658 (1987).
[34] Y.Ouchi, J.Lee, H.Takezoe, A.Fukuda, K.Kondo, T.Kitamura, A.Mukoh, *Jpn. J. Appl. Phys.*, **27**(5), L725 (1988).
[35] Y.Ouchi, H.Takezoe, A.Fukuda, , *Jpn. J. Appl. Phys.*, **27**(1), 1 (1988).
[36] E.Merck KGaA, Frankfurter Str. 250, D-64271, Darmstadt, Germany. http://www.merck.de
[37] X.Jiu-Zhi, M.A.Handschy, N.A.Clark, *Liq. Cryst.,* **2**(5), 707 (1987).
[38] M.Glogarová, J.Fousek, L.Lejček, J.Pavel, *Ferroelectrics,* **58**, 161 (1984).
[39] W.J.A.M.Hartmann, G.Vertogen, C.J.Gerritsma, H.A.V.Sprang, A.G.H.Verhulst, *Europhys. Lett.,* **10**(7), 657 (1989).
[40] F.M.Leslie, I.W.Stewart, M.Nakagawa, *Mol. Cryst, Liq, Cryst.,* **198**, 443 (1991).
[41] C.Escher, T.Geelhaar, E.Böhm, *Liq. Cryst.,* **3**(4), 469 (1988).
[42] T.Tsuchiya, H.Takezoe, A.Fukuda,. *Jpn. J. Appl. Phys.,* **25**(1), L27 (1986).
[43] L.J.Martínez-Miranda, A.R.Kortan, R.J.Birgeneau, *Phys. Rev. A.,* **36**(5), 2372 (1987).
[44] P.G.deGennes, *C. R .Acad. Sci. B (Paris),* **274**, 758 (1972).

[45] R.Shashidhar, B.R.Ratna, G.G.Nair, S.Krishna.Prasad, *Phys. Rev. Lett.*, **61**(5), 547 (1988); T.Chan, C.H.Bahr, G.Heppke, C.W.Garland, *Liq. Cryst.*, **13**(5), 667 (1993).
[46] B.W.Van-der-Meer, G.Vertogen, *J. Phys. Colloq. (France)*, **40**(4), C3-222 (1979).
[47] C.C.Huang, S.Dumrongrattana, *Phys. Rev. A*, **34**(6), 5020 (1986).
[48] R.Blinc, *Phys. Status. Solidi b*, **70**, K29 (1975)
[49] A.D.L.Chandani, T.Hagiwara, Y.Suzuki, Y.Ouchi, H.Takezoe, A.Fukuda, *Jpn. J. Appl. Phys.*, **27**(5), L729 (1988).
[50] K.Furukawa, K.Terashima, M.Ichihashi, S.Saitoh, K.Miyazawa, T.Inukai. *Ferroelectrics*, **85**, 451 (1988).
[51] A.D.L.Chandani, E.Gorecka, Y.Ouchi, H.Takezoe, A.Fukuda, *Jpn. J. Appl. Phys.*, **28**(7), L1265 (1989); A.D.L.Chandani, Y.Ouchi, H.Takezoe, A.Fukuda, K.Terashima, K.Furukawa, A.Kishi, *ibid.*, **28**(7), L1261 (1989).
[52] Y.Galerne, L.Liebert, *Phys. Rev. Lett.*, **64**(8), 906 (1990); **66**(22), 2891 (1991).
[53] Y.Takanishi, H.Takezoe, A.Fukuda, H.Komura, J.Watanabe, *J. Mater. Chem.*, **2**(1), 71 (1992).
[54] I.Nishiyama, J.W.Goodby, *J. Mater. Chem.*, **2**(10), 1015 (1992).
[55] A.Ikeda, Y.Takanishi, H.Takezoe, A.Fukuda, *Jpn. J. Appl. Phys.*, **32**(2), L97 (1993).
[56] K.Itoh, M.Johno, Y.Takanishi, Y.Ouchi, H.Takezoe, A.Fukuda. *Jpn. J. Appl. Phys.*, **30**(4), 735 (1991).
[57] H.Orihara, T.Fujikawa, Y.Ishibashi, Y.Yamada, N.Yamamoto, K.Mori, K.Nakamura, Y.Suzuki, T.Hagiwara, I.Kawamura, *Jpn. J. Appl. Phys.*, **29**(2), L333 (1990).
[58] M.Johno, Y.Ouchi, H.Takezoe, A.Fukuda, K.Terashima, K.Furukawa, *Jpn. J. Appl. Phys.*, **29**(1), L111 (1990).
[59] H.Okada, M.Watanabe, H.Onnagawa, K.Miyashita, *Jpn. J. Appl. Phys.*, **34**, L375 (1995).
[60] M.Fukai, H.Orihara, Y.Yamada, N.Yamamoto, Y.Ishibashi, *Jpn. J. Appl. Phys.*, **28**(5), L849 (1989).
[61] H.Takezoe, J.Lee, Y.Ouchi, A.Fukuda, *Mol. Cryst. Liq. Cryst.*, **202**, 85 (1991).
[62] J.Lee, A.D.L.Chandani, K.Itoh, Y.Ouchi, H.Takezoe, A.Fukuda, *Jpn. J. Appl. Phys.*, **29**(6), 1122 (1990).
[63] P.Bak, *Phys. Today*, 38, (Dec. 1986).
[64] S.Chandrasekhar, G.S.Ranganath, *Rep. Prog. Phys.*, **53**, 57 (1990).
[65] S.Chandrasekhar, B.K.Sadashiva, K.A.Suresh, *Pramana (India)*, **9**(5), 471 (1977).
[66] Lin-Lei, *Mol. Cryst. Liq. Cryst.*, **146**, 41 (1987).
[67] M.Ebert, O.Herrmann-Schönherr, J.H.Wendorff, H.Ringsdorf, P.Tschirner., *Liq. Cryst.*, **7**(1), 63 (1990).
[68] W.Weissflog, A.Wiegeleben, S.Diele, D.Demus, *Cryst. Res. Tech.*, **19**(4), 583 (1984).
[69] W.L.McMillan, *Phys. Rev. A*, **8**(4), 1921 (1973).
[70] A.Wulf, *Phys. Rev. A*, **11**(1), 365 (1975).
[71] J.W.Goodby, G.W.Gray, D.G.McDonnell, *Mol. Cryst. Liq. Cryst. Lett.*, **34**, 183 (1976).
[72] D.Coates, *Liq. Cryst.*, **2**(4), 63 (1987); **2**(4), 423 (1987).

Chapter Three

Experimental Setup, Analysis and Characterisation

An experiment is a question which science poses to Nature, and a measurement is the recording of Nature's answer.

Max Planck 1858-1947

3.1 INTRODUCTION

The fundamental properties of the liquid crystals investigated in this thesis have already been introduced. This chapter discusses the techniques and apparatus used to assess the suitability of a liquid crystal for device applications, in particular it focuses on the measurement of the important parameters which are required for assessing device performance. For example, the optical tilt angle, θ, which is important because it governs the achievable contrast. The rotational viscosity, γ, gives a measure of the ease with which switching occurs, which in combination with the spontaneous polarisation, P_s, governs the speed of ferroelectric switching, leading to an understanding of the response times, τ.

The setup and calibration of the wide range of apparatus used in this work are described along with the manufacture and measurement of cells for device analysis. The analytical methods used to measure the key liquid crystal parameters are described in detail. These methods are verified with the results of measurements of industry standard samples. In the final part of the chapter, the diverse range of methods used to characterise the various liquid crystal phases is discussed.

3.2 BASIC EXPERIMENTAL APPARATUS

The components described in this chapter allow the study of the optical and electrical properties of the materials. The setup of the basic apparatus is shown in Figure 3.1. The samples are contained in specially fabricated glass cells with electrodes affixed so that a voltage can be applied across the liquid crystal. The sample's are placed in a temperature controlled Linkam heating-stage which is mounted on a microscope bed. Simple optical and electro-optical measurements are made with an Olympus Polarising Microscope. A function generator produces A.C. fields with variable waveforms, which are amplified before being applied across the cell.

A photodiode and amplifier measure the optical response which is monitored using a digitising oscilloscope. The oscilloscope allows optical tilt angle and response time measurements to be made, along with other measurements of the cell's electrical response. Small electric currents flowing across the cell are magnified for observation with a variable gain amplifier. A computer interfaced with the heating-stage and oscilloscope allow both software control of the experiment and data collection. The individual components of the analysis rig are described in detail in the following sections.

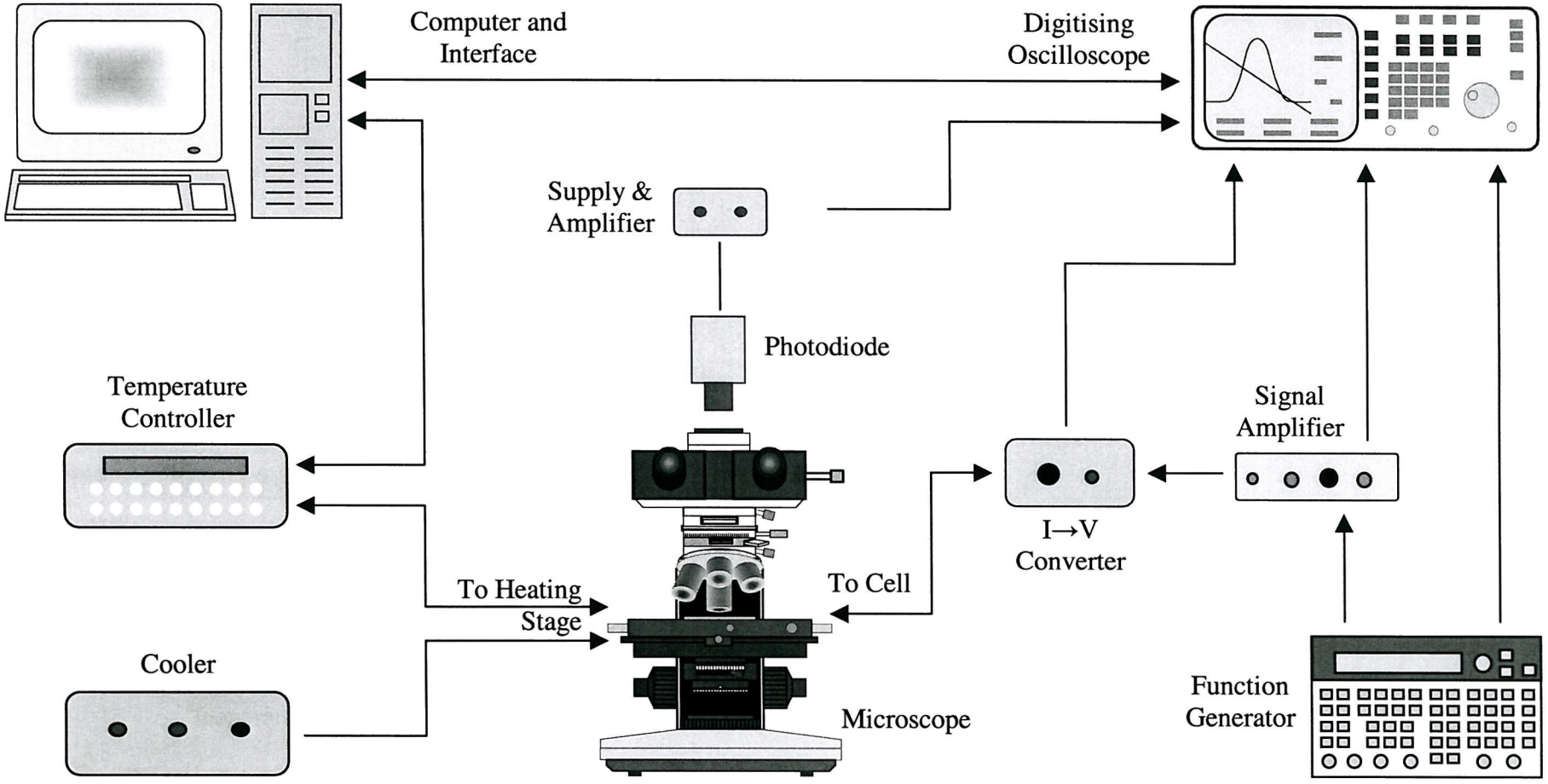

Figure 3.1 A diagram of the basic experimental setup.

3.2.1 Crossed Polariser Microscopy

One of the most useful optical analysis techniques in materials science is polarising microscopy. This technique allows the characterisation of materials, since variations in birefringence, absorption, refraction indices, thickness and orientation across a sample determine its characteristic appearance. This section will describe the workings of the Olympus Polarising Microscope[1] and its setup.

3.2.1.1 Olympus BH2 Microscope

The microscope's light source is a tungsten filament lamp, powered by either the internal A.C. or an external D.C. supply. The internal supply is regulated by a light level meter and is the most convenient to use. The A.C. driving can lead to a mains supply frequency fluctuation in the bulb's emitted intensity, and for sensitive measurements with a time period less than 10 ms this can become a problem. The microscope was therefore modified by the addition of external couplings to the bulb housing, allowing the supply to be switched to an external Thurlby Thandar[2] TS1410 12V D.C. supply. The external supply is stable to within 0.01% at 12V, providing a steady bulb emission intensity.

The light from the bulb is collimated and passes initially through a diffuser to smooth the image of the filament, then a field iris diaphragm, which allows the width of the light beam to be varied, before passing on to the condenser. At this point, the light is polarised using a Polaroid sheet with a high polarising efficiency, around 1000:1, then focussed at the appropriate place on or in the sample. The sample is placed on a heating stage fixed to the microscope bed. To allow angle calculations, the sample bed can rotate through 360° and is graduated in 0.5° increments, which represents the limit of accurate angle determination. The bed must be accurately centred on the beam path to keep the image in view during rotation. Optical resolution is improved by matching the aperture iris within the condenser to the numerical aperture of the objective mounted on the nosepiece. The objectives are MS Plan long working distance and infinity corrected with magnifying powers of 5x, 10x, 20x and 50x. The long working distance is necessary because of the extra height imposed by the heating stage. MS Plan lenses correct the curvature of the field and ensure the image is focussed on to a flat plane, which is essential for the use of cameras and instruments in the top tube.

Once collected by the objective, the light passes through a second Polaroid sheet, often called the analyser. The analyser is removable and can be rotated through 360° (to an accuracy of ±0.1°) by a vernier scale. Finally, the light is divided between the binocular eyepieces and the phototube. The division is carried out by a three-position selector toggle with partially reflective mirrors, allowing one of the following: all the light to go to the eyepieces; 25% to the eyepieces and 75% up the phototube; or all the light up the phototube. The sample stage is then brought into focus with the

coarse and fine focus knobs. The eyepieces provide a final magnification of 10x, giving a total magnification range of 50x to 500x. At a typical magnification of 100x, the field of view is 2mm in diameter. Various arms can be inserted before or after the analyser, allowing UV illumination or an optical fibre spectrometer to be fitted. The phototube permits film cameras, digital cameras, and photodiodes to be mounted on top of the assembly.

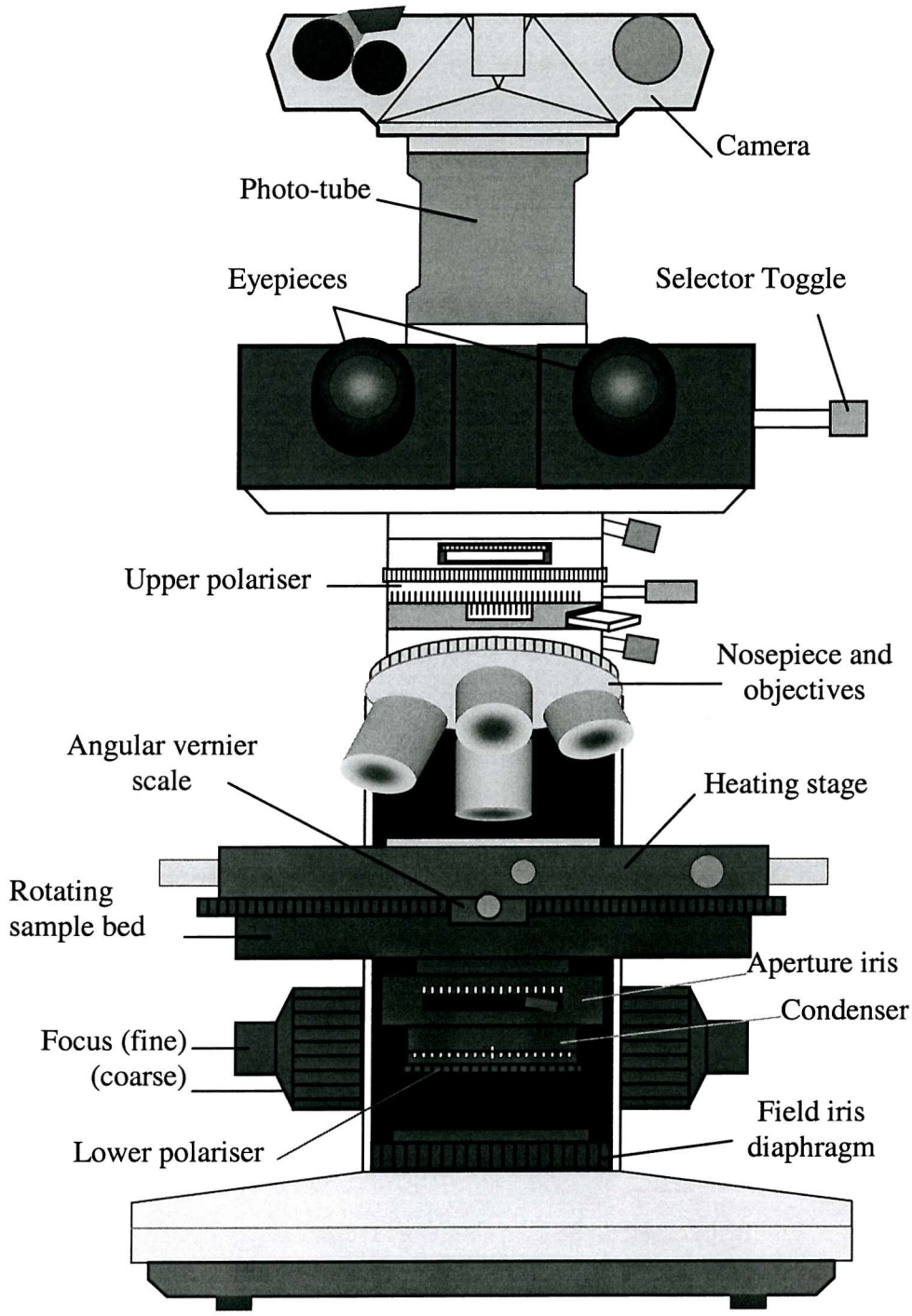

Figure 3.2 A diagram of the Olympus BH-2 Microscope.

3.2.2 Heating-stage

In order to control the temperature of the sample, a Linkam[3] (HFS91) heating-stage is fixed to the centred sample bed and the condenser is refocused at the new sample depth. The stage consists of a silver block with a built-in heating resistor, and a central mica or quartz window of 2mm diameter, corresponding to the 100x microscope setting. The block is suspended over the sample bed by two cooling tubes. Liquid nitrogen can be sucked through the sample block for cooling below room temperature. The stage is digitally controlled by a Linkam TMS91, allowing the sample to be heated at any rate from 0.1 to 50°Cmin^{-1} up to around 300°C. Above room temperature, the stage can be cooled at 0.1 to ~2°Cmin^{-1}. Faster cooling rates and temperatures to -196°C are achieved using the Linkam CS196 liquid nitrogen cooler. Once a sample cell is fixed to the silver block, a double glazed top window is screwed down. Fully enclosing the sample provides thermal insulation, reduces the condensation of water vapour when cooling, and allows the sample to be held to within ~ 0.1°C. The heating-stage was calibrated for absolute temperature using the clearing points of several organic compounds, giving results to within ±0.4°C in the temperature range –50°C to 180°C. In practice, the random error of an observed transition is determined by the intrinsic variation of repeated measurements.

Although the stage and the controller are calibrated, some temperature drift can occur, and the use of different heating methods and equipment can lead to significant differences between measurements of temperature, T, on separate apparatus. In order to allow cross comparison, a system of shifted temperature, T_S, is often used. This method uses a sharp and reproducible transition, such as I-SmC*, to remove the effect of experimental variation;

$$T_S = T_{I \rightarrow C^*} - T. \qquad 3.1$$

3.2.3 The Phototube

3.2.3.1 Photomicrography

In order to take photographs, an intermediate NFK photo-lens is placed in the phototube and a camera is secured to the top of the microscope. Depending on the choice of the photolens, the magnification is increased by a factor of between 2.5 and 7. The selector toggle is fully extended so that all of the light passes up the microscope. The focus is checked and the illumination level is set to the photo-region in the mid-point of the illumination intensity. An Olympus OM2n camera is used with Kodak film. The exposure time is selected using the camera's internal light meter, and a remote trigger and motor winder are used to obtain steadier and more reproducible conditions.

3.2.3.2 Photodiode

Light intensity measurements are made using a photodiode fixed on the phototube in place of the camera. This setup consists of a photodiode chip mounted with a dedicated intermediate photolens. The detector is a fast response, medium area, silicon photodiode, manufactured by IPL[4] and supplied by Radio Spares. It has an active area of 41.3 mm^2, a peak spectral response at 800 nm and a typical response time of 25 ns. The mount and power supply with amplifier were built in-house specifically for fast response use with ferroelectrics[5]. The complete detector package has a response time less than 4 μs. The linearity of the photodiode and amplifier system is checked using Malus's law[6],

$$I(\theta) = I_0 \cos^2 \theta, \qquad 3.2$$

where I_0 is the maximum irradiance and θ is the angle between the polarisers. Beginning with the two polarisers at 90° the analyser is rotated and the corresponding intensity noted. Figure 3.3 shows the response of the photodiode and clearly demonstrates its nearly linear nature. The small y-axis offset is due to a small bias in the amplified photodiode signal and to a small amount of light passed by the crossed polarisers.

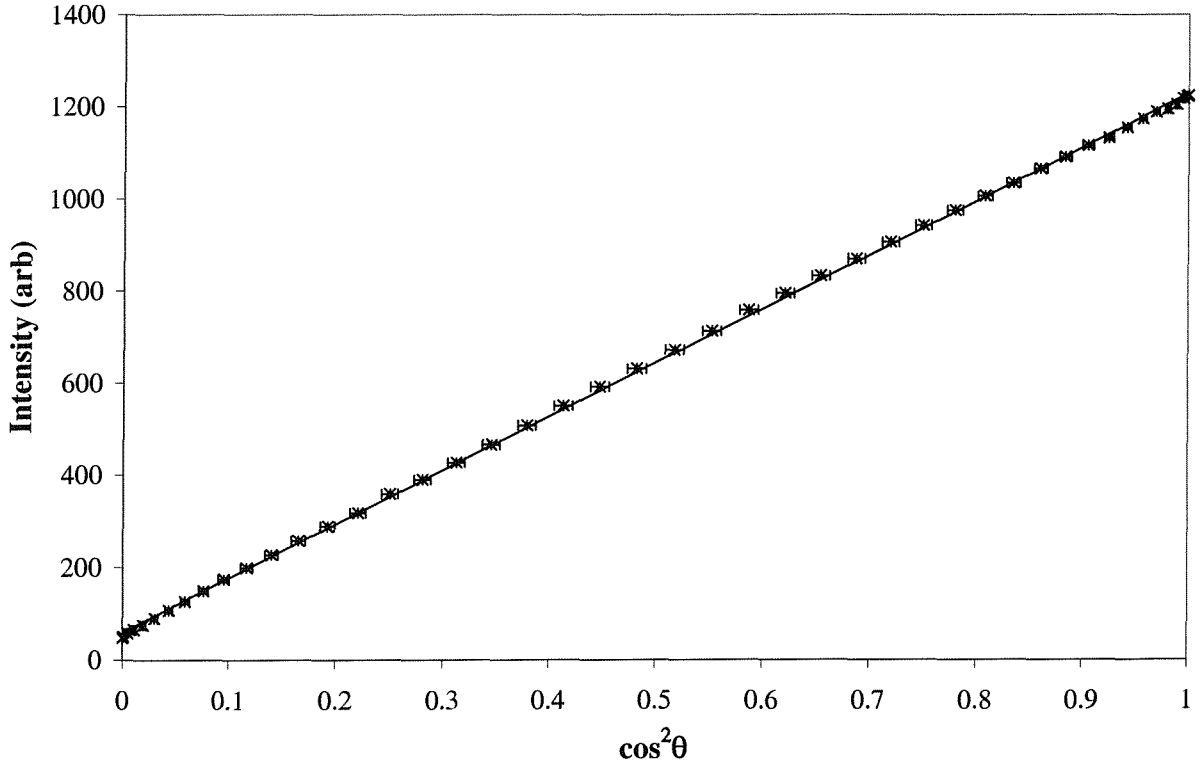

Figure 3.3 A plot of intensity against cos^2 polariser angle to demonstrate the linear response of the photodiode and amplifier.

3.2.4 Driving Methods

Liquid crystal samples are held in transparent electro-optic cells (described in §3.3). The cells are connected to a Thurlby Thandar[2] TG1304 programmable function generator, capable of providing square, triangle and sinusoidal waves at frequencies of 10 mHz – 13 MHz. This is achieved with a stabilisation of 0.01% at voltages of 1 mV to 10 V. The signals are all bipolar, although this can be altered with a DC offset. More specialised signals can be programmed into a Wavetek[7] model 75 arbitrary waveform generator. When larger driving voltages are required, the function generator signal is passed through a high voltage, wide band amplifier, EW1134B. The amplifier is custom-made[5] to provide voltages ±200 V even at high frequencies. At maximum voltage and frequency, a square wave can be seen to deteriorate and slew with a rise time of approximately 7 μs, but frequencies in the MHz range are rarely used in this work

3.2.5 Digital Oscilloscope

The driving voltages and responses from equipment are analysed with a Hewlett Packard[8] 54501a 100 MHz four-channel digitising oscilloscope. This oscilloscope is capable of a very stable display at low frequencies. Essential features include a display average up to 2048 traces and automated rise, fall and pulse width measurements. The oscilloscope's facility to plot two input signals on an x-y scale is essential for observation of hysteresis loops in ferroelectric switching. It is worth noting that in comparison to an analogue oscilloscope, the digitised nature of the signal can limit its resolution, although this is rarely seen in this work. The oscilloscope can be connected to a Hewlett Packard HP2225 Thinkjet printer for hard copies or interfaced with a desktop PC.

3.2.6 Computer Data Collection

Some of the processes involved in data collection lend themselves well to automation. In order to facilitate this, a computer workstation is fitted with an IEEE interface card[9], allowing a two-way interface with the oscilloscope. Simple programs written in Borland TurboPASCAL[10] allow the oscilloscope to be controlled and the signal levels read back to the computer. The heating-stage can also be controlled (via an RS232 interface) allowing the computer to set the heating/cooling rates and hold at any given temperature.

3.3 Electro-optic Cells

In order to facilitate measurement and identification of the liquid crystal physical parameters, the samples are examined in glass cells. This section describes the two types of cells used in the present

work. The most commonly used type is industrially prefabricated; however, when different thickness and alignment layers are required, the cells are made by hand.

Both types of cell utilise a conductive layer to allow fields to be applied to the sample. This layer is made of Indium Tin Oxide (ITO), deposited as a thin coating, (typically ~10 nm) is optically transparent and has a high conductivity. Ordinary soda-lime glass can be used in some displays, although the high concentration of alkali ions in this glass can cause particular problems in active matrix displays. The sodium ions can migrate out of the glass causing blooming, alignment degradation and increased power consumption. One solution to the problem is the use of an inert barrier layer, typically SiO_2. Specialist low ion glasses are also available and these require no coating. In commercial displays a barrier layer is often used anyway to allow the cell to be switched capacitively with no direct current passing through the liquid crystal.

3.3.1 Alignment Layers

The use of thin cells and suitable surface treatment can allow the director to be constrained in one direction over large distances such that the sample can be considered to be uniformly aligned. There are two fundamental alignment orientations: using the nematic phase as an example, when the director lies parallel to the glass substrates, the alignment is termed planar; whereas when the director is oriented normal to the substrate the alignment is termed homeotropic. Many different alignment layers can be utilised to obtain a required geometry, although their effects are also dependent on the specific properties of the liquid crystal in question[11].

Polyimide is the most commonly used alignment agent in this work. When a thin (~20 nm) layer of polyimide is uniformly rubbed, the polymer chains lie in a preferred direction[11]. Liquid crystal molecules in contact with the polyimide can orient with the rubbing direction by dipolar and Van der Waal's interactions. Polyimide is chosen commercially as a planar alignment layer because it is unreactive and very resistant to dissolving in liquid crystals, water and other solvents. It adheres well to glass and ITO, and has a good thermal stability, with tests only showing signs of decomposition above ~250°C. Studies have also shown the advantages of many other alignment layers, such as obliquely evaporated silicon monoxide films[12], to provide planar alignment layers with controllable surface pre-tilt. Other alternative alignment layers for use with hand-made cells are described in §3.3.3.

3.3.2 Prefabricated Lucid Cells

As fabrication of cells by hand can be a difficult and lengthy process, a standard cell was designed in-house and fabricated by EEV[13]. A schematic diagram of one such "Lucid" cell is shown in

Figure 3.4. The cell consists of two glass substrates, each ~0.75 mm thick, separated by glass spacer beads encapsulated in adhesive which is applied down each side of the substrates before they are joined to form a cell. The internal surfaces of the substrates are coated with a patterned electrode of ITO, with a cross-over giving an active area of 25 mm^2. Prior to cell assembly, the inner surfaces are also coated with a silane bonding agent and an alignment layer. The alignment layer is a 20 nm coating of rubbed Ciba-Geigy Probromide-32, a proprietary polyimide agent, yielding a pretilt of typically less than 2°. This induces planar alignment, such that the long axes of the molecules are ordered parallel to the glass plates. The layer is rubbed diagonally at 45° to the side of the cell. The cells are rubbed unidirectionally, ensuring the pretilt forms along the rubbing direction. If the alignment layers of both surfaces are rubbed in the same direction, the cell alignment is known as parallel. If the top substrate is rubbed in the opposite direction to the bottom substrate, the alignment directions will be anti-parallel. The anti-parallel arrangement with its opposing pre-tilt directions will favour a bookshelf alignment in the liquid crystal. The cells are fabricated with different internal gaps, typically 3-4 μm and 5-6 μm. The quoted sizes are approximate and must all be checked as described for cells in §3.3.4. Parallel-walled cells are selected by observation of a low number of interference fringes under the light of a sodium lamp.

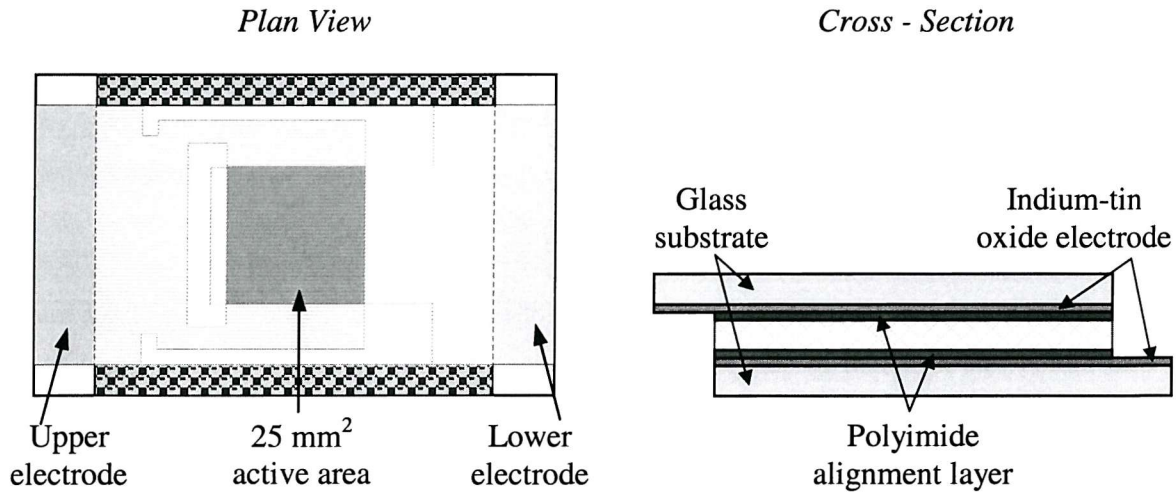

Figure 3.4 A schematic of a prefabricated Lucid cell.

3.3.3 Hand-Made Cells

If a different alignment layer or cell gap from those of the available Lucid cells is required, the cells must be hand-made. Due to the need for cleanliness, this is done in a low dust environment in a special cell preparation room. Glass pre-treated with ITO is cut up and using etch resist and a 15% (w/w) hydrochloric acid solution, any desired electrode pattern can be created. For a parallel alignment, polyvinyl-alcohol (PVA) glue has been shown to be simple to use and very effective. A swab soaked in a solution of 1% PVA in water is wiped across the surface of the glass. The glass is

then left to allow the water to evaporate. Although this is the easiest method and sufficient for the test cells needed, it can lead to small amounts of streaking due to uneven layer thickness. A more precise application method is spin coating. However, considerable skill is required to achieve an even layer as spin rate and evaporation rates are key factors. Once a layer of PVA is deposited, alignment grooves are created. The simplest method is to smoothly drag a record cleaner across the film, taking note of the rubbing direction.

Two other alignment layers are used in this work, namely polytetrafluoroethylene (PTFE) and lecithin. PTFE is used to confer a planar alignment. The deposition process involves drawing a PTFE bar across a glass substrate heated to 300°C, to create the directional alignment layer[14]. The procedure must be carried out in a clean room because the process is very sensitive to contamination. The alignment layers were deposited on the substrates by Dr Sebastien Meyer. The process of achieving even, well-fixed layers takes considerable practise and a meticulous method[15].

Lecithin can confer a homeotropic alignment. Polar interactions between the lecithin head group and glass substrate anchor the alignment layer, leaving long aliphatic chains standing perpendicular to the substrate. The upright chains encourage the liquid crystal molecules to lie normal to the glass and a homeotropic alignment is achieved. A weak solution of lecithin at ~1% in chloroform, is made up. Similar to the PVA application, the lecithin solution is spun or wiped across the glass and left to evaporate, although in this case no rubbing is required. Unlike PTFE, polyimide and PVA, which are fairly rugged and can withstand reasonably high temperatures, lecithin, a component of egg white, is not so robust and begins to break down at temperatures above ~80°C.

Once an alignment layer is deposited, the cell must be constructed. A wide range of spacer beads are available, from sub-micron to 20 microns diameter. The beads are mixed with a UV curing glue and sandwiched down the edges of the cell. Alternatively, the beads are placed in the corners and the cell is sealed externally with an epoxy glue. Another method to form thicker cells is to use optical fibre as the spacer. Choice of spacers is important, as they must be inert and their size must not be temperature dependent. Knowing the rubbing direction of an alignment layer, the cells can be sandwiched with a parallel or anti-parallel alignment. For the work in this thesis an anti-parallel alignment is favoured in order to encourage a bookshelf geometry to form in the SmC* phase. The glass plates must be held parallel whilst the glue dries or is cured. The interference fringes seen under the light of a sodium lamp show if any adjustment is needed.

3.3.4 Cell Thickness Determination

The cell gap in both commercial and homemade cells must be determined and the most accurate method is to use a spectrometer. Placing the cell in the beam path causes interference fringes to form.

These fringes, which are caused by the cell acting as an etalon, are seen as oscillations in the absorption or transmission spectra. The interference fringes are obtained as a function of wavelength by the use of a computer controlled Hewlett Packard 8453 UV-Visible spectrometer[16]. The spectrometer utilises deuterium and tungsten lamps and a photodiode array detector to achieve a range of 190-1100 nm at a resolution of 2 nm.

3.3.4.1 Etalon Theory

Light passing through a glass walled cavity is partially reflected on the inner surfaces. Some of this light will then emerge with the non-reflected beam but will have an optical retardation equal to twice the cavity width (d). If the wavelength of the incident light is equal to the extra beam path length, 2d, then the emerging beams will constructively interfere. This is true for any integer number of whole wavelengths, thus $2dn = m\lambda$ is the condition for constructive interference, where n is the refractive index in the cell gap. If the path length corresponds to half the incident wavelength, destructive interference will occur, thus $2dn = \left(m + \frac{1}{2}\right)\lambda$ is the condition for destructive interference

The refractive index of the air-filled cavity is that of air and is equal to 1 and so can be ignored in these calculations. In the spectrometer, a fixed cell gap is illuminated by a broad spectra and the two interference conditions will cause constructive and destructive interference at different wavelengths, seen in the transmission spectra. Before making any measurements, a reference spectrum is taken. A measurement with no cell in the beam path acts as a baseline or "blank". Once a blank run has been made, the cell is placed in the beam path and the full spectrum recorded. The wavelengths of the maxima and minima of any number of peaks and troughs can then be measured by the computer software. In practice 10 are usually measured.

A peak will occur every time the maxima condition, $2d = m\lambda$, is met, thus

$$2d = (m + i)\lambda_i, \qquad 3.3$$

where i is an integer or zero. Using the initial condition, where i = 0, to eliminate m yields

$$i = 2d\left(\frac{1}{\lambda_i} - \frac{1}{\lambda_0}\right). \qquad 3.4$$

Therefore a plot of i against $1/\lambda_i$ will give a straight line of slope 2d. Since the choice of the initial value of λ_0 is irrelevant, it is a simple task to pick any consecutive peaks and number them i = 1,2,3...etc. It is important to note that because these calculations are based on a cavity with an air gap, the cell must be unfilled for refractive indices to be ignored.

Since the wavelength is measured in nanometers, a plot of peak number against $2000/\lambda_i$ gives the slope as the cell gap in microns. This calculation is easily achieved in the Microsoft Excel graphing package, which can calculate the slope and associated error using a linear regression equation. Repeated measurements of the same portion of a typical 3-5 μm cell are accurate to within 0.01 μm, which is an order of magnitude higher than the cell's thickness variation. Hand-made cells can show a large thickness variation depending on the care taken in production. Industrially produced Lucid cells show good parallel alignment of the glass substrates, although the absence of any spacer beads across the cell allows some cell gap variation to occur. Repeated measurements of different parts of the cell typically have a variance ~0.1μm.

3.3.5 Cell Filling and Finishing

Once the cell gap is measured, the cell is ready to be filled. The anti-parallel Lucid cells and hand-made cells are filled by capillary action. The cell and sample are warmed on a hot-plate to reduce the sample's viscosity. Sometimes it is necessary to heat the sample into the isotropic phase to allow any air trapped in the sample to escape. Often this is carried out under mild vacuum to ensure the sample is fully degassed. A small amount of the material is placed on the lip of the cell and is drawn into and across the cell by capillary action. Once full, the cell is sealed with a Norland UV glue[17] and placed in a UV oven to cure. Care must be taken to shield the sample from the UV radiation. The final step is to solder electrodes onto the ITO contacts. With hand-made cells, the alignment layer must first be removed, which is normally done using acetone. Flying leads are then attached with indium solder. The joint is then shielded with a little more UV glue or PTFE tape to prevent short circuits.

3.3.6 Mixing

In order to achieve reproducible results, considerable care is taken when making up mixtures. Both LC/LC mixtures and dye/LC mixtures are used extensively throughout this work. A Mettler-Toledo AG 245 balance[18] allowed accurate weighing of samples down to 0.01 mg. Ideally, all mixtures are calculated utilising molecular weights to give a Mol/Mol ratio. For known compounds, the molecular weights are easily determined using ISIS draw software[19] and a Microsoft Excel spreadsheet. However, for some dyes the proprietary structure is unknown and, for comparison with earlier work, weight to weight (w/w) percentages of the total weight of the mixture are used.

Glass specimen bottles are used once they have been meticulously cleaned (by rinsing with detergent, deionised water and finally acetone) and then heat dried. Very small amounts of chemical are often needed (1% dye solutions for example) so this is weighed in the bottle with an initial idea of the required final mix, and then the liquid crystal is added. The exact weights are recorded to give an accurate value of the true molar percent ratios achieved. The samples are then mixed. When large

samples (>20 mg) are made the bottles are held in a shaker in an oven and left for several hours in the isotropic phase to mix. The scarcity of the dye and some of the liquid crystals, requires very small samples to be made making mechanical or diffusive mixing difficult. For these very small samples, spectroscopy grade DCM was used as a mixing agent. DCM was chosen in preference to chloroform due to its less hazardous nature. Once thoroughly dissolved, the samples are left to evaporate and are then heated into their isotropic phase under vacuum and left overnight. This ensures that as much solvent as possible is removed from the mixture, and that effective degassing takes place. The use of a solvent for end mixing can also allow an increase in measurement accuracy; by dissolving a larger batch of dye in the solvent, dye addition can be more accurately controlled by use of 0.1ml pipettes.

3.3.7 Alignment

For ferroelectric applications, an ideal liquid crystal would exhibit the phase sequence I→N*→SmA*→SmC* [20]. This sequence will provide the best chances for planar alignment in the SmC* phase. To encourage a defect-free alignment in a planar cell, the sample is cooled slowly from the isotropic to the N* phase, typically at <0.1°Cmin^{-1}. Slow cooling through the N*→SmA* transition allows the smectic layers to form, the presence of an already uniform planar alignment allowing this to occur, without defects, in a bookshelf geometry. Ideally, in mixtures, the pitch of the N* phase can be adjusted such that it becomes infinite just before the N*→SmA* transition allowing for easy layer formation – this is called pitch compensation[21] and is utilised, for example, in the commercial mix SCE13, which is analysed in this chapter. On further cooling to the SmC* phase, the director tilts with respect to the layer planes. The well-aligned smectic layers are pinned at the surface and thus the director tilts away from the alignment direction, which becomes the centre of the two stable states[22]. When trying to achieve alignment simply by controlled cooling, the author has found it is often helpful to connect the electrodes and short the cell.

If slow cooling and surface alignment forces are not sufficient to cause a large monodomain to form, a field can be applied. In a SmC* phase, the field will couple with the ferroelectric dipole and produce an alignment torque, encouraging the molecules to align parallel to the cell walls. Materials exhibiting the I→SmC* transition naturally form a scattering focal conic texture. If the material is cooled at ~ 0.1°Cmin^{-1} with a large field of ~ 20 Vμm^{-1} at a low frequency of ~ 0.1 Hz the focal-conic domains can sometimes be enlarged into a nearly uniform structure. This field-applied process is known as poling. Unfortunately, the use of high fields at low frequencies has a high chance of causing electrical breakdown. A better method uses electrohydrodynamic instabilities. Varying the field strength and frequency of a square-wave from a starting point of 50-200 Hz at around 10 Vμm^{-1}, and a cooling rate ~0.2°Cmin^{-1} whilst the smectic phase is just forming can induce differing levels of electrohydrodynamic instabilities and dielectric interactions[23]. This mechanism is used to disrupt the inter-molecular forces, allowing surface interactions to encourage a planar alignment.

3.3.7.1 Shearing and Magnetic Alignment

Moderate shearing motions can also be used to disrupt multiple domain-formation, allowing flow alignment or the application of a field to encourage monodomain formation. This process can be very successful in flexible displays but is often impractical with rigid glass substrates, especially if the device is fully fabricated before filling. However, a small amount of pressure on the glass can be sufficient to enhance the alignment generated by the correct field and cooling conditions.

The anisotropy of liquid crystals also extends to their magnetic properties as a consequence of the mesogen's electronic structure. This magnetic anisotropy can be utilised for alignment purposes. Most liquid crystals are diamagnetic, meaning that a magnetic moment is induced to oppose the applied magnetic field. A diamagnetic material will adjust itself to minimise this interaction with the applied field, and therefore magnetic fields can be used to promote alignment. The remote nature of the magnetic field can allow very high field strengths to be used without causing cell damage.

3.4 Material Analysis

The following section describes the different methods used to measure the fundamental electro-optic parameters of tilt angle, spontaneous polarisation and viscosity in a liquid crystalline material.

3.4.1 Tilt Angle

The definition of tilt angle depends on the method of measurement. There are two possible measurements; tilt derived from x-ray diffraction experimental data and directly measured optical tilt. X-ray diffraction techniques utilise Bragg reflection properties to determine the spacing of the smectic layers. Assumptions of molecular length and layer arrangement give an idea of the relaxed tilt angle (described further in section §3.5.5). Optical methods allow the tilt of the optic axis to be measured. The position of the optic axis relative to the molecular axis and the smectic layers is determined by the core of the molecule where most of the delocalised electrons and strongly dipolar groups are situated. The rotation of the molecule around its long axis means that the optic axis is symmetric about the rotation axis.

In complex molecules, there is a difference between the tilt angle (with respect to the smectic layer planes) of the optic axis and the mean molecular axis. Hence, the two measurement methods (optical and x-ray) can yield different results. Bartolino et al.[24] investigated several compounds of varying chain length optically and via x-ray. The optical tilt angle was always slightly larger than that derived from x-ray layer spacing calculations. The difference increased with a lengthening of the terminal alkyl chain. The application of an electric field can also slightly affect the value of tilt measured.

Although different geometries and environments lead to different apparent tilt angles, for the purpose of device manufacture in a surface stabilised geometry, it is the optical tilt angle observed in an applied field that is important in assessing the usefulness of a sample. All future references to the tilt angle are therefore assumed to relate to optical measurement unless stated otherwise.

3.4.1.1 Microscopy Measurement

Optical tilt measurements are carried out with the crossed polariser microscope described in §3.2.1. Samples are examined in the planar aligned surface stabilised geometry. The intensity transmitted through the crossed polarisers is dependent on the angle of the optic axis and governed by the birefringent equation given in the previous chapter (§2.3.2.1);

$$I = I_0 \sin^2(4\theta)\sin^2\left(\frac{\Delta n d \pi}{\lambda}\right). \qquad 3.5$$

Recalling also that Δn is the birefringence, d the cell thickness and λ the wavelength of the incident light, the equation is valid when one of the switched states lies on a polariser axis. The tilt angle, θ, is defined as the angle the molecular long axis makes with the layer normal. In order to measure the tilt, an electric field is used. When the polarity of the applied field is reversed, the molecules will move either in-plane (electroclinic) or about a cone (Goldstone). In both motions, a full switch corresponds to a switching angle equal to twice the tilt angle. In order to measure this response several methods are used.

The simplest method is to measure the position of the two extinction states. With a D.C. field applied, the molecules are held in one switched state. When the optic axis is aligned with one of the polarisers, an intensity minimum (dark state) is seen, as a consequence of $\theta=0$ in Equation 3.5. This dark state is found by rotating the microscope sample bed, and the position of the sample stage is noted. The applied field is reversed and the bed rotated until the optic axis of the new switched state is brought into extinction. The angular difference corresponds to a switch of twice the tilt angle. Although switching between two maximum intensities, (light states) will also yield the tilt angle, the dark state is easier to identify with the human eye. This method, while effective, requires the use of a D.C. or very slow A.C. field which can be damaging to the sample. The accuracy is governed by the definition of the dark state, which sometimes only shows a very slight intensity change over several degrees of rotation when viewed by eye.

A well-aligned sample can be more accurately measured using a photodiode and a digitising oscilloscope. This setup not only allows better determination of the dark state, but a faster switching frequency, typically ~100 Hz, thereby protecting the sample from potentially damaging D.C. fields. As the optic axis moves between the crossed polarisers, the transmission will follow a sinusoidal

curve, as defined in Equation 3.5. The measurement accuracy can be further enhanced if the optic axis is switched such that the two switched states show a maximised contrast. Maximisation is achieved if the mean position of the optic axis is centred around the steepest part of the sine-squared curve.

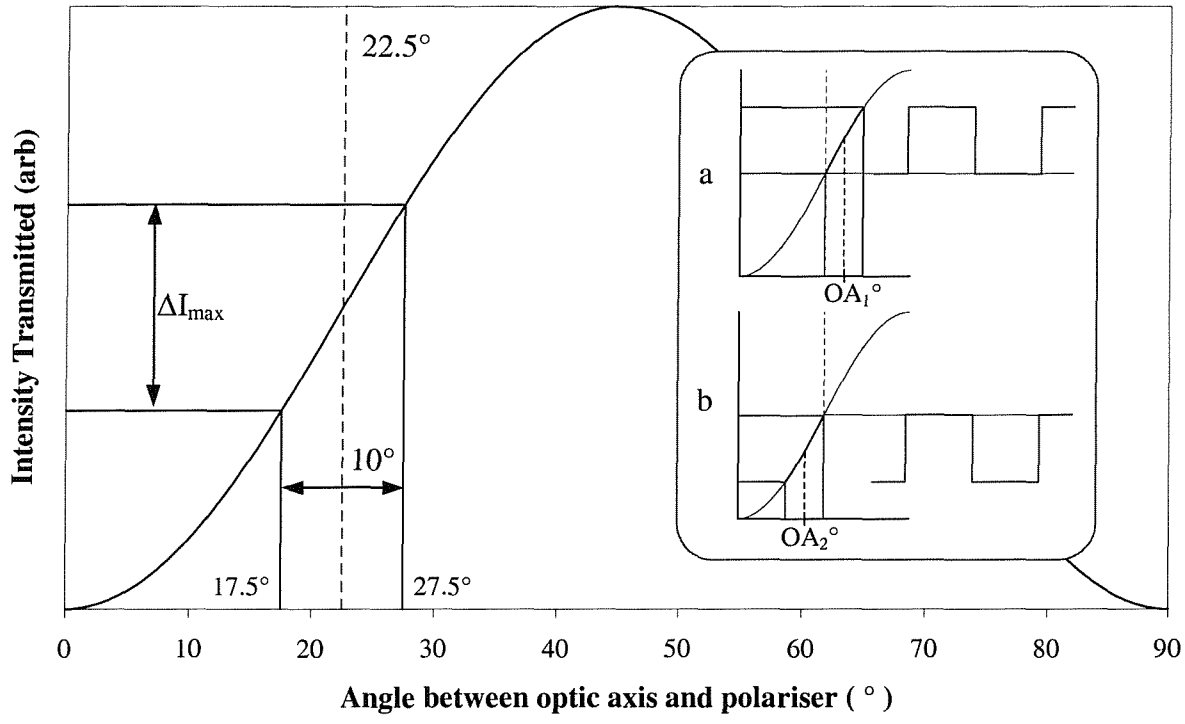

Figure 3.5 Transmission intensity curve for a varying optic axis between crossed polarisers.

As seen in Figure 3.5, the steepest part of the curve is at 22.5° to one of the polarisers. In order to locate this point, the sample is rotated until the two switched states seen on the oscilloscope have the same intensity (see Figure 3.6b). This ensures that the optic axis is switching symmetrically about either a polariser or the 45° maximum transmission axis. The sample bed is then rotated by 22.5°. A cursor is set on the voltage axis of the oscilloscope so that it lies halfway between the two switched positions, i.e. halfway between the maximum and minimum in the photodiode signal. The stage is then rotated until the minimum of the photodiode signal lies on the cursor (Figure 3.5a), and the position of the sample bed is noted. The stage is then rotated in the opposite direction until the maximum in the photodiode signal is level with the cursor and the position of the stage is noted again (Figure 3.5b). The half angle of this rotation gives the tilt angle produced by the applied field. This method allows the tilt angle to be measured to within the accuracy limit of the sample bed (0.5°).

For a sample with tilt angles less than 22.5°, both measurement methods are unambiguous. However, for tilt angles greater than 22.5°, i.e. switching angles >45°, the measurement is not so clear-cut. Problems arise due to the symmetry axes present in the crossed polariser setup. The sine-squared dependence of the intensity (Equation 3.5) will cause tilt angles greater than 22.5° to yield the same intensity as their complementary angle below 22.5°. Thus a complete switch of 30° from a polariser

will have the same appearance as a switch of 60°. If the tilt grows from zero, after, for example a second order transition such as SmA*→SmC*, Curie-Weiss like behaviour will allow the increase to be easily followed. If the SmC* phase forms directly from the isotropic, as is the case in some of this work, the transition can be almost completely first order with a spontaneous tilt appearing at the transition and showing little temperature dependence. This makes tilt identification by simple rotation and by eye on a polarising microscope difficult. The use of the photodiode setup allows the nature of the switch to be examined. For switching angles >45°, the optic axis must always pass across at least one maximum or minimum axis and cause a bounce in the transmitted intensity, which can be clearly seen on the oscilloscope, as illustrated in Figure 3.6c.

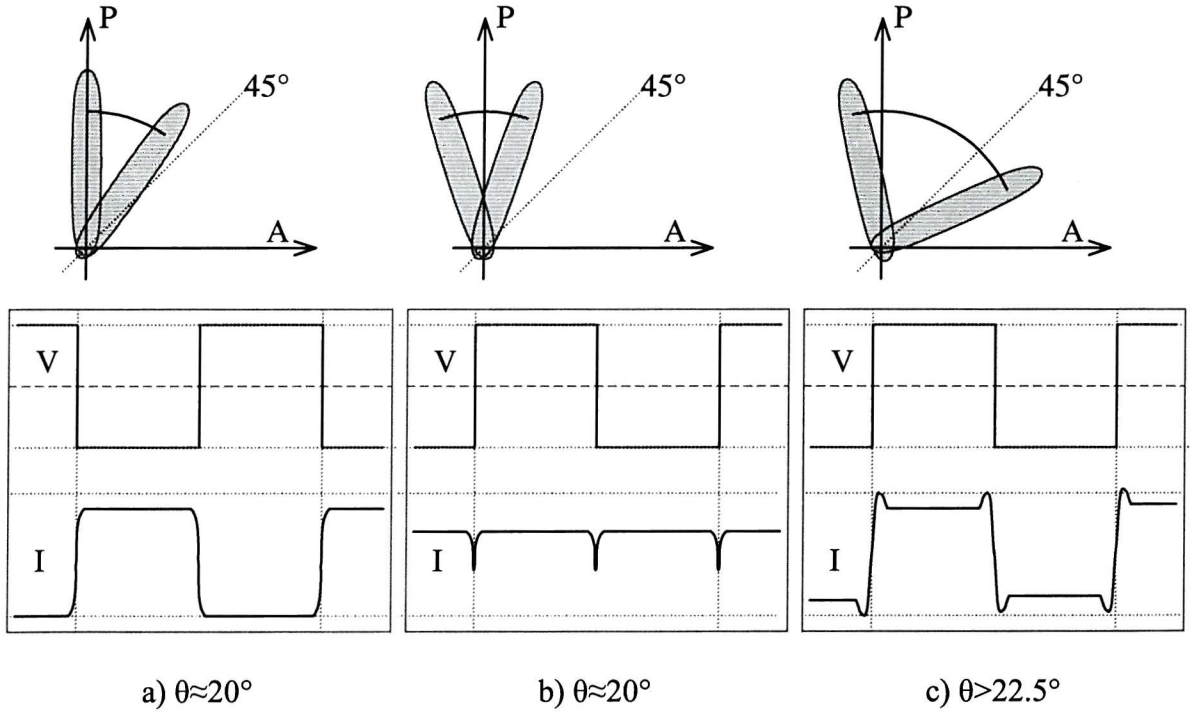

Figure 3.6 Photodiode response to square wave driving with different switched positions.

Tilt angles can be measured as a function of the applied field amplitude, the frequency of the applied (square) waveform and the temperature of the sample. With the exception of field dependence, it is important to ensure that the switching is fully saturated. The conditions required for saturated switching are material and temperature dependent, requiring a slow enough driving wave to ensure a full switch can occur and a sufficiently high field to induce it. The field must overcome the surface anchoring forces and any other defect forces pinning the cones in intermediate positions. Typically, the compounds used in this work respond completely with fields of 10-100 Hz at 10-30 $V\mu m^{-1}$. Figure 3.7 shows measurements of the BDH ferroelectric compound SCE13[25]. This is a multicomponent mix with a quoted phase range of

$$I \xrightarrow{100.8} N^* \xrightarrow{86.3} SmA^* \xrightarrow{60.8} SmC^* \xrightarrow{-20} SmI^*.$$

The graph in Figure 3.7 shows measurements of the optical tilt angle (crosses) in response to a 100Hz square wave at $5V\mu m^{-1}$. The 2nd order behaviour can be clearly seen in the Curie-Weiss curve-fit (solid line).

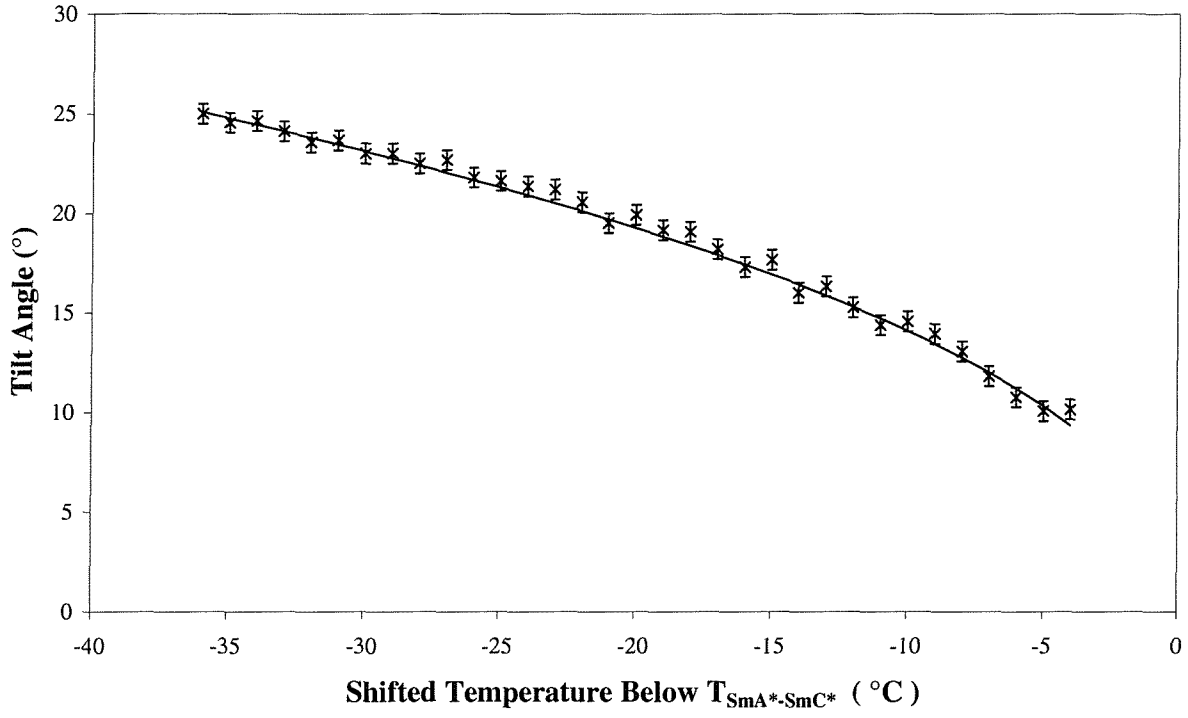

Figure 3.7 Optical tilt angle of SCE13 showing 2nd order nature.

The photodiode method represents an optical average of the part of the sample being measured and is very dependent on sample alignment. If alignment is not possible over the entire sample, higher magnification objectives are used. If the alignment is still poor, the photodiode method can be useless. Another measurement method available is the rotating analyser rig. This technique is very powerful when samples are not well aligned and has the advantage of being automated. If no alignment exists at all, rough results can still be obtained using a high magnification on the microscope and the D.C. field method described previously. Although this process risks cell degradation and is less accurate, it can be the only option to measure tilt angles in a very poorly aligned sample.

3.4.1.2 Rotating Analyser

The rotating analyser method uses separate apparatus in collaboration with C. Noot. This technique is an optical method based upon an instrument developed by Wood and Glazer[26]. The apparatus was constructed by C. Noot, and a fuller explanation of the theory and experimental setup can be found in his thesis[27].

The sample to be examined is placed on a heating-stage and illuminated with circularly polarised light. The light source is a 632.8 nm He-Ne laser, circularly polarised by a suitably oriented quarter wave plate. The light passes through the sample and on to a rotating Polaroid analyser and finally to a photodiode. The light intensity at the photodiode[28] is given by

$$I = \frac{I_0}{4}[1 - \sin(\delta)\sin 2(\omega t - \varphi)], \qquad 3.6$$

where I_0 is the incident intensity, ω is the angular frequency of the rotating analyser and φ is the angle between the optic axis and the laser's polarisation. $\delta = \frac{2\Delta n d\pi}{\lambda}$, where Δn is the sample birefringence, d is the cell gap and λ is the wavelength of the incident light. A reference signal is measured through the rotating analyser to determine the rotating analyser's angular frequency, ω. The signal and reference are displayed on an oscilloscope, where the phase delay between the two is measured. Measurements are typically carried out with a 10 Hz switching field. When the position of the optic axis is switched by this applied field, the phase delay of the intensity waveform is shifted. This method allows the rotation angle of the optic axis to be calculated directly from the change in the phase delays for the two states.

The rotating analyser technique for measuring tilt angles has several advantages. It is less sensitive to alignment problems than photomicroscopy techniques, as it can yield results (albeit with less accuracy) for quite poorly aligned samples. The geometry of the system yields a measurement of 2θ without the confusion of a $(90°\text{-}2\theta)$ ambiguity, and therefore makes the technique particularly useful where $2\theta > 45°$. The constant measurement process allows a continuous determination of the tilt angle against many factors such as field strength, frequency and temperature. By writing software to computer-control the experiment, C. Noot[27] has automated the data acquisition process. Coupled with repeated result taking and multiple runs, computer-control can significantly increase the accuracy of the results.

3.4.2 Spontaneous Polarisation

Spontaneous Polarisation (P_s) is an essential parameter in determining the field response of a ferroelectric liquid crystal. Several methods exist for its calculation. The pyroelectric effect[29] relies only on changes in the spontaneous polarisation during heating and makes no assumptions about the form of molecular motion during electrical switching. This method is highly accurate at determining the rate of change of spontaneous polarisation with temperature, and so is ideal for samples with large viscosities or complicated switching mechanisms[30]. However, to yield a plot of absolute values, it must be calibrated using another method. It is also hampered by the need for accurate estimations of the heat capacity and sample density, potentially introducing large errors.

As discussed in the previous chapter, a ferroelectric liquid crystal can be considered a capacitor and resistor connected in parallel. When a varying voltage is applied, three main contributions to the current flow across the sample are seen, due to ion flow, charge accumulation and finally dipole realignment which gives rise to the spontaneous polarisation. The standard method used to measure polarisation in solid ferroelectrics is the Sawyer-Tower method[31], designed initially for measurements of Rochelle salt. Using this method, the molecules are switched by a sinusoidal field to give a hysteresis loop of polarisation current against applied field. Such loops include contributions from all three components of the induced current flow, and considerable experience is required to select the part of the loop formed as a result of spontaneous polarisation realignment. This uncertainty led to the Diamant Bridge refinement[32]. The method utilises variable resistors and capacitors to balance out the effects of ion flow and capacitive contributions, leaving only the contribution from spontaneous polarisation realignment. The interpretation of spontaneous polarisation can still be complicated and is not easily automated. The results in this work are measured using a different method; the current pulse technique.

3.4.2.1 Current Pulse Technique

An alternative to studying hysteresis loops is to measure the transient current obtained when polarisation reversal occurs as the polarity of the applied field reverses. This current pulse technique was first used to measure spontaneous polarisation in liquid crystals by Martinot-Lagarde[33]. The method is based on measurements made of spontaneous polarisation in solid state physics using a square wave driving field. However, using a square waveform it is difficult to separate the spontaneous polarisation from the capacitive contribution. Miyasato et al.[34] pioneered the use of triangular driving waves, which allow the three separate contributions to the induced current to be identified by shape separation. A typical ferroelectric response to the triangular driving wave is shown in Figure 3.8. The ionic conduction component appears as a rising slope, following the driving wave. The slope of this baseline can be used as an estimate of the sample's ionic impurity. The capacitive contribution yields a jump in the baseline on field reversal. Finally, the response due to spontaneous polarisation reorientation is seen as a peak, which can be isolated from the background.

In order to measure the induced current, the cell is driven with a triangle wave, typically ~100 Hz at ~10 $V\mu m^{-1}$. The small current produced by the cell is measured as the voltage drop across a series of resistors in an EW251 current to voltage (I→V) converter made in-house[5]. The converter includes an adjustable gain amplifier which allows the very small currents to produce a significant signal at the oscilloscope. Recalling the results of the calculations in §2.4.2 of the theory chapter, the P_s can be calculated from the charge, Q, produced by the current flow due to dipole reorientation,

$$P_s = \frac{Q}{2A}. \qquad 3.7$$

All P_s measurements are carried out in the prefabricated Lucid cells where the electrode area, A, is known (25 mm^2). Since the ionic and capacitive contributions are baseline contributions, the charge (Q) is calculated using the oscilloscope trace from the area bounded by the spontaneous polarisation peak and the interpolated ionic current baseline (see shaded region in Figure 3.8). This method of shape identification allows much of the measurement process to be computer automated.

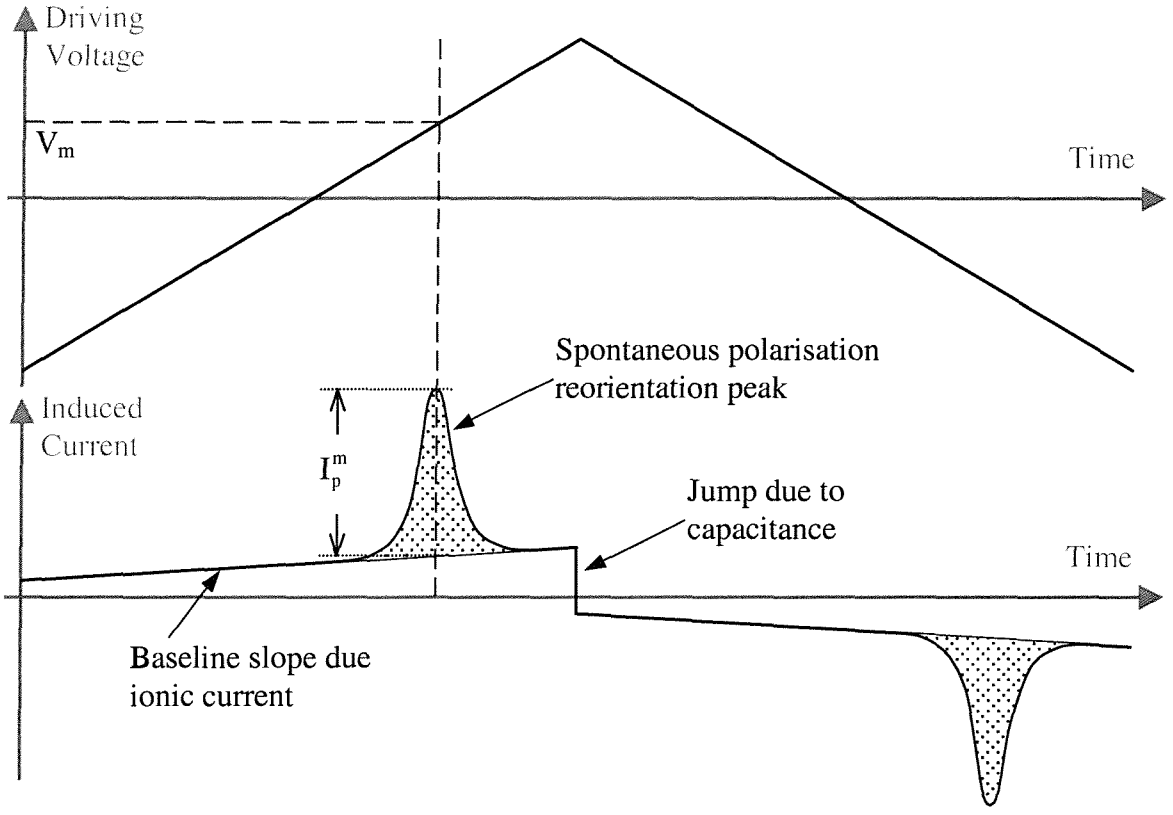

Figure 3.8 A typical induced current response to a triangular driving wave highlighting the three components of the induced charge.

Computer automation has been used previously and the method described here is a further refinement of the original work of H. Walton[35] and W. Robinson[36], who wrote control software in Borland TurboPASCAL[10]. The oscilloscope is triggered by the stable driving wave from the function generator. The time-base is adjusted to ensure that the peak is as broad as possible to maximise the resolution, whilst leaving enough baseline to enable accurate determination of the peak area. The I→V amplifier is adjusted to maximum gain without saturation, thus maximising the signal to noise ratio. The signal is digitally averaged on the oscilloscope, usually 32 times to minimise noise and random error. The driving voltage, current pulse waveforms, and oscilloscope settings are then read by the computer. The slope of the baseline is measured by taking eleven data points on either side of the current pulse peak and carrying out a least squares regression on them. The area bounded by the calculated baseline and the current pulse curve is then determined using a trapezium rule. In order to obtain an accurate measure of spontaneous polarisation, ten acquisitions are made and an average

value of the area under the curve is obtained. Using the oscilloscope settings, I→V gain and electrode area, the spontaneous polarisation is calculated automatically. The computer can also interface with the Linkam temperature controller, allowing a series of readings at different temperatures to be fully automated.

3.4.2.2 Measurement Limitations

If the temperature is lowered, typically the viscosity increases and the reorientation is slowed down. The current pulse peak broadens until complete switching no longer occurs. To give an idea of the complexity of the role of the components in the molecular switch, Skarp and Handschy[37] derived an equation of torque balance between the ferroelectric driving torque and the viscous damping torque. This is represented graphically in Figure 3.9, which shows the variation of the current response trace after a voltage step at time t=0. The area of the peaks, which is proportional to the spontaneous polarisation, is held constant and the rotational viscosity increases by ~10% between each curve.

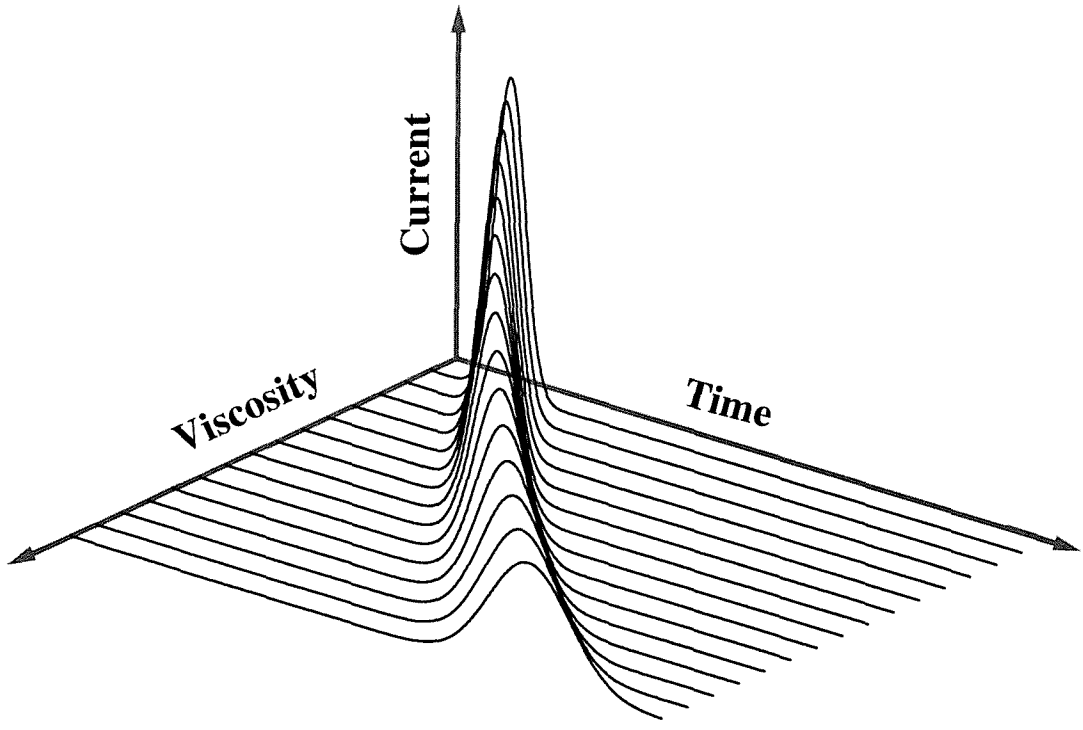

Figure 3.9 The effect of increasing viscosity on peak height, width and position.

With increasing viscosity, the time delay before the current pulse occurs increases (i.e. the peak shifts along the time axis) and the frequency of the driving field must be reduced in order to allow a complete switch to take place. Another consequence of increased viscosity is an increase in the voltage required to cause switching. Sometimes higher voltage and lower frequency fields can disrupt the liquid crystal, particularly if ionic or other impurities (such as a dye) are present, limiting the range and accuracy over which full automation can occur. The size of these effects is sample-specific

and requires careful choice of switching fields and frequencies to ensure saturated switching for all readings. The effect of altering the driving field is seen with SCE13 in Figure 3.10 in which the spontaneous polarisation of the material is given as a function of shifted temperature at a range of field amplitudes. Below 2 Vμm^{-1} the switch is not fully saturated, which drastically affects the magnitude of the P_s and results in deceptive measurements. The application of fields greater than 2 Vμm^{-1} has only a small effect on the shape of the curve and the switch is considered to be fully saturated. The results are plotted against shifted temperature below the SmA*→SmC* transition, and once more the Curie-Weiss like behaviour is clearly seen. The solid line represents a Curie-Weiss fit using the manufacturer's quoted values[25].

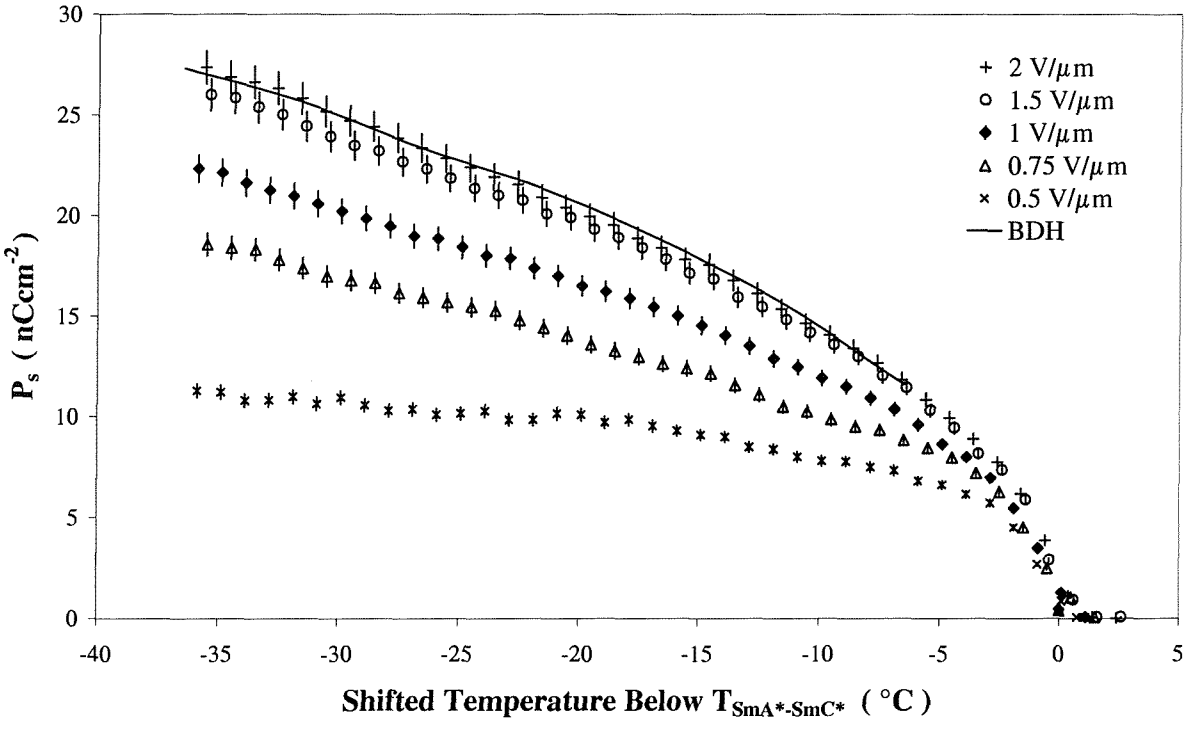

Figure 3.10 The effect of fields below saturation on the measurement of spontaneous polarisation in SCE13.

As mentioned in the preceding section, the quality of alignment can greatly affect the measurement of optical tilt angle. The spontaneous polarisation, on the other hand is a molecular property and as such is far less strongly influenced by the quality of material alignment. As with tilt angle measurements, the validity of the spontaneous polarisation measurements is dependent on establishing fully saturated switching which must occur over the entire active region and across the cell. However, molecules are pinned at cell walls and at the surface defined by the apex of the chevron[38]. Both these considerations are factors affecting the saturation voltage level. In the ferroelectric liquid crystals used in this work, the required saturation field is typically in the region of 15-20 Vμm^{-1}. The use of a 100 Hz field removes the risk of exposing the cell to prolonged D.C. voltages. These experimental conditions required to induce saturated switching and the use of A.C. fields are essential to ensure the validity of

the assumptions made in the previous chapter when discussing the contributions of dielectric permittivities and the formation of fully-unwound stable bookshelf-like structures.

Not all transitions occur over a narrow temperature range, some mixtures can have biphasic regions over more than 10°C. If biphasic behaviour occurs, for example, at an I→SmC* transition, the occurrence scales down the measured value of P_s since the isotropic areas do not contribute to the size of the current pulse peak. The automated calculation, however, assumes that the entire active area is switching ferroelectrically. The proportion of the active area that is in the isotropic phase can be estimated with the use of a computer and C.C.D. camera. The camera is mounted in the microscope phototube and computer software counts the number of pixels that have a colour value equivalent to black. This measurement indicates the percentage of sample in the isotropic phase and allows the spontaneous polarisation results to be scaled appropriately.

3.4.2.3 Ionic Effects

In a commercial ferroelectric liquid crystal material, the amount of ionic impurity is usually small and the switch is well defined. Many of the compounds used in this thesis are synthesised specifically for this work and are not always 100% pure. Very small amounts of synthetic pre-cursor or solvents such as DCM can greatly affect the number of free ions in the cell. The addition of another compound such as a dye can have a similar effect. The presence of ions increases the slope of the baseline in the current pulse measurements and this can make automated reading difficult. The effect is reduced via a feedback circuit following the method of ohmic current removal of Gießelmann et al.[39]. The slew of the baseline caused by ionic motion follows the applied field. To counter this slew the inverse of the driving wave is scaled down and fed back to the outgoing current. The level of feedback is controlled with an operational amplifier/resistor circuit to allow the baseline to be fully flattened. The circuit is built into the I→V converter and could be switched in when required. Repeated measurements with poor samples showed that the absolute value of the spontaneous polarisation is unaffected. The spontaneous polarisation measurement software is also written to allow the user to choose the end points for baseline calculations. This manual method can improve the accuracy when measuring samples with poor response characteristics (i.e. noisy data) but is also essential for measurement of antiferroelectrics described later in §3.4.5.

When levels of ionic impurity are high and the field is reversed, after some delay a diffuse peak may be observed in addition to the spontaneous polarisation reorientation peak[40]. This additional peak is due to fully mobile ions within the cell releasing a drift current density at the electrodes. The author has observed that the diffuse peak occurs typically ~0.1 s after field reversal. Hence, it is only seen at low frequencies (<10 Hz) and is far slower than a typical dipole reorientation of ~100 μs. With the frequencies used in this work, the ion contribution is either not seen, or is clearly distinguishable.

3.4.2.4 Accuracy

The I→V converter provides a resistance across which the charge liberated by the cell generates a voltage. The resistance differs dependent on the gain selected, but for a typical conversion gain of 10 $V\mu A^{-1}$ has a value of 1 KΩ, which does not greatly affect the rise time of ~1 μs. The calibration of the I→V converter was carried out by feeding a known current through the converter, and this test yielded results equivalent to the error of the resistors, ~0.5%. Many sources of error are sample-dependent, such as biphasic contribution and incomplete switching. Measurement errors are dominated by the choice of baseline. A slow response can give a very broad peak with long tails giving errors of ~5-10%. The use of oscilloscope averaging and repeated measurements yield results that are reproducible to ~3%, confirmed by comparison with previous work and standard samples.

3.4.3 Switching or Response Time

The time taken for an SSFLC cell to switch between its two states can be measured optically with an experimental setup similar to that used when obtaining tilt measurements on the microscope. In order to measure the optical switching time, the sample must also be reasonably well aligned. A square driving wave is used at ~100 Hz and ~20 $V\mu m^{-1}$, dependent on the individual sample. As with the tilt measurements, intensity changes detected by a photodiode are plotted on the oscilloscope. The measurement accuracy is greatest when the switch causes the largest intensity change, and this is identified, as previously described for tilt analysis (§3.4.1.1), at a mean optic axis position of 22.5°. This position is essential as the optical response curve is symmetrical about this axis. Once the intensity response is shown on-screen, the oscilloscope cursors are used to measure the peak levels and calculate the time taken for the switch. It can be very difficult to determine accurately the exact times when the switch begins and ends. Thus, it is more practical to measure the time taken for the intensity to rise or fall from a 10% to 90% level. The optical response time is then quoted as a rise time, $\tau_{10\text{-}90}$, and fall time, $\tau_{90\text{-}10}$.

With tilt angles greater than 22.5°, the optical switch complicates this method. As demonstrated in the discussion of tilt measurement (Figure 3.6), switching of a sample with $2\theta>45°$ results in a bounce in the intensity response and makes the identification of 10% and 90% levels difficult. One alternative is to calculate the optical phase using similar methodology to that of the rotating analyser technique. Another alternative to measuring the optical response time in samples with large tilt or poor alignment is found by utilising the current pulse technique once more.

Before considering the current pulse technique, it is necessary to examine the definition of response time. Upon application of a field, the responding molecules can lift slightly on their cones, but may lag for a significant period of time before undergoing significant optical switching. Thus, measurements of 10-90% rise and fall times might be more accurately called switching times. The

true response time is measured from the reversal of the driving voltage to some point on the intensity response. This is far harder to define experimentally, and is considered less important when analysing device characteristics. The measurement of switching time is preferred as it is a molecular characteristic, whereas the effect of the field response lag can be compensated for in pre-addressing. The distinction between the two possible measurements is important.

3.4.3.1 Current Pulse

When measuring switching or response times via the current pulse technique a square-wave is used instead of the triangle-wave used for spontaneous polarisation measurements. The use of a square wave can result in a much sharper peak than that seen with a triangular voltage waveform since the entire driving signal is above threshold. The width of the peak corresponds to the switching time of the molecules, although once again, the tails of the peak are hard to identify accurately.

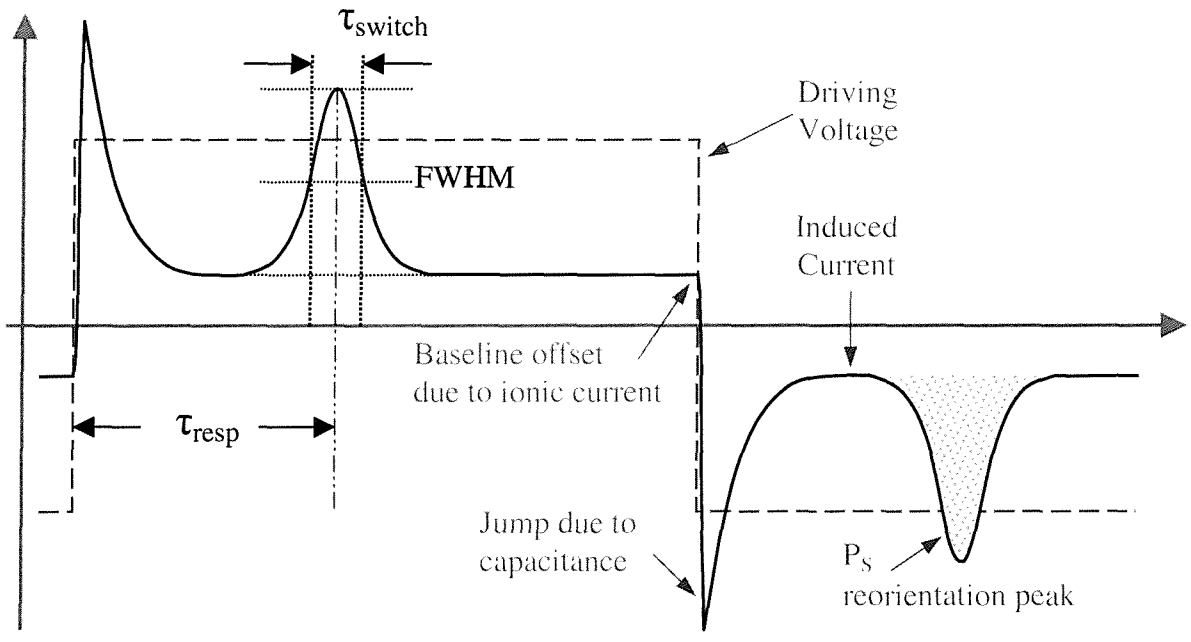

Figure 3.11 Measurement of current pulse response and switching times from a square driving wave.

The most appropriate measurement is the full width at half maximum (FWHM), as shown in Figure 3.11. As with the spontaneous polarisation measurement, the three contributions to the measured current are seen. The capacitance jump can cause a long decay, which often merges with the spontaneous polarisation reorientation peak. Although the area under the peak, and thus the value of the spontaneous polarisation, will be the same as with triangular waveform driving the switch, the merging of the two contributions often prevents accurate measurement. The use of a square-wave also gives an indication of the time taken for the ferroelectric liquid crystal to respond to the applied field.

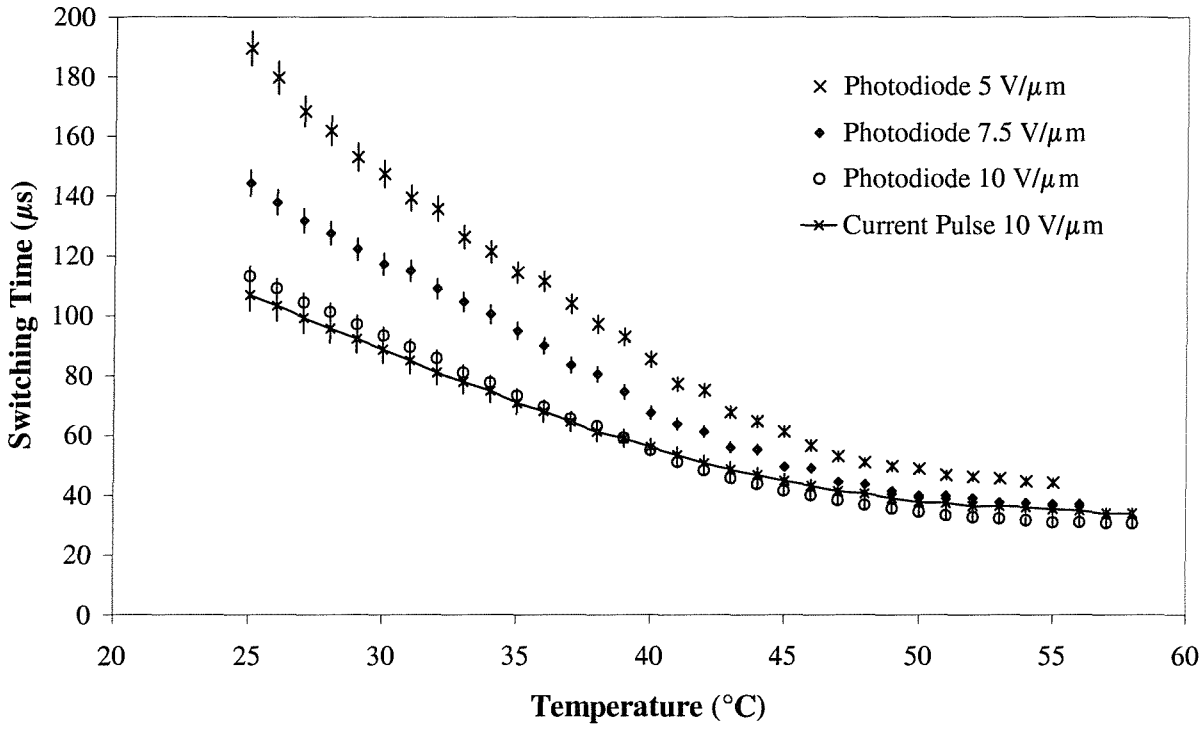

Figure 3.12 Measurement of switching times for SCE13 by current pulse technique and photodiode.

Measurements of the switching times of SCE13 as a function of temperature are shown in Figure 3.12; the effect of varying the driving field can be clearly seen. SCE13 can be easily aligned, making it ideal for a comparison of the two measurement methods. The optical results are measured for a 10-90% transmission change. The current pulse results are highlighted with a line. The optical and current pulse switching times differ slightly; at the same field amplitude there is typically <5% difference between the measured values. The accuracy of both methods is estimated by reproducibility considerations. Readings from the optical method are governed by the response of the photodiode setup and the ability to measure the trace on the oscilloscope. Using oscilloscope averaging and maximising the area of interest on the screen, the results are found to be reproducible to within ~3%. The accuracy of the current pulse technique is governed by similar factors as the spontaneous polarisation. The estimation of a baseline can be complicated by the capacitive decay. Repeated measurements typically yield results with a reproducibility of ~5%.

3.4.4 Rotational Viscosity

The rotational viscosity can be measured by several methods. Recalling the relationship of the rotational viscosity (γ_φ), response time (τ), and spontaneous polarisation, given in §2.5.2,

$$\tau_\varphi = \frac{\gamma_\varphi}{P_s E}. \qquad 3.8$$

This equation allows the viscosity to be estimated from spontaneous polarisation and switching time measurements obtained in similar experimental conditions. In reality, the different methods of measurement of these parameters require a proportionality constant to be included for the expression to be valid. Theoretical predictions[41] estimate a value of 1.76 for switching times derived from the FWHM. Other authors' measurements[42] yield a range of 2.2-1.8 for $\tau_{10\text{-}90}$. The size of the numerical constant varies between samples because the constant depends on the dielectric anisotropy of the material.

The rotational viscosity can be measured from the current pulse response concurrently with the measurement of spontaneous polarisation as described in §3.4.2.1. This is derived from the viscosity equation as a consequence of the dipole motion[43] discussed in the theory chapter (§2.4.3),

$$\gamma = \frac{AP_s^2 E_m}{I_p^m \sin^2\theta}, \qquad 3.9$$

where A is the sample area, I_p^m is the peak value of the current reversal and E_m is the value of the driving field at that time. The measurements of P_s and θ have already been discussed and the value of A is known (25 mm^2). I_p^m is detected using a peak maximum algorithm carried out simultaneously with the P_s measurements[44] (see Figure 3.8 earlier). The value of the driving field at this maximum V_m is also easily read from the oscilloscope and yields E_m when divided by the cell thickness, d. Thus, the rotational viscosity can be measured whenever the spontaneous polarisation is measured, whether semi-manually or by a fully automated process. The accuracy of this part of the experiment is governed by similar factors to those governing the measurement of P_s. The assumptions used in the derivation of the equation and the combination of errors from P_s^2 and tilt measurements give an estimated error of 10%. Since the viscosity typically follows an Arrhenius type behaviour, it is usual to plot the results on a log scale as a function of the reciprocal of absolute temperature.

$$\gamma = \gamma_h \exp\left(-\frac{\varepsilon_A}{k_B T}\right), \qquad 3.10$$

where k_B is Boltzmann's constant, ε_A is the rotational activation energy required for motion, T is the temperature in Kelvin and the factor γ_h represents a measure of the rotational hindrance with the units of viscosity. Results for SCE13 are shown in Figure 3.13 with a straight line fit. The gradient of the fit can be used to calculate an activation energy for the switch ε_A, allowing comparisons to be made between similar compounds.

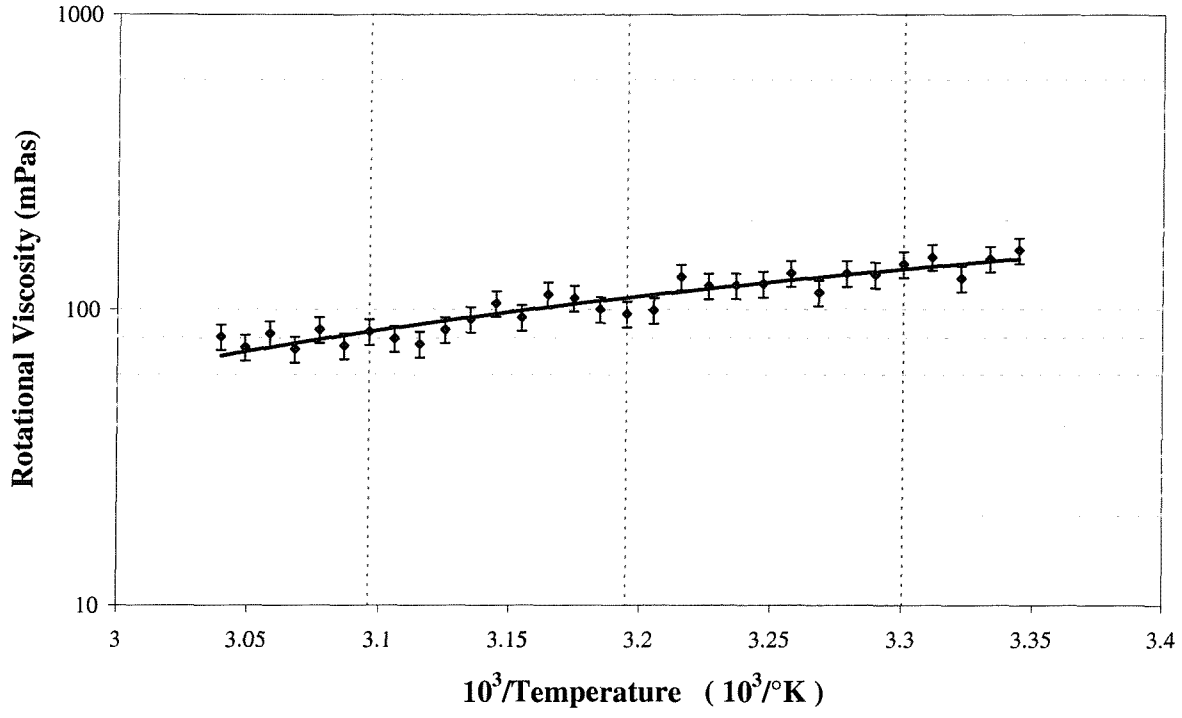

Figure 3.13 Rotational viscosity of SCE13 calculated from I_p^m measured from the current pulse peak.

3.4.5 Antiferroelectric Switching

As described in the theory section, an antiferroelectric material switches from an undisturbed state into two opposite ferroelectric states. When a bipolar triangle wave is applied across an antiferroelectric liquid crystal material, these two switched states are seen separately. The presence of three possible states can alter many of the switching characteristics, and necessitates slightly different measurement methods to those used when characterising ferroelectric liquid crystals. Beginning with the relaxed antiferroelectric state, the driving wave builds from V=0 until it exceeds some threshold level and the sample is driven into a ferroelectric state. This transition results in a sharp current pulse peak. The driving field falls off until the realignment forces take over and the sample relaxes back into its antiferroelectric state, yielding another current pulse peak. The peaks are not identical in shape because of the different processes involved. As shown in Figure 3.14, the driven peak will be sharper, whilst the relaxed peak is broader and exhibits long tails. The added complexity of the induced current response requires each peak to be considered individually when using the automated P_s measurement system or for the endpoints to be selected manually. The presence of a relaxed state necessitates a distinction between the different switching mechanisms. It is now important to consider what spontaneous polarisation value is reported. If the driven and relaxed peaks give the same value of P_s, the driven peak could simply be doubled to give a value for the spontaneous polarisation of the material. However, the two peaks rarely return the same P_s value, and a consideration of the full switch is required. One method would be to quote half of the value of one

driving cycle, i.e. ½(Af→F^+→Af→F^-→Af), corresponding to all four peaks. However, typically the two ferroelectric states are identical and therefore positive and negative fields yield the same result. Thus, the P_s values in this thesis are either quoted separately or as the addition of one driven and one relaxed peak.

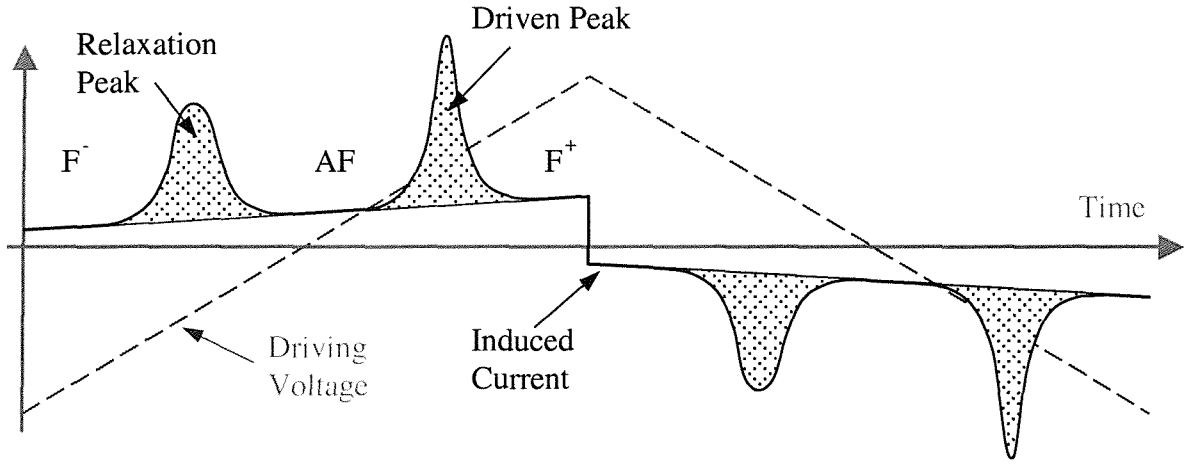

Figure 3.14 A schematic showing the twin peak spontaneous polarisation response of an antiferroelectric liquid crystal.

In the absence of an electric field, the SmC^*_A phase has no macroscopic tilt. The application of a sufficiently large bipolar square wave will switch it between its two fully induced ferroelectric states. This induced tilt can be measured in the same manner as that of the normal ferroelectric phase as described earlier.

The measurement of response time also requires a distinction between the switching processes. A monopolar square wave pulse will cause a switch into a ferroelectric state, followed by a relaxation. Unlike a normal ferroelectric this gives two distinctly different times, a τ_{on} and τ_{off}. An alternative is to drive the switch with a sufficiently large bipolar square wave, as with the tilt, and measure the response time of the fully driven switch.

3.4.5.1 Higher Order Smectics

The switching characteristics of the SmI* and SmF* phases are more complex due to the hexatic molecular arrangement in the layers. Unlike the SmC* phase in an SSFLC cell, where the molecules switch with bistability around the cone, the hexagonal arrangement can yield four different optically switched states[45]. In an SSFLC geometry with a large chevron effect, the SmI* phase has been reported to have as many as eight stable switched states[46].

The current reversal technique relies on a complete reversal of the dipole, and the complexity of the switching process in higher order smectic phases yields multiple overlapped peaks that are difficult to

analyse. The tilt and response measurements are similarly affected[47]. The higher viscosity of the hexatic phases can also create other difficulties for electro-optic measurement. Although the results can be confusing, they can be used as an identifier for a change of mesophase in cases where textural changes are indistinct.

3.5 Other Analytical Techniques

3.5.1 Light Scattering – Dynamic and Raman

Although the lowest energy configuration in a liquid crystal is that of uniform director alignment, the director still fluctuates due to the thermal energy of the material. Many of these fluctuations are on the visible wavelength scale, and lead to the characteristic turbidity of some liquid crystals. This has many effects on the properties of a sample, making light scattering a valuable investigative technique. The transmitted intensity of light incident on a turbid liquid crystal is related to the mean square of the fluctuation amplitude, and the angle dependence of the scatter is governed by the fluctuation correlation length. Analysis of the spectrum of scattered light is used in Dynamic Light Scattering and can provide information on the viscosity coefficients, which is especially effective when studying nematic phases. Raman scattering makes use of inelastic scattering due to vibrational excitement of the molecular normal modes. Measurements of the scattered light yield information on the local molecular organisation and order[48].

3.5.2 Techniques for Measuring Refractive Index

The measurement of refractive indices can be achieved by several methods, all of which require a well-aligned film. The use of a refractometer treated with a suitable alignment layer allows one of the easiest methods for measuring refractive indices in nematic and SmA phases, but the measurement is not as simple with the more complex SmC phases. Measurements within the group are carried out using a Bellingham and Stanley 60/HR Abbé refractometer[49]. A homeotropic alignment is required, in this case lecithin is chosen because it can be easily removed from the experimental optics. The use of lecithin in conjunction with water heating limits the upper range of measurements to ~80°C.

3.5.3 Absorbance

As mentioned previously, the Olympus microscope setup allows the use of a fibre spectrometer arm. This was built by B. Musgrave and utilises an Ocean Optics S2000 fibre optic spectrometer[50]. This apparatus has a CCD array with a resolution of 1 nm across the range 300-800 nm. The detector is coupled to a desktop computer via an internal card allowing the collected spectrum to be software-analysed.

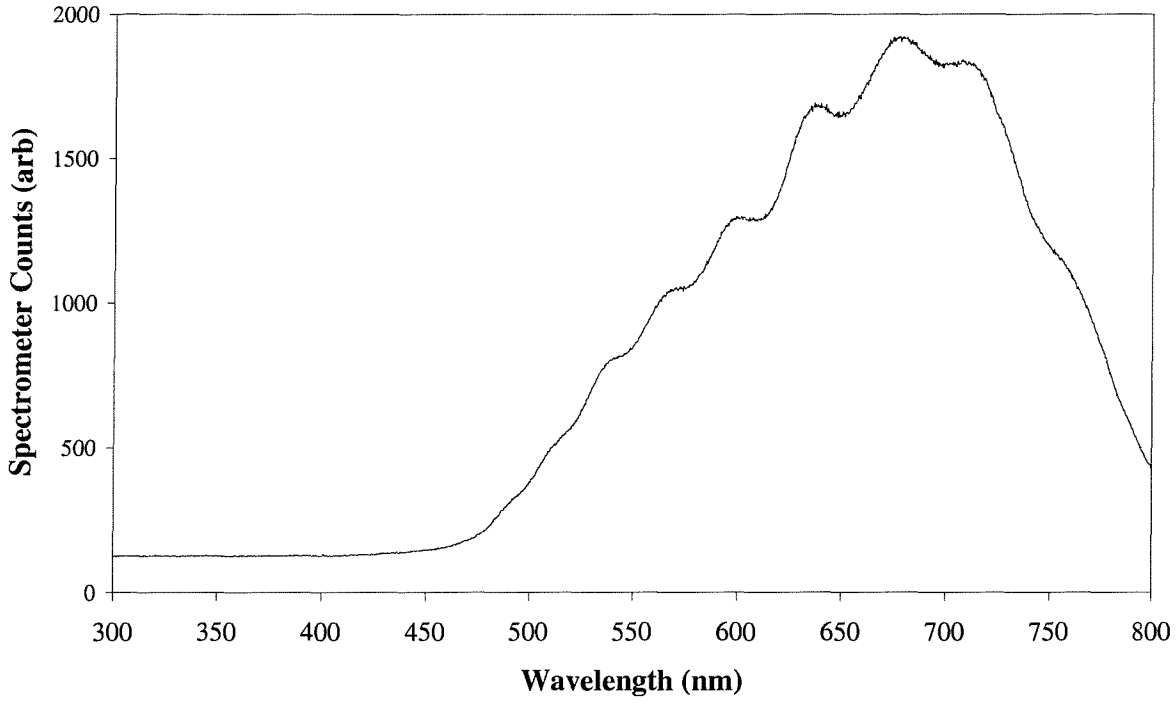

Figure 3.15 Spectrometer measurement of the Olympus Microscope bulb emission spectrum.

An example of a reading is seen in Figure 3.15, which shows the raw data obtained when measuring the spectrum of the microscope bulb. Reference signal readings are then taken to compensate for the spectral response of the CCD array and the non-uniform emission spectrum of the light source. The use of a reference spectrum allows the raw data of subsequent measurements to be corrected so that the absorption and transmission spectra can be calculated. The use of a microscope setup is advantageous as it allows the sample to be monitored visually and measurements can also be made in reflection mode.

A wider and better resolved spectral range is available for transmission measurements from the Hewlett Packard 8453 UV-Visible spectrometer[16] discussed earlier in §3.3.4. In order to control cell temperature, a Mettler[18] FP82 heating stage is placed in the spectrometer which is capable of generating temperatures from ambient to 120°C via a Mettler FP80 controller. The heating block is double-sided to ensure good thermal stability and to hold the cell in place. Great care is taken to ensure the cell is placed centrally and normal to the beam path axis. The spectrometer is capable of a 0.1 ms scan speed and thus can be used to monitor slow switching, however, the inability to observe the cell in situ makes the microscopy method preferable in some cases.

The UV-Visible spectrometer is ideal for measuring absorbance spectra of samples of liquid crystal and dye compounds. The Lucid cells used widely in this work strongly absorb UV light (because of their glass substrates) and this causes a problem when trying to evaluate the UV characteristics of a sample such as a dye. In order to observe high quality spectra, very weak solutions are made ~0.01 M

in a suitable solvent, usually DCM. The samples are placed in special cuvettes that have low absorbance across the UV and visible spectral ranges. The absorbance of a particular dye is governed by the Beer-Lambert law,

$$A_{dye} = \varepsilon cd = \log_{10}\left(\frac{I_0}{I_T}\right), \qquad 3.11$$

where I_0 is the intensity of the incident light and I_T is intensity of the light transmitted through a sample of concentration c and thickness d. The molar absorption coefficient ε represents the efficiency of a dye's absorption. This value is normally quoted at its peak wavelength and a "good" dye can have an absorption efficiency of $\geq 10^4 Lmol^{-1}cm^{-1}$.

3.5.4 Differential Scanning Calorimetry

Known commonly as DSC, Differential Scanning Calorimetry is a very powerful technique for determining transition temperatures and heats of transition. Rather than simply determining the energy needed to heat and cool a sample, DSC exploits the difference in energy requirements of maintaining a sample at the same temperature as that of a reference. A Perkin-Elmer DSC7[51] is connected via a TAC 7/DX controlling unit to a computer to allow recording and software analysis of results. The accuracy of the technique relies heavily on the calibration of the experiment which can take several hours; it is therefore often practical to analyse multiple batches in one session. The apparatus has two main parts, the head where the samples are held and the glove box where they are loaded. Both parts have oxygen free, dry nitrogen gas to purge them. The use of a refrigeration unit gives the head a temperature range of -70°C to 300°C. Prior to calibration, the cooler and gasses are turned on and the system left to stabilise for around three hours. The experiment is calibrated with the solid-fluid transitions of gallium (T_{fusion}=29.78°C) and indium (T_{fusion}=156.60°C, $\Delta H = 28.45 Jg^{-1}$).

Samples are weighed in specially designed, lightweight aluminium pans on the Mettler-Toledo AG245 balance. These are then sealed with a crimping tool. The samples are heated with respect to a reference, which in this case is simply a sealed empty pan. Due to the sensitive nature of the experiment, great care is taken to avoid contaminating the sample head and pans, thus all operations are carried out in a semi-clean cell preparation room. Sample sizes in this work are typically in the range 3-4 mg. An initial heating run is always carried out to make certain the sample is melted into the pan and to ensure a constant thermal history. The sample temperature is then cycled a number of times over the region of interest. Heating and cooling runs are performed in order to expose any monotropic phases with typical heat/cool rates of $5°Cmin^{-1}$. The amount of energy required to keep the sample and reference at a constant heating rate is recorded by the computer, and a plot of endotherms and exotherms is generated. An example thermograph is shown in Figure 3.16 for the compound SCE13. This trace shows a heating run, with positive melting peaks (upper curve) and a cooling run with negative endothermic peaks (lower curve).

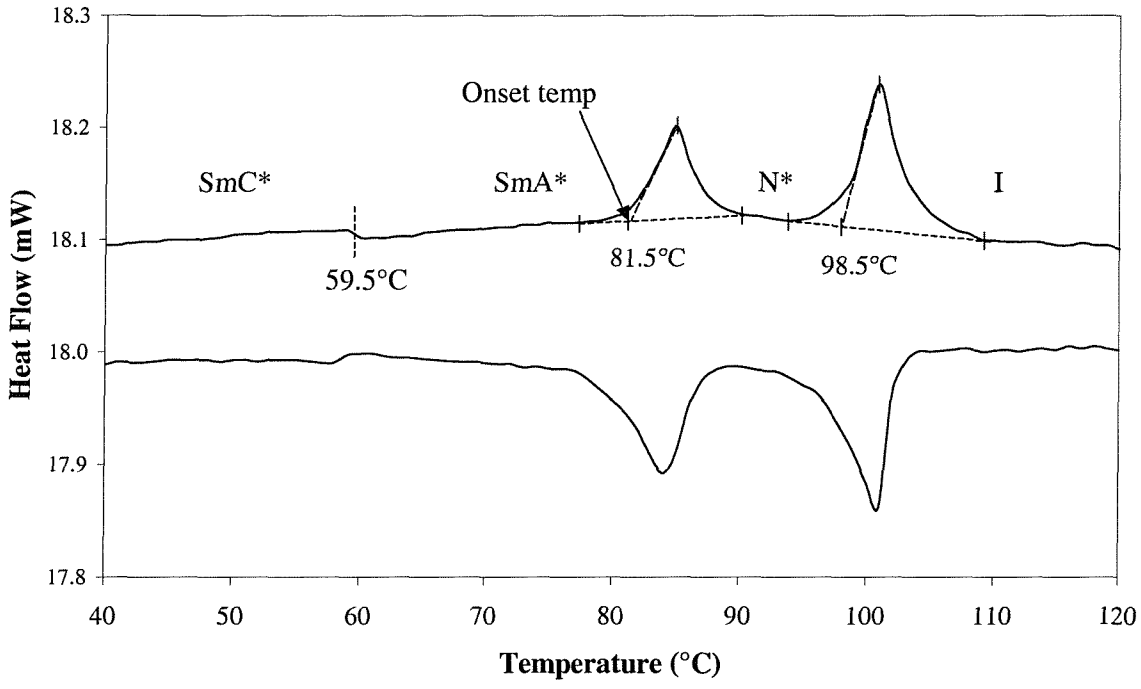

Figure 3.16 A typical DSC trace for the compound SCE13

3.5.4.1 Interpretation

First order phase transitions are characterised by discontinuous jumps in the first derivative of free energy, resulting in a discontinuity in the enthalpy (H) at the transition temperature. Second order transitions are continuous in enthalpy but show a specific heat capacity, C_p, and thus will not be seen on the DSC trace as there is no latent heat associated with the transition. However, as discussed in the previous chapters, liquid crystal transitions such as SmA*↔SmC* are not fully second order and sometimes will show a small heat of transition. This small heat of transition can be made more prominent if the run speed is increased and the approximate area of the transition is focussed upon. In Figure 3.16 the SmA*↔SmC* transition is just identifiable at 59.5°C. The largest peaks are typically associated with enthalpy changes at the crystal melt.

First order transition temperatures are measured at the point of the intersection of the baseline with the extrapolation of the first inflection of the onset of the latent heat peak, as shown in Figure 3.16. The onset temperature is quoted in preference to the temperature of the peak maximum as the value is more reproducible and less dependent on sample size and heating rate. The degree of accuracy is determined by the quality of the peak and baseline, and this varies between samples. Factors affecting the accuracy of the onset temperature measured include the purity of the sample, the thermodynamic nature of the transition and any pre-transitional effects. Although the curve inflection point is computer-determined, it is based on the operator's choice of baseline limits, which can have a significant effect on the accuracy of the result. Enthalpy values are similarly affected by the choice of limits because they are calculated by measuring the area bounded by the peak and the chosen baseline by software integration.

DSC is particularly useful when examining polymer transitions which are not always easily identified visually and can be used to detect the glass transition characteristics of the polymer backbone. A glass transition typically shows up as a discontinuity in the baseline and is measured at the midpoint between the tangents of the initial and final baselines. While mesophase-mesophase and isotropic-mesophase transitions characteristically show little supercooling, a large amount of supercooling is often seen at the mesophase–crystal transition and in such cases, results are very dependent on the cooling rate.

In comparison with measurements from the heating-stage/microscope setup, sample equilibrium and temperature accuracy are far higher. This results in very accurate trace reproducibility, although the need to extrapolate the baseline introduces typical uncertainties of ±0.5°C for a first order transition and ±0.3 Jg^{-1} for an enthalpy of transition. DSC is used as a complementary technique to thermo-optic polarising microscopy observations. The transition temperatures returned by the two methods can differ slightly due to the effects of alignment layers and boundary conditions. Anchoring effects can increase a sample's stability and raise its phase transition temperatures. Although heating-stage calibrations are not as regularly checked as the DSC, the use of a shifted temperature scale can normalise measurements made by both techniques. DSC traces are chiefly used to determine latent heats and transition temperatures, and by giving an indication of the order of a transition, can sometimes assist with phase identification when explicit identification via microscopy is not possible. This additional information is particularly important for a transition where no texture change is seen or when a transition such as a recrystallisation or melting point is difficult to accurately identify optically. It is important to note that not all optical transitions correspond to a phase transition, and conversely, that a change in optical texture is not always seen at every phase transition.

3.5.5 X-Ray

X-ray diffraction is widely used to probe structural ordering. Electrons within a sample scatter the incident radiation, yielding an intensity distribution corresponding to the spatial Fourier transform of the molecular structure. The sharp peaks produced by a well-defined crystal are related to the structure's reciprocal lattice and can allow the calculation of the molecular or atomic spacing. An isotropic fluid has no crystalline order and therefore produces no sharp diffraction pattern. A liquid crystal mesophase yields a diffraction pattern of peaks and broad bands that give an idea of the type and level of order present. The two main types of x-ray diffraction experiment applicable in liquid crystal studies relate to aligned and unaligned samples.

Samples aligned by surface forces or externally applied fields allow precise structural studies to be carried out because the diffraction pattern obtained is very detailed. X-ray diffraction experiments can require samples 0.5 mm thick. It is difficult to create an aligned sample of such a thickness by

surface interactions, and the use of an external field complicates the experiment. It easier to perform unaligned powder diffraction experiments, in which the liquid crystal is held in a capillary tube with a 0.5mm bore. This method is derived from use with crystals and relies on fundamental parameters such as layer-spacing to form a diffraction pattern. When used for liquid crystals this negates the need for complex alignment and is thus widely used. The results obtained in this work are all from powder diffraction experiments.

A smectic phase will yield broad Bragg peaks due to its layered structure. These peaks are broader and weaker than those produced by a crystal and often only the first two orders are seen. The Bragg spacing can then be used in conjunction with the molecular length calculated using computer modelling to assess the form of the layer ordering and degree of interdigitation and to obtain an estimate of the steric tilt angle. If a sample exhibits both a SmA and SmC phase, the tilt can be estimated from the reduction in layer spacing in the SmC phase. Skilful interpretation of the diffraction pattern can often be used to infer the nature of the phase, however, it is difficult to distinguish between a SmA and SmC phase if only one of these phases is present. Smectic hexatic phases are characterised by extra peaks in the spectrum caused by their increased ordering, while the sharper structures of the crystal hexatic phases produce further peaks.

3.6 PHASE CHARACTERISATION

The first stage of assessing a new compound is to establish the transition temperatures and mesophases present. Initially, a simple cell, made by placing the sample between two cover slips, is placed on the heating-stage of the microscope between crossed polarisers. Textural changes observed during a quick heating and cooling run will give approximate values for the transitions. The sample can then be more slowly scanned to give more accurate readings. This is also a good time to gauge the sample's purity by examination of the width of any biphasic regions. Biphasic regions of 5-10°C in width are a good indicator of the presence of impurities.

3.6.1 Optical Texture

While the optical textures of liquid crystals are often characteristic of particular phases, they can sometimes be paramorphotic, which means that after a phase transition the texture retains features of the preceding phase. This memory can complicate phase identification. For consistency most phase classification is carried out on cooling. Studying textures on cooling allows the first phase encountered to form a natural texture, although the textures of underlying phases may be affected by its structure. The formation of a mesophase from the isotropic phase gives many clues to its nature. Texture reference books such as those by Demus and Richter[52] and Gray and Goodby[53] can be used as aids in the identification of mesophases from characteristic textures. In this section some of the

individual characteristics of the thermotropic calamitic mesophases are described. These are all viewed between crossed polarisers unless otherwise specified. Thus, the isotropic phase is dark in any alignment state due to its lack of birefringence. The use of an unprepared cover slip is important because many of the characteristic textures of the mesophases outlined in this section are best seen when the alignment is disrupted by boundary surface defects. Planar and homeotropic alignment layers are also used in shearing and wedge cells to aid mesophase identification.

3.6.1.1 Nematic Textures

The mesophase forms as rounded droplets from the isotropic phase demonstrating the low viscosity, fluid nature of the phase. In uniaxial achiral nematics the optic axis lies parallel to the director and thus if the texture forms a fully planar orientation, a uniform birefringence colour is seen. An imperfect planar alignment reveals a texture consisting of a network of dark "brushes" ending at point disclinations, and is called a schlieren pattern. The dark, irregularly curved brushes correspond to areas where the director is parallel to the extinction positions of the polariser or analyser. It is always the case that either two or four brushes intersect at the disclination points. These points occur at singularities in the structure. The disclination points are referred to as $S = \pm ½$ or ± 1 junctions respectively, where the parameter S indicates the "strength" of the disclination, and $|S|$ = no. of brushes/4. Full homeotropic alignment on the other hand causes complete extinction between crossed polarisers as the optic axis aligns normal to the cell walls. No birefringence effects are observed, which demonstrates the uniaxial nature of the phase. If this homeotropic alignment is disturbed, by pressing the cover slip for example, bright flashes are seen. Figure 3.17a shows 5CB exhibiting the characteristic nematic droplets forming from the extinct background of the isotropic phase. Figure 3.17b shows the schlieren pattern of 5CB, with two and four point defects.

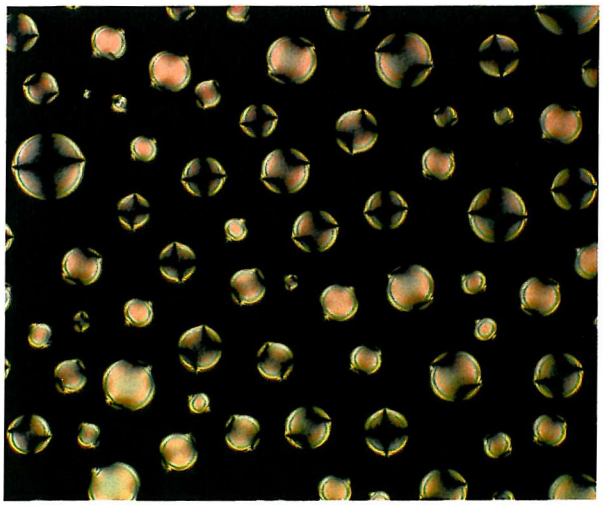

a) Droplets forming from the isotropic phase

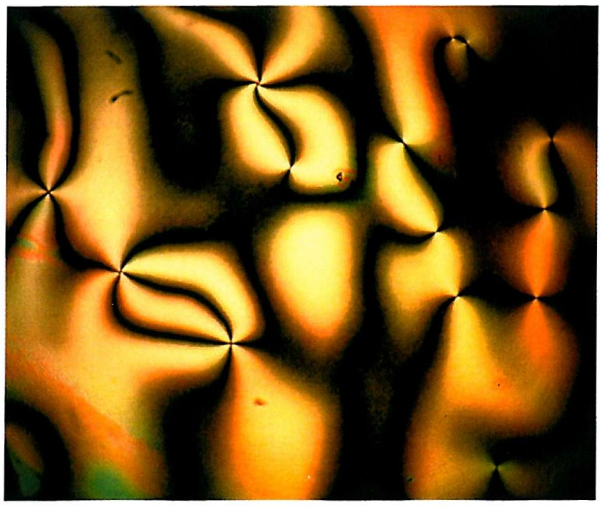

b) Schlieren texture with two and four point defects

Figure 3.17 Photomicrographs of typical nematic textures of 5CB at 50x magnification.

3.6.1.2 Chiral Nematics

The added complexity of the chiral structure causes more complicated defects to appear in the chiral nematic phase than are observed in the nematic mesophase. As with the achiral nematic phase, circular droplets of chiral nematic phase form on cooling from the isotropic melt. A disturbed structure can exhibit oily streak defects, and formation of a focal conic structure is also possible (see smectic phases below). A homeotropic alignment layer causes the helix to lie parallel to the substrates, and in long pitch mesophases (pitch>1 μm) gives rise to a fingerprint structure. This structure is demonstrated by SCE13 in Figure 3.18a. Shearing promotes a planar alignment of the molecules and a standing helix configuration, resulting in what is called the Grandjean texture. When confined in a wedge cell treated with planar alignment layers, a Grandjean texture shows a series of steps corresponding to a discontinuous change of the number of turns of the helix. An example is shown in Figure 3.18b examining the compound 7CB doped with a chiral additive to induce the N* phase. Due to surface anchoring the pitch is forced to lengthen with increasing sample thickness until the deformation energy becomes too high and a disclination line forms allowing the number of helical turns to increase by ½ and thereby introducing a discontinuous change of pitch.

a) Fingerprint texture *b) Grandjean Texture*

Figure 3.18 Typical chiral nematic textures of a) SCE13 and b) 7CB doped with a chiral additive.

3.6.1.3 The Smectic A Phase

At the transition from the isotropic melt, the SmA phase is characterised by the formation of elongated bâtonnets as shown in Figure 3.19a. Due to the necessity of maintaining layer integrity, the only allowed elastic deformation of smectic layers is the splay deformation. Energy minimisation causes the bâtonnets to form a "cooling tower" type structure due to the effects of circular splay. This packing of the layer structure gives a system of curved equidistant layers that correspond to geometrical figures called Dupin cyclides[53]. These coalesce to form the focal-conic texture observed

in thin samples as shown in Figure 3.19b. In thick samples, the focal-conic texture is characterised by dark lines outlining ellipses and hyperbolae, as shown in Figure 3.19c. Shearing the cover glass encourages a homeotropic alignment as the layer planes slide over one another and form parallel to the plane of the substrates. The optic axis of the phase lies parallel to the direction of light propagation and extinction is seen. Disturbing the cover slip does not cause the texture to flash, differentiating this homeotropic texture from that of the nematic phase. A schlieren texture can also form but will contain only four brush defects (S ± 1).

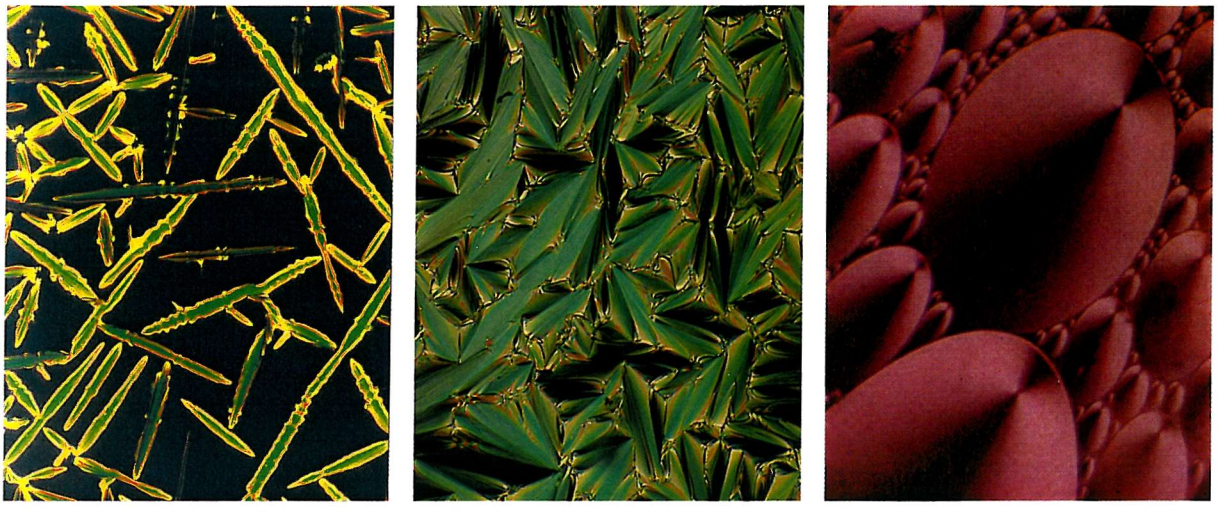

a) Bâtonnets *b) Focal Conic* *c) Ellipses*

Figure 3.19 Different textures exhibited by SmA materials.

3.6.1.4 The Smectic C Phase

The SmC phase can show very similar textures to the SmA phase, and when formed directly from the isotropic melt the two can be indistinguishable. If a SmC phase forms below a SmA phase, the focal-conic texture becomes distorted, the fans are seen to break and some banding may also be observed. In comparison to a SmA phase, the fans are less regular and are distorted by additional disclinations. This change is demonstrated in the photographs shown in Figure 3.20; note that the same part of the sample is shown in both pictures. While the banding of the SmC* fans is clearly seen in this case, the transition is not always this obvious.

As with the SmA phase, shearing encourages the layers to lie parallel to the substrates. However, the tilt of the molecules prevents the light (travelling perpendicular to the cell) from propagating along the optic axis. Thus, unlike the SmA phase, the SmC phase cannot display an optically extinct homeotropic texture. In a SmC* phase aligned with its layer planes parallel to the substrates, the precession of the tilt around the helical axis (perpendicular to the layers) means that for light travelling along the axis, the overall tilt angle averages to zero. This is termed a pseudo-homeotropic alignment, and in cases where the pitch length is comparable to the visible spectrum, light can be reflected from the helical structure causing a coloured, petal-like structure to be seen. With poor

alignment a schlieren texture with four brush defects is observed. The SmC* phase has many optical similarities to the N* phase, and in some geometries this can make identification difficult. In the N* phase the director is perpendicular to the helix axis, while in the SmC* phase the director is inclined at the tilt angle with respect to the helix axis. This difference can be probed with oblique transmission or reflection spectra measurements, as was first suggested by Berreman[54]. These techniques alongside others, such as conoscopy allow even apparently identical phases to be distinguished.

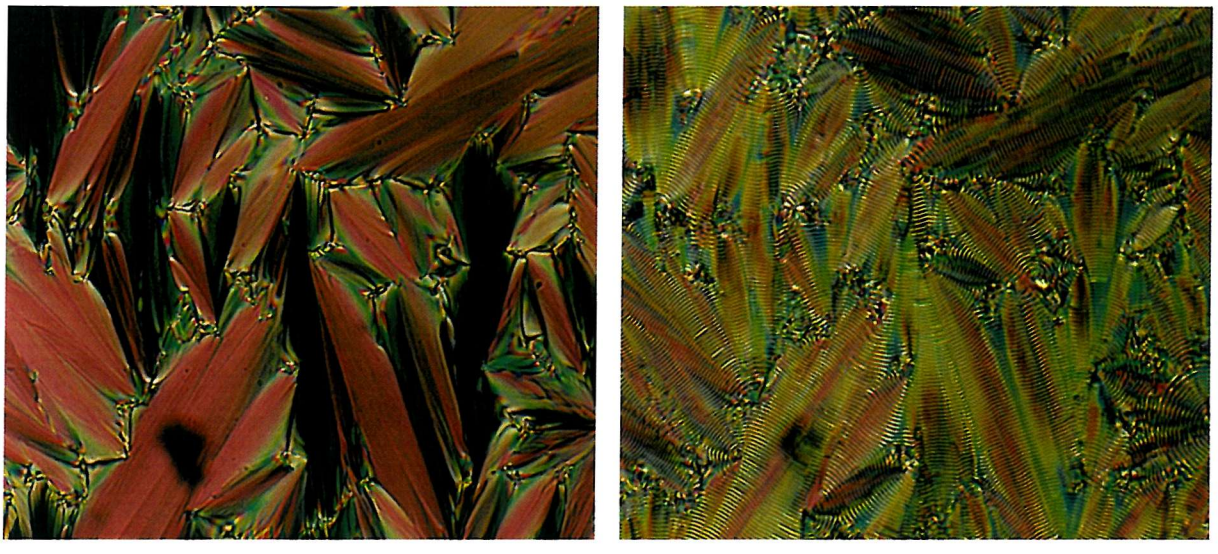

a) SmA Texture* *b) SmC* Texture*

Figure 3.20 Photomicrographs at 50x magnification showing the texture of the same sample above and below the SmA-SmC* transition.*

3.6.1.5 The SmC$_A$ Phase*

Antiferroelectrics differ from the SmA and SmC phases in that there is some evidence that they can exhibit both S = ±½ and ±1 defects[55]. Although it is difficult to uniquely identify the SmC*$_A$ phase by inspecting its texture alone, a transition from the SmC* to the SmC*$_A$ phase is often easily identified in thin planar aligned cells because long stripe shaped domains grow along the smectic layer. In thicker cells, extra focal conic domains can form at the transition[56]. These effects are attributed to the increased strain on the structure due either to the extra antiferroelectric ordering[56] or to the change in layer spacing at the transition[57].

3.6.1.6 Higher Order Phases

Although a lot of information can be gained from simple textural observations, it is often difficult to identify a transition from the SmC* to SmF* or SmI* phases solely from observation of texture changes. The additional hexagonal ordering has only a slight effect on the focal-conic texture and causes additional narrow concentric arcs in the fan shaped domains. The paramorphotic textures can be helpful; the SmI phase shows a blurring effect whereas the SmF phase has a tendency to form mosaic structures that may be seen as an overlaid or background effect in the texture.

3.6.2 Complementary Methods

3.6.2.1 Thermo-optic Analysis

Different phases exhibit varying birefringence levels and so transmit different levels of light when placed between crossed polarisers. Use of the microscope, photodiode and oscilloscope setup allows this sometimes very subtle effect to be magnified. Ideally, observations are made using a narrow wavelength band by employing a light filter. The use of a photodiode allows transmitted intensity to be measured as a function of temperature and can reveal phase transitions not seen by eye. So, for example, for a SmA* to SmC* phase transition the greatest effect is seen with the cell aligned for a minimum transmission in the SmA* phase. The formation of tilt at the transition will change the optic axis and alter the intensity of light transmitted. Figure 3.21 demonstrates this effect in SCE13. The sample is cooled from the isotropic phase and even without careful alignment, the transitions can be seen clearly.

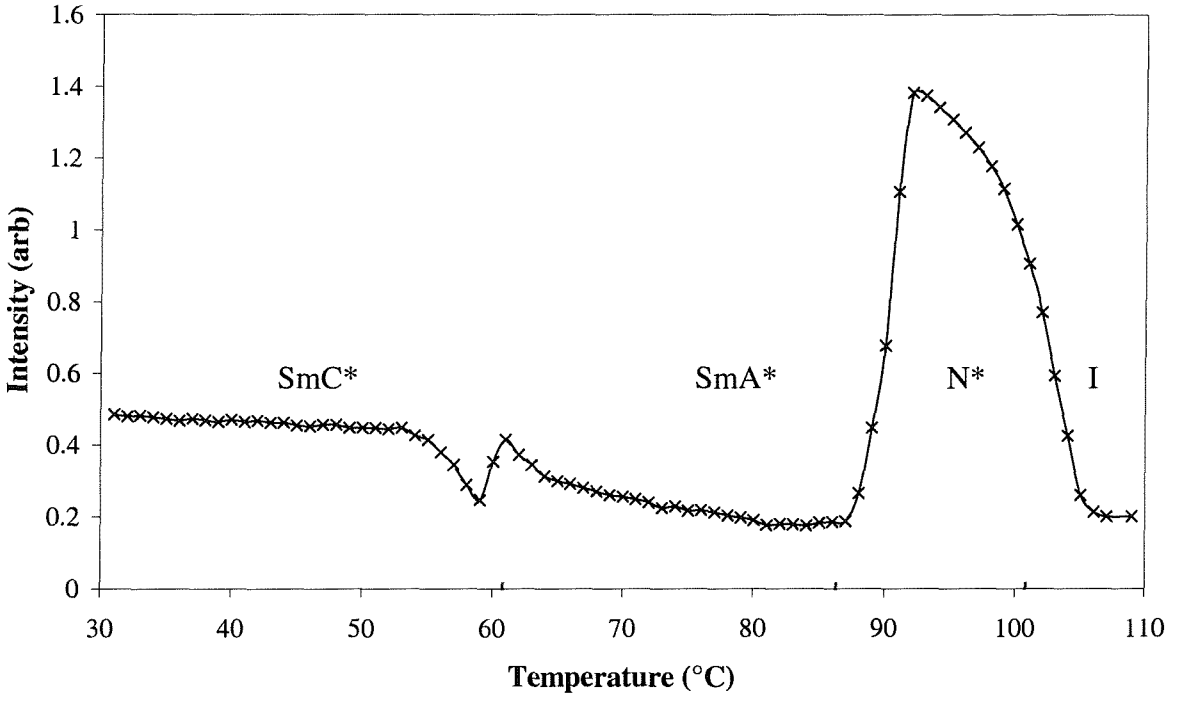

Figure 3.21 A thermo-optic trace for SCE13.

3.6.2.2 Contact Preparation

A contact preparation is a small miscibility study carried out to demonstrate whether two materials mix easily and are isomorphic. A sample of known phase sequence is introduced on one side of a cell with the unknown sample introduced at the other and both allowed to capillary fill the cell. If miscible, diffusion creates a concentration gradient at the interface. If this gradient is smooth and continuous, the two phases can be considered miscible and are likely to be the same. Different phases will show a discontinuity such as a sharp texture change or other disclination demonstrating the

immiscibility of the two phases. Immiscibility with a standard material does not prove the identity of a phase. The method does not provide an absolute proof as it is a reduced version of the more rigorous miscibility studies typically carried out to identify a phase using a large series of mixtures.

3.6.2.3 Field Effects

The effects of electric fields on a sample give many vital clues as to the nature of the phase. The sample is placed in an electro-optic cell (which is normally a prefabricated cell - chiefly for speed, since the cell is sometimes tested to destruction). Initially, low fields are used with an aim to show up any switching and to characterise the phase sequence. The field can then be raised to determine thresholds. Initial measurement of parameters such as tilt can be essential in pinpointing other more subtle transitions. All the electro-optic responses described earlier can give information on phase transitions. Previous work[35] has shown that the measurement of direct parameters, such as the peak height of the current pulse response (I_p^m), can give a rough indication of a phase change in ferroelectrics; the increased complexity in the more ordered smectic phases can allow the observer to differentiate between SmC* and SmI* phases. It is important to note that an applied field can affect the transition temperatures measured; they can be shifted by up to several degrees due to the change in energy of the system. Plotting the driving voltage (x) against the optical transmission (y) reveals a hysteresis trace, which can be crucial in identifying the nature of a switching mechanism[58]. Application of a triangle wave of sufficient magnitude gives rise to a square wave optical response in a suitably aligned ferroelectric material, due to the switching threshold. The corresponding SmA* phase has no threshold in its electroclinic switching and at low fields the optical response follows the applied field.

3.7 SUMMARY

The apparatus that comprises the measurement rig used throughout the thesis has been outlined. The full measurement route has been discussed, beginning with cell fabrication and testing, leading to filling, then sample analysis. The theories of the previous chapter, in particular the switching dynamics are the basis of the main analytical methods for measurement of tilt angle, spontaneous polarisation, switching time and rotational viscosity. These measurements have been demonstrated using the standard ferroelectric compound SCE13. The chapter is completed with a discussion of the many methods of phase characterisation. In the next chapter we will use these techniques to study the latest organosiloxane compounds.

3.8 REFERENCES

[1] Olympus Optical Co. Ltd, Great Western Industrial Park, Dean Way, Southall, Middlesex, UB2 4SB, UK. http://www.olympus.co.uk

[2] Thurlby Thandar Instruments Ltd, Glebe Road, Huntingdon, Cambs, PE18 7DX. UK. http://ttinst.co.uk

[3] Linkam Scientific Instruments Ltd, 8 Epsom Downs Metro Centre, Tadworth, Surrey, KT20 5HT, UK. http://www.linkam.co.uk

[4] IPL 10050CW, Radio Spares No.651-995, Data Pack F 232-3894.

[5] Electronics workshop, Schuster Physics Laboratory, University Of Manchester, Brunswick Street, Manchester, M13 9PL, UK.

[6] E.Hecht, *Optics – 2nd Ed,* **§8.2.1** (Addison-Wesley, 1987).

[7] Wavetek-Datron, Hurricane Way, Norwich, Norfolk, NR6 6JB, UK. http://wavetek-datron.com

[8] Agilent Technologies Ltd, Test & Measurement, Eskdale Road, Winnersh Triangle, Wokingham, Berkshire, RG41 5DZ, UK. http://www.agilent.com

[9] Brainboxes, Unit 3C Wavertree Boulevard South, Wavertree Technology Park, Liverpool, L7 9PF, UK. http://www.brainboxes.com

[10] Borland-Inprise Corp., 100 Enterprise Way, Scotts Valley, CA 95066, USA. http://www.borland.com

[11] B.O.Myrvold, *Mol. Cryst. Liq. Cryst.,* **202**, 123 (1991); *Liq. Cryst.,* **3**(9), 1255, (1988).

[12] J.L.Janning, *Appl. Phys. Lett.,* **21**(4), 173 (1972).

[13] EEV Ltd., Waterhouse Lane, Chelmsford, Essex, CM1 2QU, UK. http://www.eev.com

[14] J.C.Wittmann, P.Smith, *Nature*, **352**, 414 (1991).

[15] S.Meyer, *Thesis*, Université Louis Pasteur, Strasbourg, France (1995).

[16] Supplied by Anachem Ltd., Anachem House, Charles Street, Luton, Beds, LU2 0EB, UK. http://www.anachem.co.uk

[17] Norland Optical Adhesive 81, Norland Products, 695 Joyce Kilmer Av., New Brunswick, N.J., 08902, USA. http://www.norlandprod.com

[18] Mettler-Toledo Ltd., 64 Boston Road, Beaumont Leys, Leicester, LE4 1AW, UK. http://www.mt.com

[19] ISIS Draw 2.3. MDL Information Systems, Building 4 Archipelago, Lyon Way, Camberley, Surrey, GU16 5ER, UK. http://www.mdli.co.uk

[20] J.F.Clerc, *Ferroelectrics,* **85**, 3 (1988).

[21] M.J.Bradshaw, V.Brimmell, E.P.Raynes, *Liq. Cryst.,* **2**(1), 107 (1987).

[22] T.P.Rieker, N.A.Clarke, G.S.Smith, D.S.Parmer, E.B.Sirota, C.R.Safinya, *Phys. Rev. Lett.,* **59**(23), 2658 (1987).

[23] D.Coates, W.A.Crossland, J.H.Morrissy, B.Needham. *J. Phys. D,* **11**, 2025 (1978).

[24] R.Bartolino, J.Doucet, G.Durand, *Ann. Phys,* **3**, 389 (1978).

[25] E.Merck KGaA, Frankfurter Str. 250, D-64271, Darmstadt, Germany. http://www.merck.de

[26] I.G.Wood, A.M.Glazer, *J. Appl. Cryst.,* **13**, 217 (1980).

[27] C.Noot, *Ph.D. thesis (in preparation),* Univ. Southampton, U.K., (2002).

[28] J.Etxebarria, A.Remón, M.J.Tello, A.Ezcurra, M.A.Pérez-Jubindo, T.Sierra, *Mol. Cryst. Liq. Cryst.,* **150b,** 257 (1987).

[29] L.M.Blinov, L.A.Beresnev, N.M.Shtykov, Z.M.Elashvili, *J. de Phys. (Paris),* **40**(4), C3-269 (1979).

[30] L.M.Blinov, V.A.Baikalov, M.I.Barnik, L.A.Beresnev, E.P.Pozhidayev, S.V.Yablonsky, *Liq. Cryst.,* **2**(2), 121 (1987).

[31] C.B.Sawyer, C.H.Tower, *Phys. Rev.,* **35**, 269 (1930).

[32] H.Diamant, K.Drenck, R.Pepinsky, *Rev. Sci. Instrum.,* **28**(1), 30 (1957).

[33] Ph. Martinot-Lagarde, *J. de Phys. (Paris),* **38**, L17 (1977);

[34] K.Miyasato, S.Abe, H.Takezoe, A.Fukuda, E.Kuze, *Jpn. J. Appl. Phys.,* **22**(10), L661 (1983).

[35] H.Walton, *Ph.D. Thesis,* University of Manchester (1994).

[36] W.Robinson, *Ph.D. Thesis,* University of Manchester (1995).

[37] K.Skarp, M.A.Handschy, *Mol. Cryst. Liq. Cryst.,* **165**, 439 (1988).

[38] P.C.Willis, N.A.Clark, C.R.Safinya, *Liq. Cryst.,* **11**(4), 581 (1992).

[39] F.Gießelmann, A.Heimann, P.Zugenmaier, *Ferroelectrics,* **200**, 237 (1997).

[40] Z.Zou, N.A.Clark, M.A.Handschy, *Ferroelectrics,* **121**, 147 (1991).

[41] S.Kimura, S.Nishiyama, Y.Ouchi, H.Takezoe, A.Fukuda, *Jpn. J. Appl. Phys.*, **26**(4), L255 (1987).
[42] V.M.Vaksman, Y.P.Panarin, *Mol. Mats.*, **1**, 147 (1992); M.Nakagawa, *Mol. Cryst. Liq. Cryst.*, **173**, 1 (1989).
[43] C.Escher, T.Geelhaar, E.Böhm, *Liq. Cryst.*, **3**(4), 469 (1988).
[44] M.R.de-la-Fuente, A.Ezcurra, M.A.Pérez-Jubindo, J.Zubia, *Liq. Cryst.*, **7**(1), 51 (1990).
[45] T.Uemura, Y.Ouchi, K.Ishikawa, H.Takezoe, A.Fukuda, *Jpn. J. Appl. Phys.*, **24**(4), L224 (1985).
[46] R.Shao, Z.Zhuang, N.A.Clark, *Ferroelectrics*, **122**, 213 (1991).
[47] I.Dierking, F.Gießelmann, J.Kußerow, P.Zugenmaier, *Liq. Cryst.*, **17**(2), 243 (1994).
[48] S.Meyer, H.J.Coles, *Mol. Cryst. Liq. Cryst.*, **331**, 27 (1999).
[49] Bellingham & Stanley Ltd, Longfield Road, Tunbridge Wells, Kent. TN2 3EY. UK. http://www.bs-ltd.com
[50] B.Musgrave, *Ph.D. Thesis*, University of Southampton (2000); Ocean Optics Inc., 380 Main Street, Dunedin, FL 34698, USA. http://www.oceanoptics.com/
[51] Perkin-Elmer Ltd, Post Office Lane, Beaconsfield, Bucks. HP9 1QA, UK. http://www.instruments.perkinelmer.com
[52] D.Demus, L.Richter, *Textures of Liquid Crystals*, (Verlag Chemie, 1978).
[53] G.W.Gray, J.W.G.Goodby, *Smectic Liquid Crystals: Textures and Structures*, (Leonard Hill, 1984).
[54] D.W.Berreman, *Mol. Cryst. Liq. Cryst.*, **22**, 175 (1973).
[55] Y.Takanishi, H.Takezoe, A.Fukuda, H.Komura, J.Watanabe, *J. Mater. Chem.*, **2**(1), 71 (1992).
[56] M.Johno, Y.Ouchi, H.Takezoe, A.Fukuda, K.Terashima, K.Furukawa, *Jpn. J. Appl. Phys.*, **29**(1), L111 (1990).
[57] A.Suzuki, H.Orihara, Y.Ishibashi, Y.Yamada, N.Yamamoto, K.Mori, K.Nakamura, Y.Suzuki, T.Hagiwara, I.Kawamura, M.Fukui, *Jpn. J. Appl. Phys.*, **29**(2), L336 (1990).
[58] C.Reynaerts, A.deVos, *J. Phys. D*, **22**, 1504 (1989).

Chapter Four

Low Molar Mass Organosiloxanes

One should not pursue goals that are easily achieved.
One must develop an instinct for what one can just barely achieve through one's greatest efforts.

Albert Einstein 1879-1955

4.1 INTRODUCTION

Much of the work in this thesis is based around an investigation of the properties of a new series of low molar mass organosiloxane liquid crystal compounds. These compounds are synthesised in-house and are the result of an evolution in synthesis and electro-optic testing within the group over the past 5-10 years. The development of the materials from polymer and low molar mass systems is discussed. The compounds in this work are built around a common unit. This unit, or precursor, is responsible for the liquid crystalline nature of the materials. Following an examination of the basic precursor unit, this chapter examines the characteristic tilt angle, spontaneous polarisation, switching time, and viscosity of some of the latest ferroelectric and antiferroelectric organosiloxane materials.

4.2 MULTI-COMPONENT COMPOUNDS

It is common in liquid crystal fabrication to combine different units in the hope of realising a compound exhibiting the preferential properties of its component parts. Any chemical group usually associated with the formation of liquid crystal phases is known as a mesogenic unit. The compounds synthesised within the Southampton Liquid Crystal Group contain low molar mass mesogenic units attached to polymer-like siloxane head groups.

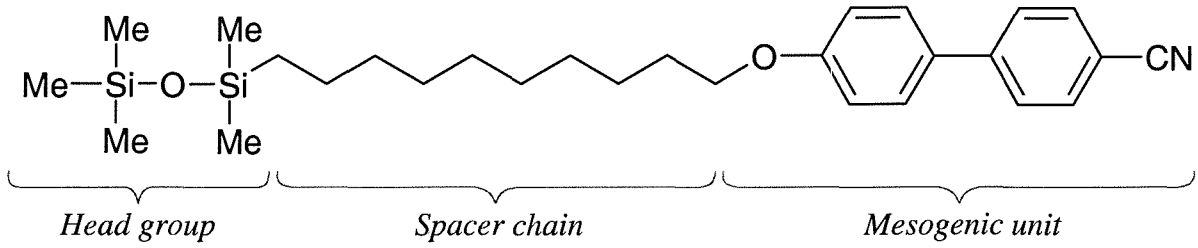

Figure 4.1 A schematic of a multi-component compound.

A typical multi-component structure is illustrated in Figure 4.1. A mesogenic unit is attached to a siloxane head group by an alkyl spacer chain. The compound is designed to combine the properties of its two components; the mesogenic unit is chosen for its ability to produce preferential parameters such as a fast switching time, high tilt and high spontaneous polarisation, while the siloxane unit, typically found in polymers, favours the formation of smectic phases.

4.2.1 Polymer Systems

The development of ferroelectric compounds has led to materials with exceptionally short switching times, making large, fast, ferroelectric displays a possibility. However, the complex process required to align the materials makes the final device fragile and susceptible to shock and damage by

deformation. One possible solution to the problem of device fragility is the use of polymers[1] as the long polymer chains stabilise the structure and alignment against deformation. Although they can be harder to align initially, owing to their increased viscosity compared to low molar mass liquid crystals, polymers are more rugged and have greater shock resistance[2]. The development of polymer liquid crystals for display work is a recent phenomenon. Although the first polymeric mesophase was seen in the lyotropic tobacco mosaic virus by Bawden and Pirie in 1937[3], it is only in the past twenty years that controllable optically active polymers have been reported for device applications[1,2,4].

One common problem in polymer synthesis is that in any end product there can be a range of molecular weights; this is known as polydispersity. A side effect of polydispersity is that there can be a biphasic region below the isotropic phase. Control of polydispersity is difficult in linear structures. One important and useful feature of polymer liquid crystals is their ability to undergo a glass transition. Polymers typically exhibit a glass transition on cooling because the polymer backbone freezes, no molecular re-orientation occurs and the compound enters a glassy state. Thus, incorporating a polymer into a liquid crystal system can both broaden the mesophase range and improve the mechanical properties[5,6]. There are two main types of commercially available polymer, called main chain and side chain polymers, and these are described in the following sections.

4.2.1.1 Main Chain Liquid Crystal Polymers

In a main chain liquid crystal polymer, the mesogenic unit is built into the backbone as shown in Figure 4.2. The mesophase is formed as a zigzag arrangement of the backbone allows the moieties to align and form liquid crystal mesophases. Once oriented in the liquid crystal state, the order can be frozen in by cooling the polymer to below the glass transition temperature. A good example of commercial utilisation of main chain polymer liquid crystal order is the production of high modulus fibres, and products such as Kevlar. Main chain liquid crystal polymers are often highly viscous and are not usefully optically active. For display applications, the focus turns to side chain liquid crystal polymers.

4.2.1.2 Side Chain Liquid Crystal Polymers

In side chain liquid crystal polymers, mesogenic units are attached to the polymer backbone via pendent spacer groups (see Figure 4.2). The pendent spacer groups are used to decouple the mesogenic moieties from the backbone and can often allow the resultant polymer material to retain some or all of the pendent side group's liquid crystalline properties[7]. Work by Finkelmann et al.[7] demonstrated the potential of thermotropic side pendents to form smectic phases. Side chain liquid crystal polymers enhance smectic phases due to their inherent lamellar nature. In the mesophase, the pendent side chains interdigitate, and the backbone gives the phase a high degree of stability.

The properties of the liquid crystal phase are governed by the physical parameters of the units making up the side chain liquid crystal polymers. Typically, a longer backbone yields higher transition temperatures. The viscosity is extremely temperature dependent and scales as a power law with molecular weight; hence longer chains give slower switching times[8]. Three typical backbone units are shown in Figure 4.2, where R denotes a possible position for attaching a mesogenic unit. The flexibility of the backbone increases from polymethacrylates to polyacrylates to polysiloxanes. This trend results in lower glass transitions for simple backbone derivatives, from around 60°C in polymethacrylates to –123°C in polysiloxanes. The large degree of rotational freedom exhibited by the Si-O bond gives polysiloxane backbones some of the lowest polymer viscosities[9] and is therefore often used to encourage room temperature mesophases. However, despite the flexibility of the backbone and decoupling chains, movement of the moieties is still restricted since the backbone functions as an anchor. Although side chain liquid crystal polymers exhibit high viscosities, they still have many potential applications; these range from variable transmission devices based on the ability of the liquid crystal to scatter light[10], to dye guest host devices[11].

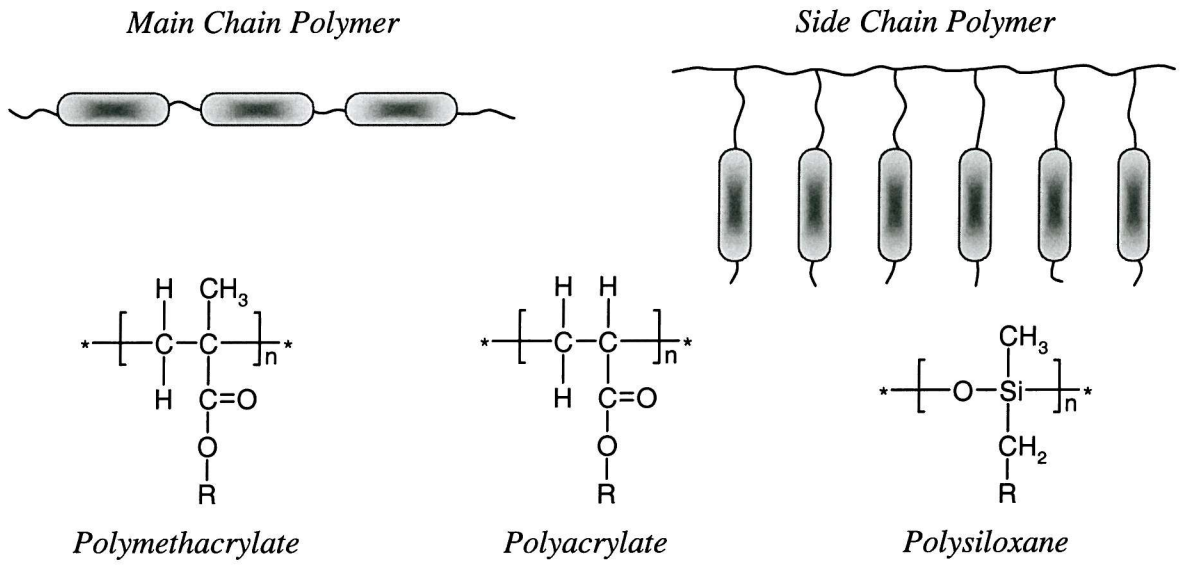

Figure 4.2 A schematic of different polymer structures.

4.2.2 Low Molar Mass Compounds

Low molar mass refers only to the mass of the molecule in comparison to a polymer and does not give any information about the shape or activity of functional groups. When comparing low molar mass materials and side chain liquid crystal polymers, many similarities are seen[12], such as their electro-optic switching effects and phase ranges. LMM materials consist of small molecules, and consequently have a dynamical response that is one or two orders faster than that of many polymers.

4.2.3 Low Molar Mass Organosiloxane Liquid Crystals

Side chain liquid crystal polymers have long been a subject of research interest in the group[1]. Polymers have been mixed with low molar mass materials in attempts to realise a mixture with preferential properties of both components[6]. This work was evolved by combining low molar mass and polymeric moieties in a single molecule. The addition of a head group, consisting of a short chain of homologous dimethyl siloxane units, onto a mesogenic unit has been shown to encourage a significant stabilisation of phase properties and broadening of the mesophase. This addition has resulted in low molar mass mono-mesogenic compounds that show a tendency to build a polymer-like backbone[13,14]. The siloxane head groups micro-phase separate, resulting in a structure similar to a fully-joined side chain liquid crystal polymer. This structure strongly encourages the formation of smectic phases. Thus, even when typical nematogenic moieties, such as cyanobiphenyls, form the decoupled moiety, a layered smectic phase is usually formed[15]; an example molecular structure of such a compound was shown in Figure 4.1.

Micro-phase separation is considered to cause the formation of a 'virtual' or 'pseudo' backbone. The backbone effect confers polymer ruggedness on the mesophase[16], while retaining the rapid response of low molar mass liquid crystals to electric fields. The siloxane units increase the 'flow' viscosity of a system, giving added shock resistance. The effect of the virtual backbone should not adversely affect the phase transitions and switching times in the same manner as a fully-linked side chain polymer backbone, due to the absence of covalent bonds between the microphase separated siloxane groups, which means that they are relatively flexible. Such organosiloxane materials are found to have properties typical of low molar mass liquid crystals such as low micro and macroscopic viscosities.

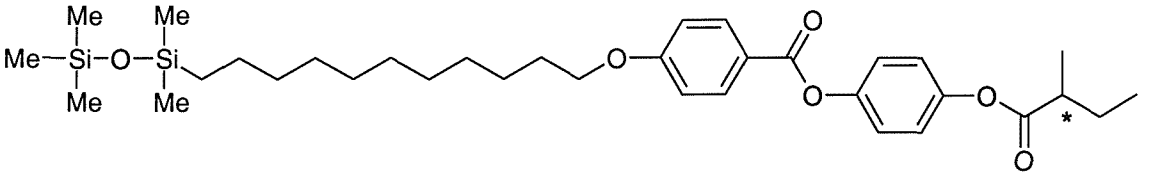

*Figure 4.3 A typical previous organosiloxane low molar mass material (C11A*B).*

Early work within the group focussed on the use of cyanobiphenyls on polysiloxane side chain liquid crystal polymers[10], and oligomeric mono- and bi-mesogens[15]. Material development led to ferroelectric compounds such as the material called C11A*B which is shown in Figure 4.3. The electro-optic properties of this material have been extensively studied and further information can be found in the references[17]. This particular material has a high tilt angle of ~35°, combined with a switching time of ~200 μs at 20 Vμm^{-1}. The spontaneous polarisation of 18 nCcm^{-2} is essential for

producing a significant dipole realignment torque, but without excessive electrode polarisation effects. The success of the multi-component structure has led a drive to synthesise and investigate a wide range of such compounds.

4.2.4 The Latest Low Molar Mass Organosiloxane Liquid Crystal Materials

The latest low molar mass organosiloxane materials are the culmination of synthetic development work by P. Kloess[18]. Part of her work concentrated on the use of a new molecular structure with a mesogenic moiety known to promote high tilt and spontaneous polarisation[14].

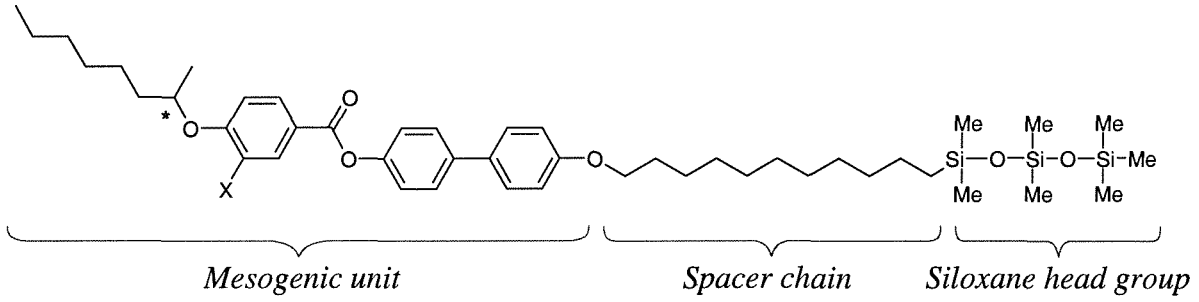

Figure 4.4 A schematic of the basic structure of the latest low molar mass organosiloxane.

The typical structure is illustrated in Figure 4.4, and once more shows the multi-component nature of the molecule. The mesophase inducing component consists of a biphenyl benzoate with a halogen attached laterally at X. The position of the chiral centre, essential for ferroelectric behaviour, is marked with an asterisk. The moiety is attached to the siloxane group by eleven methylene spacers. The idea is to combine the high tilt and high spontaneous polarisation found in the analogous side chain liquid crystal polymer[19] with the siloxane head group's ability to provide temperature independent properties[20].

Systematic variation of the spacer-chain length and head-group size yields a range of materials with different properties[14]. In particular, variation of the alkyl spacer results in an odd-even effect in transition temperatures. This effect is typical of low molar mass compounds with terminal or linking chains[21]. The longest chain length synthesised (eleven carbon atoms) yielded the widest mesophase range. Many materials require a minimum chain length in order to exhibit a mesophase; such behaviour is evident in the homologous series, as short chain lengths yield monotropic behaviour[18]. Ferroelectricity is only seen with alkyl chains containing more than six carbon atoms. With less than eleven carbons in the chain, the spontaneous polarisation and tilt angle show strong temperature dependencies. Therefore, compounds with spacers containing eleven CH_2 units are chosen for examination in this thesis because of their tendency to promote stable smectic phases with minimal temperature dependent properties.

Variation of the number of siloxane units also yields a small odd-even effect[22]. Synthesis of small head groups (those containing five silicon atoms and less) yields monodisperse compounds (i.e. all the same size and weight), whilst those containing greater than five silicon atoms are highly polydisperse[14,22]. The effect of siloxane variation on phase range is well documented [18,20]. A three silicon head group is chosen because it is monodisperse and tends to promote wide, stable mesophase ranges.

The siloxane unit can be used as a central linking group with two moieties attached. This results in the possibility of single 'mono-mesogen' materials or twin dimer 'bi-mesogen' materials. In this work, a compound is identified by the type of laterally substituted halogen, X, the length of the alkyl chain, n, and the number of silicon atoms in the head group, m. Mono-mesogen labels are of the form Xn-Si_m and bi-mesogens are identified by Xn-Si_m-nX. Before studying the electro-optic properties of these compounds, the effect of varying the laterally substituted halogen is examined by studying the series of mesogenic precursors. These mesogenic units are the precursors for later attachment to the siloxane units, and are labelled Xn.

4.3 MESOGENIC PRECURSORS

The laterally substituted biphenyl benzoate mesogen shown in Figure 4.5 was selected for investigation because of its tendency to promote phases with high tilt and spontaneous polarisation[23,24]. The chiral centre necessary for ferroelectricity is found on the terminal chain (once again denoted with an asterisk). The substitution of a lateral halogen on the mesogen (denoted X) is known[23] to strongly influence the electro-optic properties of the biphenyl benzoate mesogen. As this section will show, substituting a halogen onto the benzoate phenyl ring yields highly tilted lamellar phases. The lateral substitution also has a steric effect, which is essential in hindering rotation and promoting ferroelectric behaviour. The magnitude of the spontaneous polarisation and tilt are dependent on the halogen employed. The electronegativity of the halogen attracts electrons from the ring system but is partially countered by the effect of the halogen's free electron pairs. This balance allows changes in atomic radii and electronegativity to have a considerable effect on the material properties. In this work, mesogenic precursors substituted with bromine, chlorine and fluorine have been synthesised for examination.

The generation of a lateral dipole is fundamental to creating a spontaneous polarisation. Bromine has a high electronegativity and can induce a dipole and enhance molecular polarisability. Chlorine, although similar in electronegativity to bromine, has a smaller atomic size and can therefore create a larger dipole. Fluorine is the smallest halogen, but possesses the highest electronegativity of any element. Fluorine is often substituted into liquid crystals to reduce the viscosity and bring down transition temperatures[25].

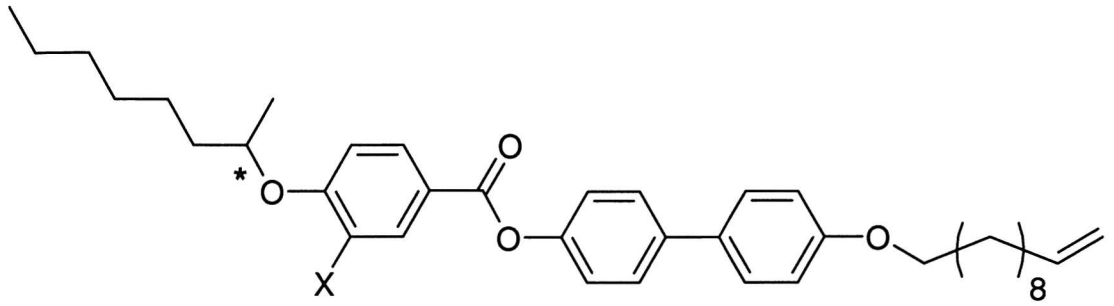

Figure 4.5 A schematic of the structure of the X11 mesogenic biphenyl benzoate precursor.

The precursors were synthesised by P.Kloess[18] who determined their phase range by differential scanning calorimetry and the results are shown in Figure 4.6. The measurements are quoted on heating because a large amount of supercooling occurs at the smectic to crystal transitions. All three compounds exhibit a wide SmC* phase and a narrow N* phase. The Br11 and F11 compounds both show a crystal-crystal transition. As demonstrated by the DSC data, increasing halogen size leads to a decrease in clearing temperature, partly because the lateral substitution disrupts the packing and reduces phase stability.

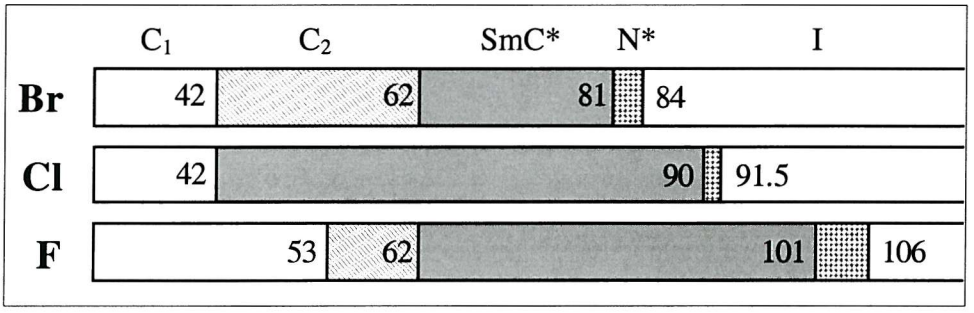

Figure 4.6 Phase transitions determined by differential scanning calorimetry of the biphenyl benzoate precursors with different laterally substituted halogens.

4.3.1 Electro-Optic Analysis of X11 Compounds

Small amounts of the vinyl terminated biphenyl benzoate were available from the initial work of P. Kloess and it is interesting to investigate the differences the change in halogen promotes. In order to study the electro-optic effects, the compounds were examined in ~4 μm Lucid cells. Once filled the materials all show a sanded texture with no alignment. A variety of D.C. and A.C. fields were applied while the materials were cooled slowly at ~0.1°Cmin^{-1} from the isotropic and through the N* phase. The applied field resulted in very small regions of alignment in the SmC* phase; however, no particular field strength or waveform consistently proved beneficial to the alignment process. The small regions of alignment were not stable, and upon removal of the field, often revert to a sanded texture.

4.3.1.1 Tilt Angle

The difficulties encountered when aligning the sanded texture of the SmC* phase in all three compounds makes optical measurements difficult. Thus, tilt measurements were carried out by eye, at maximum magnification on the crossed polariser microscope. The direct switching method was used with a 0.5 Hz square wave at 20 $V\mu m^{-1}$. Identification of extinction regions is hampered by the poor alignment, which leads to a higher than usual estimated error of ±1°. The results in Figure 4.7 show the weak temperature dependence of the tilt angle in the mesogens. The magnitude of the tilt angle roughly follows the halogen size.

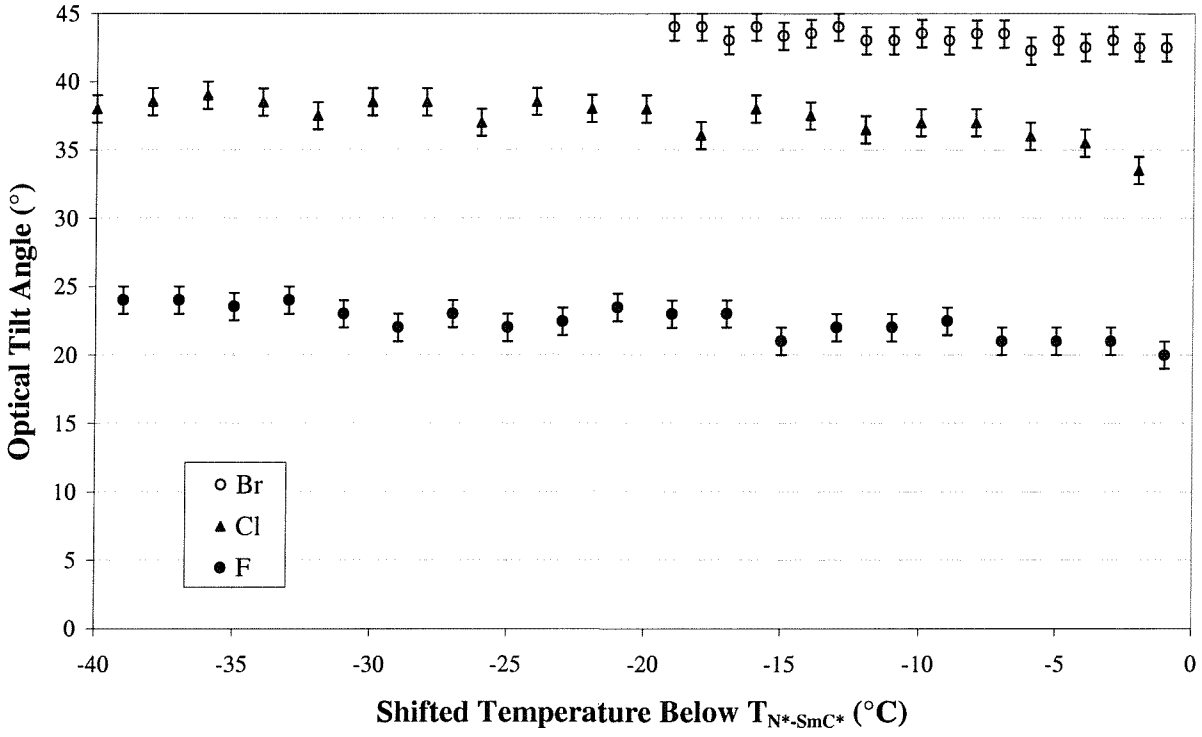

Figure 4.7 The optical tilt angle of mesogenic precursors as a function of shifted temperature.

4.3.1.2 Spontaneous Polarisation

The spontaneous polarisation current switch was not well defined and fluctuated widely, so the end-points of the spontaneous polarisation realignment peak were selected by hand (as described in the experimental chapter §3.4.2). A triangular driving wave at 10 Hz and 20 $V\mu m^{-1}$ was used. The oscilloscope trace was averaged 256 times and each measurement was repeated ten times. The lack of peak stability results in an estimated error of ~±5% on the spontaneous polarisation measurements. The poor alignment and current peak instability hampered the measurement of either optical or current pulse switching times. However, despite the very noisy nature of the signal and long peak tails, the spontaneous polarisation results in Figure 4.8 still clearly indicate the relative magnitude and trends of the spontaneous polarisation values as functions of temperature and lateral substituent. As

with the tilt angle measurements, only a weak temperature dependence is seen. The differences in the magnitudes of the spontaneous polarisation are due to the different halogen sizes and electronegativities. Spontaneous polarisation is a result of a combination of dipole and steric hindrance effects: in general the stronger the dipole at the chiral centre, the larger the lateral component relative to the long axis and the greater the spontaneous polarisation. A small amount of spontaneous polarisation is seen around the $T_{N^*\text{-}SmC^*}$ transition due to the electroclinic effect.

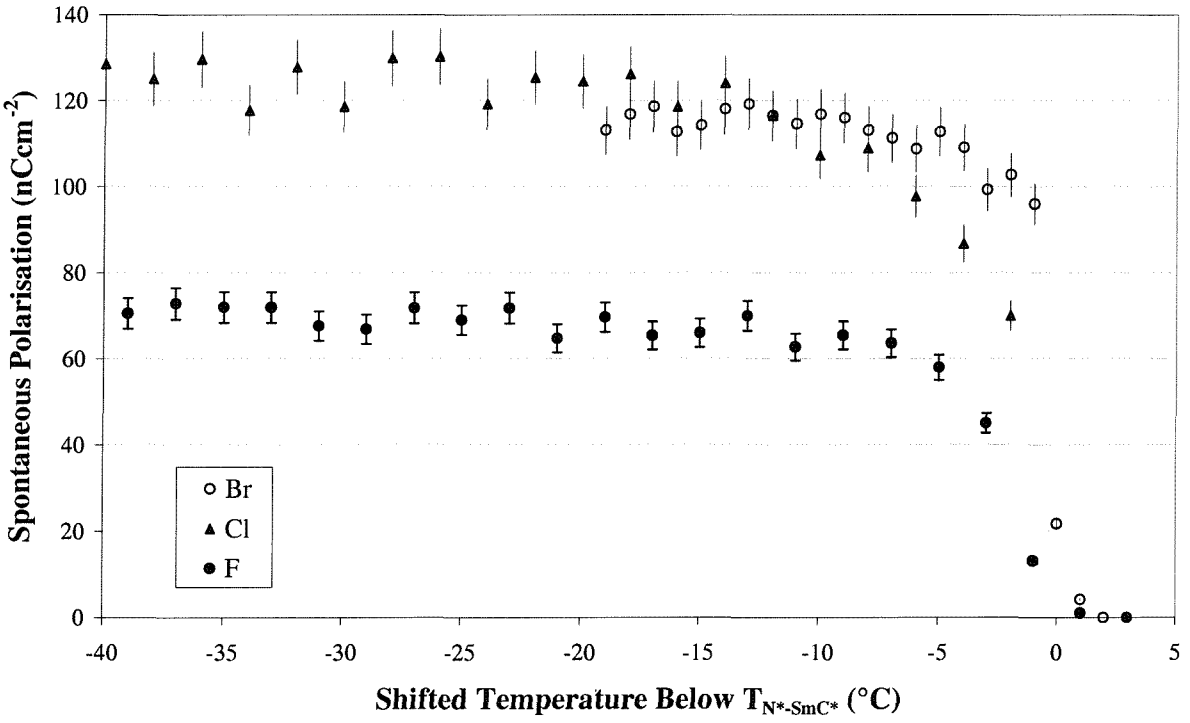

Figure 4.8 The spontaneous polarisation of mesogenic precursors against shifted temperature.

4.3.1.3 Effect of the Lateral Halogen

The effect of varying the lateral substituent is highlighted by comparison with the work of Sunohara et al.[9], who prepared several similar structures. Most relevant is a material identical to those considered here but without the lateral substituent (denoted IIb-9 in the work of Sunohara et al.). Although the same liquid crystal phases were seen, the transition temperatures of the biphenyl benzoate molecules were ~20°C higher than the F11 compound examined in this work. Spontaneous polarisation results were ~40 $nCcm^{-2}$ for IIb-9 compared with ~70 $nCcm^{-2}$ for F11 and >100 $nCcm^{-2}$ for the Cl11 and Br11 (see Figure 4.8). These comparisons clearly demonstrate the influence of dipolar and steric factors in producing a large spontaneous polarisation. Furukawa et al.[23] synthesised biphenyl benzoate laterally substituted with a halogen, but with a vinyl terminated chain consisting of eight carbons atoms instead of the eleven carbon atoms in the chain used in this work. Furukawa's results reveal an almost identical trend in transition temperatures, tilt angle and spontaneous polarisation as is seen in the X11 materials.

4.4 LOW MOLAR MASS ORGANOSILOXANE MONO-MESOGENS

The mono-mesogenic structure was shown earlier in Figure 4.4. The F11-Si_3 compound was synthesised by P.Kloess[18] and the Br11-Si_3 and Cl11-Si_3 compounds by S.Perkins[22]. The phase ranges are determined by differential scanning calorimetry and are shown in Figure 4.9. The addition of the siloxane head group and the resulting virtual backbone effect have exclusively promoted the formation of the smectic phases. The tilt of the mesogens has ensured that this is a tilted phase, the SmC* phase. The increased stability of the mesophase gives ~50°C wide phase ranges. Supercooling occurs at the SmC*→Crystal transition but only by around 2-5°C. The lines in the SmC* phase indicate a small anomaly, which is discussed later in §4.4.2.

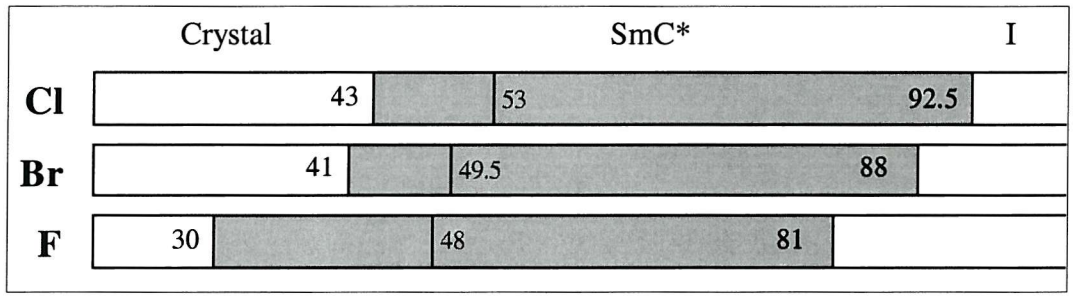

Figure 4.9 Phase transitions determined by DSC of the mono-mesogenic organosiloxanes with different laterally substituted halogens. The lines in the SmC phase indicates an anomaly seen in the DSC trace, and not a change of mesophase.*

4.4.1 Electro-Optic Analysis of X11-Si_3 Organosiloxane Compounds

4.4.1.1 Alignment

The mono-mesogens take the form of a near-white, waxy powder at room temperature, which melts into an almost clear, colourless, viscous liquid on heating. An unaligned sample exhibits a sandy texture similar to that of the precursors (see Figure 4.10a), which under high magnification (x500) is seen as a fine schlieren texture. Alignment for electro-optic switching is not straightforward, although repeated testing has uncovered the most effective conditions. The sample is heated into the isotropic phase then cooled at 0.5°Cmin^{-1} to ~1°C below the I→SmC* transition where bâtonnets have just formed, as shown in Figure 4.10b. An A.C. field is applied which induces turbulence in the bâtonnets. Charge liberated from the electrodes is moved back and forth, disturbing the bâtonnets as they form. Typical triangle-wave field values used are around 100 Hz and 15 Vμm^{-1}. The break-up of the bâtonnets requires the choice of field to be tailored to each sample. The effect of the alignment process for the first cooling run on Br11-Si_3 in a 4 μm Lucid cell is shown in Figure 4.10c. Sinusoidal waves can also be effective with higher field strengths, particularly with slower cooling. In order to enhance the alignment the sample is annealed by cycling between 1°C below and 5°C below the

I→SmC* transition whilst under the influence of the alignment field. The effect of ten cycles at $0.3°Cmin^{-1}$ is seen in Figure 4.10d. The pictures in Figure 4.10 are taken using the bromo compound, but are generally representative of all three mono-mesogenic organosiloxanes.

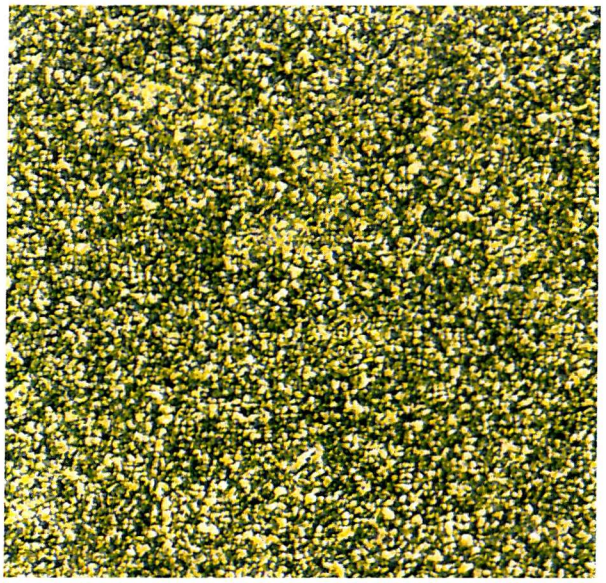

a) No alignment.

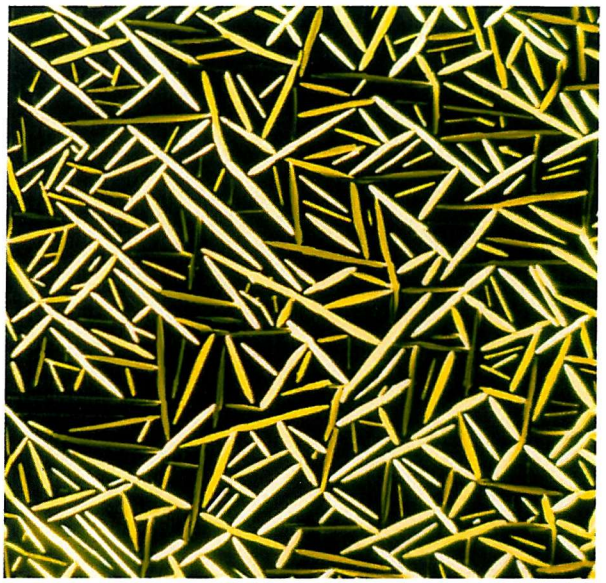

b) Bâtonnets forming on cooling through the I→SmC transition.*

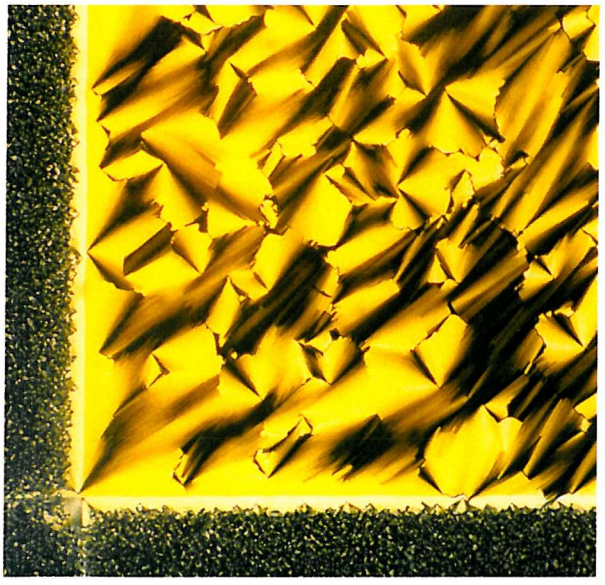

c) Broken alignment on first cooling.

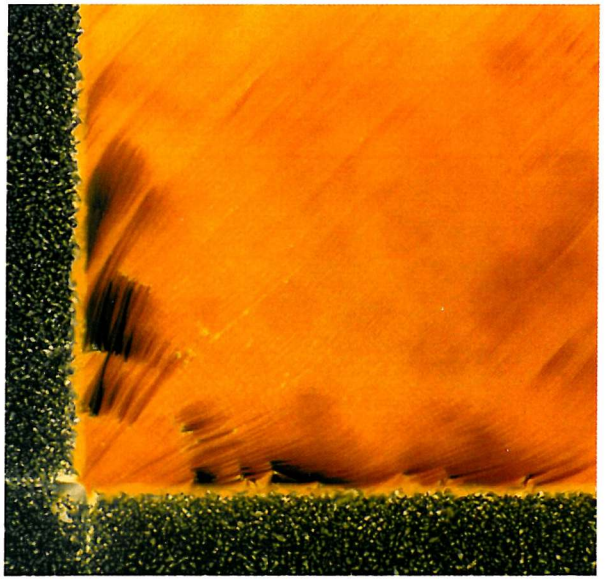

d) Final alignment after repeated annealing.

Figure 4.10 Photomicrographs at 50x magnification showing the effect of the alignment process on the mono-mesogen Br11-Si3.

Obtaining a fully-aligned sample requires considerable time, and alignment cannot always be reproduced. In an attempt to enhance the alignment, cells were fabricated by hand with a PTFE alignment layer. Although the use of PTFE usually gave good alignment in small areas, large reverse domains were often seen. On balance, the advantages of using hand-made PTFE treated cells did not justify the time necessary to fabricate the cells. The outcome of the alignment process with the

Br11-Si_3 and Cl11-Si_3 compounds was almost identical. F11-Si_3, although responding to similar treatment, was the hardest to align and exhibited the most defects. The use of controlled cooling to obtain alignment means that most electro-optic work is carried out on cooling unless otherwise stated.

4.4.1.2 Tilt Angle

The optical tilt angle is measured using the photodiode method described in §3.4.1.1. An 80 Hz A.C. square-wave at 20 $V\mu m^{-1}$ was sufficient for the tilt to be fully saturated in each material. The tilt angles of the materials as functions of shifted temperature are shown in Figure 4.11. The consequence of a first order transition from I→SmC* is seen with the instantaneous appearance of high tilt angles. All three compounds show temperature dependencies only in narrow temperature ranges near the transitions. The high tilt of the bromo- and chloro-substituted precursors has been slightly enhanced after addition to the siloxane head group, with the tilt angle of Br11-Si_3 reaching 45° over a wide part of its smectic phase range. Somewhat surprisingly, the fluoro-substituted compound has shown a vastly increased tilt to ~43° in comparison with the precursor's 20-25° tilt angle. These effects are attributed to the impact of the virtual backbone that enhances the smectic layer order. Thus, this arrangement clearly favours a near 45° tilt of the mesogens.

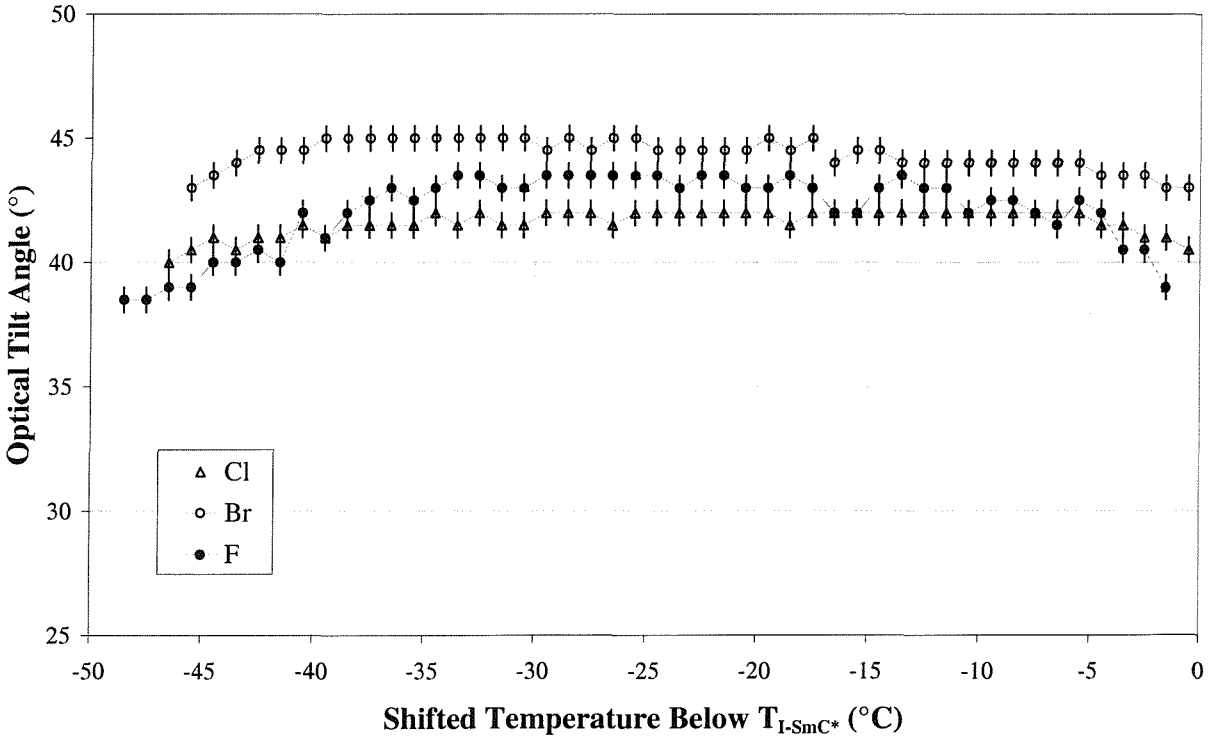

Figure 4.11 Optical tilt angle measurements of mono-mesogenic organosiloxane compounds X11-Si_3, against shifted temperature.

The temperature independence of the tilt over a wide range, as exhibited by these materials, is essential for a temperature independent, high contrast, electro-optic device.

4.4.1.3 Spontaneous Polarisation

The spontaneous polarisation switch of the organosiloxane materials is considerably smoother than the traces seen with the precursors. The Br11-Si_3 and Cl11-Si_3 compounds yield smooth well-defined curves which are shown in Figure 4.12a. The F11-Si_3 curve is noisier and far less stable, therefore more averaging is used; 256x in comparison with 32x used when examining the other compounds. The curves show the typical ferroelectric spontaneous polarisation realignment current pulse peak. Very little baseline slope is seen, indicating that only a very small amount of ionic impurity is present. The different switching times of the three compounds result in peaks of different widths. The peaks appear at different positions along the time axis because the materials have different threshold voltage, switching times and viscosities. If the photodiode response is plotted against the triangular driving wave, a hysteresis curve is seen, as in Figure 4.12b, which was obtained using Br11-Si_3. This plot, measured at 75°C and 15 Vμm^{-1}, clearly demonstrates the ferroelectric nature of the phase.

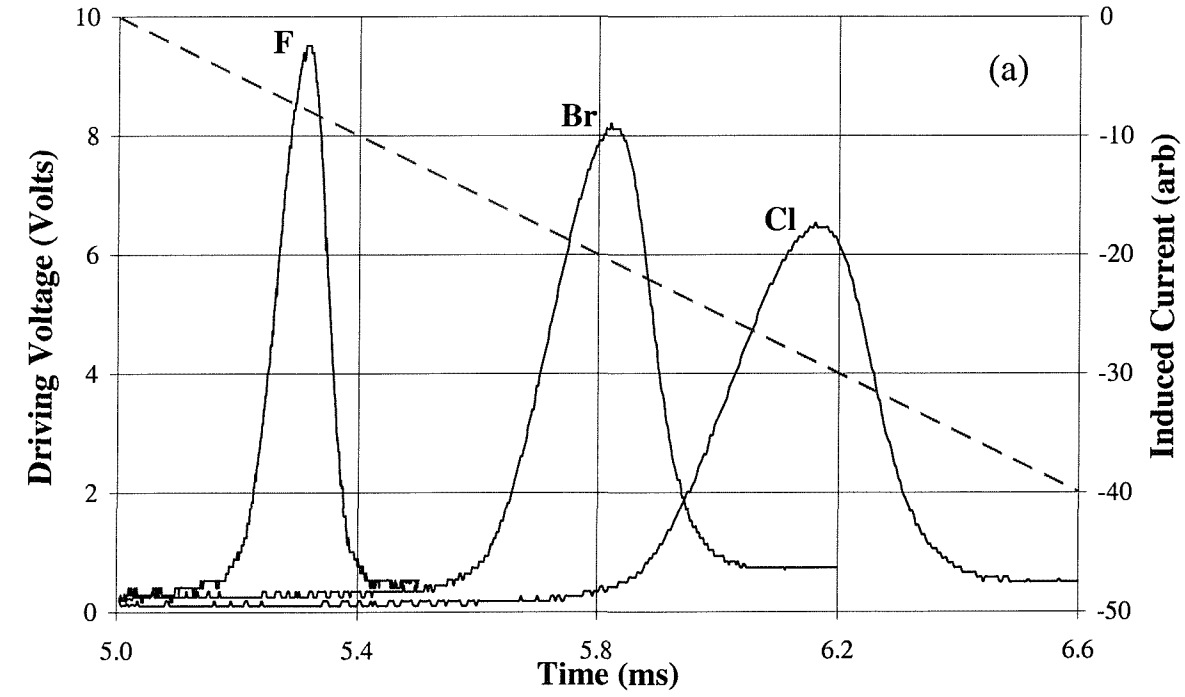

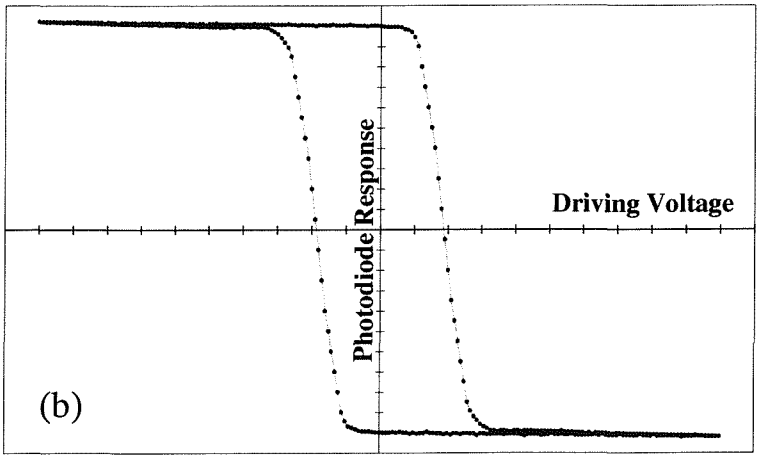

Figure 4.12 a) Spontaneous polarisation traces for the three mono-mesogenic compounds.

b) Photodiode response against triangular driving wave for Br11-Si_3 showing typical ferroelectric hysteresis.

The clarity of the realignment peak allows the spontaneous polarisation to be measured using the computer-controlled current pulse technique described in §3.4.2.1. Thus, the increased ease of measurement enables not only extensive averaging of individual readings, but also reduced run times, allowing more repeated measurements to be made. The spontaneous polarisation measurements shown in Figure 4.13 for the three materials were made using a triangular driving wave of 20 $V\mu m^{-1}$ at 80 Hz. Once more, the almost temperature invariant nature of the precursors is retained. Overall, values of spontaneous polarisation are lower than those of the precursors. This result is not surprising given the reduced number of dipoles per unit volume. With the grafting of the siloxane, the mesogenic precursor now accounts for roughly 75% of the molar mass of the overall material and this is matched by an approximately 25% decrease in the value of the spontaneous polarisation for each material.

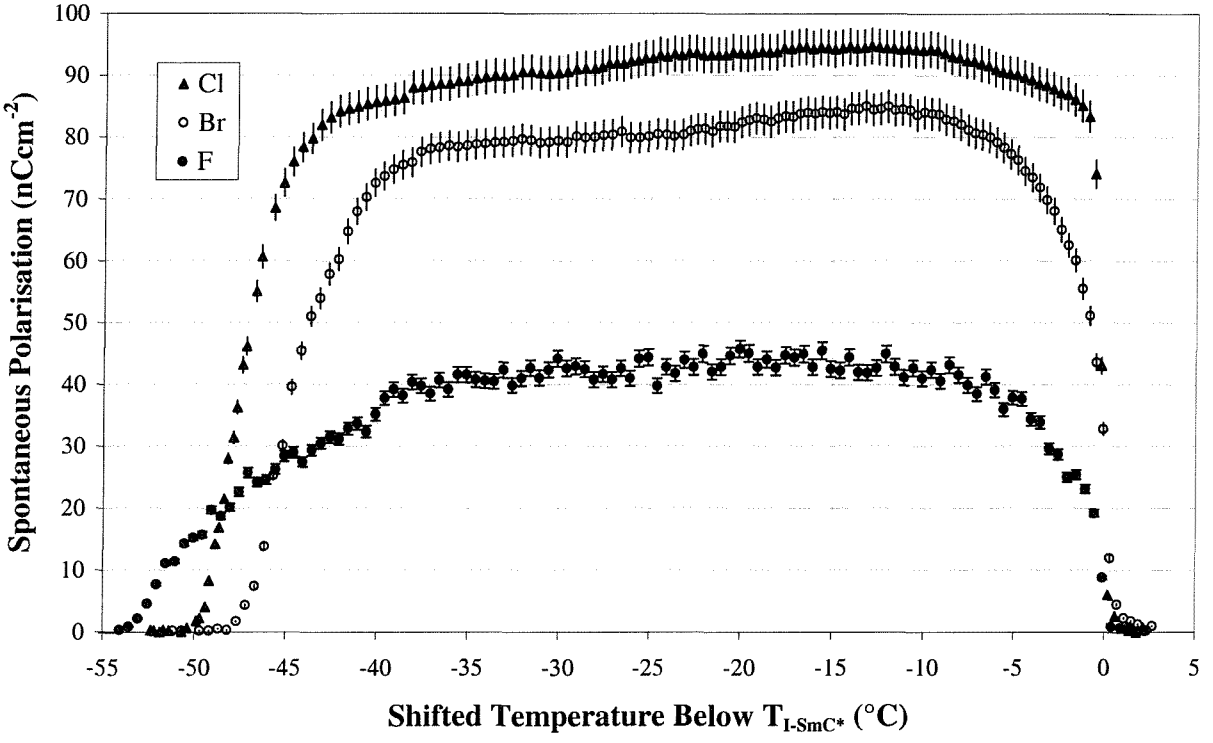

Figure 4.13 Spontaneous polarisation measurements of mono-mesogenic organosiloxane compounds against shifted temperature.

4.4.1.4 Switching Time and Viscosity

The quality of alignment differed between samples and individual cells. In some cases, switching time measurements could be made using the photodiode setup. When this was not possible, particularly with F11-Si_3, the current pulse technique was used. Both measurement methods yielded similar results to within the limits of measurement accuracy. The switching times were measured as a function of shifted temperature with square-wave driving fields at 80 Hz and 20 $V\mu m^{-1}$ and are shown in Figure 4.14. The materials demonstrate the fast switching times in the hundred microsecond or less regime that are sought for display applications.

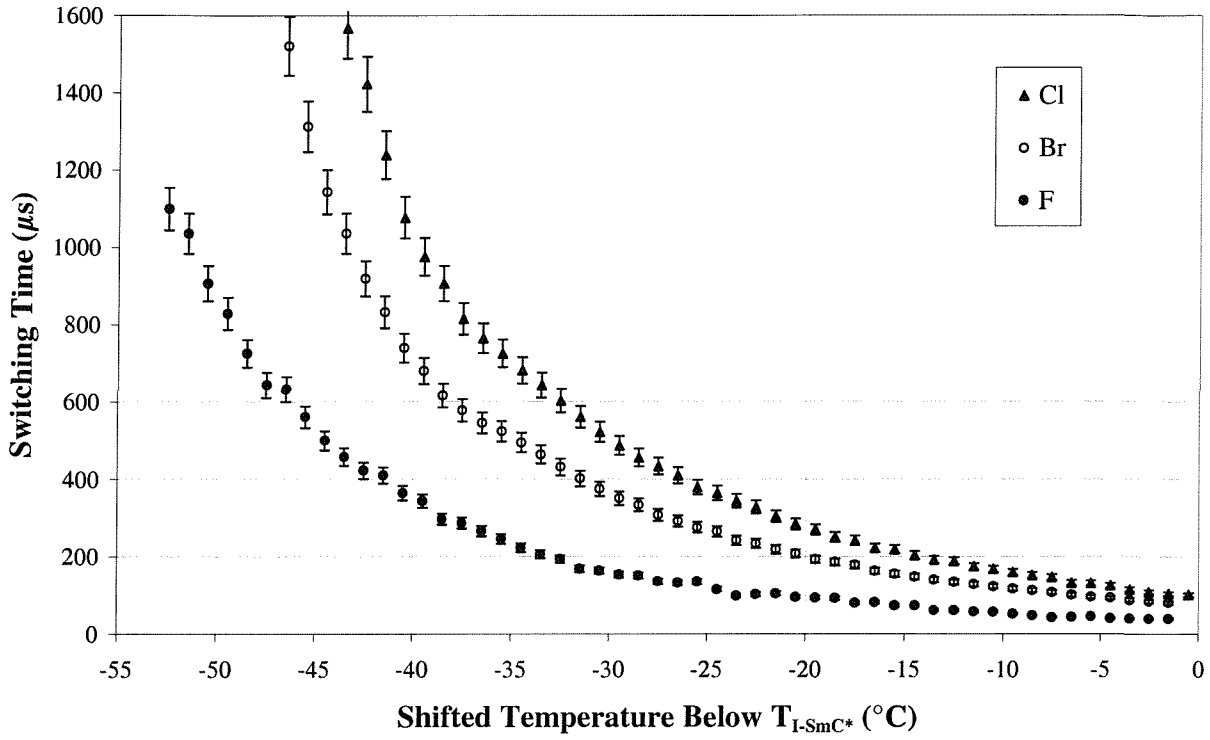

Figure 4.14 Switching time measurements of mono-mesogenic organosiloxane compounds against shifted temperature.

The computer-control of spontaneous polarisation measurements also yields results for the current peak height and driving field at reorientation. As described in the previous chapter these oscilloscope readings in conjunction with tilt angle results allows the calculation of rotational viscosities (§3.4.4). A semi-log plot against the reciprocal of absolute temperature is shown in Figure 4.15. The data follows the expected Arrhenius behaviour as described in the previous chapter. This trend allows line fits to be applied, with the gradient proportional to the activation energy of the switch.

As Figure 4.15 shows, F11-Si_3 has the lowest viscosity, which corresponds with its faster switching times. The activation energy of the switch is also the smallest. This is attributed to a number of factors. Lateral substitution on a mesogen usually increases the viscosity of a mesophase because it disrupts the molecular arrangement; this effect is minimised with the fluorine atom. As shown in the table in Figure 4.15, fluorine is the smallest halogen and is only slightly larger than the hydrogen it replaces[26]. The viscosity is also highly dependent on the magnitude of spontaneous polarisation, which is smallest in F11-Si_3. The higher viscosity of Cl11-Si_3 over Br11-Si_3 is a consequence of its larger spontaneous polarisation; this overrides the reduced steric viscous effect due to smaller atomic size. The data fits well to the expected exponential behaviour as can be seen on examining the straight-line fits. The activation energies have no significant meaning in isolation, but can be used for comparing the effects of varying the laterally substituted halogen. The activation energies loosely follow the atomic size[26] of the laterally-substituted halogens.

UNIVERSITY OF SOUTHAMPTON LIBRARY

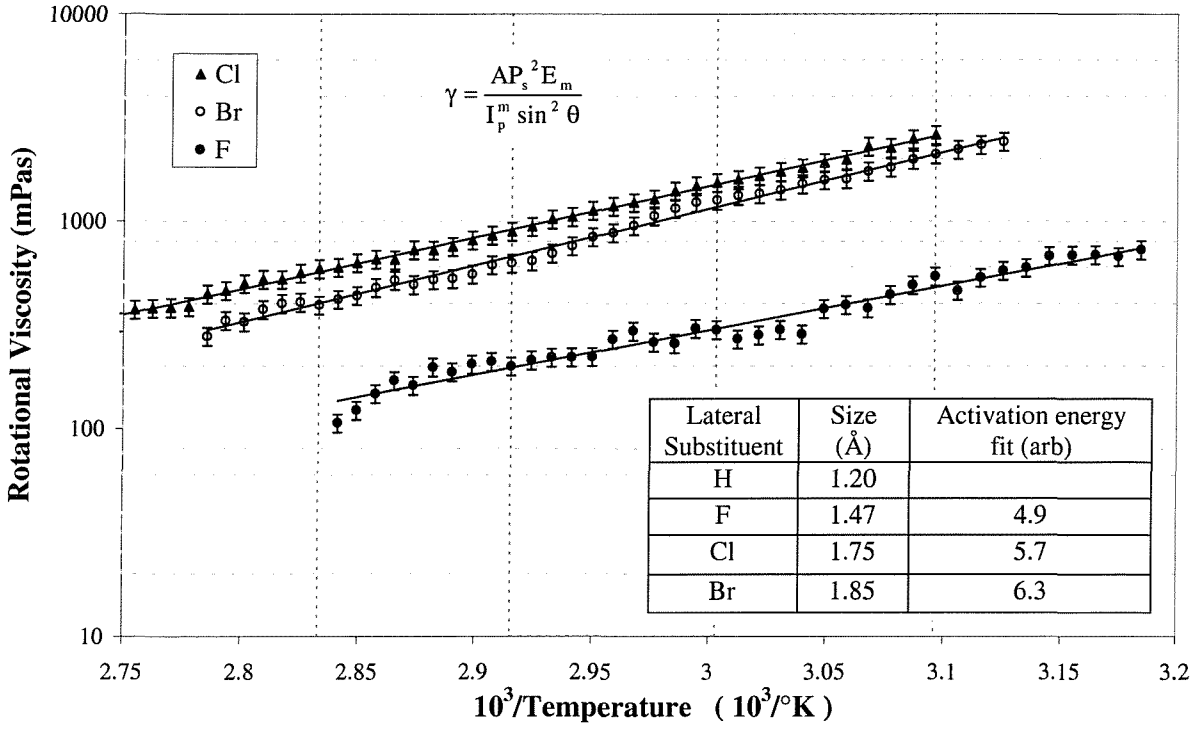

Figure 4.15 Rotational viscosity for mono-mesogenic organosiloxane compounds derived from electro-optic readings using the Escher equation (inset). The data follows an Arrhenius behaviour, allowing straight line fits giving activation energies. These are shown in the table with their corresponding halogen sizes.

The rotational viscosity can also be estimated from the relationship $\gamma_\varphi \propto \tau_\varphi P_s E$, where $\gamma_\varphi = \gamma \sin^2\theta$. This treatment yields very similar results to those calculated from the current pulse technique. A comparison of the two methods allows the proportionality constant to be calculated. The results are shown in Figure 4.16.

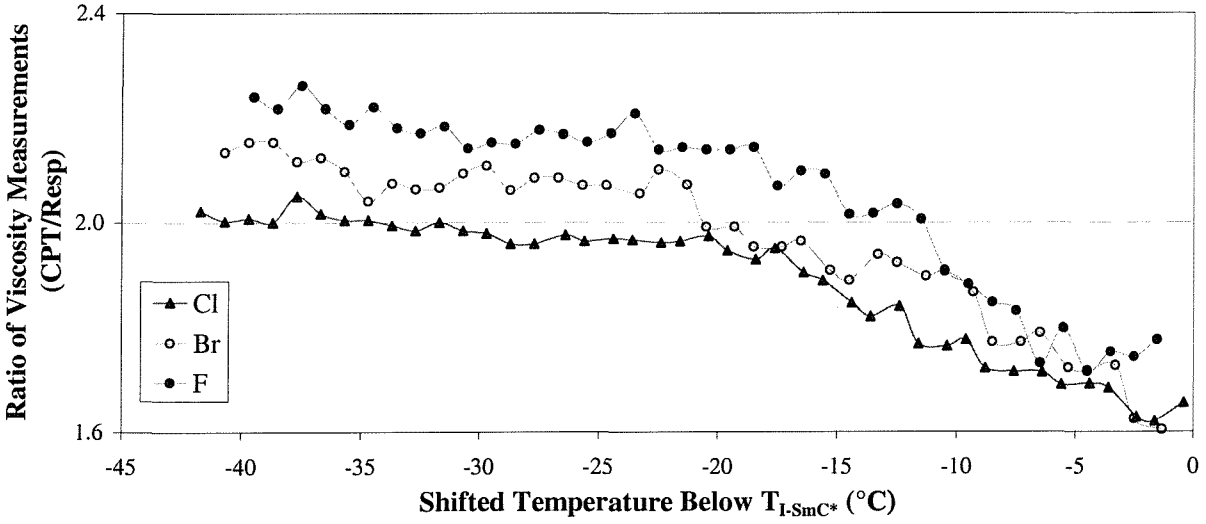

Figure 4.16 A comparison of the results of rotational viscosity measurements by current pulse technique and response measurements in the mono-mesogenic organosiloxanes.

The values compare favourably with the range of values 1.8-2.0 seen in different materials by other researchers as discussed in §3.4.4. The gradual variation of the ratio of the two methods with decreasing temperature is attributed to the greater dependence of the current pulse technique calculations on spontaneous polarisation. Both methods are based on an approximation of coupling of tilt angle and spontaneous polarisation, and this relationship breaks down at low temperatures. The breakdown is seen in the continued temperature invariance of the high tilt in contrast with the slow drop-off in spontaneous polarisation, particularly for F11-Si_3 (see Figure 4.11 and Figure 4.13).

4.4.2 Phase Anomalies

Differential scanning calorimetry was used to examine the phase ranges of the compounds. An example of a trace for Cl11-Si_3 is shown in Figure 4.17. The sharpness of the peaks indicates the purity of the sample. However, an additional small peak can be clearly seen on heating, at 53°C. Similar peaks are seen for all three compounds, as indicated on the DSC phase ranges (Figure 4.9). No textural change is observed at the temperatures of the anomalies. X-ray analysis by P. Kloess[18] and E. Corsellis[27] on the series did not show any change in layer spacing or any anomalies at these temperatures. The electro-optic results in this temperature region were examined in detail. The spontaneous polarisation realignment peaks show no abnormal behaviour on heating or cooling, or multi-mode switching as might be expected if the sample were to undergo a phase change to a higher ordered phase. A very small jump in the spontaneous polarisation curves can just be made out in Figure 4.13 at the temperatures shown in the DSC traces, but this is at the limit of measurement accuracy and the behaviour is similar on cooling and heating. Any effect in the tilt angle is negligible.

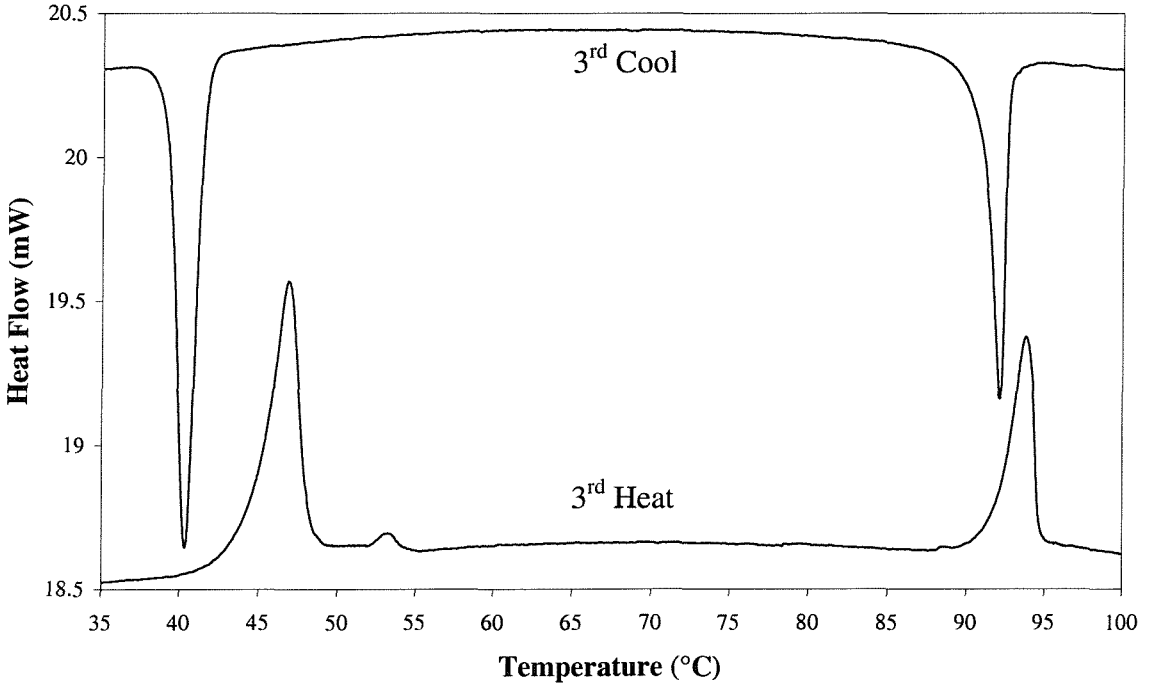

Figure 4.17 Differential scanning calorimetry trace for Cl11-Si_3.

The most obvious effect of any possible change is seen in the switching time measurements. As expected, the results follow an exponential trend and thus a semi-log plot is appropriate. The result is shown in Figure 4.18. A slight change in the exponential behaviour is emphasised with straight-line fits extrapolated from the beginning and end of the runs. This clearly highlights a change in the nature of the switching times at temperatures that coincide well with the anomalies identified in the DSC curves.

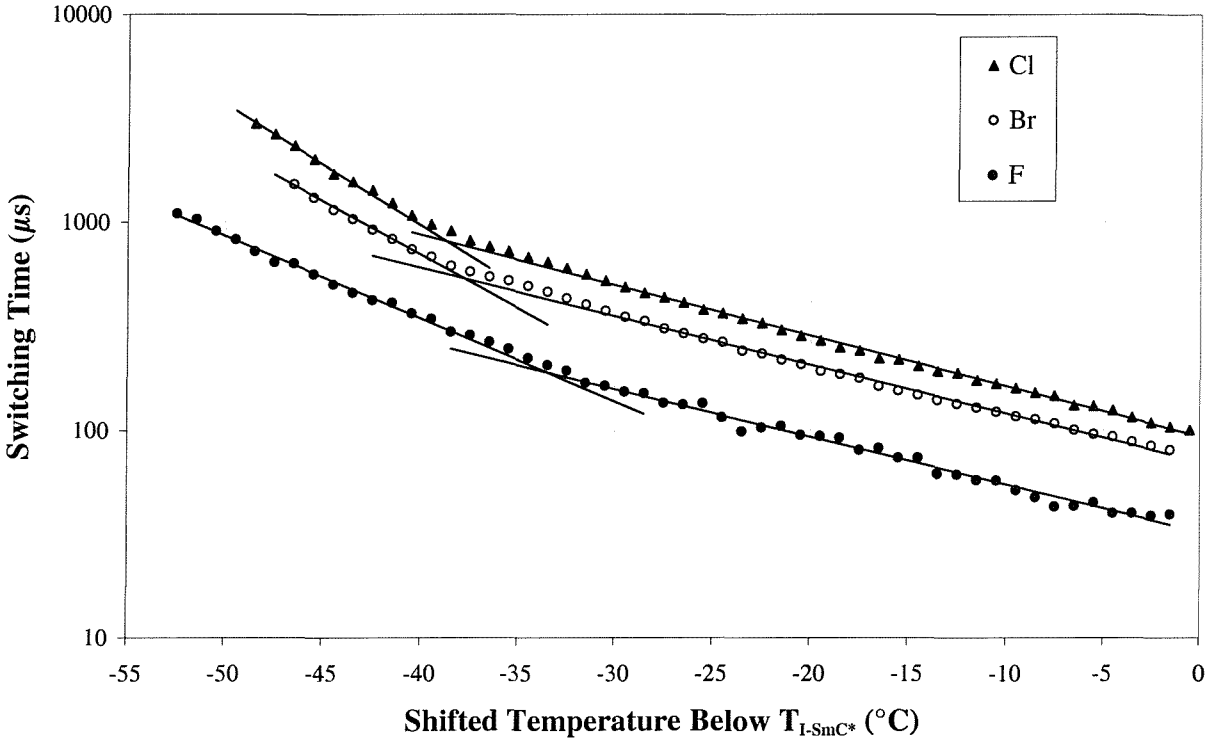

Figure 4.18 Switching time measurements from Figure 4.14 re-plotted on a semi-log scale.

A comparable anomaly has been observed in similar mono-mesogenic compounds with cyanobiphenyl moieties[20] (the structure is illustrated in Figure 4.1). Although the cyanobiphenyl is very different from the biphenyl benzoate, and the phase ranges are not the same, the size and nature of the peak is similar. This analogy indicates that the effect is more likely to be associated with the siloxane and alkyl chain rather than the mesogen. The multi-component nature of the low molar mass organosiloxane materials allows for many energetically driven reconfigurations of its component parts, without a macroscopic phase change. The aromatic core of the mesogen is mainly responsible for the material's birefringent properties. The eleven-unit methylene spacer chain provides a high degree of decoupling, and thus a rearrangement of the siloxane head group may be possible without an obvious change in phase. Little is known of the dynamics of siloxane head groups and spacers. In polymer systems, DSC analysis is often used to highlight conformational changes of the backbone. A similar effect is hypothesised to occur here, due to the polymer-like nature of the virtual backbone.

4.5 Low Molar Mass Organosiloxane Bi-Mesogens

In order to produce bi-mesogenic organosiloxanes, mesogens are grafted at both ends of the short siloxane group. Two bi-mesogenic compounds were synthesised in large quantities by S. Perkins: Br11-Si_3-11Br and Cl11-Si_3-11Cl. This section looks at the analysis of the two compounds whose basic structure is shown in Figure 4.19.

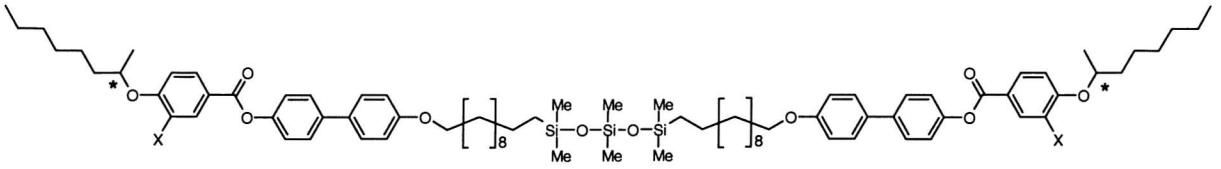

Figure 4.19 A schematic of the basic structure of the latest bi-mesogenic low molar mass organosiloxane.

The phase range of this structure is shown in Figure 4.20. As with the mono-mesogenic organosiloxane compounds, the only phase exhibited by the bi-mesogens is a smectic phase. This phase is identified by electro-optic study as antiferroelectric. The differential scanning calorimetry peaks were smooth and sharp and showed no evidence of extra peaks as seen with the mono-mesogens. Once again, the mesophase has a wide temperature range, ~60°C, slightly larger than seen with the mono-mesogens. This increased phase range is typical of the slightly higher ordering of antiferroelectric phases in comparison to ferroelectric phases.

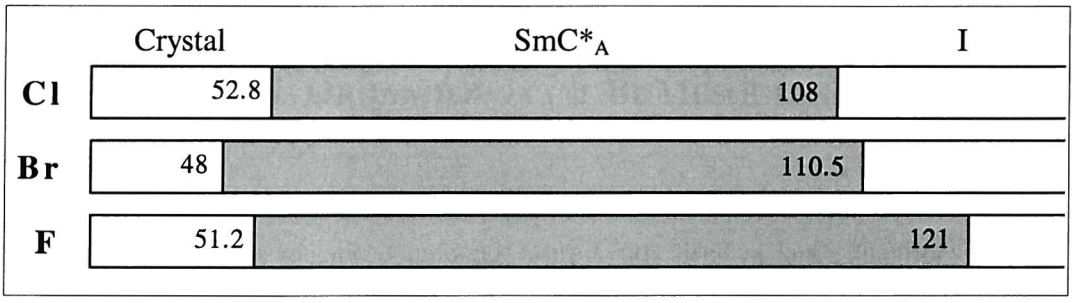

Figure 4.20 Phase transitions determined by differential scanning calorimetry of the bi-mesogenic organosiloxane compounds with different laterally substituted halogens.

4.5.1 Electro-Optic Analysis of X11-Si_3-11X Organosiloxane Compounds

The fluoro-substituted compound was not synthesised for this study due to difficulties in the synthetic process. A comparison is made with the small amount of F11-Si_3-11F synthesised by P. Kloess and analysed by R. Campin[28]. The F11-Si_3-11F compound was synthesised under different conditions than the Br11-Si_3-11Br and Cl11-Si_3-11Cl compounds. The different synthetic route affects the levels of impurity, ionic and otherwise, which can have a large influence on the results of the material's analysis. The study of F11-Si_3-11F was carried out on different apparatus using different fields and

experimental methods. These differences must be taken into account when comparing the data published for F11-Si_3-11F with those obtained in the current work for Br11-Si_3-11Br and Cl11-Si_3-11Cl.

4.5.1.1 Alignment

The alignment techniques are similar to those used to align the mono-mesogenic compounds. The sample is heated into the isotropic phase and then cooled at 0.1-0.5°Cmin^{-1} to ~2° below the I→SmC*$_A$ transition where bâtonnets have just formed. A triangular A.C. field is applied at ~100 Hz and high field strengths are used, 25-35 Vμm^{-1}. The use of such high field strengths means that extra care must be used throughout sample fabrication and the cell filling process to avoid contaminants. The high fields often cause the cell to short-out dramatically, particularly if seeded by a contaminant. Obtaining a satisfactory alignment took considerably more time than with the mono-mesogenic ferroelectric samples. The result of the first cooling run at 0.2°Cmin^{-1} with Cl11-Si_3-11Cl in a 4 μm Lucid cell is shown in Figure 4.21a. Repeated cycling with varying cooling rates between a shifted temperature of -5°C and the isotropic phase transition yielded some success. The results of extended annealing are shown in Figure 4.21b. In general, the alignment quality was poorer than that of the ferroelectric compounds. This can be seen by comparing the alignment in Figure 4.21b, typical of the bi-mesogenic antiferroelectric compounds, with that of the mono-mesogens in Figure 4.10d. The transition to the antiferroelectric phase directly from the isotropic requires a large amount of order to spontaneously form. Without a lower ordered phase such as a SmA* or N* phase to introduce the order gradually, alignment is difficult to produce. The use of PTFE alignment in hand-made cells showed promising results, especially in thin (~2 μm) cells. However, despite careful manufacture, the thin cells shorted and failed too easily.

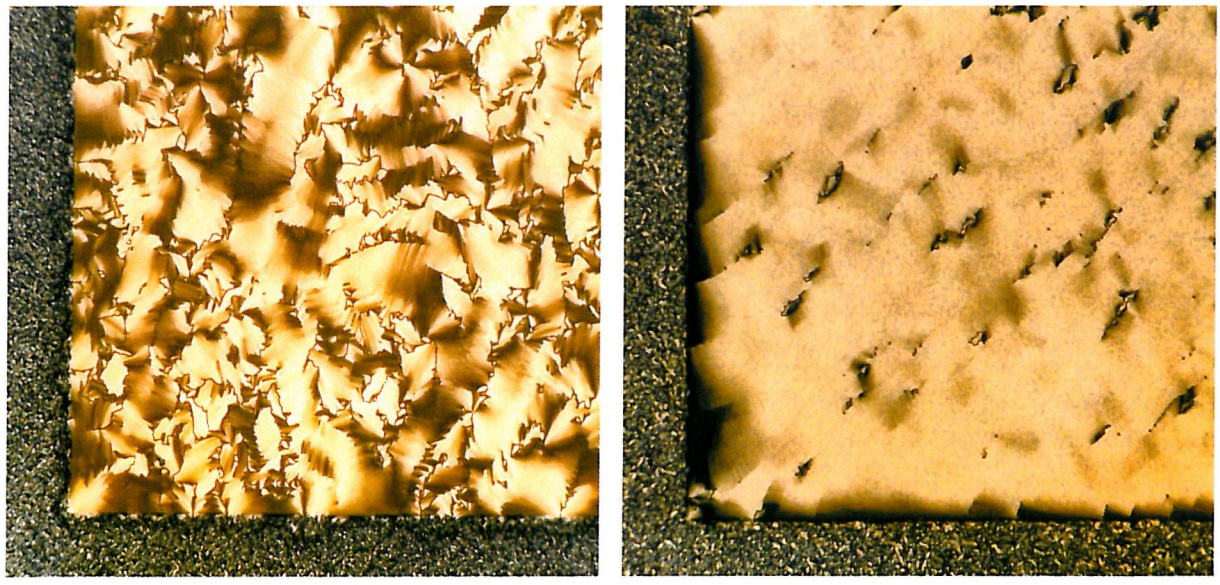

a) Broken alignment on first cooling *b) Final alignment after repeated annealing*

Figure 4.21 Photomicrographs at 50x magnification showing the effect of alignment processes on the bi-mesogen Cl11-Si_3-11Cl.

4.5.1.2 Tilt Angle

Antiferroelectric compounds have no macroscopic optical tilt because they have an alternating layer structure. A macroscopic tilt is only seen in the presence of a field and thus a field induced optical tilt angle is measured here. The poor alignment quality necessitated the use of the D.C. field method. A field of 25 $V\mu m^{-1}$ was required for the tilt to become saturated. The tilt angles as a function of shifted temperature are shown in Figure 4.22. Once again a first order transition, this time from I→SmC*$_A$, is clearly seen with an almost temperature independent nature. The high tilt exhibited in the mono-mesogens is retained. The dotted line represents the tilt of F11-Si$_3$-11F measured under similar conditions by R.Campin[28].

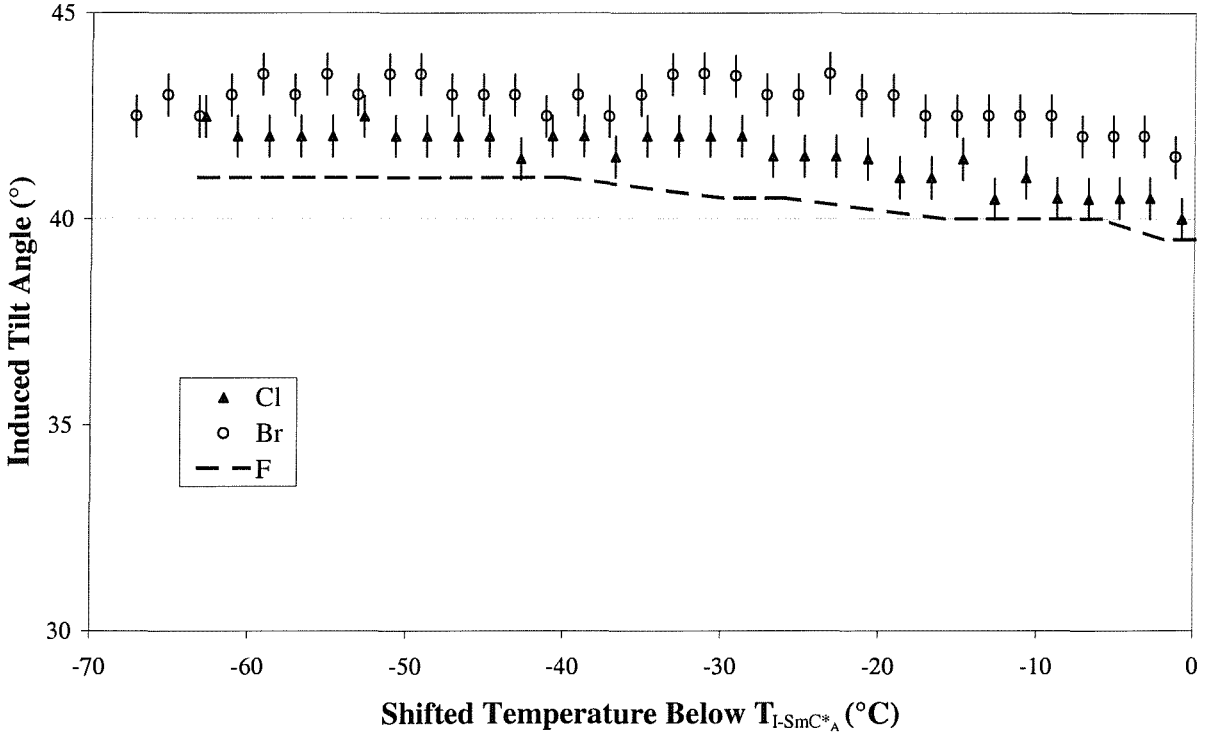

Figure 4.22 Field induced optical tilt angle measurements of bi-mesogenic organosiloxane compounds against shifted temperature.

4.5.1.3 Spontaneous Polarisation

After averaging (64x) the spontaneous polarisation switch is smooth, yielding well-defined traces, as shown in Figure 4.23a for Br11-Si$_3$-11Br and Cl11-Si$_3$-11Cl at a shifted temperature of -20°C. The trace clearly shows the characteristic twin realignment peaks of an antiferroelectric switch. A larger baseline jump is observed in comparison to the mono-mesogens, although a similarly small amount of baseline slope indicates the absence of excessive ionic impurities. The traces show the variation in peak shape for the relaxed and driven ferroelectric ↔ antiferroelectric switches. Although different in shape, the area under the two peaks only differed moderately, with the "relaxation" peak area ~10% smaller than the "driven" peak area at most temperatures.

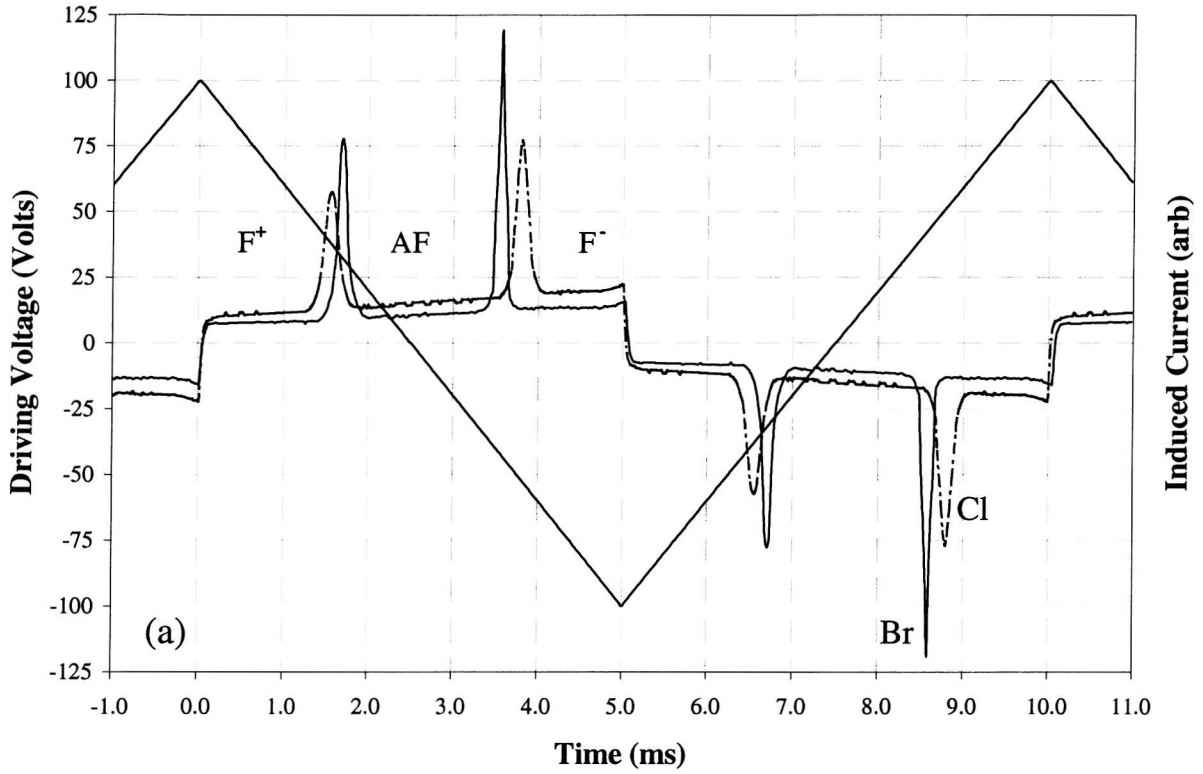

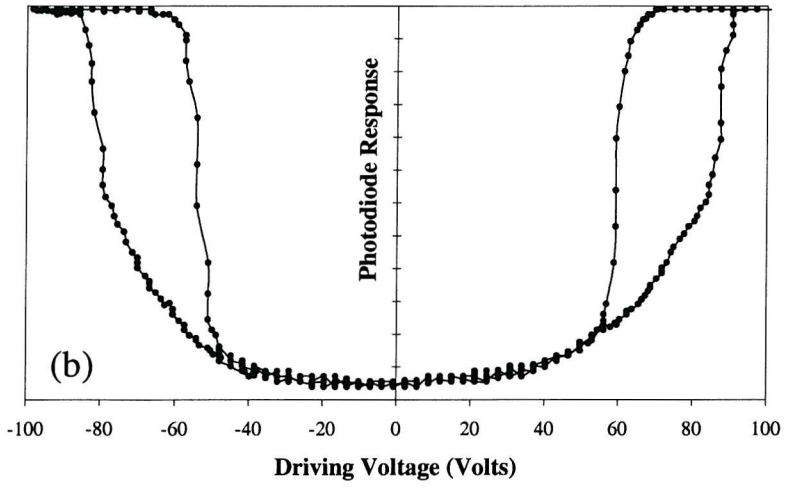

Figure 4.23 a) Spontaneous polarisation traces for the antiferroelectric Br11-Si3-11Br and Cl11-Si3-11Cl bi-mesogenic organosiloxane compounds.

b) Photodiode response against triangular driving wave for Cl11-Si3-11Cl showing typical antiferroelectric hysteresis.

The antiferroelectric nature of the switching is also confirmed by examination of the hysteresis curve. Measuring the photodiode response to the triangular driving wave yields the characteristic antiferroelectric trace shown in Figure 4.23b.

The measurement of the two spontaneous polarisation realignment peaks requires a longer experimental method. Each peak is treated separately in the same manner as a ferroelectric peak, as described in §3.4.5. The bi-mesogenic compounds yield a slightly noisier signal, and the peak shift on the time-base is greater than that observed with the mono-mesogens. However, if the temperature run is restricted to ~10°C intervals, automation can still be used. This method produces the measurements shown in Figure 4.24. The spontaneous polarisation results are quoted as the addition of individually measured driven and relaxed peaks.

The choice of driving signal depends strongly on the sample's temperature. Fully saturated switching requires larger fields than those used with the mono-mesogens. Lower frequencies are used to allow the relaxed antiferroelectric phase to form and the two spontaneous polarisation realignment peaks to remain separated. At the high temperature end, a triangle-wave of 20 $V\mu m^{-1}$ at 80 Hz allowed saturated switching in all cases, as with the mono-mesogens. As the temperature was reduced, the voltage was increased and the frequency lowered to maintain saturated switching. Below approximately -40 °C shifted temperature, a maximum voltage of 35 $V\mu m^{-1}$ was applied at 5 Hz. Any further reduction in frequency resulted in chemical degradation of the sample and often the cell shorted. With shifted temperatures below -50°C, however, the switch was no longer fully saturated under such an applied field. The high fields yield a large baseline slope. The slope is flattened by feedback adjustment, as explained in §3.4.2.3. The high field also causes the quality of the peak trace on the oscilloscope to deteriorate significantly and this becomes more noticeable with decreasing temperature, requiring manual measurement of the traces. The change in the nature of the switch and the driving fields give a significant drop off in the magnitude of the spontaneous polarisation below – 40 °C of shifted temperature, which is clearly seen in Figure 4.24. However, the magnitude of the spontaneous polarisation is larger than that seen in the mono-mesogens. The spontaneous polarisation of F11-Si_3-11F was measured differently[28]. The compound was driven between its two ferroelectric states at higher fields and lower frequencies than the Br11-Si_3-11Br and Cl11-Si_3-11Cl compounds could withstand and thus no drop-off in the spontaneous polarisation is seen with decreasing temperature.

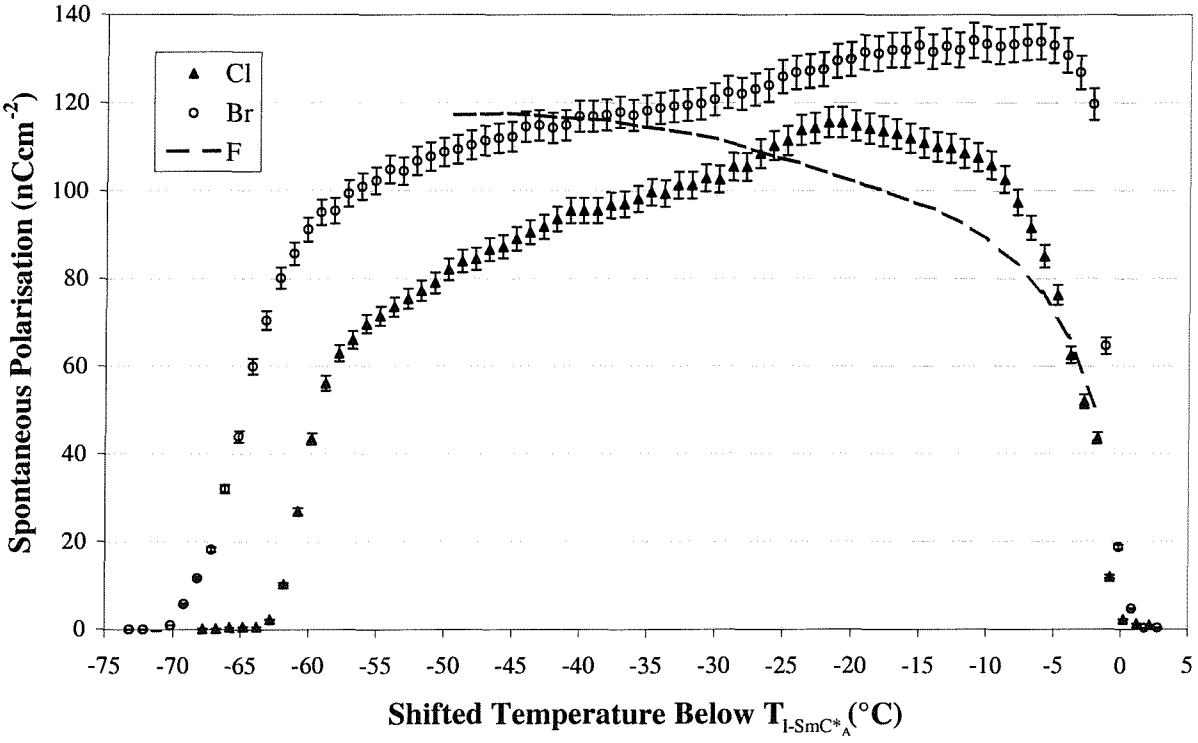

Figure 4.24 Spontaneous polarisation measurements of antiferroelectric bi-mesogenic organosiloxane compounds against shifted temperature.

4.5.1.4 Switching Time and Viscosity

Switching time measurements for the bi-mesogens were carried out using the current pulse technique. Similar fields were used to those of spontaneous polarisation measurements. The switching times shown in Figure 4.25a are of the same order as those recorded with the mono-mesogenic compounds.

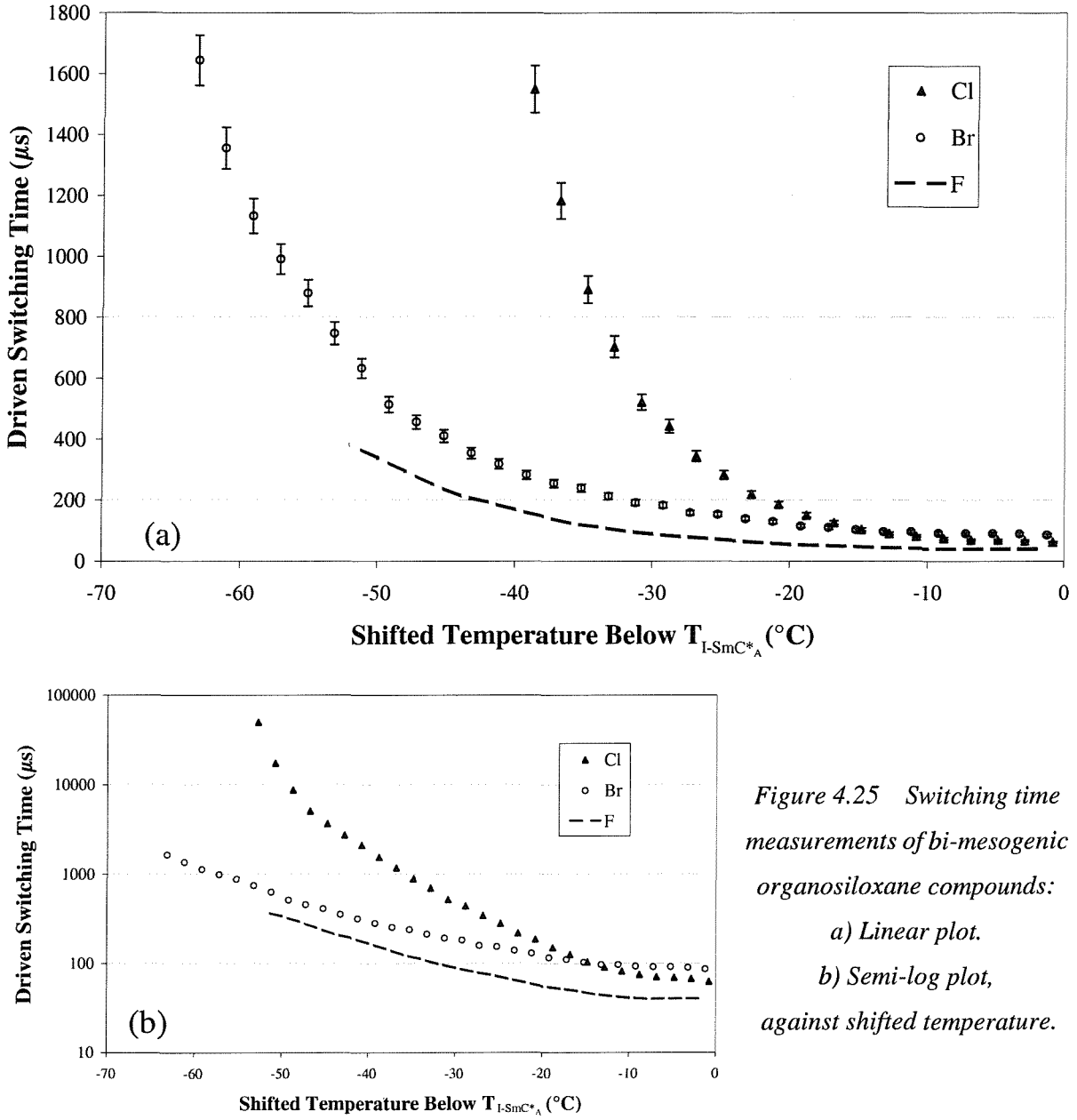

Figure 4.25 Switching time measurements of bi-mesogenic organosiloxane compounds: a) Linear plot. b) Semi-log plot, against shifted temperature.

This result may initially seem surprising given the larger size of the bi-mesogenic molecules, but the antiferroelectric nature of the compound means that only half the molecule is oriented by an electric field, making the nature of the switch similar to that of the mono-mesogens (the mechanism of the switch is examined in §4.5.2). Figure 4.25b shows the switching times as a function of shifted temperature on a semi-log plot. The switching times are expected to follow an exponential relationship, and should therefore allow a straight line fit, as seen for parts of the mono-mesogenic compound traces in Figure 4.14. However, the behaviour of bi-mesogens is not in agreement with the theoretical predictions given earlier. All the results show a curved nature, indicating a more complex

switching relationship. The curve of the results to slower switching times as the sample temperature falls is a consequence of the sharp decrease of the spontaneous polarisation, and thus a reduction in the effect of the dipole realignment torque.

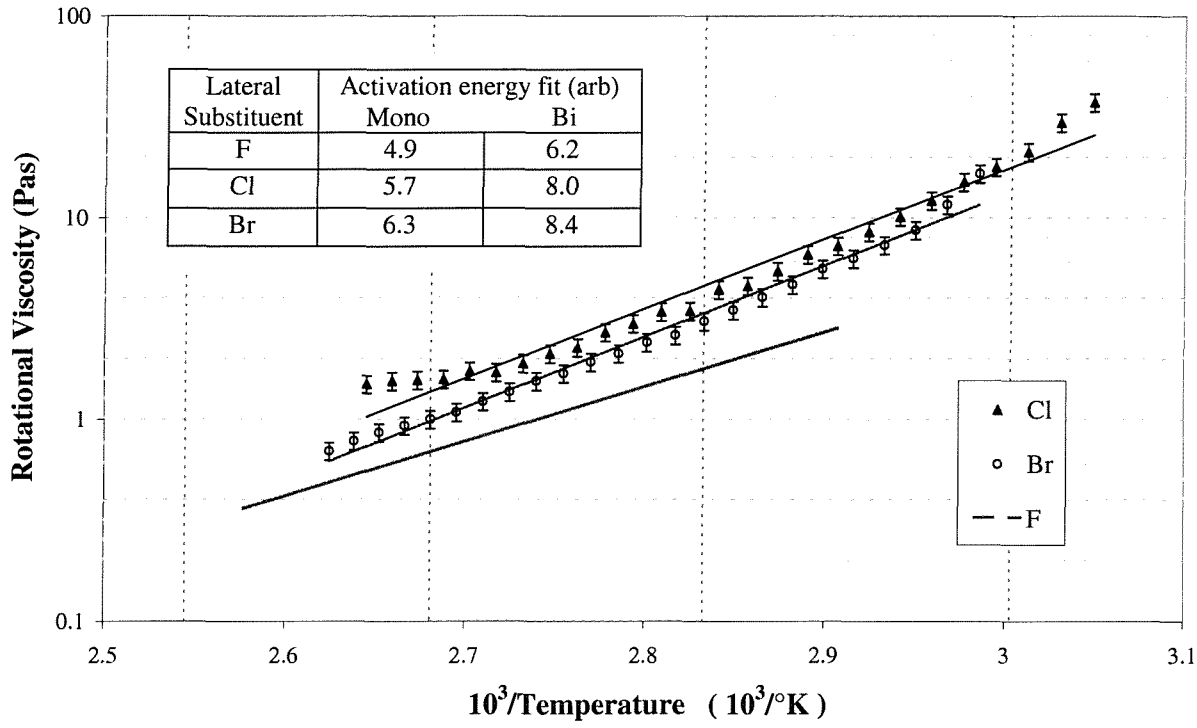

Figure 4.26 Rotational viscosity derived from electro-optic readings for bi-mesogenic organosiloxane compounds.

The results of rotational viscosity estimated by the current pulse technique are shown in Figure 4.26. No results were available for F11-Si3-11F. A proportionality constant is estimated for F11-Si3-11F, to give an estimate of probable viscosity for comparison, using calculations from switching time and spontaneous polarisation. In comparison with the mono-mesogens viscosities, the viscosities of the bi-mesogens are increased by about one order of magnitude for all compounds, with commensurately higher activation energies. There is some slight non-linearity in the data, which is attributed to a change in the nature of the switching mechanism at higher viscosities as with the switching times.

4.5.2 Antiferroelectric Switching

Unlike a conventional antiferroelectric where the director alternates from layer to layer to give the herringbone structure, in the bi-mesogenic organosiloxane materials the antiferroelectric nature is thought to be built into a single molecule. This structure yields the unusual I→SmC*$_A$ phase transition and the high phase stability. Antiferroelectricity is typically accompanied by large transverse dipoles and therefore large spontaneous polarisations. One argument used to explain the formation and stabilisation of the SmC*$_A$ phase, in preference to the SmC* phase, is antiparallel

alignment of the transverse dipoles[29], with pairs forming between adjacent layers. Some evidence has been found to support this argument. X-ray diffraction measurements by Ikeda et al.[30] have shown the influence of antiferroelectric stability on smectic layer spacing. They found that molecular dimerisation in adjacent layers played a crucial role in SmC^*_A phase stability.

Work on a series of F11-Si_n-11F bi-mesogens, varying the number, n, of siloxane units has shown that the ferroelectric behaviour is governed by the number of Si atoms in the core[22]. Even numbers of silicon atoms yield ferroelectric order. Antiferroelectric order is only seen with three and five silicon atoms. Antiferroelectric behaviour, although dominant in the three-length unit, is weaker when the number of silicon atoms is increased to five, and disappears completely when there are seven silicon atoms. Modelling of the core and alkyl chains has indicated that there is a bent conformation for odd numbers of silicon atoms and a straight conformation for even numbers[18].

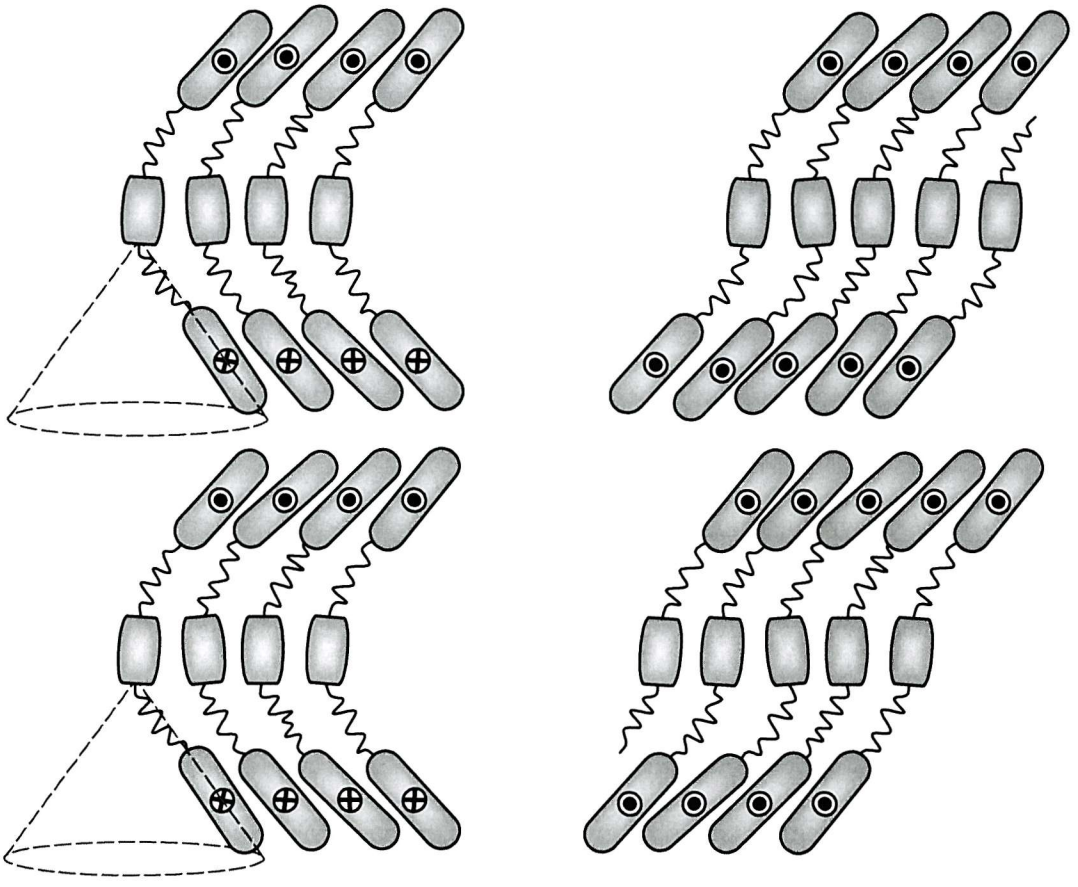

Relaxed Antiferroelectric State *Switched Ferroelectric State*

Figure 4.27 Schematic of the possible switching mechanism in bi-mesogenic organosiloxane molecules with a virtual backbone.

The influence of the siloxane core on the ferroelectric nature of the sample has led to a switching model for the bi-mesogenic compounds[31]. It is proposed that the antiferroelectric behaviour is caused by a bent confirmation of the entire molecule, as shown in Figure 4.27. The molecules are arranged

in 'effective bi-layers' with the siloxane cores once more forming a virtual backbone. The bent conformation is strong in the siloxane core containing three siloxane atoms and weakens with increasing core length (5-7-9). The even core lengths are thought to promote a straight conformation, and thus only ferroelectric phases are seen. The concept of a bent molecular structure fits well with the results. The idea that the herringbone structure is 'built into' the molecule, in conjunction with the formation of a virtual siloxane backbone, is one explanation for the high stability of the antiferroelectric phases. The mesogens are arranged with an antiparallel alignment of the dipoles between layers. The application of an electric field causes a dipole torque and reorients one half of the bi-mesogen with the field. The orientation will follow a Goldstone switch around a cone as proposed in Figure 4.27. The switching mechanism is similar to that expected in the mono-mesogenic molecules.

4.6 SUMMARY

This chapter has analysed the latest series of low molar mass compounds. Measurements made at a shifted temperature of -20°C are summarised in the table below.

Compound	I→Sm	Sm→Cr	Tilt	P_s	Switch	Viscosity
			(Deg)	($nCcm^{-2}$)	(μs)	(Pas)
Cl11-Si_3	92.5	43	42	93.5	277	0.93
Br11-Si_3	88	41	44.5	82.5	201	0.70
F11-Si_3	81	30	43	45	94	0.30
Cl11-Si_3-11Cl	108	48	41.5	115	171	2.3
Br11-Si_3-11Br	110.5	51.2	43	130	122	1.7

Table 4.1 A summary of the results of measurements of the latest series of low molar mass organosiloxane liquid crystal compounds at a shifted temperature of -20 °C.

The effect of varying the laterally substituted halogen highlights the complex balance between electronegativity and atomic size. All the compounds exhibit a high (40-45°) tilt angle, particularly important in single polariser applications, which are discussed in the following chapter. The high spontaneous polarisation of the Br11-Si_3-11Br and Cl11-Si_3-11Cl compounds is also very promising and gives scope for mixing. While mixing with a non-ferroelectric material would reduce the spontaneous polarisation, the inclusion of such an additive has the potential to reduce the viscosity of the resultant mesophase. A careful choice of the materials could therefore retain or improve the fast switching times.

4.7 REFERENCES

[1] H.J.Coles, H.F.Gleeson, G.Scherowsky, A.Schliwa, *Mol. Cryst. Liq. Cryst. Lett.,* **7**(4), 117 (1990).
[2] H.Finkelmann, U.Kiechle, G.Rehage, *Mol. Cryst. Liq. Cryst.,* **94**, 343 (1983); H.Finkelmann, *Phil. Trans. R. Soc. Lon. A,* **309**, 105 (1983).
[3] F.C.Bawden, N.W.Pirie, *Proc. R. Soc. Lon. B,* **123**, 274 (1937).
[4] S.Uchida, K.Morita, K.Miyoshi, K.Hashimoto, K.Kawasaki, *Mol. Cryst. Liq. Cryst.,* **155**, 93 (1988).
[5] A.I.Hopwood, H.J.Coles, *Polymer,* **26**, 1312 (1985).
[6] G.A.Lester, H.J.Coles, A.Murayama, M.Ishikawa, *Ferroelectrics,* **148**, 389 (1993).
[7] H.Finkelmann, H.Ringsdorf, J.Wendorff, *Makromol. Chem,* **179**, 273 (1978).
[8] P.J.Collins, M.Hird, *Introduction to Liquid Crystals,* Chpt **5**, (Taylor & Francis, 1998).
[9] K.Sunohara, K.Takatoh, M.Sakamoto, *Liq. Cryst.,* **13**(2), 283 (1993).
[10] R.Simon, H.J.Coles, *Mol. Cryst. Liq. Cryst. Lett.,* **102**, 43 (1984); *Liq. Cryst.,* **1**(3), 281 (1986).
[11] H.J.Coles, *Faraday Discuss. Chem. Soc.,* **79**, 201 (1985).
[12] M.Dumon, H.T.Nguyen, M.Mauzac, C.Destrade, H.Gasparoux, *Liq. Cryst.,* **4**(10), 475 (1991).
[13] M. Ibn-Elhaj, A.Skoulios, D.Guillon, J.Newton, P.Hodge, H.J.Coles, *Liq. Cryst.,* **19**(3), 373 (1995); *J. de Phys. II (Paris).,* **6**, 271 (1996).
[14] P.Kloess, J.McComb, H.J.Coles, R.Zentel. *Ferroelectrics* **180**, 233 (1996).
[15] J.Newton, H.J.Coles, P.Hodge, J.Hannington, *J. Mater. Chem.,* **4**(6), 869 (1994).
[16] H.Poths, R.Zentel, *Liq. Cryst.,* **16**(5), 749 (1994).
[17] H.J.Coles, I.Butler, K.Raina, J.Newton, J.Hannington, D.Thomas, *SPIE,* **2408**, 14 (1995); H.J.Coles, H.Owen, J.Newton, P.Hodge, *ibid.,* **2408**, 22 (1995)
[18] P.Kloess, *Ph.D. Thesis,* The University of Southampton (1997).
[19] H.Kapitza, R.Zentel, R.J.Twieg, C.Nguyen, S.U.Vallerien, F.Kremer, C.G.Willson, *Adv. Mater.,* **2**(11), 539 (1990).
[20] J.Newton, *Ph.D. Thesis,* The University of Manchester (1994).
[21] A.T.M.Marcelis, A.Koudijs, E.J.R.Sudhölter, *Liq. Cryst.,* **18**(6), 843 (1995).
[22] W.K.Robinson, C.Carboni, P.S.Kloess, S.P.Perkins, H.J.Coles, *Liq. Cryst.,* **25**(3), 301 (1998).
[23] K.Furukawa, K.Terashima, M.Ichihashi, S.Saitoh, K.Miyazawa, T.Inukai, *Ferroelectrics,* **85**, 451 (1988).
[24] T.Inukai, S.Saitoh, H.Inoue, K.Miyazawa, K.Terashima, K, Furukawa, *Mol. Cryst. Liq. Cryst.,* **141**, 251 (1986).
[25] D.J.Byron, A.S.Matharu, R.C.Wilson, J.W.Brown, *Mol. Cryst. Liq. Cryst.,* **258**, 95 (1995).
[26] P.J.Collins, M.Hird, *Introduction to Liquid Crystals,* Chpt **3**, (Taylor & Francis, 1998).
[27] E.Corsellis, D.Guillon, P.Kloess, H.J.Coles, *Liq. Cryst.,* **23**(2), 235 (1997).
[28] R.Campin, Ph.D. Thesis, *University of Manchester,* (1998).
[29] Y.Takanishi, K.Hiraoka, V.K.Agrawal, H.Takezoe, A.Fukuda, M.Matsushita, *Jpn. J. Appl. Phys.,* **30**(9A), 2023, (1991).
[30] A.Ikeda, Y.Takanishi, H.Takezoe, A.Fukuda, *Jpn. J. Appl. Phys.,* **32**(2), L97, (1993).
[31] W.K.Robinson, P.S.Kloess, C.Carboni, H.J.Coles, *Liq. Cryst.,* **23**(2), 309 (1997).

Chapter Five

Dye Guest Host Systems

A pessimist sees the difficulty in every opportunity;
an optimist sees the opportunity in every difficulty.

Winston Churchill 1874-1965

5.1 INTRODUCTION

Practical liquid crystal systems are often composed of a mixture of compounds with different properties, chosen to achieve a desirable result. This chapter looks at the effects of adding dyes to the organosiloxane materials discussed in the previous chapter. The concept of dye addition in liquid crystal systems is not a new one: in 1968[1] Heilmeier and Zanoni introduced a dye (or guest) into a nematic liquid crystal host. If the guest molecules are suitably anisotropic in shape the guest is aligned via steric forces with the host. Reorientation of the host molecules can then reorient the guest as the dopant dye molecules prefer to remain aligned with the liquid crystal solvent. If the anisotropy of the dye molecules is sufficient, they will also be anisotropic in their absorption characteristics. Thus, if the mixture is illuminated with suitably oriented polarised light, the two states of the dye can be accessed without a second polariser. These properties are termed the Dye Guest Host (DGH) effect, as originally suggested by Heilmeier and Zanoni[1].

The many advantages offered by dye guest host displays, such as increased brightness and wide viewing angle, are discussed in this chapter. Until recently, the DGH effect was only demonstrated in nematics. Although nematic DGH devices achieved some commercial success in displays such as those used on some petrol pumps, the technology was never refined sufficiently for large-scale, flat panel display use. The advantages of dye addition were outweighed by their adverse effect on the nematic systems. A non-liquid crystalline dye will act as an impurity in the system and may affect all the electro-optic properties, in particular switching time, conductance and alignment. The drawbacks hampered DGH development and only specialist applications were found, in contrast to the large-scale production of the twisted nematic family of displays.

In the last decade, the possibility of reviving interest in the DGH effect has come about with the discovery of ferroelectric liquid crystals. The surface stabilised ferroelectric liquid crystal cell (SSFLC) offers a new wealth of possibilities and entirely new geometries. The main requirement for a single polariser ferroelectric DGH device is a 45° tilt compound. The latest development of the low molar mass organosiloxanes made within the group and described in the previous chapter has made the ferroelectric DGH device a possibility for the first time.

This chapter looks at the concepts behind single polariser devices and the application of the SSFLC geometry to DGH work. The feasibility of such a device is assessed with a number of commercial dyes. The unusual characteristics of the low molar mass organosiloxanes have also created the possibility for a unique DGH antiferroelectric geometry, resulting in three different transmission states.

5.2 DYES

One effect of a dissolved dye is to increase the absorption of the sample in a particular wavelength region. The guest-host effect utilises the fact that the dye's absorption coefficients are different for light polarised perpendicular or parallel to the dye molecule.

5.2.1 Dye Theory

If a molecules absorbs light most strongly along a single axis, it is called a dichroic dye. The molecule absorbs light of a certain spectral range if its polarisation is parallel to the dye's absorbing axis and transmits the light if its polarisation is normal to the absorbing axis. As with liquid crystal molecules, the shape anisotropy of a dye can take many forms, however, in this theoretical treatment of the DGH effect, the dye molecule is approximated by a rod shape. A transition moment, **T,** is defined, along which the electronic field vector, **E,** is most likely to be absorbed. Figure 5.1 demonstrates the absorption characteristics of two types of dye; positive and negative. A positive, or p-type dye, has a transition moment in the direction of its long axis. When illuminated with circularly polarised light, the transition moment will interact with the parallel component of the E-field whilst passing the perpendicular component. A negative, n-type, dye has the opposite effect; the transition moment lies perpendicular to the molecular long axis. Since the dye is spinning about its long axis, **T** interacts with the E-field in any direction orthogonal to the axis but passes the parallel component.

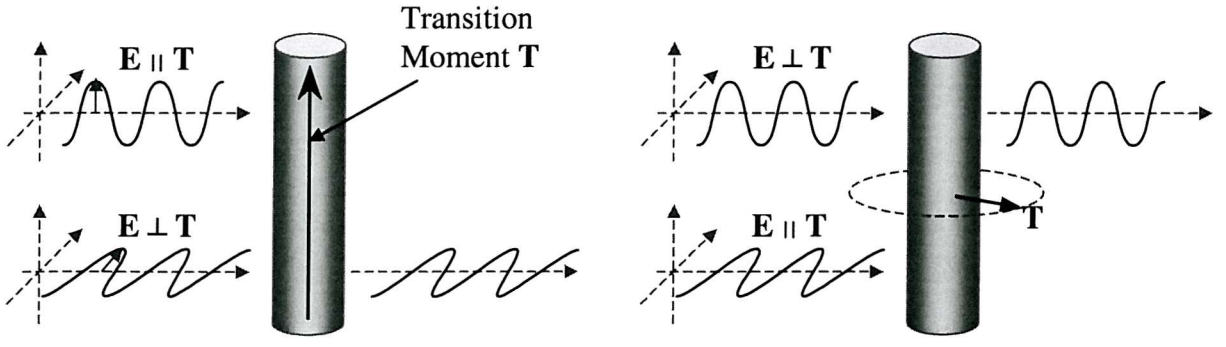

a) P-Type Dye *b) N-Type Dye*

Figure 5.1 A schematic demonstrating the interaction of P-type and N-type dyes with the orthogonal linear components of circularly polarised light.

Figure 5.1 is a simplistic view of the interactions, as **T** and **E** are wavelength-dependent. This dependence results in incomplete absorption of the components of **E** || **T** and hence the characteristic colour of the dye is passed. If the incident light is plane-polarised and switched between parallel and perpendicular alignment, relative to **T**, the transmitted light will alter between two states. In one state the characteristic colour of the dye will be seen, whilst in the other state the incident light will be

passed almost unaffected. Alternatively, reorienting the dye whilst maintaining the same polarised illumination will produce the same optical effect.

These selective absorption characteristics are the basis of the dye-guest host effect. If a suitably small amount of dye dopant is introduced into a liquid crystal host, the dye molecules are ordered with the liquid crystal. This interaction allows the dye to be switched with the host, which can allow a display to be switched from clear, to a colour and back to clear. The use of both n- and p-type dyes can allow a display to switch from one colour to another.

5.2.1.1 Dichroic Ratio

In order to align with the host, the guest dye molecule must be suitably anisotropic. It is worth remembering that no liquid crystal is perfectly ordered. Thermal fluctuations mean that each molecule makes a small angle, θ, with the director **n**. The distribution of the molecules about the director is defined by an order parameter (as discussed in §1.4). When the dye molecules align with the liquid crystal, their long axes will also make a small angle, ϕ, with the director of the host. The dye molecules can then also be defined by an order parameter in ϕ. In practical applications it is the arrangement of the transition moment, **T,** that is important. The different order parameters of host, dye and transition moment all have consequences when describing the relationships within the mixture mathematically. These are discussed in greater depth in the work of B.Bahadur[2] and W.S Park[3].

The efficiency of a dye in a DGH device is governed by the dichroic ratio *(DR)* and is defined as[4]

$$DR = \frac{A_{\parallel}}{A_{\perp}}, \qquad 5.1$$

where $A_{\parallel}$ and $A_{\perp}$ are the absorption characteristics parallel and perpendicular to the long axis of the molecule. This simple ratio has the advantage of being independent of dye concentration and the thickness of the liquid crystal layer[5]. Clearly, a positive dye will have a dichroic ratio > 1 and a negative dye will have a dichroic ratio < 1. Ideally, the dye will possess very similar properties to the liquid crystal host, so it is often useful to consider the relationship between the order parameter of the transition moment, S_T, in terms of the anisotropic absorbancies or the dichroic ratio[3],

$$S_T = \frac{A_{\parallel} - A_{\perp}}{A_{\parallel} + 2A_{\perp}} = \frac{DR - 1}{DR + 2}. \qquad 5.2$$

5.2.1.2 Absorbance

The absorbance of a particular dye is governed by the Beer-Lambert law as discussed in §3.5.3,

$$A_{dye} = \varepsilon cd = \log_{10}\left(\frac{I_0}{I_T}\right), \qquad 5.3$$

where I_0 is the intensity of incident light and I_T the intensity of light transmitted through a sample of dye concentration c, thickness d and molar absorption coefficient, ε. In order to measure the values of $A_{\parallel}$ and $A_{\perp}$, the dye is aligned with the host in an electro-optic cell. A cell of similar thickness is filled with the undoped host liquid crystal. These cells are placed in a double beam spectrometer. The cells are oriented in the same manner and both illuminated with the same polarised light. The cell with no dye acts as a compensator and corrects for scattering, reflection, transmission and other effects of the host molecules. By switching the cell or altering the plane of polarisation, both absorption coefficients can be determined.

5.2.1.3 Contrast Ratios

A major issue in device manufacture is the sharpness of the display's response, determined by the ability to differentiate a pixel from the background, which is measured as a contrast ratio. The contrast ratio is directly related to the dichroic ratio[2] and thus also has the advantage of being independent of dye concentration and sample thickness. Many different measures of contrast ratio exist, depending on the nature of the display. The most simply defined contrast ratio measures the maximum/minimum transmitted intensity for an active pixel. To differentiate a character from its background by eye, a minimum contrast ratio of ~2:1 is required, and the contrast ratio should preferably be >5:1, with 10:1 sufficient for good quality character recognition (for example, newsprint normally has a contrast ratio ~7:1). A typical nematic cell can have contrast ratios 20:1–100:1, although it is worth noting that in these cases the contrast ratio falls drastically with obtuse viewing[2].

When measuring contrast ratios using a photodiode on the microscope it is important to consider carefully the initial reference level. The contrast ratio is more accurately defined as the ratio of the maximum luminance to the minimum luminance between the symbol and the background. The background can either be the luminance of the off-state or the inactive part of the cell. The idea of a blank spectrum, discussed previously in the experimental chapter (§3.3.4.1), is utilised in much of this work. One important consideration is the wavelength response of the eye. The contrast ratio is typically quoted at the wavelength corresponding to an intensity maximum, giving an idea of the maximum capability of the dye but not the true photo-optic response. This discrepancy leads to many other definitions of contrast ratio that include weighting factors for the eye's response such as Bloom and Priestley's perceived contrast ratio[6].

Another consideration is the excellent sensitivity of the eye when discriminating colour. A lower contrast ratio is acceptable if the character and background have different chrominance. Hence contrasts such as red lettering on a green background can be detected even if the two states have the same luminance. This leads to complicated definitions of colour difference ratio, and is studied in depth in the work of Shimomura et al.[7] In summary, the true contrast ratio must take account of not only the amount, but also the wavelength of the light transmitted. A further complication is the environment in which the readings are made. Very rarely does a display operate in a totally dark room, and different colours will be seen when viewed in different illuminations[8], thus environment luminance levels also play a part. The purpose of contrast ratios in this work is only to assess a given cell's ability to function as a display. The actual values are more important for comparison between dyes, and thus a simple ratio of maximum/minimum transmitted intensity for an active pixel is used.

5.2.2 Dye Qualities

The ability of a dye to function in a guest-host device is determined by many different parameters; this section identifies some of the qualities investigated.

- *Long lifetimes* - the guest dyes must be extremely stable in the host:[9]
    - *Chemically* - it should not react with the host;
    - *Photochemically* - the colour should not change or fade;
    - *Electrochemically* - as all devices require the use of driving voltages; in order to avoid electrochemical degradation, the dye should have a high electrical resistivity of $\sim 10^8$ -$10^9\ \Omega cm^{-1}$ with a non-ionic nature to reduce current consumption.
- *High solubility and thermal stability* - the dye must remain dissolved in the host over a wide temperature range and can expect to meet very stringent requirements, for example -40°C ↔ +90°C for applications such as those found in automobiles. The temperature requirements are even more stringent for military applications.
- *Colour of hue and spectral width* - this is important for determining the possible useful optical range.
- *Absorption coefficient* - the higher the efficiency of a dye, the more economical it is because less material needs to be dissolved in a sample.
- *Dichroic ratio* - this is related to the anisotropic nature of the dye. The higher the dichroic ratio the greater the contrast between the two states.
- *Order parameter* - ideally this is matched to the host to encourage a well ordered sample.
- *Effect on viscosity* - dramatic increases in viscosity caused by bulky or mismatched dyes will impair switching.
- *Purity* - as in all liquid crystal work, the dye must be pure to avoid being a source of contaminants in the system.

Finally it is noteworthy that although liquid crystalline dyes are becoming more common, the dye is not necessarily liquid crystalline. The most common dye guests are azo and anthraquinone dyes.

5.2.3 Azo Dyes

Many of the dyes for liquid crystal work are based around an azo group. The structure consists of a double nitrogen bond (-N=N-), typically between phenyl or naphthalene rings. One of the unique features of the azo linkage is its ability to adopt different configurations. Figure 5.2 shows a schematic of two possible isomeric forms, where R and R' are the aromatic components. The arrangement is referred to as *trans* in the straight configuration and *cis* in the bent configuration. The *trans*-isomer is more stable than the *cis*-isomer. The transition moment of a dye containing an azo linkage lies along the molecular long axis from the donor group, D, to the acceptor group, A (Figure 5.2c). The molecule can be switched from *trans* to *cis* by the application of ultra-violet light. This is known as photoisomerisation or the photomechanical effect.

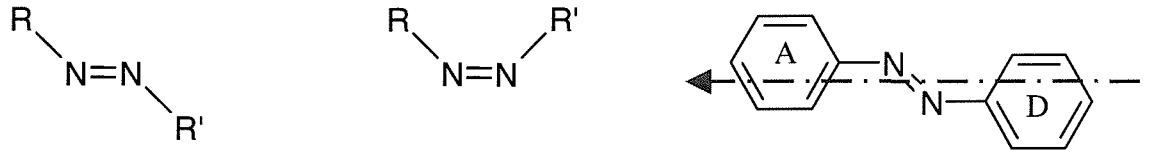

a) Trans *b) Cis* *c) Dipole Moment*

Figure 5.2 Schematic of the trans and cis configurations of an azo dye.

5.2.3.1 Photochromism and Photoisomerisation

Photochromism is the ability to undergo a reversible change between states with different absorption properties. Such switching can occur due to molecular excitation or a configurational change such as photoisomerisation. Photoisomerisation occurs when a molecule undergoes a steric (*cis-trans*) change when illuminated by light of the appropriate wavelength. Photoisomerising molecules can be introduced directly as a dopant or attached as a pendent molecule in, for example, a side-chain polymer. Liquid crystal properties are very sensitive to changes at a molecular level, thus small steric changes can have an amplified effect on the liquid crystal phase. These effects can be seen in many of the thermotropic classes, recently Ikeda et al.[10] demonstrated optical switching in an FLC with a photochromic compound.

The *cis*↔*trans* orientation in the azo linkage is a good example of a possible photoisomerisation. A great deal of work has been done within the Southampton liquid crystal group on azobenzene dyes. Previous work investigated the photomechanical effect in commercial smectic liquid crystals[11] and showed the effects of even low power illumination. Ultra-violet light at 360 nm and <10 $mWcm^{-2}$

converted an azobenzene dye from its *trans* to its bent *cis* isomer. The change caused the spontaneous polarisation of the DGH system to fall, consistent with the expectation of disrupted packing. This added disruption due to the bent conformation can also reduce phase transition temperatures. The effect is fully reversible upon removal of the illumination.

5.2.4 Anthraquinone Dyes

Another popular dye structure is that of the anthraquinone. Anthraquinone dyes are synthesised by attaching electron donating groups at the numbered points on the rings of the polyaromatic core structure shown in Figure 5.3. The molecule is planar with its transition moment in the plane of the molecule.

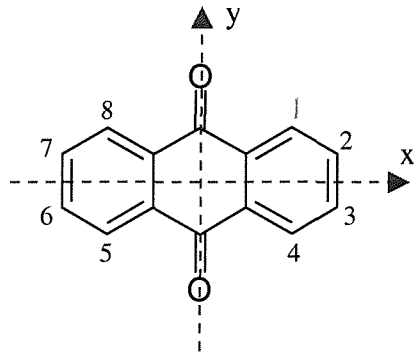

Figure 5.3 Core structure of an anthraquinone dye.

Anthraquinone dyes used in dye guest-host work typically have their transition moment almost parallel to their molecular long axis and have a positive dichroism[12]. Anthraquinone dyes do not absorb light as strongly as azo dyes. The absorption coefficient of a typical azo dye ($\varepsilon \approx$ 1-2 x10^4 Lmol^{-1}cm^{-1}) is roughly twice that of an anthraquinone, and thus typically around twice as much anthraquinone dye is needed in a mixture for a similar effect to that of an azo dye. Azo dyes (particularly compounds with multiple azo groups) also typically have slightly higher order parameters ($S_{op}\approx$0.6-0.8) than anthraquinones ($S_{op}\approx$0.5-0.7). However, anthraquinones are still popular choices for DGH work because of their high chemical and thermal stability, these properties coupled with a high photostability and strong colouring, leads to a good light 'fastness' in comparison with azo dyes[13].

5.2.5 Nematic Dye Guest Host Cell Arrangements

The earliest single polariser colour display was proposed by Heilmeier and Zanoni[1]. A positive blue dye (indophenol blue) was dissolved in a nematic host with positive dielectric anisotropy. The mixture was placed in a 12 μm cell where the molecules adopted a planar alignment. The incident light was polarised parallel to the transition moment of the dye and the blue colour of the dye was

observed as shown in Figure 5.4. Upon the application of a field, the liquid crystal molecules adopt a homeotropic arrangement, the transition moment no longer lies parallel to E, and hence the light is not absorbed. The result is a display with a blue field-off state and an almost colourless field-on state. Although offering enhanced brightness, the development of the display was hampered by several factors. The response times were slow (1-5 ms), with relaxation times of ~20 ms, and the contrast ratio of the dye was poor.

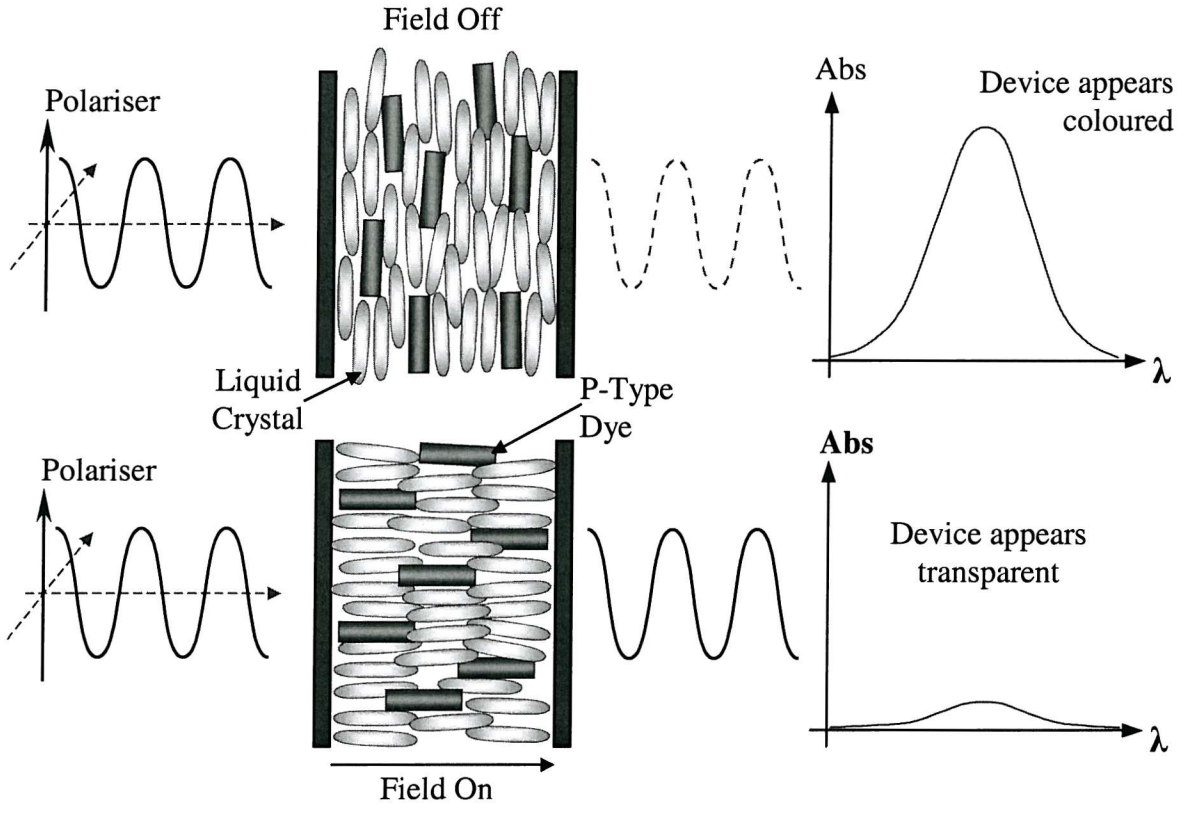

Figure 5.4 A schematic of the operating principles of the earliest dye guest host display by Heilmeier and Zanoni[1].

The brightness levels were improved by the complete removal of polarisers and the use of higher order parameter dyes. White and Taylor[14] accomplished this by utilising the phase change effect in a chiral nematic. Using a planar alignment layer, a Grandjean texture forms with a "standing" helix. The dye is aligned with the liquid crystal and follows the helix. The twist of the helix results in the positive dye interacting with all incident polarisations, and the coloured state is seen. The application of a small field results in a scattering texture as the Grandjean texture is disrupted and causes the absorption of the dye to drop off. Finally, with a sufficient field, the helix is unwound into a fully homeotropic texture, and as with the Heilmeier display, there is very little absorption. The absence of any polarisers improves brightness and viewing angle, however, effective operation requires a chiral nematic pitch $<3\ \mu m$ and this requires a very high switching voltage to achieve full contrast[15]. Hysteresis effects can also often lead to undesired scattering in the off state.

Cole and Kashnow[16] used a quarter wave plate and a reflector to allow a Heilmeier display to function without polarisers. In the field-off state, half of the unpolarised light interacts with the transition moment. The unaffected component passes through a quarter wave plate, on to a reflector, and back through the wave plate, finally returning to the cell with its polarisation state rotated by 90°. It can then interact with the dye molecules with the result that all the incident light interacts with the dye to give a coloured state. When a field is applied and the mixture is reoriented into a homeotropic state, the unpolarised light no longer interacts with the dye, and a clear state is seen.

Many other types of DGH display exist, most using a variant of the Heilmeier idea. Uchida et al[5] proposed a double layer arrangement. Two Heilmeier cells are fabricated and sandwiched at 90° to one another. Each cell acts as a controllable polariser giving a clear and fully dyed state with no external polarisation. The double DGH geometry has the advantage of high brightness, wide viewing angle, and low-operating voltage[17].

The use of positive dyes in these geometries results in displays with a negative contrast (light symbols on a dyed background). However, under conditions of weak illumination, a positive contrast is preferable[18] (dark symbols on a bright background), and this can be achieved with the use of negative dyes.

5.2.5.1 Benefits and Drawbacks

Most liquid crystals do not absorb in the visible spectrum and their refractive indices and polarisabilities are only weakly frequency dependent[19]. Therefore, in order to produce a coloured display, most applications rely on colour filters, which reduce the performance of a display. The colour filter in a liquid crystal display is similar to a conventional cathode ray screen, with a red, green and blue spot, hence each pixel has three colour elements. Thus to achieve a red display, for example, the green and blue filters must be blocked and only a third of the available light is used. Colour filter transmission can be as low as 25%, and in full colour active matrix liquid crystal displays[2] the overall transmission can be as low as 5%. The use of a colour filter with a polariser and analyser in conjunction with the liquid crystal cell can also lead to parallax problems. The inherent thickness of a typical twisted nematic device limits the angle over which the display is observed with the correct colour and makes the large contrast of twisted nematic cells strongly angle dependent[15].

Fabricating a Heilmeier-type single polariser dye guest-host device allows some of the problems to be solved. The use of dyes gives direct access to coloured states and can avoid the need for the front polariser and colour filters. Removal of the analyser has several advantages. The first is an increase in the brightness of the transmitted state; a higher transmission characteristic reduces the illumination required. This reduction has substantial knock-on effects. The need for high battery power, largely to meet screen power requirements, is one of the main factors limiting the reduction in size and weight

of many lap-top computers[20]. Another advantage is a reduction of the complexity of the optical elements, thus reducing parallax problems and increasing the viewing angle. Incorporating the colour filter directly into the liquid crystal cell reduces parallax problems still further. Thus a fully transmitting state has no filters or polarisers in the optical path and a coloured state only has the dye.

Dye guest host devices have had trouble competing as an alternative technology to the twisted nematic display. One factor affecting dye guest host devices arises from the fact that the effective order parameter of a dichroic dye is lower than a polarising filter, making it difficult for a dichroic display to match the contrast ratio of a device such as the twisted nematic display. Other reasons for a lack of commercialisation lie in the limitations in large displays since the multiplexing ability depends on threshold sharpness and static response, which is poorer than a twisted nematic. This is due to the shallow nature, or hysteresis, of the transmission/voltage characteristics[21].

5.2.6 The Surface Stabilised Ferroelectric Liquid Crystal DGH Geometry

Any liquid crystal display performance depends on the materials used. Many of the requirements for a ferroelectric DGH display are no different from the nematic DGH display. These requirements include properties such as a broad phase temperature range, stability in a wide range of environments, and a low viscosity for fast switching. However, there is the extra requirement of 45° tilt, that should remain temperature independent. The 45° requirement is a consequence of the surface stabilised geometry. Recalling the discussion in the theory chapter, a conventional bistable crossed polariser surface stabilised ferroelectric liquid crystal (SSFLC) display utilises a 22.5° tilt material. This setup allows the effective optic axis to be switched from lying parallel to one polariser's transmission axis (dark state) to a 45° position between the polarisers, giving a maximum transmission state. In the DGH geometry, the anisotropic dye acts as the second polariser. Thus maximum transmission will occur when the transmission axis of the dye is aligned with the polariser, and minimum transmission (the dyed state) will occur when the transmission axis of the dye is oriented at 90° to the polariser. Hence, for a 90° switch to occur in the SSFLC geometry, the host liquid crystal must have a 45° tilt angle. A diagram of the working principal of a typical SSFLC dye guest host cell is shown in Figure 5.5. This schematic shows how the interaction of a positive green dye with the incident plane polarised light allows a suitably oriented cell to be switched between a white and a coloured state.

There has been minimal research into the possibility of a DGH mode in SSFLC cells, in comparison with the number of studies of the more standard crossed polariser application. Thus, the majority of ferroelectric liquid crystals for display purposes are designed to have the optimum 22.5° tilt necessary for a crossed polariser SSFLC application. It is only in the past 10 years, with the synthesis of higher tilt materials, that the use of the SSFLC geometry has become a possibility in single polariser DGH work.

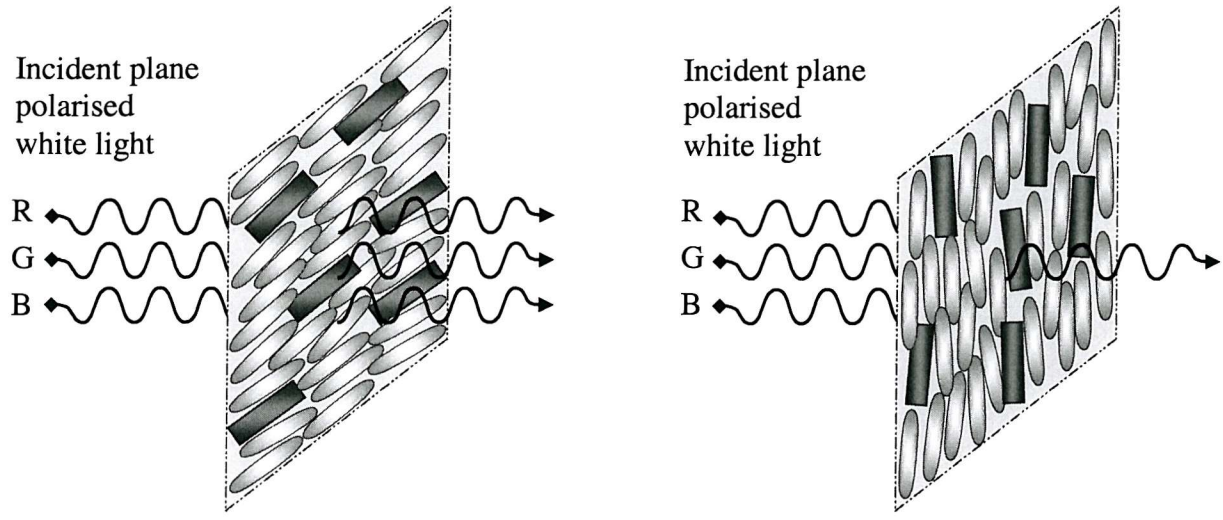

White 'off' state *Coloured 'on' state*

Figure 5.5 A schematic of a surface stabilised ferroelectric dye-guest host cell.

The possibility of using ferroelectric liquid crystals for DGH applications was first investigated in 1985 by Kondo et al.[22] This work was carried out using a ferroelectric host with a 23° tilt angle and a very low spontaneous polarisation. The results were poor, highlighting the need for improved materials. Work began to synthesise materials with improved tilt angles and spontaneous polarisation characteristics in the U.K. in the Manchester group of H.J.Coles[23]. Although 45° is desirable for a full contrast DGH display, the sine-squared nature of the transmission equation for a SSFLC means that a device can still work well with a non-ideal switching angle. A transmission change of around 70% can be achieved with as little as a 28° tilt angle[24]. However, for the geometry to work at maximum efficiency, a 45° material is required. This has only become possible with the evolution of the organosiloxane materials studied in the previous chapter.

5.2.6.1 Advantages of the Surface Stabilised Ferroelectric Liquid Crystal Geometry

The potential benefits of ferroelectric liquid crystals over nematics are well known. Primarily, with ferroelectric materials, switching responses are in the microsecond regime and surface alignment induced bistability leads to almost permanent memory states. The application of these benefits to many display devices has long been sought. The ferroelectric effect has the advantage of being linear in applied field E, whereas a twisted nematic device approximately follows an E^2 switching relationship and is thus insensitive to field direction. Hence, while the twisted nematic device is electrically driven, it relaxes back elastically. Although nematic liquid crystals are capable of millisecond switching times they are still an order of magnitude slower than the ferroelectric switching times and high video refresh rates in the microseconds. The SSFLC bistability, with almost permanent memory states, allows a pixel to be switched with a short voltage pulse. Removing the need for permanently driven states permits smaller and more closely packed pixels without cross-talk.

A primary concern with any liquid crystal display is ease of production and manufacture. The use of SSFLC geometry can remove the need for the more complicated switching methods and thin film transistor back-planes used in many current flat panel nematic displays.

The difference in switching dynamics between the twisted nematic and SSFLC modes can also be advantageous. A ferroelectric switches in-plane and hence there is very little azimuthal variance in birefringence and colour because the optic axis is always roughly parallel to the cell plane. In a twisted nematic device the optic axis points out of this plane in the field-on state, and the device is highly sensitive to angular variation and even contrast inversion. Another advantage of in-plane switching is colour neutrality: in a twisted nematic, intermediate field values while bestowing some grey-scale capability, tilt the optic axis and change the material's birefringence. The dye guest host SSFLC geometry also remains insensitive to colour and brightness variations when the cell gap fluctuates[22].

As discussed earlier, an ideal ferroelectric host must have a 45° tilt angle. Clearly, an ideal material would possess a wide temperature range over which its electro-optic properties do not change. First order materials, i.e. with an I –SmC* transition have the advantage of smaller tilt variance with temperature, as was shown in the previous chapter. For a second order material to be practical it must be used in the lower part of its temperature range where the tilt variance with temperature is less pronounced. Thus, the organosiloxane liquid crystals introduced in chapter four are ideal candidates for testing the possibility of realising the advantages of the ferroelectric mode in dye guest host work.

5.3 Dyes Used in this Work

The choice of dye is clearly very important. Initially, three commercial dyes have been used; a dark mauve azo dye from Mitsui (M777), a blue dye from Merck (D102) and a black dye from ICI. These provide a mix of dye types, azo and anthraquinone, and different colours for comparative studies of the SSFLC dye guest host geometry.

5.3.1 M777

M777 is a dark mauve, highly conjugated diazo dye from the Mitsui Toatsu Chemical Company[25] the chemical structure of which is shown in Figure 5.6. The compound is a 1:1:1 mix of three similar naphthyl-azo compounds. It was chosen because of a good record for stability in a wide range of liquid crystal mixtures[26] and a high dichroic ratio[25] of ~13 at the peak absorption wavelength ~560 nm in standard nematic mixtures.

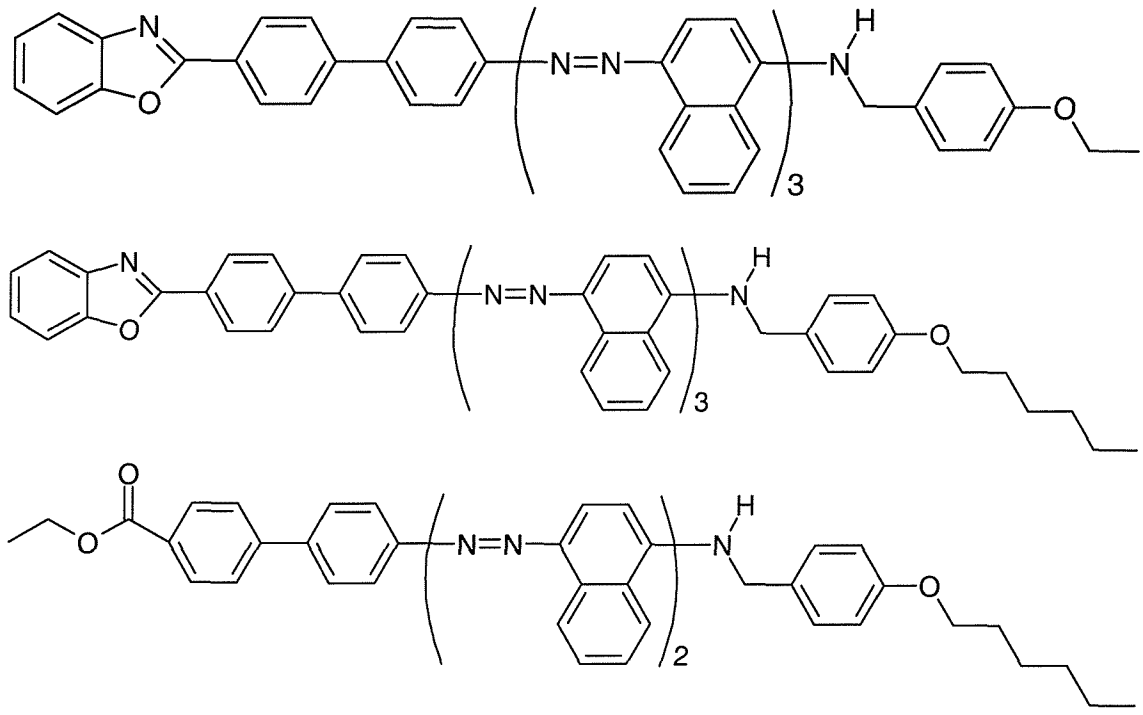

Figure 5.6 The chemical structure of the three components of Mitsui dye - M777.

5.3.2 D102

D102 is a deep blue diamino-anthraquinone dye from BDH/Merck[27]. The exact structure is proprietary but is thought to be very similar to that shown in Figure 5.7. This is sufficient for a good approximation of the molar mass of the dye.

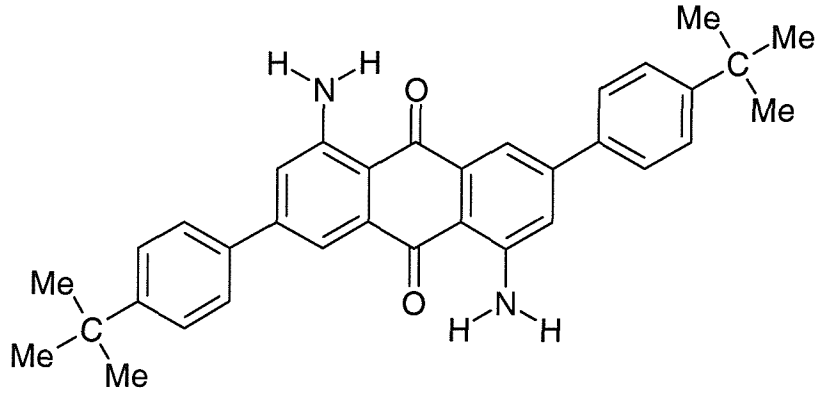

Figure 5.7 The basic chemical structure of the BDH/Merck D100-series dyes.

Although it is bulkier than simple anthraquinones, the structure of this dye does not necessarily hamper its solubility. Work by Foitzik and Haase on the solubilities of a range of similar anthraquinone dyes synthesised by Merck, showed that the size of the molecule had very little influence on its solubility[28]. This was highlighted in their work by the fact that the dye molecules with the smallest dimensions were the least soluble. D102 was chosen because it had been used in previous nematic DGH work, it has a high order parameter[27] (~0.8), a solubility in excess of 4% in commercial nematic mixtures and it was readily available.

5.3.3 ICI Black

The ICI black dye was chosen to assess the possibility of a DGH monochrome display. Typically, several dyes are mixed to form a black dye. Many examples in nematic DGH work are based around anthraquinone dyes and have had some success in applications such as dashboard displays[29]. This ICI dye is also proprietary, and although the exact structure is unknown it is thought to contain a mix of anthraquinone dyes including D102.

5.3.4 Mixing and Cell Preparation

The amount of non liquid-crystalline dye used in DGH applications is often less than 5% and this can present problems when preparing the mixtures. The organosiloxane hosts are synthesised in-house in small amounts (grams), and only very small amounts of dye are available (milligrams). This makes accurate measurement and minimisation of waste very important. The procedures used are discussed in §3.3.5. In order to fill several cells, mixtures typically consist of ~10 mg of liquid crystal and 0.5 mg of dye. Maintaining high levels of purity is of paramount importance in order to achieve accurate and reproducible results. It was sometimes found that the D102 dye contained small flecks, thus the dye was dissolved in chloroform and filtered. It is important to restate the need to remove all the chloroform used in solution mixing prior to cell filling. As discussed previously this is achieved with a combination of evaporation, and mild heating under vacuum. For this single polariser DGH application, a surface stabilised geometry is required. To achieve this, the mixtures are capillary filled in LUCID cells with anti-parallel rubbed alignment layers.

5.3.5 Dye Spectra

The absorption spectra of the dyes are examined using the Hewlett Packard 8453 UV-Visible spectrometer. The dyes are in powder form and are dissolved in a solvent to enable the spectra to be measured accurately. Chloroform was chosen as the solvent because the dyes were readily soluble and unreactive in solution. The effect of the solvent on the spectra is small as chloroform has very little absorption in the visible wavelength and will not significantly shift the absorption wavelength of the spectra[30]. To enable a comparison between the spectra, similar strength solutions are made. The structure and molecular mass of the black ICI dye is unknown so the molecular mass is estimated to be similar to that of D102, since D102 is thought to be a major constituent of the mix. Solutions are made at 1, 10, 100 and 1000 μM in spectroscopy grade chloroform. A cuvette containing only chloroform is measured and the resultant spectrum used as a reference spectrum. Taking such a reference allows the spectra to be corrected for the effects of the small amount of absorption of the cuvette and chloroform, and flattens the illumination spectra so that the subsequent measurements show only the effects of the dye.

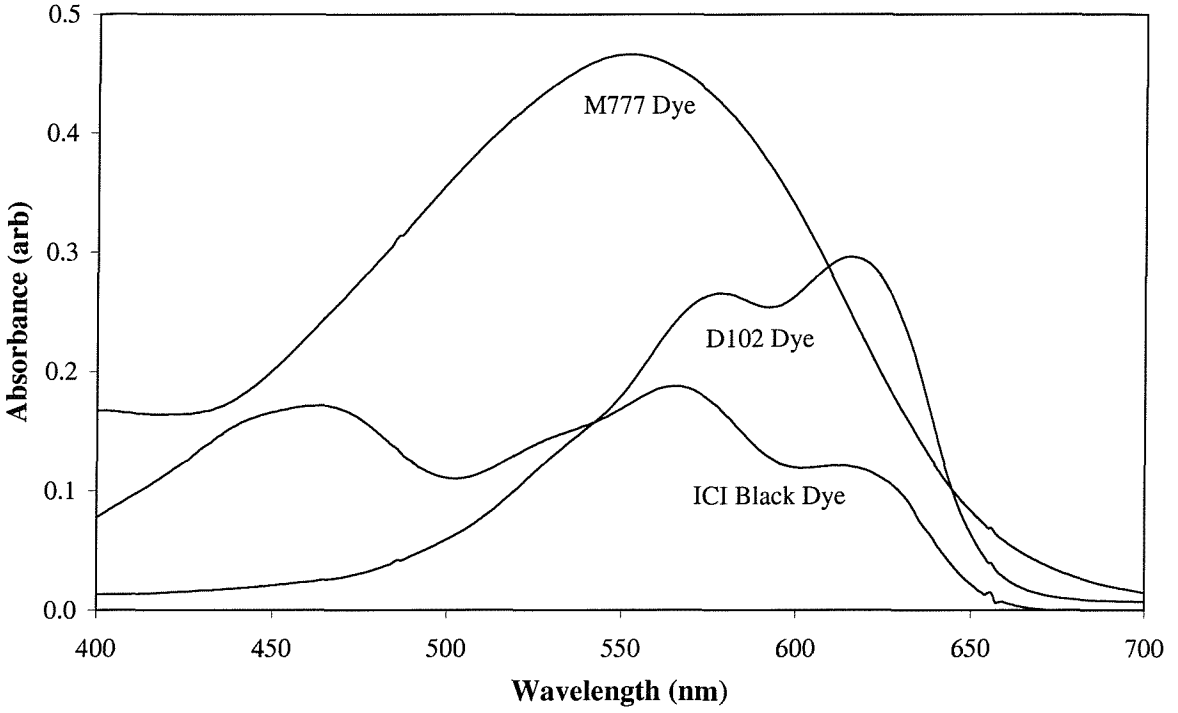

Figure 5.8 Absorption spectra of the three dyes at 10 μM solution in chloroform, measured relative to the same reference.

The 100 and 1000 μM solutions produced very noisy spectra, particularly with the black ICI dye, and hence the results obtained using the 10 μM solution were used since they produced a strong, smooth signal. The results, (Figure 5.8) show the broad absorbance of the black ICI dye, with a strong absorption peak for M777 and twin D102 peaks. The weaker absorption of the two anthraquinone dyes in comparison to the azo dye M777 is clearly seen. The absorption spectra of Cl11-Si_3 and Cl11-Si_3-11Cl were also measured, but are found to be insignificant at a 10 μM concentration.

5.4 Cl11-Si_3 AS A HOST IN THE SSFLC DYE GUEST HOST EFFECT

The main purpose of this study is to realise the potential of a ferroelectric liquid crystal in a DGH geometry. In order to accomplish this, the organosiloxanes studied in the previous chapter are used as the host materials. The feasibility of an organosiloxane DGH display is tested with the azo and anthraquinone dyes. M777 has already been thoroughly studied and shown to be an excellent dye for addition in low tilt ferroelectric and nematic DGH applications[26]. In order to test whether the desirable properties of M777 translate well to a ferroelectric material, whether organosiloxanes are a stable host medium, and whether D102 and ICI black are useful for display applications, electro-optic measurements are carried out. The development of the DGH device is reliant on the advantages offered by a 45° SSFLC geometry. Thus, it is critical that the dye does not affect the properties of the host in an adverse manner. In order to ascertain that the dye and host are compatible, the important characteristics to measure in an FLC DGH device are principally tilt, spontaneous polarisation (P_s) and optical performance.

This section examines the effect of the addition of the three dyes to a mono-mesogenic organosiloxane host, Cl11-Si_3. The chloro-substituted compound was chosen for use as the host after examination of the three halogen substituted mono-mesogens in the previous chapter: all three X11-Si_3 compounds examined had near 45° tilt, but the chloro-compound showed the highest spontaneous polarisation. Other factors, such as high reproducibility of results and slightly lower voltage thresholds for switching, made Cl11-Si_3 the first choice for investigation.

5.4.1 Dye Usage

Choosing the amount of dye to be used involves a compromise. At a high concentration, adverse effects on device performance are observed, whereas at a low concentration poor contrast is seen. The dyes were tested at concentrations from 1-10% weight for weight (w/w). It was found that the current mono-mesogenic organosiloxanes can accept the addition of up to around 4% w/w of any of the three dyes. At 5% w/w concentration and higher, dye aggregation can occur, particularly at the lower temperature end of the smectic range. The onset of the isotropic to smectic phase transition is depressed by over 10°C and the mixture remains biphasic down to 10°C below the transition. These effects are similar with all three dyes and particularly strong with the ICI black dye.

Another important concern is the level of switching voltage. It was found that 20 $V\mu m^{-1}$ was more than sufficient for saturated switching in the pure liquid crystal, and although dye addition did not necessitate an increase in driving voltage, concentrations above 5% caused conductance and dramatic shorts to occur. Therefore 4% w/w was chosen as the standard dye concentration for our measurements. Weight for weight concentrations are used throughout much of the DGH work in the literature and this convention is continued here.

5.4.2 Phase transitions

The first step in characterising the mixtures was to identify the phase transitions. The examination was carried out initially by crossed polariser optical microscopy, and confirmed by differential scanning calorimetry (DSC) using the Perkin-Elmer DSC7. The samples were heated and cooled at a rate of 5°min^{-1} and calculations of onset carried out on the third cooling run. The results are shown in Figure 5.9. These results indicate that the isotropic to liquid crystal transition temperatures are slightly depressed by the addition of the dyes. This is also true for the crystal transition and consequently the SmC* phase range with M777 addition is as wide as that of the pure host. The effect is a little more pronounced with the addition of the two anthraquinone dyes; these result in a slightly wider phase range in comparison to the host. The small peak at ~54°C seen in the heating run of the DSC trace for the pure compound (§4.4.2) is reduced with dye addition and is barely perceptible. The shapes and sizes of the phase transition peaks remain unchanged with the addition of M777 and D102. However, the ICI dye causes the peak widths to increase from ~4°C to ~7°C with a corresponding drop in amplitude.

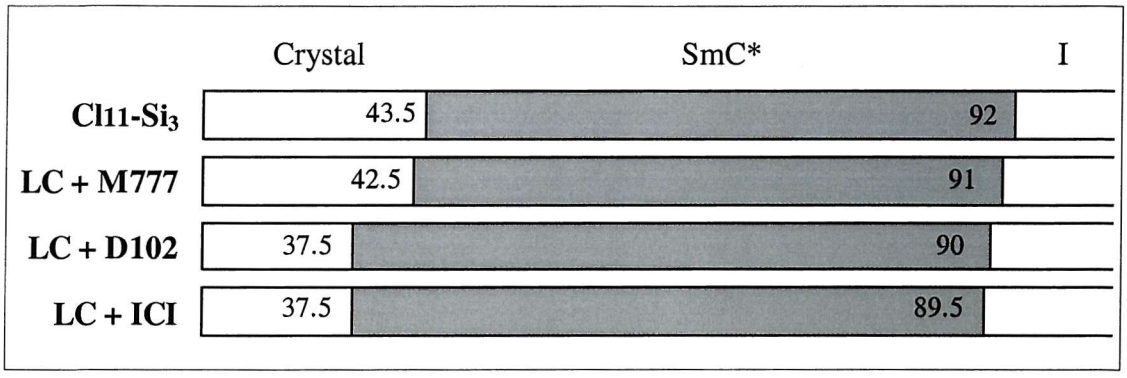

Figure 5.9 Phase transitions determined by DSC for Cl11-Si$_3$ with 4% w/w concentration of the three dyes.

5.4.3 Alignment and Photomicrography

Once the cells are filled, the alignment process is the same as that of the host materials - as outlined in §4.4.1.1. The sample is heated into the isotropic phase and then cooled at 0.2°Cmin^{-1} to ~2° below the I→SmC* transition under the influence of a triangle-wave field at 100 Hz and 15 Vμm^{-1}. This treatment produced alignment in the M777 mixtures that was of a higher quality than the pure host liquid crystal. The alignment of the D102 mixtures was of similar quality to that of the host, with large mono-domains but also with reverse domains and small areas of sanded texture. The addition of the ICI compound had a detrimental effect on alignment and it proved difficult to produce large monodomain areas in the mixtures containing this dye. This can be seen in the photomicrographs in Figure 5.10 taken at 50x magnification. The sample is illuminated with polarised light with the analyser removed. No further improvement in alignment was observed after 5 alignment cycles in the 5°C below the isotropic transition. Although the two states are clearly distinct, a fine sandy structure underlies both states severely hampering electro-optic measurements.

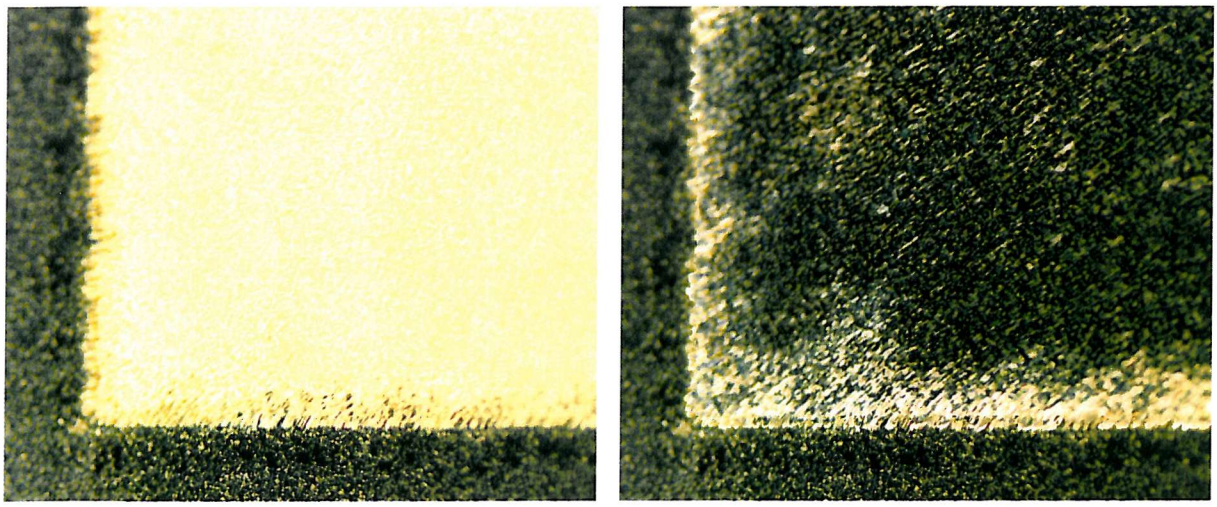

Figure 5.10 Single polariser photomicrographs at 50x magnification showing the white off-state and the near black on-state of 4% w/w of the ICI Black dye in Cl11-Si$_3$.

Figure 5.11 shows microscopy photographs of Cl11-Si_3 with 4% w/w M777, and illustrates the high degree of alignment that is possible. The influence of the alignment field is crucial in obtaining a well aligned sample. In this instance, variation of the field frequency by as little as 10% can greatly reduce its effect. In order to achieve the alignment shown, the sample was repeatedly cycled between 0.5°C and 10°C below the isotropic transition at 0.1°C for 24 hours. The sample is illuminated with polarised light and the pictures are taken at 50x magnification without an analyser. The photographs correspond directly with the operation shown schematically in Figure 5.5 and clearly illustrate the two switched states observable with a single polariser. At the edge of the cell's switching area, the non-aligned dye strongly absorbs the light. Of particular interest is the presence of a small reverse domain along the bottom edge showing the true contrast between the two states.

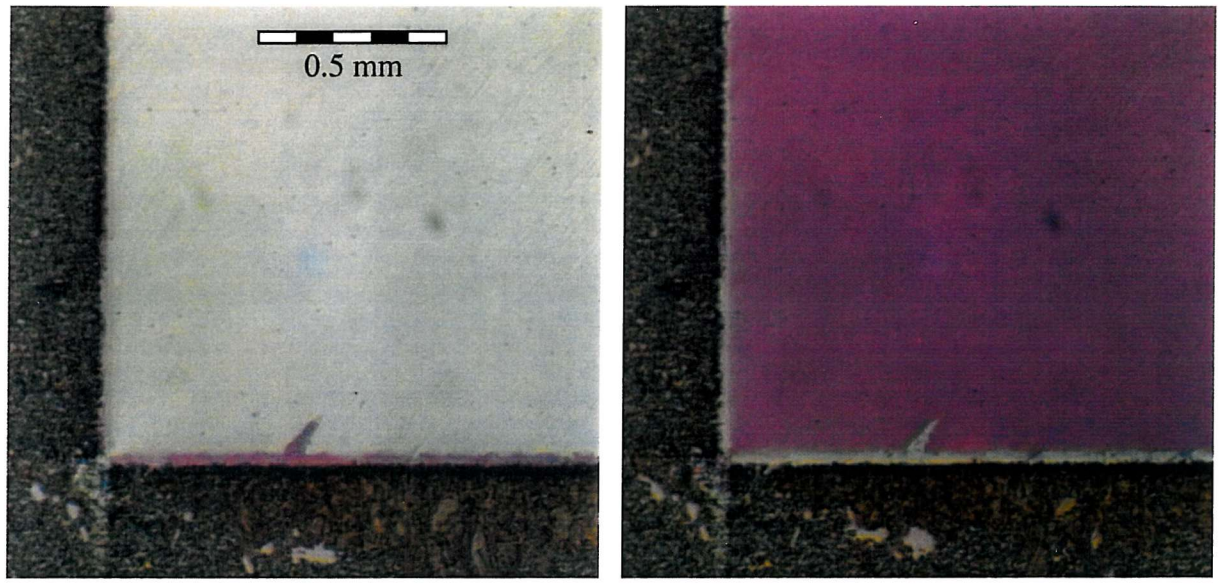

Figure 5.11 Single polariser photomicrographs at 50x magnification showing the white off-state and the coloured on-state of 4% w/w M777 in Cl11-Si_3.

5.4.4 Electro-Optic Measurements

Once it was clear no new phases had formed and the dye had only a small effect on the transition temperatures, the electro-optic response was examined

5.4.4.1 Tilt Angle

One of the main reasons for using the X11-Si_3 series for DGH work is the near 45° tilt angle obtained. It is important to measure the effects of dye addition on the tilt angle, the results of which are shown in Figure 5.12. In the shifted temperature range down to 40°C below the isotropic transition, the addition of the dye causes a small increase in the value of the tilt angle by a maximum of 1.5°. It is important to note the narrow range of the y-axis scale used to highlight the small differences. As with the pure compound, an 80 Hz A.C. square wave at 20 $V\mu m^{-1}$ was used to ensure full saturation. In

order to measure the small differences, the measurements were repeated twenty times. Different cells were used with a range of thickness from 3-6 μm. The spread of the results for the pure compound and with the addition of M777 and D102 yields an error of 0.25°. The addition of the ICI black dye caused slightly more erratic results, which in conjunction with the increased difficulty of measuring the sample due to poor alignment gave a larger error of ~0.75°.

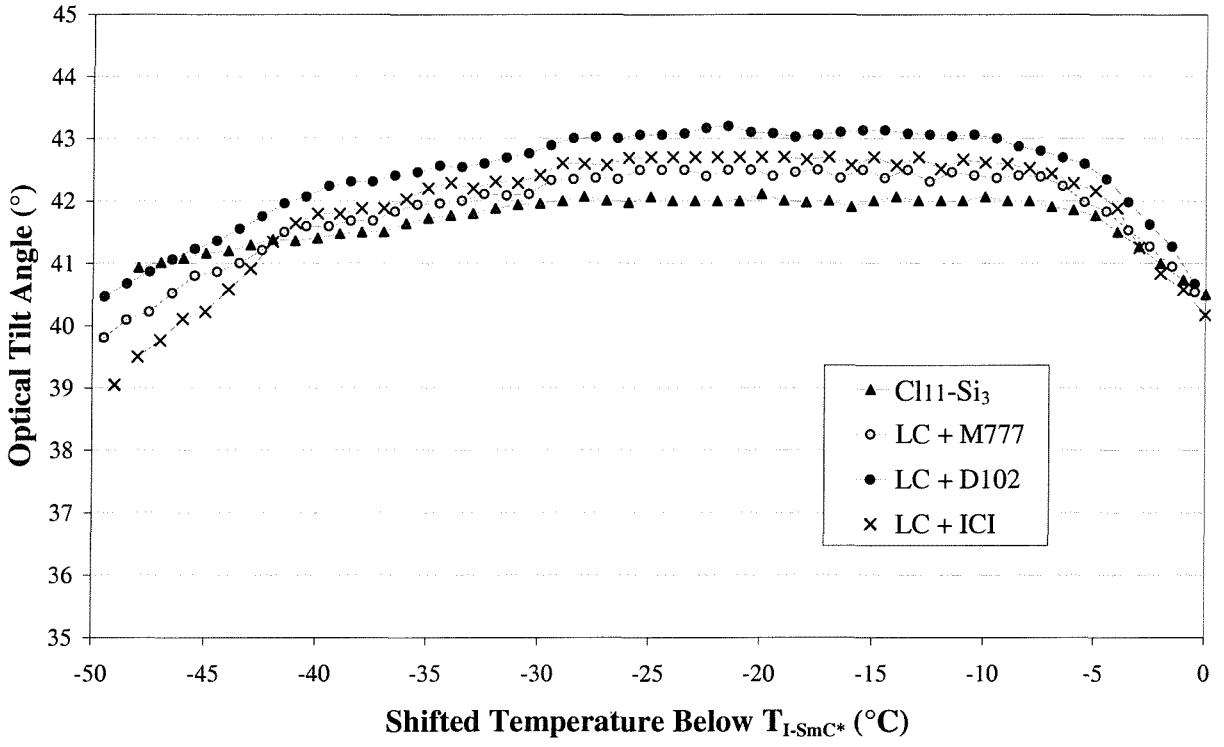

Figure 5.12 Optical tilt angle measurements of Cl11-Si3 showing the effects of 4% w/w dye addition.

All three dyes have a small effect on the magnitude of the tilt angle. As the smectic-crystal transition is approached, there is a gradual drop off in the values of the tilt angles in the mixtures, while in the pure material the tilt angle remains relatively constant. Although the effect is small, the dye addition appears to slightly enhance the size of the tilt angle. In the previous chapter it was seen that the biphenyl-benzoate precursor for the liquid crystal host has a tilt of ~37° which is increased to ~42° with the addition of the siloxane unit. This change is attributed to the siloxane virtual-backbone effect. The tilt angle in a smectic compound is closely linked to the spacing of the smectic layers. In the present case the addition of dye molecules is likely to affect the molecular packing, resulting in a small further enhancement of the tilt angle. In summation, the above 40° tilt of the host material is retained on the addition of the three dyes.

5.4.4.2 Spontaneous Polarisation

The spontaneous polarisation of the samples was measured using the current pulse technique with a triangle-wave field of 20 $V\mu m^{-1}$ at 80 Hz. The addition of M777 and D102 had very little effect on the size and shape of the spontaneous polarisation realignment peak. However, the addition of the ICI dye caused a widening of the current pulse peak over the entire smectic range. The effect was most pronounced at the low temperature end of the smectic range, necessitating a reduction in driving frequency to 40 Hz. The quality of the signal deteriorated at these lower temperatures and more averaging was used. The spontaneous polarisation measurements are shown in Figure 5.13.

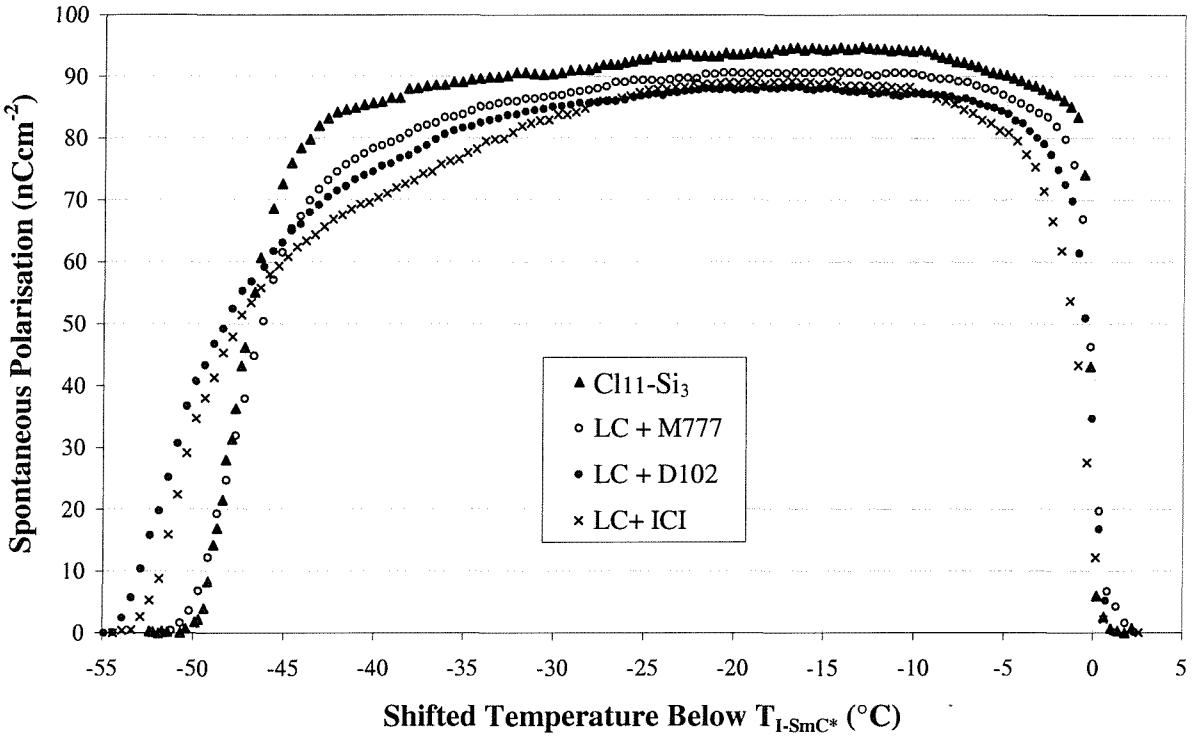

Figure 5.13 Spontaneous polarisation measurements of Cl11-Si3 showing the effects of 4% w/w dye addition.

The results show a reduction in the magnitude of the spontaneous polarisation with the addition of the dyes. This is to be expected because the dyes are not liquid crystalline and therefore will not contribute to the spontaneous polarisation. Thus, the reduction in P_s is attributed to the small dilution effect, this is better explained when considering molar mass. M777 causes a reduction in P_s by 4% over most of the smectic phase range and this correlates with the similar molar masses of guest and host; 827.8 $gmol^{-1}$ for Cl11-Si_3 compared with 854.0 $gmol^{-1}$ for M777. The molar mass of D102 is not known exactly but is thought to be in the region of 500 $gmol^{-1}$, thus a 4% w/w mix is equivalent to ~6.5% M/M. This mol/mol ratio agrees well with the ~6% reduction seen over most of the smectic range. The ICI black dye also causes a reduction in P_s of ~6% but has a significant drop off at the low temperature end of the smectic range. This drop off occurs with the deterioration of the spontaneous

polarisation realignment peak and highlights the adverse effect the dye has on the switching process in this temperature range. The enhancement of the phase range caused by the addition of the anthraquinone dyes can also be seen. Although the addition of a non-liquid crystalline dye reduces the spontaneous polarisation, such small reductions in P_s would not be expected to seriously hamper a display application.

5.4.4.3 Switching Time

The good quality alignment achievable in most cells allowed switching time measurements to be made using the photodiode setup. However, this was not possible with the ICI dye mixture, and in this case the current pulse technique was used. To verify the consistency of the two measurement methods, the pure host, M777 and D102 mixes were also checked with the current pulse technique. In all cases the two methods yielded near identical results within the experimental accuracy. The switching times were measured as a function of shifted temperature with square-wave driving fields at 80 Hz and 20 $V\mu m^{-1}$ and the results are shown in Figure 5.14.

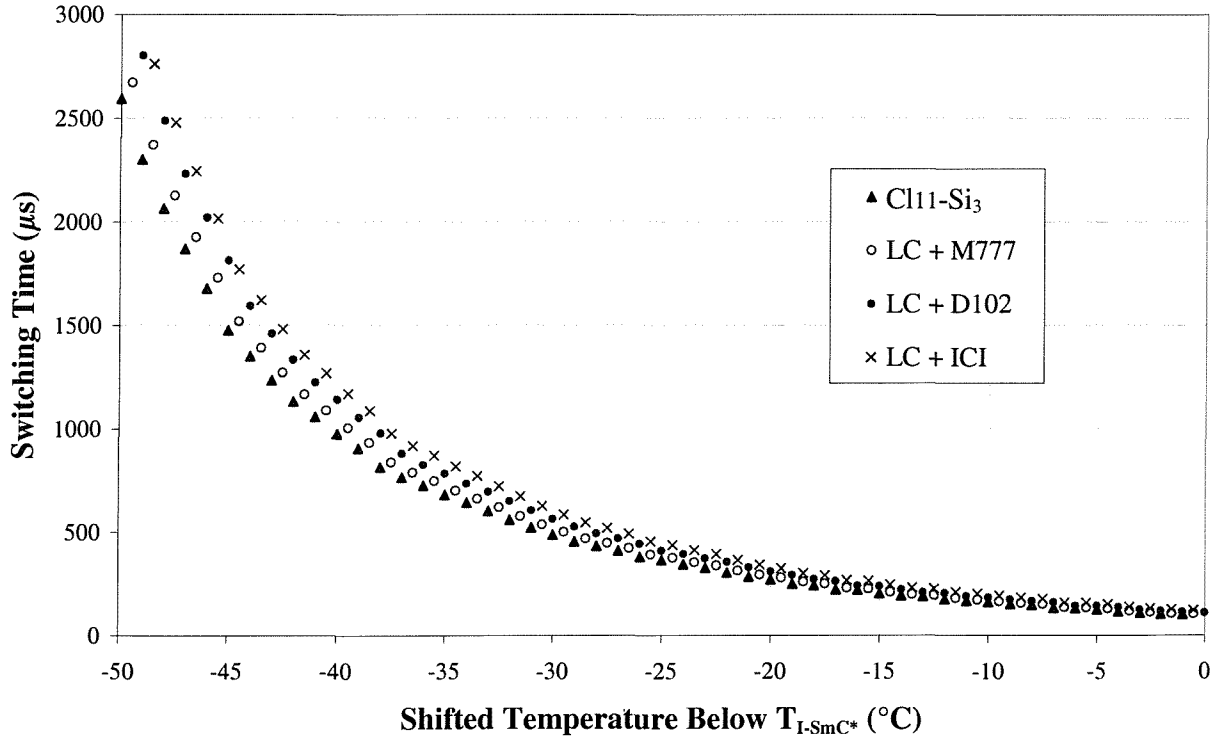

Figure 5.14 Switching time measurements of Cl11-Si3 showing the effects of 4% w/w dye addition.

The addition of the dye causes a small increase in the switching times. The differences are too small to be seen clearly on a semi-log plot so the results are shown on linear axes. The effects measured are small but it is not surprising to find that with an increased tilt angle and reduced spontaneous polarisation, the switching time is longer. Although the switching time readings are repeated many times and different cells are examined, the nature of the results obtained for the four samples makes

them susceptible to slight displacements of the shifted temperature scale. A small shift along the x-axis will not affect the relationships between the tilt angle or spontaneous polarisation curves for the four samples, however, a small shift in the x-axis will greatly affect the comparison of switching time results. Thus, the accurate identification of the I→SmC* transition temperature is crucial. The switching time is also very susceptible to temperature gradients in the sample and changes in field strength, therefore great care is taken to ensure the sample is in thermal equilibrium at each measurement and the conditions are the same for all the measurements. Dye addition has slowed the switching time of the host but once more the effect is small and the mixtures are still capable of switching times in the hundred microsecond regime.

5.4.4.4 Contrast Ratios

In order to assess the contrast ratios of the three dyes in the Cl11-Si_3 host, transmission levels were measured using the microscope and photodiode setup. To provide an initial reference for all the readings, the illumination was kept constant in the centre of the photo regime of the microscope. White light was used as this matches the conditions found in a working display application. An empty Lucid cell was placed on the microscope with the analyser removed and illuminated with polarised light. Once the microscope was focussed on the cell, the photodiode signal level was noted as the 100% transmittance level. The microscope light source was turned off and the photodiode level noted once more. The small oscilloscope reading accounts for any stray light entering the system and any small current from the electronics of the photodiode amplifier system causing a 'dark current'. This result gives a level for zero transmittance. The photodiode has a linear response (ascertained in §3.2.3.2); thus knowing the zero and 100% transmittance levels it is then a simple task to assign a transmission percentage for the measurements of the cell. As discussed previously, there are many different methods for determining contrast ratios, but for comparative purposes a simple ratio of transmittance levels is used here.

Different amounts of each dye were dissolved in the Cl11-Si_3 host prior to choosing a level for electro-optic study and this allowed measurement of transmission against dye concentration. In order to make the measurements of transmission it is important to ensure that the cell is aligned well and is undergoing fully saturated switching. The alignment quality of the M777 and D102 samples were sufficient to allow a mono-domain region to be selected for observation. At 5% w/w the M777 showed some dye aggregation but adequate regions of monodomain sample remained for measurement. The ICI black dye was reasonably well aligned up to a concentration of 3%, but above 3%, even at maximum magnification, it was difficult to select a single monodomain sample for observation. The results are shown in Figure 5.15 and are taken at a shifted temperature of 20°C below the I→SmC* transition.

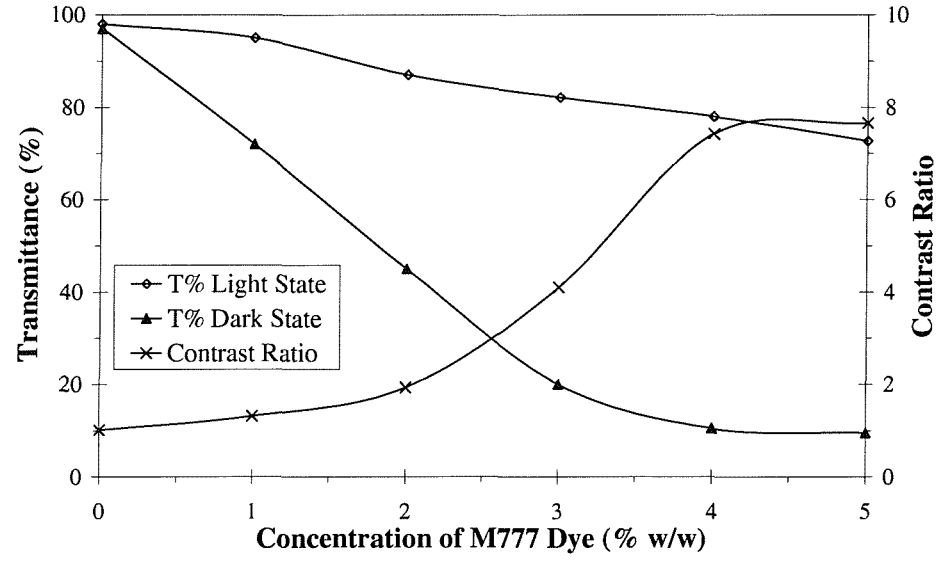

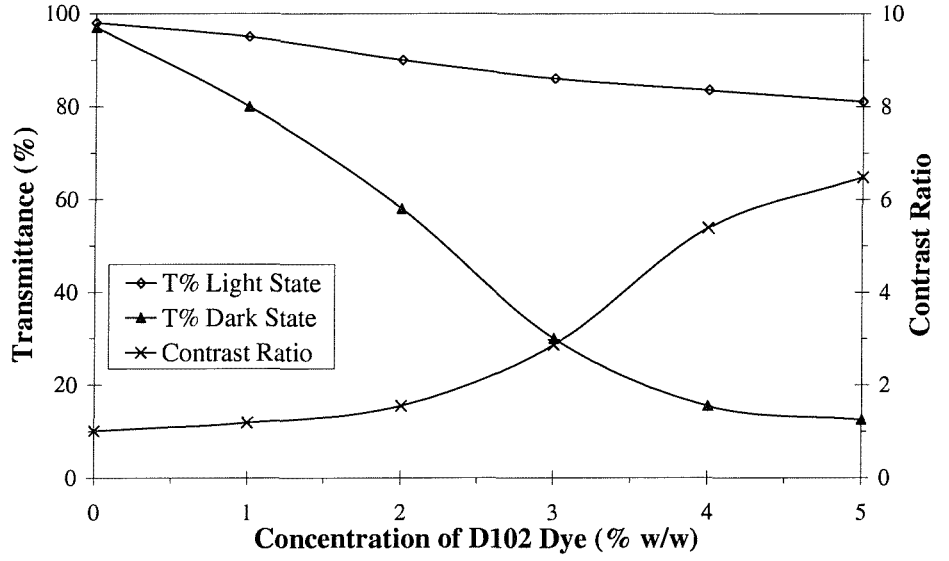

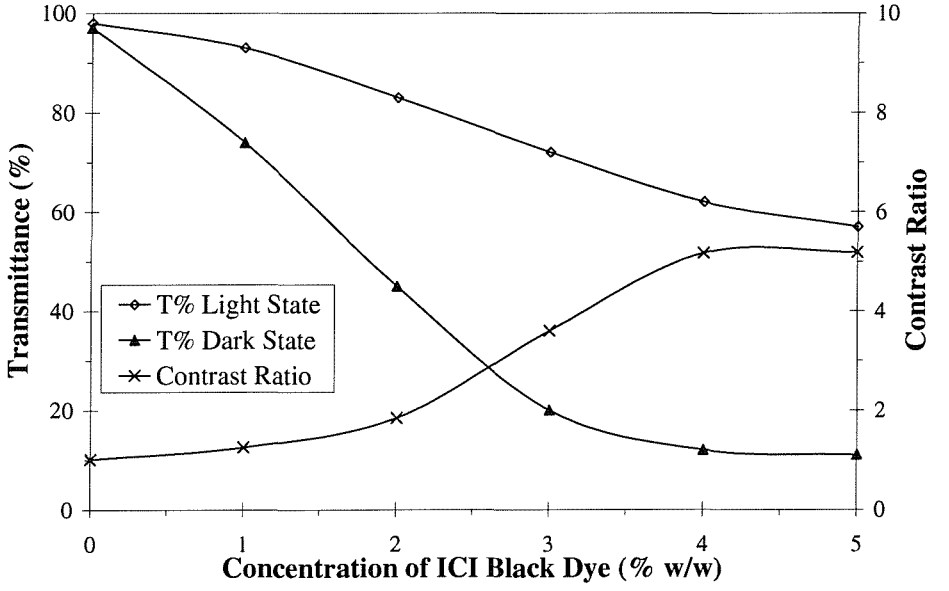

Figure 5.15 Graphs showing the effect on transmittance in the light and dark states and the calculated contrast ratios when varying dye addition in the host Cl11-Si3.

The mixture containing M777 shows the highest contrast ratios of the three dyes. As the dye concentration is increased, the transmittance of the light state gradually decreases. The dark state transmittance initially falls rapidly, then more slowly at concentrations in excess of 4%. The contrast ratio curve flattens off and thus even if addition of M777 at higher levels was possible, the contrast ratio may not improve significantly. D102 has a lower contrast ratio than M777, although its bright state transmits more light. If further addition of dye was possible the contrast ratio could be improved. The ICI black dye has the lowest contrast ratio but the results must be considered in the context of the poor alignment quality achievable in the samples containing this dye. The presence of small amounts of the "opposing" state, even when the measurements are made at maximum magnification, decreases the transmittance of the light state whilst allowing light to leak through in the dark state. This lack of a monodomain region reduces the contrast ratio, particularly at dye concentrations above 3% where alignment was poorest. It was observed that even at 1% concentration the reasonably well aligned white state had a distinct grey tinge. In summary, the use of 4% w/w dye yields near optimal contrast ratios for M777 and ICI black, with some potential for improvement with D102.

5.5 Mono-Mesogenic Organosiloxanes as Hosts

Small amounts of Br11-Si_3 and F11-Si_3 were available, allowing one or two cells to be made with each of the three dyes. Although the measurements of Br11-Si_3 and F11-Si_3 with dye addition were not repeated with the number of cells used for Cl11-Si_3 measurements, the electro-optic measurements yield almost identical trends to those obtained with dye addition to Cl11-Si_3.

5.5.1 Summary of Dye Addition in the Mono-Mesogens

A summary of the effects of dye addition in all three mono-mesogenic organosiloxanes is given in Table 5.1. These measurements are all taken at a shifted temperature of 20°C below the I→SmC* transition.. At this point all the samples were fully smectic without any biphasic behaviour and are undergoing fully saturated switching under the same measurement conditions. As with the pure compounds an 80 Hz A.C. square wave at 20 $V\mu m^{-1}$ was used for switching time measurements and for tilt angle measurements when the alignment allowed the photodiode method to be used. Spontaneous polarisation measurements were carried out with a triangle-wave field of 20 $V\mu m^{-1}$ at 80 Hz. Table 5.1 summarises the measurements using Cl11-Si_3 as the host (described in the previous section) and the results of measurements with Br11-Si_3 and F11-Si_3 as the host compounds (discussed in the following sub-sections).

	I→SmC*	SmC*→C	Tilt	P_s	Switch
			(Deg)	($nCcm^{-2}$)	(μs)
Cl11-Si_3	92	43.5	42	93.8	275
Cl11-Si_3 + M777	91	42.5	42.5	90.5	286
Cl11-Si_3 + D102	90	37.5	43	87.8	307
Cl11-Si_3 + ICI	89.5	37.5	42.8	89	315
Br11-Si_3	88	41	44.5	82.5	201
Br11-Si_3 + M777	87	40	44.5	79.5	210
Br11-Si_3 + D102	86	36	44.5	77.5	225
Br11-Si_3 + ICI	86	35.5	44.5	77.5	225
F11-Si_3	81	30	43	45	94
F11-Si_3 + M777	78	29	43.5	43.5	99
F11-Si_3 + D102	76	28	43.5	42	106
F11-Si_3 + ICI	75.5	28	43.5	42	113

Table 5.1 Results summarising the effects of dye addition in Cl11-Si_3, Br11-Si_3 and F11-Si_3 at 20°C below the isotropic to SmC transition.*

5.5.2 Br11-Si_3

As was seen with the DSC measurements of Cl11-Si_3 the addition of the three dyes slightly affects the smectic range. With dye addition to Br11-Si_3 the I→SmC* transition temperature is reduced by 1-2°C alongside a reduction in the crystal transition temperature of up to 5°C. A small amount of biphasic behaviour was noted at the I→SmC* transitions with dye addition. The DSC transition peaks were ~1°C broader than seen with the Cl11-Si_3 host, with a corresponding slight decrease in peak amplitude. The alignment quality seen in the Cl11-Si_3 mixtures, particularly when doped with M777, could not be matched with Br11-Si_3 as the host, as shown by the photomicrographs in Figure 5.16. Comparing the high quality alignment shown by the Cl11-Si_3 and M777 mixtures in Figure 5.11 with the Br11-Si_3 and M777 mixtures in Figure 5.16a, a large number of reverse domains are seen, despite similarly extensive alignment treatment. The alignment quality of the Br11-Si_3 and D102 mixtures, was also reduced in comparison to that of the Cl11-Si_3 host. Figure 5.16b show a typical defect seen in the Br11-Si_3 and D102 mixtures. However, sufficient alignment existed to carry out accurate photodiode measurement of the mixtures of Br11-Si_3 with M777 and D102. The results yielded no discernable change in the optical tilt angle in comparison with the pure host. The near 45° tilt angle exhibited by the Br11-Si_3 host over nearly the entire phase range is maintained. The mixture

containing the ICI dye also exhibited near 45° tilt angles over the majority of the SmC* phase range. However, in the 10°C below the I→SmC* transition and the 10°C before the SmC*→Crystal transition, the tilt angle was depressed by an extra 2° more than the host, as was seen with the ICI and Cl11-Si_3 mix in Figure 5.12.

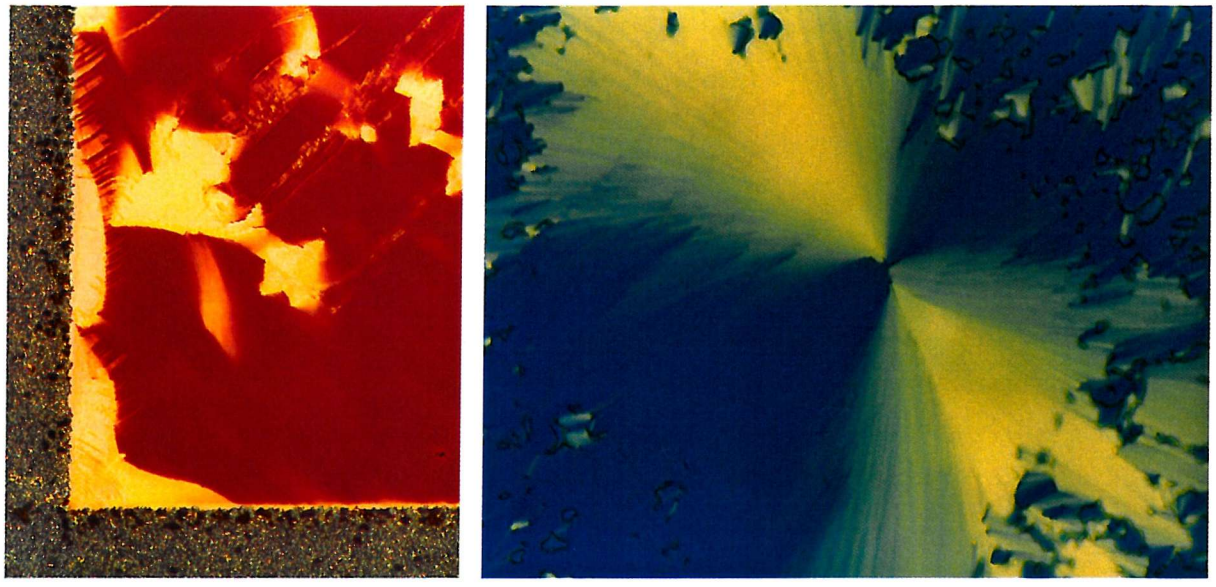

a) 4% w/w M777 in Br11-Si_3. at 50x magnification

b) 4% w/w D102 in Br11-Si_3. At 100x magnification

Figure 5.16 Single polariser photomicrographs, showing alignment quality.

The spontaneous polarisation was measured under the same conditions as the Cl11-Si_3 mixes, with a triangle-wave field of 20 $V\mu m^{-1}$ at 80 Hz. The spontaneous polarisation realignment peak was unchanged with the addition of M777 and D102 and showed some widening with the ICI mix. The graph of spontaneous polarisation against shifted temperature in Figure 5.17 shows the same trends as those seen with Cl11-Si_3 as the host in Figure 5.13. The addition of M777 has reduced the spontaneous polarisation by ~4% over most of the smectic range, with a slightly higher reduction of ~6% for the D102 and ICI mixes. The reduction in spontaneous polarisation is attributed to a dilution of the dipoles per unit volume, consistent with the results for Cl11-Si_3 in §5.4.4.2.

The switching times were measured using the current pulse technique. Once again the results followed the general trend seen with Cl11-Si_3 as the host: the addition of the dye increased the switching time by a small amount. The differences in switching time between the mixes is too small to be plotted and the curves completely overlap over the majority of the smectic range. As before, the curves are particularly sensitive to small variations in the determination of the I→SmC* transition, which was complicated by the small amount of biphasic behaviour at the transition. Multiple runs with extended periods were used to ensure full thermal equilibrium, but this did little to separate the curves.

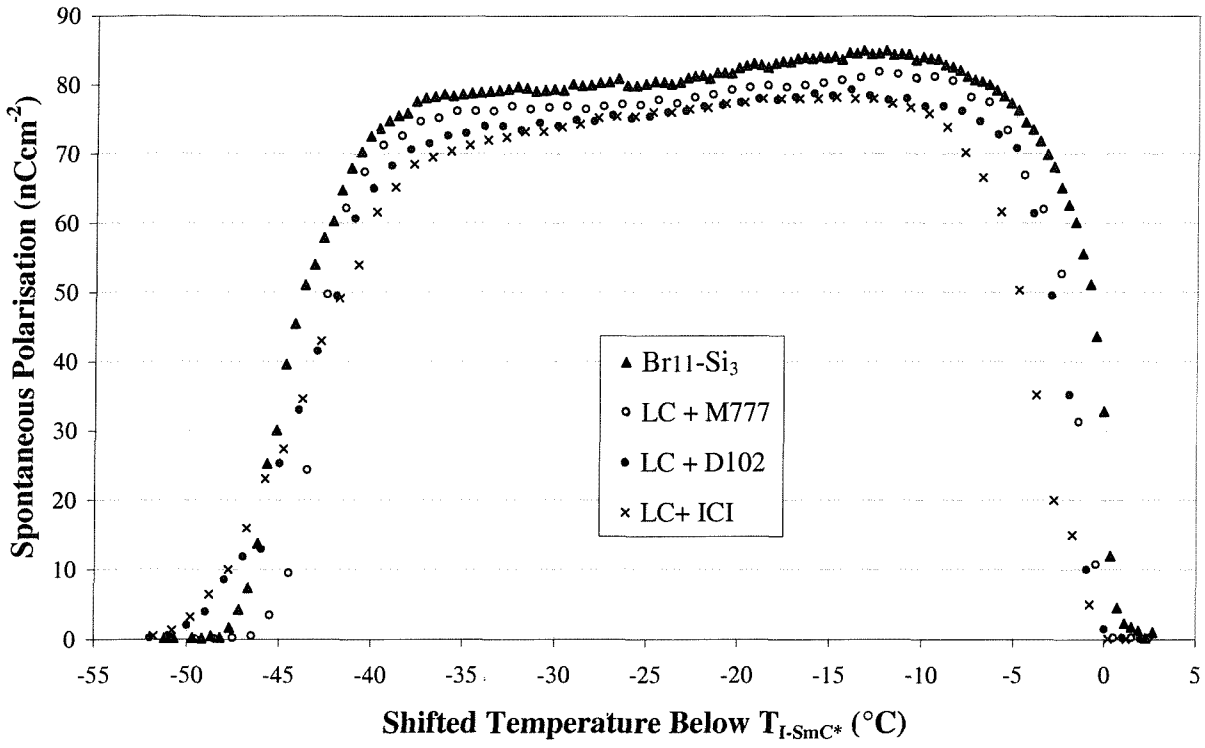

Figure 5.17 Spontaneous polarisation measurements of Br11-Si3 showing the effects of 4% w/w dye addition.

5.5.3 F11-Si3

Of the three host materials, F11-Si3 was the most sensitive to the addition of the dyes, and showed the greatest deterioration in material properties. The I→SmC* transition temperature was difficult to identify precisely due to a small biphasic region. Although the biphasic region was only ~3°C wide with M777 as the dopant, the width of the region increased to ~10°C with the ICI dye and biphasic behaviour was also seen at the crystal transition. The biphasic nature of the transitions widened the DSC transition peaks, making onset temperatures difficult to assess. The alignment quality was very poor, particularly with the ICI dye. The optical tilt angle of the M777 doped sample was measured on the microscope but the poor alignment quality of the anthraquinone doped samples prevented microscope based electro-optic measurements from being made. All three dyed mixtures were measured at a shifted temperature of 20°C below the I→SmC* transition by Chris Noot[31] using the rotating analyser rig described in §3.4.1.2. The results obtained in this way for the M777 mixture agree with the microscopy readings.

Although the rotating analyser results are not as accurate as those on the microscope, the addition of the dye shows the same trends demonstrated by the Cl11-Si3 host in Figure 5.12. The addition of the three dyes yields a small enhancement in the peak values of the optical tilt angle. Although the tilt angle increase is at the limit of measurement accuracy, repeated measurements consistently showed an increase of 0.5° of tilt in the range 20°C to 30°C below the I→SmC* transition. Measurements at

a shifted temperature of 10°C below the isotropic transition, yielded tilt angles around 35° with the addition of either of the dyes. The results were not consistent and varied by around ±3° of tilt between runs, depending on the biphasic nature of the sample. A similarly sharp drop off was seen towards the SmC*→Crystal transition. The previously almost temperature independent behaviour of the host is lost and the value of the tilt falls to 30°-35° from around 40°C below the I→SmC* transition in all three dye samples. Once again the exact nature of the biphasic behaviour varied on each run, making accurate reproducible measurement difficult. Recalling the results of the previous chapter, the addition of the siloxane core to the fluoro-substituted biphenyl benzoate precursor caused a tilt enhancement from ~23° to 43° in F11-Si_3. The substantial enhancement seen with fluorine was the largest effect of the three halogen substituted compounds measured. It is therefore not surprising that F11-Si_3 is the most sensitive to the addition of an impurity such as a dye, which can disrupt the delicate structural balance yielding the high tilt compounds.

The spontaneous polarisation measurements were hampered by very poor spontaneous polarisation realignment peaks, requiring baseline compensation and a large amount of averaging. The results follow the general trends seen with the two other halogenated mono-mesogens studied. In the middle of the SmC* range, away from the biphasic regions, the value of the spontaneous polarisation is reduced by a few percent from that of the host. The magnitude of the decrease follows the reduction in the dipoles per unit volume, hence, as before, this is attributed to dilution effects. In the regions below the I→SmC* transition and before the SmC*→Crystal transition, the biphasic behaviour of the dye mixed samples caused the spontaneous polarisation to fall sharply. The switching times were measured using the current pulse technique. The biphasic nature of the samples at either end of the smectic range made measurements very difficult. Once again the dye mixes exhibit slightly increased switching times in comparison to the pure host and the trend matches that seen with the Cl11-Si_3 host in Figure 5.14.

5.6 Antiferroelectricity in the Dye Guest Host Effect

After observing favourable results with the ferroelectric mono-mesogenic compounds, it is a natural progression to examine the effect of the dyes on the antiferroelectric bi-mesogenic organosiloxanes. In comparison with the ferroelectric DGH effect, the use of the antiferroelectric mode is more complicated. The need for a field to maintain a driven state means the loss of the bistable memory states of the surface stabilised ferroelectric. The bi-mesogenic organosiloxanes also require higher field strengths in order to switch states and are harder to align. However, the major difference between the ferroelectric and antiferroelectric modes, of interest in this study, is the possibility of three separate optical states. In a typical surface stabilised antiferroelectric liquid crystal (SSAFLC) sample examined between crossed polarisers, the 90° symmetry does not take full advantage of the

three states of a 45° tilt compound. On removing the analyser and adding a dye, the three states should be distinctly different in appearance. In order to test this hypothesis, the antiferroelectric material Cl11-Si_3-11Cl was used as the host and the same three dyes added.

5.6.1 Cl11-Si_3-11Cl as a Host in the SSAFLC Dye Guest Host Effect

In a similar manner to the studies of the mono-mesogens, different levels of dye concentration were tested. The voltages required to switch the antiferroelectric compounds are greater and thus the addition of a dye has a greater potential to cause shorting and other adverse effects. Although it was found that M777 was soluble over the entire smectic phase range up to ~5% w/w, the application of sufficient fields to induce saturated switching caused the cell to short. The concentration of the dye was reduced to ~2% w/w before saturated switching could be maintained. The same effects were seen with the ICI black dye. The problems of shorting and restricted switching were not as prominent with D102 addition but the doping concentration was also cautiously set at 2% w/w.

The phase transitions were once again examined initially by crossed polariser optical microscopy, and then differential scanning calorimetry. The results are shown in Figure 5.18. Although the phase transitions are affected by the addition of the dye, the antiferroelectric nature of the host is not lost and the SmC^*_A phase is the only liquid crystalline phase observed.

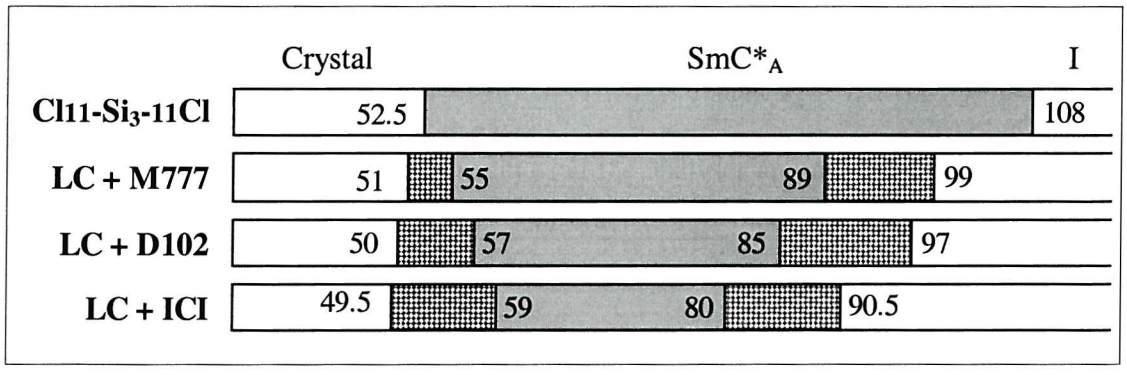

Figure 5.18 Phase transitions determined by DSC for Cl11-Si_3-11Cl with 2% w/w of the three dyes (the hatched areas indicate the width of the biphasic regions).

The addition of the dyes causes the I→SmC^*_A transition temperature to be greatly reduced and wide biphasic regions appear at both ends of the smectic range. The presence of the biphasic regions widened the DSC peaks to such an extent that meaningful analysis of this data was impossible. However, measurements on the microscope allowed consistent identification of the onset of the biphasic region and the fully smectic phase to within 0.5°C. The transition from the smectic phase to the crystal phase could not be identified without the application of a field. The strength of the field was kept below 0.5 $V\mu m^{-1}$ to avoid influencing the phase transition, however, even with small voltages it was possible to highlight the onset of crystallisation. Although greatly less than the values

required for saturated switching, the small voltage is enough to "flick" the molecules and identify the region in which the sample stops switching and enters the crystal state. The final value of the transition temperatures recorded for the fully crystallised state can be dependent on the amount of time the sample is left near the transition. If the temperature is reduced at a rate of 0.3°Cmin^{-1} or faster, a large amount of supercooling was observed. The final values quoted in Figure 5.18 were obtained using a cooling rate of 0.1°Cmin^{-1}, with the sample temperature maintained at a constant level for one hour for every 1°C by which the sample was cooled.

5.6.1.1 Electro-Optic Measurements

The alignment quality of the antiferroelectric host is considerably poorer than that exhibited by the ferroelectric compounds, as discussed in the previous chapter. The addition of M777 had no noticeable beneficial effect on the alignment, in contrast with the improvements in ease and resultant quality of alignment observed in the ferroelectric Cl11-Si$_3$ mixes. In order to align the samples, they were heated into the isotropic phase and then cooled at 0.5-0.1°Cmin^{-1} through the biphasic region, under the influence of a triangular A.C. field at ~100 Hz and 20-35 Vμm^{-1}. Annealing improved the alignment of the M777 and D102 mixtures for the first 3-4 cycles, after which no further improvement was noted. The addition of the ICI dye made alignment impossible in the antiferroelectric.

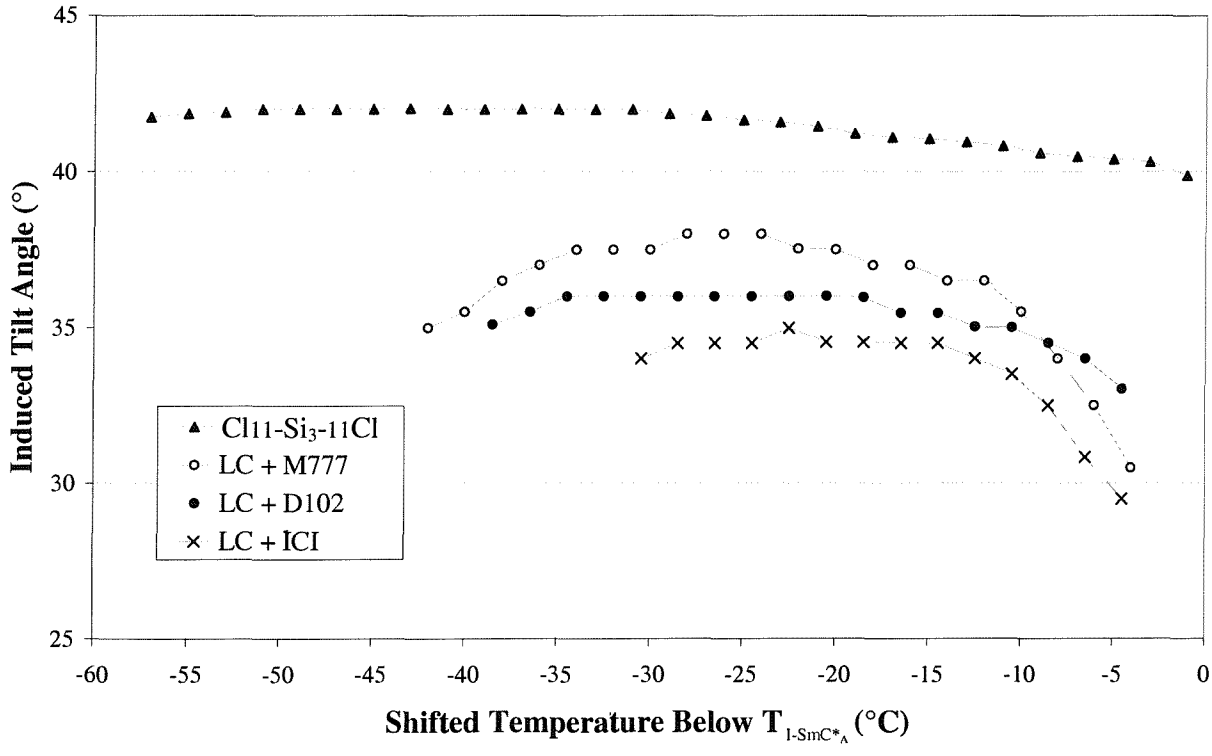

Figure 5.19 Induced optical tilt angle measurements of Cl11-Si$_3$-11Cl showing the effects of 2% w/w dye addition.

As discussed in the previous chapters, an antiferroelectric compound has no macroscopic tilt, thus once again field-induced optical tilt angles are measured. In order to ensure complete switching, the guest-host mixtures were switched between their two states at low frequencies and a field of 30 $V\mu m^{-1}$. Microscope based electro-optic measurements were made for the M777 mixture and a limited temperature range of the D102 mixture. These were repeated on the rotating analyser rig with all three dye mixtures by Chris Noot[31]. The results from the two methods were consistent and are combined in Figure 5.19. The results of the tilt angle measurements show the reduced phase range of the guest-host mixtures. Although some tilt angle measurements were possible in the high temperature biphasic region, the voltage required for saturated switching was too great at the low temperature end of the smectic phases. In overview, the addition of the dye has reduced the induced tilt by ~5°. In comparison to the slight enhancement of the tilt angle seen with the ferroelectric Cl11-Si_3 mixtures, the structure of the Cl11-Si_3-11Cl compound is more easily disrupted by the presence of an impurity. The normally well defined herringbone structure of the antiferroelectric phase in the Cl11-Si_3-11Cl host is disturbed, reducing the magnitude of the induced tilt.

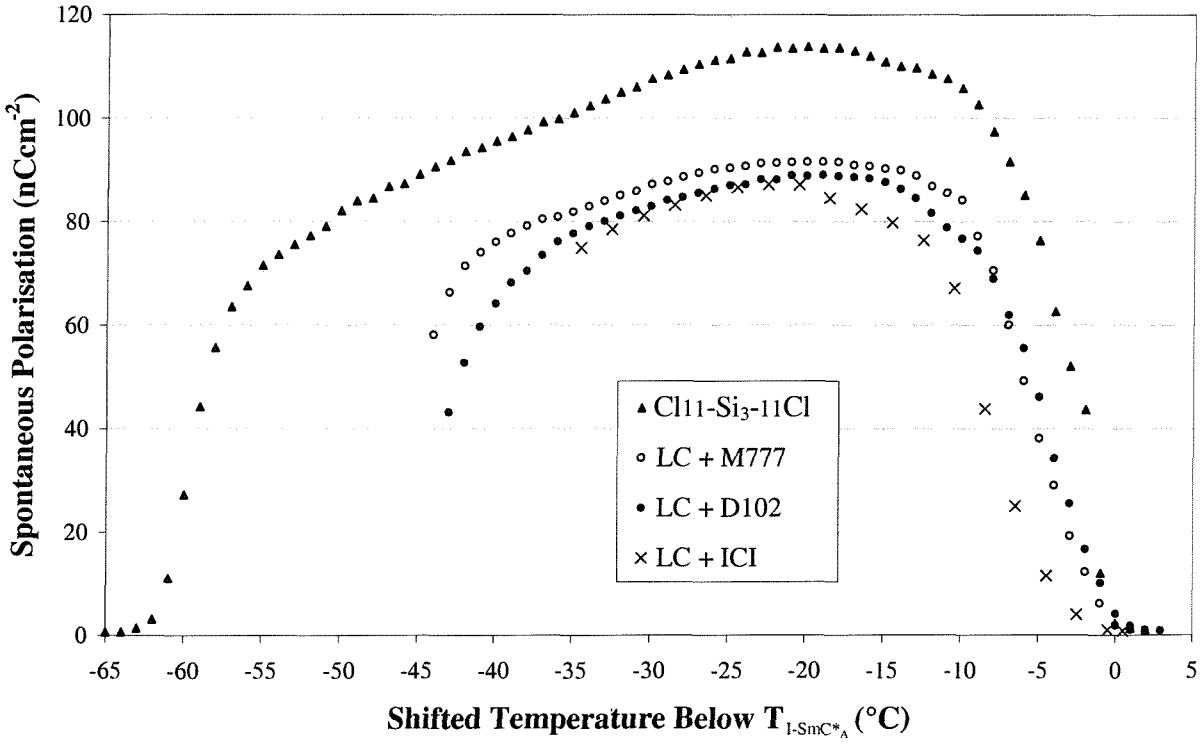

Figure 5.20 Spontaneous polarisation measurements of Cl11-Si_3-11Cl showing the effects of 2% w/w dye addition.

The twin spontaneous polarisation realignment peaks observed in antiferroelectric switching make the measurement of spontaneous polarisation more complex than that of the ferroelectric mixes. The peaks of the antiferroelectric dye mixes were measured separately, and in order to smooth the spontaneous polarisation switch, the maximum averaging of 256x was used. As with the measurement of the host material discussed in §4.5.1.3 the applied voltage was increased to the

maximum of 35 $V\mu m^{-1}$. Beginning with 75 Hz at the high temperature end of the smectic range, the frequency of the applied waveform was gradually reduced with temperature to ensure fully saturated switching. The frequency could not be reduced below 10 Hz however, without the cell shorting. The high voltage and low frequencies used caused considerable baseline slope, which was countered by feedback adjustment. Some degree of automation was possible when measuring the spontaneous polarisation of the M777 and D102 doped mixtures whilst the ICI doped mixture required manual measurement. The spontaneous polarisation measurements in Figure 5.20 are the result of the addition of the two antiferroelectric peaks: driven and relaxed. With respect to these two components of the full switch, the relaxation peak was ~10-15% smaller than the driven peak for mixtures containing M777 and D102, and in the ICI doped mixture the relaxation peak was up to 20% smaller than the driven peak at the extremes of its range. The results are shown in Figure 5.20 and once again the reduced smectic range induced by the addition of the dye is seen. The magnitude of the spontaneous polarisation in the dye mixtures is reduced by ~20%, a far greater effect than the reduction in magnitude of around 4% observed with the ferroelectrics. The reduction cannot be attributed to dilution effects. It is likely that as with the tilt angle measurements, the interaction of the dye with the liquid crystal host disrupts the antiferroelectric structure and reduces the effect of spontaneous dipole realignment.

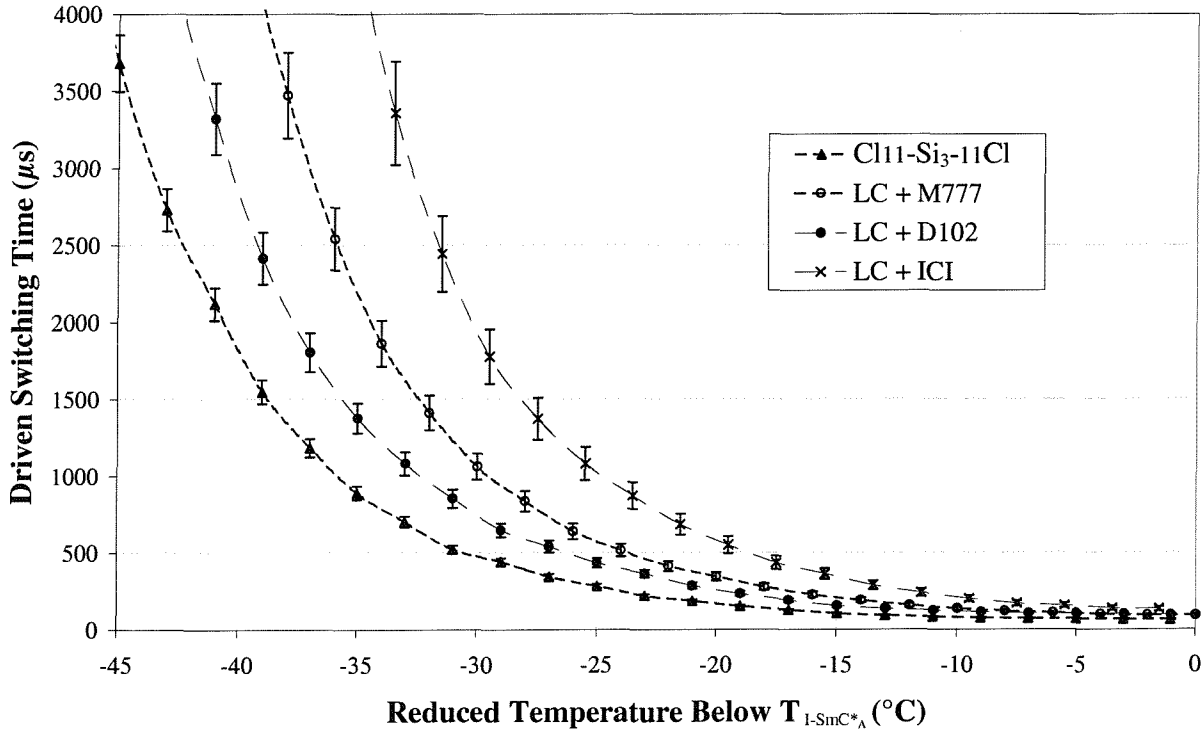

Figure 5.21 Switching time measurements of Cl11-Si3-11Cl showing the effects of 2% w/w dye addition.

The switching time measurements were carried out using the current pulse technique with similar fields to those used when making spontaneous polarisation measurements. Once more, the maximum

level of averaging was used to smooth the signal. Although the technique was effective with the M777 mixture, the responses of the D102 and in particular the ICI dyed mixtures were erratic and noisy. The lack of good signal quality, especially at the low temperature end of the smectic phase ranges, is reflected in higher errors associated with the results shown in Figure 5.21. The addition of the dyes causes a marked increase in the switching time of the host. In agreement with the spontaneous polarisation results, the dye guest interaction disrupts the antiferroelectric switching.

5.6.2 Towards a Tri-State Device?

Although the addition of the dyes had an adverse effect on the Cl11-Si_3-11Cl host, it was interesting to note that in some orientations the three antiferroelectric states appeared to have different colour and brightness levels. In order to investigate this further, the effect needed to be enhanced with greater dye addition. The M777 and ICI black dyes were already near their dissolution limits at 2% w/w concentration, but more D102 could be dissolved in the host yielding significant contrast improvements. Adding ~8% w/w of D102 reduced the non-biphasic smectic range to 65-75°C. Partial alignment was achieved as before by annealing at 0.5-0.1°Cmin^{-1} through the biphasic region under the influence of a triangular A.C. field at ~100 Hz and 20-35 Vμm^{-1}. In order to photograph the three states, a square wave at 1 Hz and 35 Vμm^{-1} was used. The sample gradually degraded and the cell shorted after several hours, however the sample lasted long enough for photographs to be taken and these are shown in Figure 5.22. Due to the automatic light adjustment of the camera, the pictures do not show the full contrast achieved.

The photomicrographs in Figure 5.22 show the three distinctly different states; the relaxed state with no field (Figure 5.22a), one switched state with a field applied into the page (Figure 5.22b), and the other switched state with a field out of the page (Figure 5.22c). In order to observe the different states, the alignment of the cell with respect to the incident polarised light is crucial. If the relaxed state is aligned with the polarisation direction of the incident light, the two switched states are identical. However, if the polariser is aligned along the effective optic axis of a switched state, a tri-state colour switch is observed.

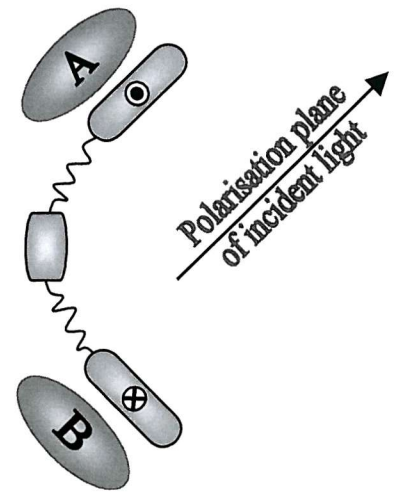

a) No Field

Dye A Active and Dye B Passive

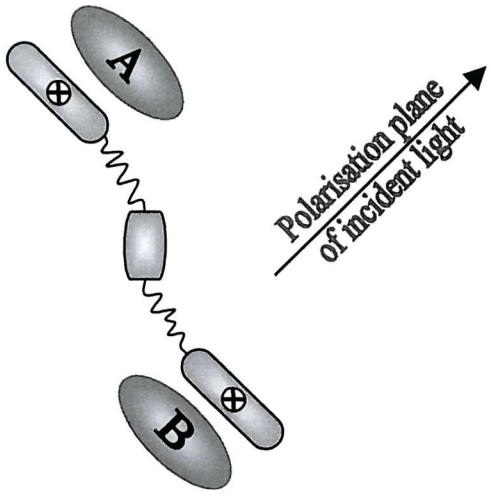

b) Applied field into page

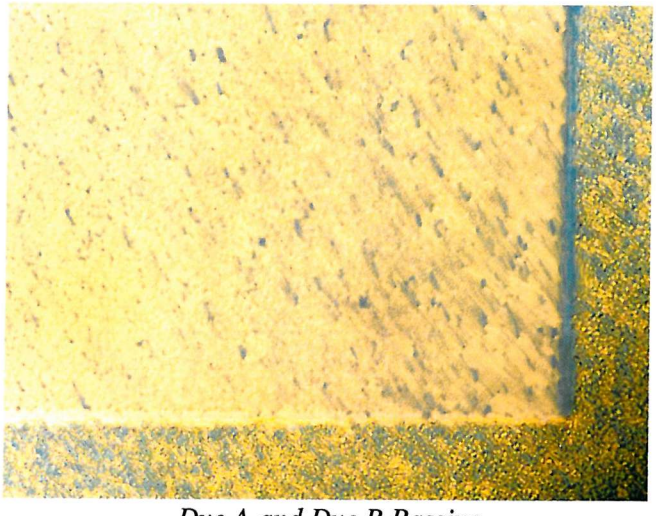

Dye A and Dye B Passive

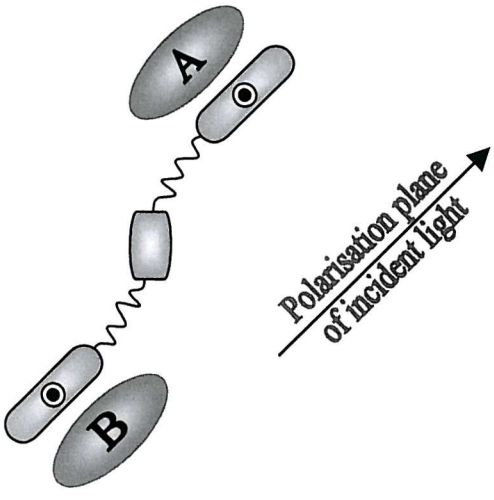

c) Applied field out of page

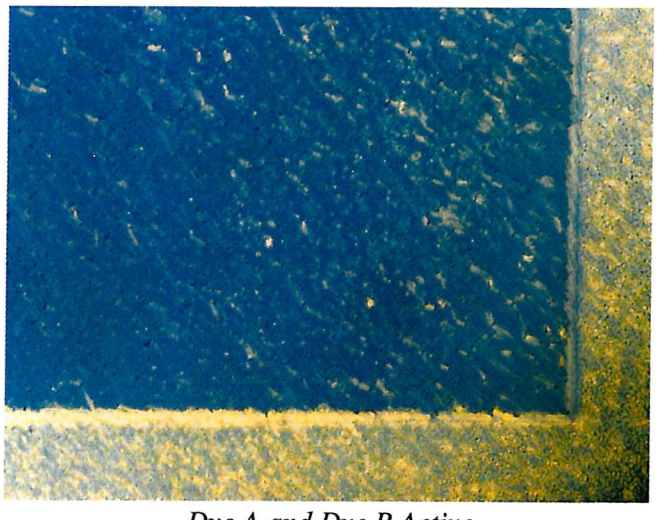

Dye A and Dye B Active

Figure 5.22 A schematic of the possible arrangement of guest and host in the three states of antiferroelectric Cl_{11}-Si_3-$_{11}Cl$ with 8% w/w D102. The corresponding microscopy pictures at 50x magnification show the switching effect with plane polarised light illumination.

The schematic diagrams in Figure 5.22 offer a possible explanation for the three states observed. To maintain layer integrity, a Goldstone mode switch of the pendent biphenyl benzoate around the siloxane core is hypothesised, as discussed in the previous chapter. The alignment of the siloxane cores forms the virtual backbone whilst the dye molecules align with the flexible biphenyl benzoate moieties. In the relaxed state, p-type dye molecules aligned along the polariser transmission axis (dye molecule A) will interact with the incident light and the characteristic colour of the dye will be passed. Over the entire cell area this will equate to half of the dye molecules lying in their active state. The application of a field into the page will realign the antiferroelectric host into the switched ferroelectric state. Provided that the guest-host interaction also realigns the dye, neither dye molecule will interact with the incident polarised light, giving a near-colourless state, as illustrated. Alternatively, the application of the oppositely directed field (out of the page) realigns the sample in the other switched ferroelectric state. Now both dye molecules A and B will interact with the incident light and a fully dyed state is seen. This intuitive explanation combines considerations of the steric interactions of the guest host mode with the switching mechanisms of the antiferroelectric host[32].

This device represents a clear new geometry and application of the dye guest host effect. The observation of the three states is only possible with the recently synthesised 45° tilt angle antiferroelectrics. In order to investigate this device further, dyes that are better matched to the antiferroelectric host are required.

5.7 SUMMARY

This chapter has shown the potential of the application of ferroelectric and antiferroelectric liquid crystals to dye guest host applications. The mono-mesogenic ferroelectric organosiloxanes Cl11-Si_3 and Br11-Si_3 proved stable hosts with the addition of small amounts of the commercial dyes M777 and D102. A level of 4% w/w of dye addition was chosen, which provided near optimum contrast for the three dyes, without dye aggregation and excessive adverse effects such as shorting and electro-optic signal degradation. The problems of alignment and the poor switching characteristics encountered with F11-Si_3 in the previous chapter were further exacerbated by the addition of a dye. The ICI black dye was intended to provide the strongest contrast and possible mono-chrome applications, but was found to cause the most adverse effects on electro-optic and phase properties of the three dyes investigated.

Considering all the mono-mesogenic mixes, the phase ranges of the hosts were slightly altered by the dye addition. The SmC* phase remained the only liquid crystal state observed with transition temperatures reduced by up to 6°C. One of the problems for display applications of the organosiloxane hosts in this work is the high temperature of the smectic ranges, thus any reduction in

transition temperature, whilst maintaining the width of the smectic range, is welcome. From the perspective of a display application, in general the addition of the dyes to the mono-mesogenic hosts did not significantly alter the 42°-44.5° tilt angles of the hosts. The effect of the dyes on the spontaneous polarisation was a small reduction due to dilution of the dipoles per unit volume. This reduction was at its greatest around 6%, which in the context of the high spontaneous polarisation of the mono-mesogens, particularly Cl11-Si_3 and Br11-Si_3, will not impact a display application. Some drop off in the magnitudes of the spontaneous polarisation and tilt angle measurements with temperature were seen near the transitions, particularly in samples displaying biphasic behaviour. However, over most of the smectic range the temperature independent nature of the host was largely maintained. The most significant effects are observed in the small slowing of the switching times. Although the increase is no larger than ~15%, any increase in the switching time is undesirable.

The best results were observed with the mixtures of 4% w/w M777 which produced a responsive single polariser dye guest host cell that retained the properties of fast bistable switching and wide smectic phase range. This success provides much encouragement for further investigations of other dyes and high tilt hosts for single polariser applications.

The use of the antiferroelectric organosiloxane Cl11-Si_3-11Cl as a host for the three dyes illustrates the adverse effects of disrupting the SmC^*_A liquid crystal structure. However, with the addition of sufficient dye, the possibility of a novel tri-state device is seen. Clearly, different dyes are required to capitalise on any potential uses of these states. The results shown here provide a good basis for further investigation.

The promising results of this chapter point the way to a possible regeneration of the dye guest host effect using ferroelectric hosts. In order to continue this work, several problems need to addressed, such as the limit on the amount of dye addition and subsequent hampering of the contrast levels obtainable. An ideal host would exhibit a room temperature ferroelectric phase with an overlying, less ordered phase for alignment. The next chapter tackles some of the problems observed thus far and advances the possible applications of the ferroelectric dye guest host effect.

5.8 REFERENCES

[1] G.H.Heilmeier. L.A.Zanoni, *Appl. Phys. Lett.,* **13**(3), 91 (1968); G.H.Heilmeier. J.A.Castellano, L.A.Zanoni, *Mol. Cryst. Liq. Cryst.,* **8**, 293 (1969).
[2] B.Bahadur, *Handbook of Liquid Crystals – Low Molecular Weight Liquid Crystals I,* (ed D.Demus, J.Goodby, G.W.Gray, H.-W.Spiess, V.Vill) Vol.**2A**,Chpt.3-**§3.4** (Wiley-VCH, Germany, 1998); *Mol. Cryst. Liq. Cryst.* **209**, 39 (1991).
[3] W.S.Park, T.Uchida, *Liq. Cryst.,* **5**(5), 1405 (1989).
[4] L.M.Blinov, V.G.Chigrinov, *Electrooptic Effects in Liquid Crystal Materials,* Chpt. 2, (Springer-Verlag, 1994).
[5] T.Uchida, M.Wada, *Mol. Cryst. Liq. Cryst.,* **63**, 19 (1981).
[6] A.Bloom, E.B.Priestley, *IEEE Trans. Elec. Dev.* **ED-24**, 823 (1977).
[7] T.Shimomura, S.Kobayashi, *Appl. Optics,* **20**(5), 819, (1981); T.Shimomura, H.Mada, S.Kobayashi, *Jap. J. Appl. Phys.,* **19**(5), 891, (1980).
[8] T.J.Scheffer, *J. Appl. Phys.,* **53**(1), 257 (1982).
[9] I.A.Shanks, *Contemp. Phys.* **23**(1), 65 (1982).
[10] T.Ikeda, T.Sasaki, K.Ichimura, *Nature*, **361**, 428 (1993).
[11] H.J.Coles, H.G.Walton, D.Guillon, G.Poetti, *Liq. Cryst.,* **15**(4) 551 (1993); *ibid.,* **17**(3) 333 (1994).
[12] X.Q.Yang, J.R.Wang, G.D.Ren, *Mol. Cryst. Liq. Cryst.,* **199**, 1 (1991).
[13] H.V.Ivashchenko, V.G.Rumyantsev, *Mol. Cryst. Liq. Cryst.,* **150A**, 1 (1987).
[14] D.L.White, G.N.Taylor, *J. Appl. Phys.,* **45**(11), 4718 (1974).
[15] M.Schadt, *J. Chem. Phys.,* **71**(6), 2236 (1979).
[16] H.S.Cole, R.A.Kashnow, *Appl. Phys. Lett.,* **30**(12) 619 (1977).
[17] H.L.Ong, *Jap, J. Appl. Phys.,* **27**(11), 2017 (1988).
[18] T.J.Scheffer, *Phil. Trans. Roy. Soc. London,* **A309**, 189 (1983).
[19] D.A.Dunmur, *The Optics of Thermotropic Liquid Crystals*, (ed. Steve Elston, Roy Sambles), Chpt. **2**, (Taylor & Francis, London, 1998).
[20] P.D.Semenza, *Stanford Resources, Web Reviews*, http://www.stamfordresouces.com
[21] Y.Nara, S.Kobayashi, A.Miyaji, *J. Appl. Phys.*, **49**(7), 4277, (1978).
[22] K.Kondo, S.Era, M.Isogai, A.Mukoh, *Jpn. J. Appl. Phys.,* **24**(11), 1389 (1985).
[23] H.J.Coles, H.F.Gleeson, *Mol. Cryst. Liq. Cryst. Lett.,* **6**(2), 53 (1988).
[24] H.J.Coles, H.F.Gleeson, J.S.Kang, *Liq. Cryst.,* **5**(4), 1243 (1989).
[25] Mitsui Toatsu Chemicals Inc. http://www.mitsui.co.jp
[26] J.Kang, *Ph.D. Thesis,* University of Manchester, (1991).
[27] E.Merck KGaA, Frankfurter Str. 250, D-64271, Darmstadt, Germany. http://www.merck.de
[28] J.K.Foitzik, W.Haase, *Mol. Cryst. Liq. Cryst.,* **97**, 231 (1983).
[29] S.Matsumoto, K.Mizunoya, H.Hatou, H.Tomii, *Mol. Cryst. Liq. Cryst.,* **122**, 285 (1985).
[30] N.S.Bayliss, E.G.McRae, *J. Phys. Chem.,* **58**, 1002, (1954).
[31] C.Noot, Ph.D. thesis (in preparation), Univ. Southampton, U.K., (2002).
[32] W.K.Robinson, C.Carboni, P.S.Kloess, S.P.Perkins, H.J.Coles, *Liq. Cryst.,* **25**(3), 301 (1998).

Chapter Six

Dyed Organosiloxanes : Nitrostilbenes

The most exciting phrase to hear in science, the one that heralds new discoveries, is not "Eureka!" but "That's funny..."

Isaac Asimov 1920-1992

6.1 INTRODUCTION

In an ideal dye containing display, the guest host effect might be replaced by the use of dyed liquid crystals. This could yield all the advantages of the dye guest host (DGH) effect without the problems of introducing what is essentially a contaminant into the liquid crystal. Until recently the focus of DGH work has been on the nematic phase although very few stable nematic liquid crystalline dyes have been found. Thus, the nematic DGH effect has typically relied on non-liquid crystalline guest dye doping. With the work of the last chapter, the ferroelectric dye guest host effect has become a more realistic possibility. The move to the smectic phase opens up new possibilities for dyed liquid crystals.

Initially the purpose of this chapter is to investigate the possibility of introducing larger amounts of dye into the liquid crystal matrix then later to move towards dyed ferroelectric devices. The work with the organosiloxanes in this thesis and within the group has encompassed the idea of the 'virtual backbone' effect. The addition of the siloxane unit has stabilised smectic phases with polymer-like ruggedness. As an initial step, it was thought that by attaching a dye molecule to the siloxane group, the backbone effect might allow larger amounts of dye to be added without the concomitant adverse effects on the liquid crystal structure.

The original concept behind this work is partly based on polymer work carried out within the group[1], which looked at the possibility of dye addition in nematic polymer devices. An appropriate dye molecule was attached as a side pendent to a polymer backbone and aligned by steric forces in a dye guest-host effect. As work within the group turned to the fabrication of ferroelectric polymer devices, the concept of pendent dye molecules was pursued and the result was a dye guest host effect in a ferroelectric polymer[2]. The structural similarities between organosiloxanes and polymers prompted research into the substitution of dye molecules onto siloxane backbones. Newton et al.[3], investigating the early organosiloxanes, found that by using the siloxane as a template, the virtual backbone effect could allow guest material to be added in far higher concentrations than achieved by simple solution of a dye molecule in a liquid crystal phase.

6.2 NITROSTILBENE AND SILOXANE COMBINATION

If a guest molecule, not necessarily mesogenic, is attached to a siloxane group and mixed with an organosiloxane liquid crystal, the siloxane moieties from the guest and from the smectic host may aggregate in the same layer. The guest moiety thus behaves in an analogous way to a pendent group on a side chain polymer liquid crystal, and its concentration can be significantly increased above the normal amount added by simply dissolving the dye in the host. The idea is simply to graft a dye

molecule onto the siloxane unit via an eleven length alkyl chain where it will, it is hoped, align with and mimic the organosiloxane hosts as closely as possible. The dye molecule chosen is 4-hydroxy-4'-nitrostilbene. This unit was selected because the molecule was already under investigation for another project and the synthetic process was well understood, allowing a relatively large amount to be synthesised[4]. The dye molecule met many of the criteria for a guest dye, in terms of its chemical, electrical and photo-stability, and it provides a stable structure for further chemical alteration to vary the colour[5]. There was also the possibility of the resultant combination exhibiting fluorescence. It was hoped that the similarly sized anisotropic shape, would fit well with the biphenyl-benzoate moieties of the organosiloxane hosts.

6.2.1 Structures

Although the 4-hydroxy-4'-nitrostilbene moiety has no liquid crystal phase, somewhat surprisingly after grafting it was found that the resultant organosiloxane nitrostilbene dye was itself liquid crystalline, exhibiting a SmA and a SmC phase[6]. A large amount of the dye was synthesised and is denoted NS11-Si_3 following the nomenclature developed in the early organosiloxane work. In later development work the idea of dye addition in the bi-mesogenic structures was investigated and consequently a dimeric dye was also synthesised NS11-Si_3-11NS. The structures of the dyes are shown in Figure 6.1 with a comparison to the structure of the organosiloxanes.

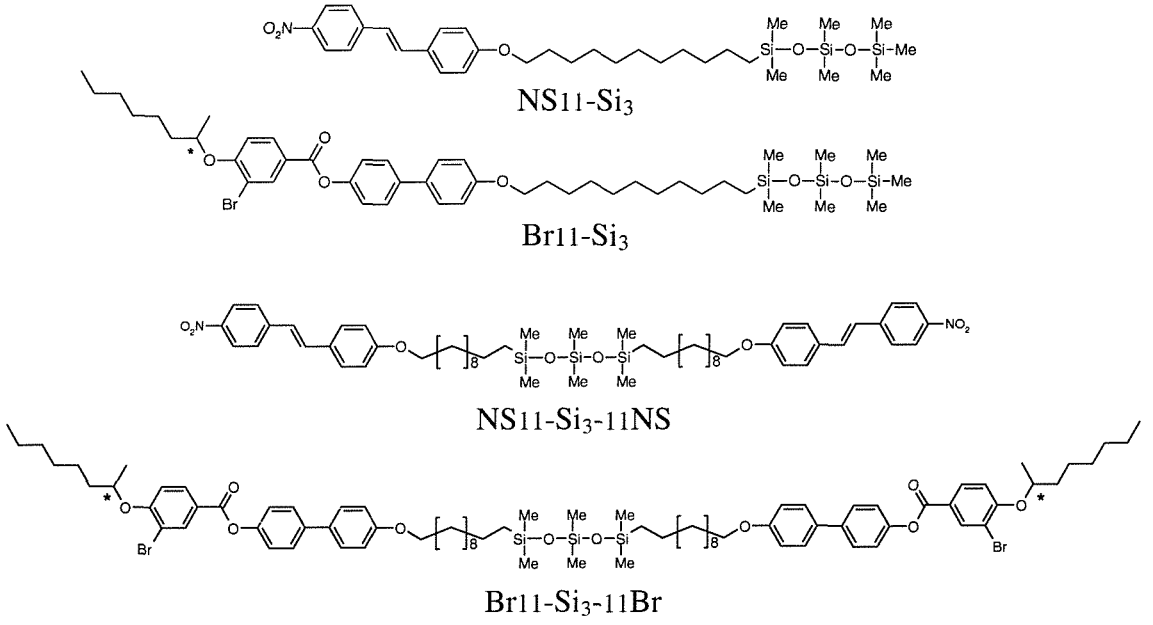

Figure 6.1 Schematic of the chemical structure of the nitrostilbene monomer and dimer alongside the bromo-substituted structures.

When choosing a suitable host material, the fluoro compounds were rejected due to their poorer alignment and electro-optic responses. The development of the synthetic route and material

availability allowed greater amounts of the mono- and bi-mesogenic bromo-substituted compounds to be synthesised and thus these were chosen as the preferred hosts.

To avoid confusion between the components of the mixtures, all of which are liquid crystalline, the bromo-substituted biphenyl benzoates Br11-Si_3 and Br11-Si_3-11Br are referred to as the hosts whilst the nitrostilbene compounds NS11-Si_3 and NS11-Si_3-11NS are referred to as the dyes.

6.2.2 Initial Study

The differential scanning calorimetry thermographs of NS11-Si_3 taken on cooling show a strong sharp peak with an onset temperature of 108°C. At 31.5°C, a distinct shoulder is seen and identified as a glass transition. A small diffuse peak was seen in the region of 45-50°C. Varying the run-times helped to resolve the peak, which suggested a very weak first order transition of the type sometimes seen at predominantly second order smectic-smectic transitions. With electro-optic study, NS11-Si_3 was found to have a phase range of

$$\mathrm{I} \xrightarrow{108} \mathrm{SmA} \xrightarrow{47} \mathrm{SmC} \xrightarrow{31.5} \mathrm{G}\,.$$

The presence of a smectic phase was identified initially by the characteristic bâtonnets that formed on cooling from the isotropic phase. A simple squidge cell with no alignment layers showed some focal conic texture and some schlieren texture with only four brush defects. With homeotropic alignment and shearing the cell appears black. The bâtonnets, appearance of four brush defects exclusively, and extinct homeotropic texture identify the initial smectic phase formed on cooling from the isotropic as SmA. On further cooling through 47°C the homeotropic texture showed birefringence colours. In the unaligned sample, the backs of the focal conic fans exhibited distinct banding. These effects suggest the transition to a SmC phase.

The grafting of the dye sample onto the siloxane core has once again promoted exclusively smectic phases, however, in this case the lack of a chiral centre in the nitrostilbene structure leads to non-chiral phases. To ascertain if the NS11-Si_3 and the Br11-Si_3 host are compatible, a contact preparation was made. No discontinuities were seen and the two compounds appeared to be fully miscible. As discussed in §3.6.2.2, apparent miscibility is not absolute proof of compatibility or phase determination, but is a promising sign[7].

Two mixtures were made at 16% and 36% w/w of NS11-Si_3 in Br11-Si_3. A brief study revealed ferroelectric smectic phases with 30-40° tilt angles[6]. Both the mixtures appeared to be completely miscible. This provided the impetus for an electro-optic examination of a full mixture range, the results of which are discussed in the following sections.

6.2.2.1 Spectra

Once it was established that the nitrostilbene organosiloxane was miscible with the Br11-Si_3 host, the spectra were studied. The nitrostilbene yields a yellow colour, and although not as striking as the mauves and blues described in the previous chapter, yellow dyes are still important in DGH work not only as one of the primary colours but as an ingredient in multi-component mixtures[8]. For the purposes of this chapter, the study of the compatibility of siloxane grafted compounds and the usefulness of the siloxane dye concept is of more interest than the dye's absorption spectrum. However, it is important to assess the effect on its absorption spectrum of grafting the precursor, 4-hydroxy-4'-nitrostilbene, onto the siloxane unit.

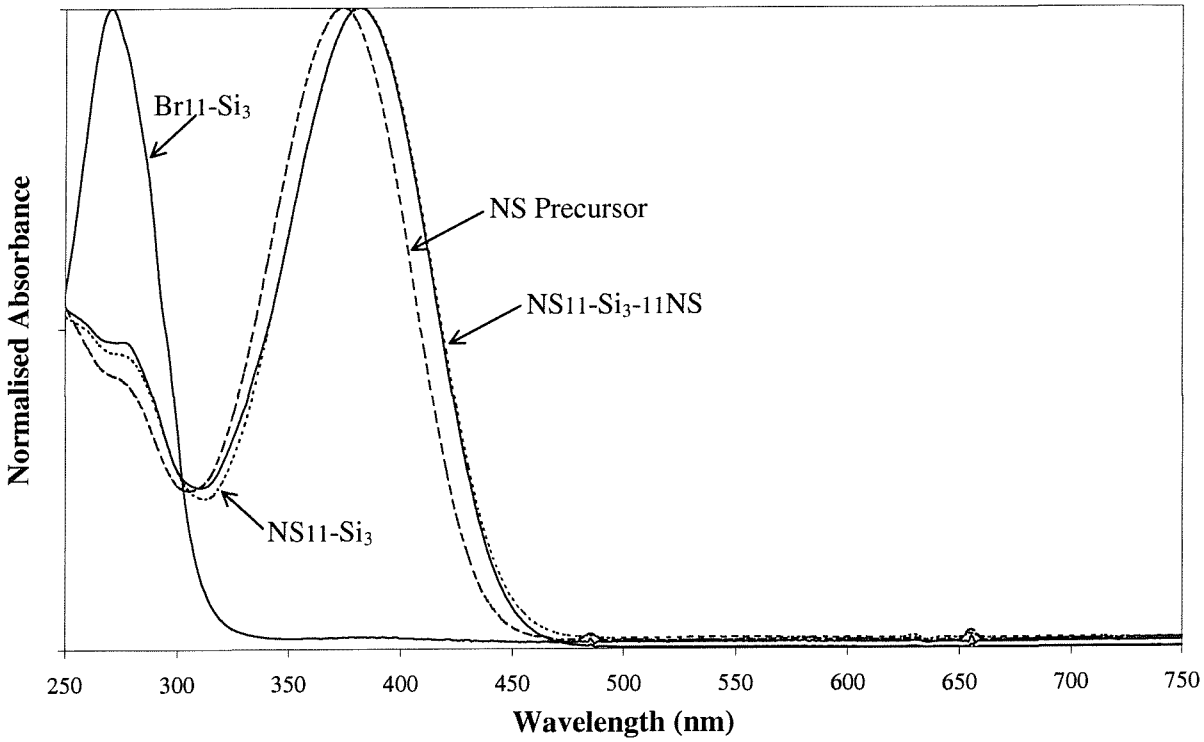

Figure 6.2 Comparison of the normalised absorption spectra of NS11-Si_3 and NS11-Si_3-11NS with the nitrostilbene precursor and the host Br11-Si_3.

The absorption spectra are examined using the method described in §5.3.5. Each compound is dissolved at 10 μM concentration in spectroscopy grade chloroform. As before; the samples are placed in ultraviolet transmissive cuvettes and are compared against a chloroform reference. The spectra in Figure 6.2 are normalised to allow easy comparison of the peaks' positions and shapes. The results show that the absorption spectrum of the precursor, 4-hydroxy-4'-nitrostilbene, is red-shifted by around 8 nm when it is grafted onto a siloxane unit. It can be seen from Figure 6.2 that the spectra of NS11-Si_3 and NS11-Si_3-11NS are almost identical and overlap for the majority of the spectrum. This is a promising result, showing that grafting of the dye onto the three-siloxane unit via an eleven-length alkyl chain has not dramatically altered the absorption properties of the dye. For

comparison, the spectrum of the host liquid crystal Br11-Si_3 is also shown (the spectrum of Br11-Si_3-11Br is identical to this and so is not shown). The absorption of the host is in the ultraviolet and does not overlap with that of the dye. No fluorescence was observed in the spectra of the 4-hydroxy-4'-nitrostilbene, NS11-Si_3 or NS11-Si_3-11NS compounds. The compounds were also investigated on a microscope ultraviolet rig and with an ultraviolet laser. No fluorescence was observed, so it was assumed that the fluorescent modes often associated with nitrostilbenes are quenched in this particular dye. Overall, the results indicate that if successfully grafted, a dyes' colours may be maintained, and other dyed liquid crystals may be produced by this substitution technique.

6.3 MONO-MESOGEN Br11-Si_3 WITH MONO-NITROSTILBENE NS11-Si_3

Building on the apparent miscibility and success of the test mixtures[6], a full mixture range was studied[9]. All the compounds are synthesised in-house and their exact chemical structures are known; this allowed mixtures to be made, varying concentration by molar mass. All the mixture ratios in this chapter are expressed in terms of the percentage of nitrostilbene in the bromo-organosiloxane host as a Mol/Mol ratio. Initially, mixtures of NS11-Si_3 and Br11-Si_3 were made near each end of the concentration range, i.e. at 5%, 10%, 90% and 95% with larger steps at 25%, 50% and 75%. The mixtures were examined in ~5 μm Lucid cells with an anti-parallel rubbing direction.

6.3.1 Phase Diagram

The temperature ranges and phase identification shown in Figure 6.3 are the result of differential scanning calorimetry (DSC) and optical microscopy. The two compounds are fully miscible over the entire concentration range. In general terms, the addition of the nitrostilbene has yielded a SmA phase over much of the concentration range. This is extremely beneficial for alignment purposes.

The wide temperature range of the phase diagram required the use of the Linkam CS196 liquid nitrogen cooler, described in §3.2.2 to reduce the temperature of the sample sufficiently. On cooling from the isotropic, the first liquid crystal phase is identified as smectic by the appearance of bâtonnets and focal conic textures. The mixtures of 75% and above also show homeotropic extinction, indicating presence of the SmA phase. Below the SmC* phase an additional liquid crystalline phase is seen. For example the 25% mixture's DSC thermographs show a small diffuse bump with an onset of 17.5°C and a sharper peak at -18°C. On the microscope between crossed polarisers, the focal conic structure of the unaligned SmC* phase breaks up and blurs slightly at ~17.5°C with no further changes in appearance on cooling. However, with the application of an electric field, a slight electro-optic switching effect (flickering) is seen between crossed polarisers down to –18°C. This evidence

points to a switchable liquid crystal phase below the SmC* phase. The most likely candidates for the more ordered smectic phase are SmI* and SmF*, as discussed further at the end of this section in §6.3.2.6.

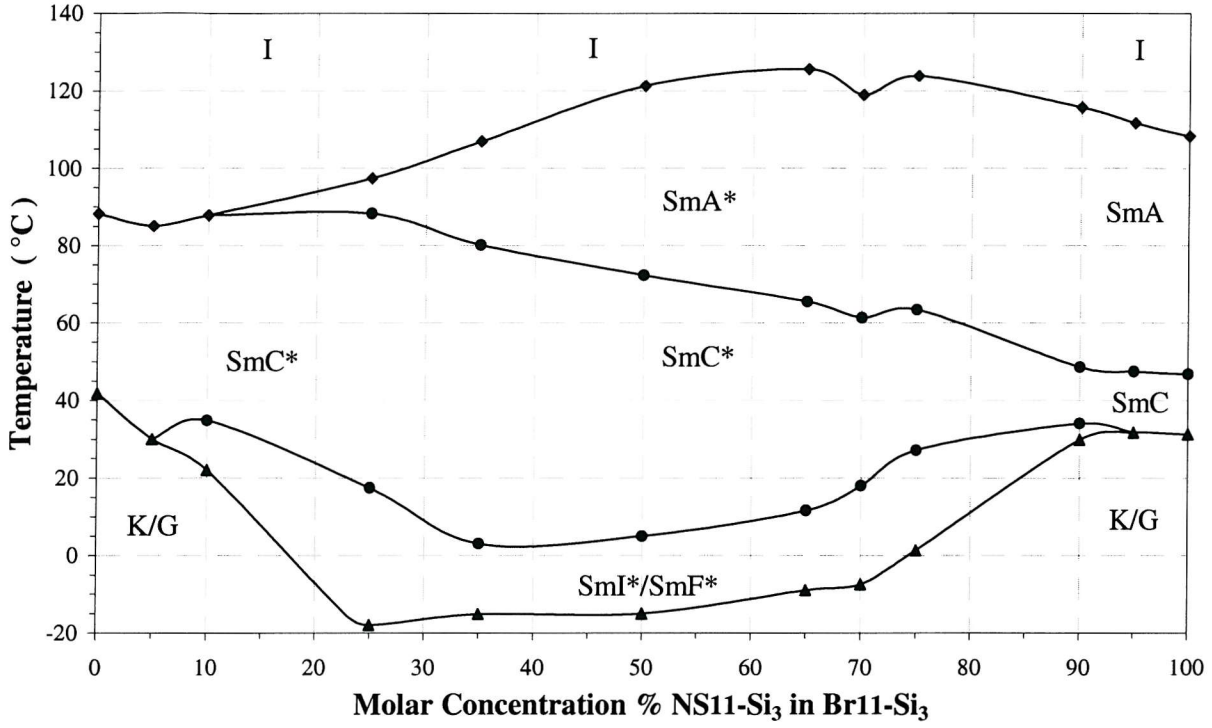

Figure 6.3 Phase diagram of molar concentration of NS11-Si3 in Br11-Si3.

The sharp DSC peaks and optical observations indicate that the pure Br11-Si_3 cools into a crystal state. At the other end of the scale, the pure NS11-Si_3 compound appears to cool into a glassy state. The mixtures in between are a combination of both and it is difficult to categorically identify the final cooled state. In addition to the appearance of a SmA phase over much of the mixture range, the SmC* phase occurs at room temperature. Although it is not the original intention of this study, the addition of the nitrostilbene to the host liquid crystal has created a room temperature ferroelectric with an overlying lower order phase; both desirable characteristics for an ideal ferroelectric device.

It is also difficult to identify which of the mixtures possess useful chiral phases. With 75% dye addition and higher, no effects are seen which would indicate that the bulk phase is chiral. However, it is difficult to study the phases accurately with the constraints imposed by boundary alignment conditions. It would be expected that even small amounts of what is, in essence, a chiral dopant in the 95% dye mix would result in a chiral phase, albeit with a long pitch, but the effect is too delicate to be seen in this work. Extra mixtures were made at 35%, 65% and 70% in order to examine where the presence of sufficient chirality to yield electro-optical effects vanishes, and fill some of the larger gaps in the phase range.

6.3.2 Electro-Optic Analysis

6.3.2.1 Alignment

One of the disadvantages of the organosiloxanes examined in the previous two chapters is the lack of an overlying lower ordered phase. In commercial compounds, a lower ordered phase is often a desirable property as it promotes planar alignment of the ferroelectric phase. High quality alignment is obviously essential for any commercial application. In this work, although good planar alignment is not essential for purely electrical studies such as spontaneous polarisation, reasonable alignment is required for tilt angle and optical switching time measurements.

One of the reasons that good planar alignment is more easily achieved in the SmA phase is that it is easier to induce a small amount of electrohydrodynamic instability in this phase. The focal conic structure is more readily disturbed in the un-tilted phase and so a monodomain texture forms more easily than it would in the tilted SmC phase. A good example of the alignment that can be achieved is shown in the crossed polariser photomicrographs in Figure 6.4. The alignment of the mixture was promoted by slow cooling from the isotropic through the SmA* phase at between 0.5°Cmin^{-1} to 2°Cmin^{-1} in the presence of an electric field. The applied field was typically around 100 Hz and 10 Vμm^{-1} but could be greatly varied with equally good results. If a simple cooling run was insufficient, the sample was annealed by cycling through ~5°C in the SmA* phase just above the SmA*→SmC* transition. In Figure 6.4 both samples have gone through a single cool 0.5°Cmin^{-1} and been exposed to the same electric field alignment conditions. The increase in alignment quality with dye addition is clearly seen.

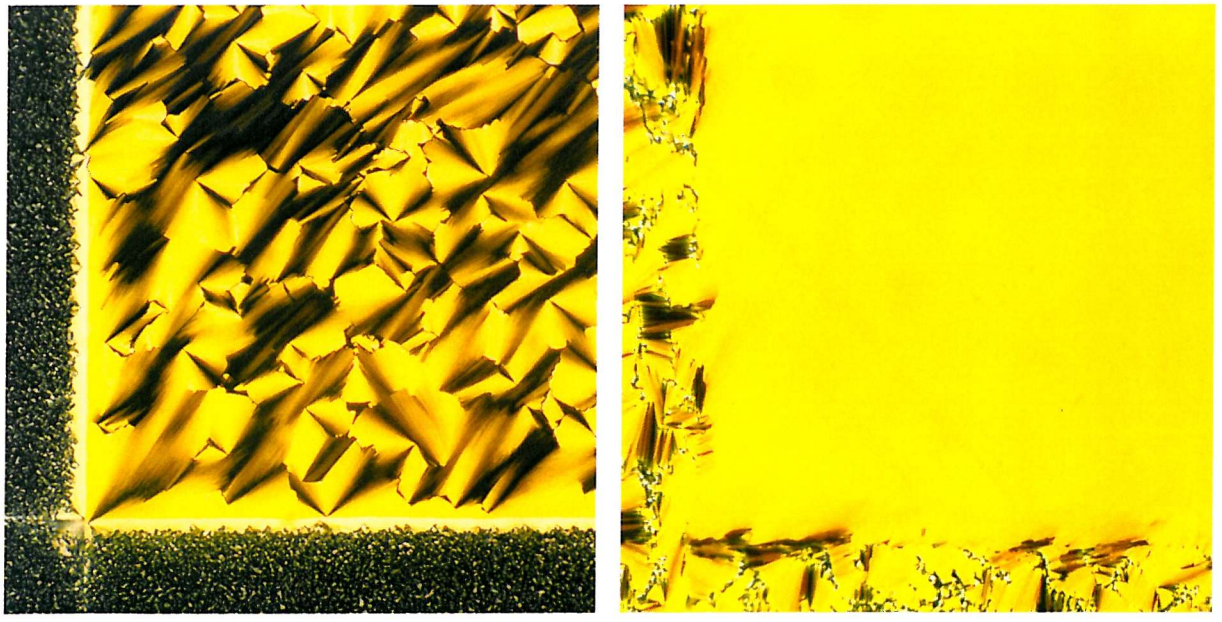

Figure 6.4 Photomicrographs taken at 50x magnification, demonstrating the alignment variation between pure host material Br11-Si$_3$ (left) and that with 25% NS11-Si$_3$ addition (right).

The setup of new equipment within the lab also allowed the possibility of using magnetic alignment to encourage the formation of mono-domain textures[10]. This technique has the advantages of being less invasive and not relying on high electrical fields. A low electric field of ~2-3 $V\mu m^{-1}$ at ~50 Hz is applied to help stimulate the molecules. The sample is then slowly cooled from the isotropic with a ~1T magnetic field applied. The use of the magnet slightly enhanced the alignment of the pure host, 5%, 10% and 25% dye mixtures, but was of no further benefit above 25% where good alignment was already possible.

6.3.2.2 Tilt Angle

The high quality of the alignment, particularly with larger amounts of NS11-Si_3, allowed the tilt angle measurements to be made using the most accurate photodiode method described in §3.4.1.1. The level of illumination is carefully controlled with a red-gel filter. The results in Figure 6.5 show that with small amounts of dye addition the tilt is reduced by several degrees, but as the concentration of dye increases this reduction in tilt angle becomes more pronounced. At 50% the tilt angle is reduced to ~28° and falls further to ~15° at 65%. A 70% mixture was made specifically to look for electro-optical effects. With high fields, some flickering was seen between crossed polarisers, but no tilt angles could be reproducibly measured.

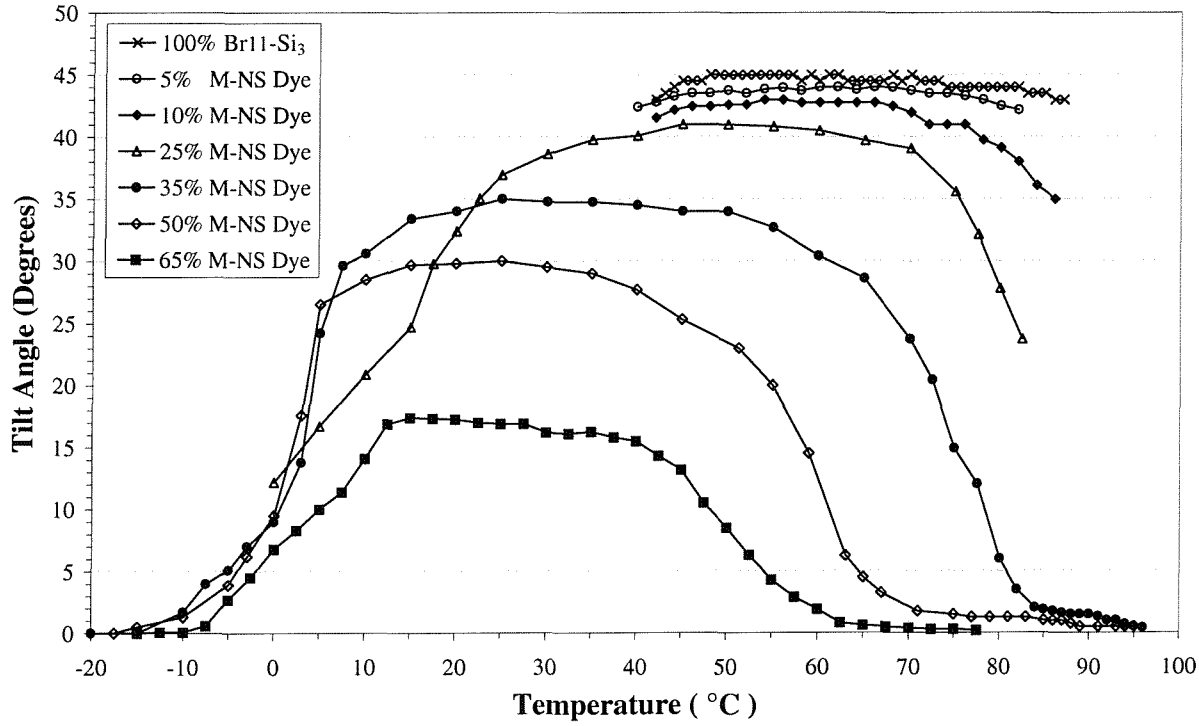

Figure 6.5 Optical tilt angle measurements of mixtures of NS11-Si_3 in Br11-Si_3.

Figure 6.5 shows that as the percentage of nitrostilbene increases and the SmA* phase becomes wider, the tilt angle becomes dependent on temperature over most of the SmC* range. This second order behaviour is a consequence of the SmA*→SmC* transition.

As was seen with the fluoro-precursors in the organosiloxane chapter, altering the layer structure can cause large changes in the tilt angle. The alkyl chain allows a great amount of flexibility of molecular length and tilt. An extensive x-ray study of organosiloxanes in earlier work revealed that even small variations in the structure of the mesogenic unit, whilst maintaining chain length, could strongly affect layer spacing[11,12]. The tilting mechanics of the mesogens are not well understood. It is hoped that future x-ray studies will shed some light on possible layer spacing changes, perhaps indicating a straightening of the ferroelectric Br11-Si_3 host within the mixtures, increasing the smectic layer spacing and reducing the tilt in this case.

6.3.2.3 Electroclinic Tilt Angle in the SmA phase*

As can be seen in the long tails at the high temperature end of the phase range in Figure 6.5, the tilt angle appears to extend into the SmA* phase. In the SmA* region the molecules do not favour a tilted arrangement and the Goldstone mode no longer exists. As discussed in §2.2.3 molecules in the SmA* phase can undergo 'soft mode' or 'electroclinic' switching. In the SmA* region away from the SmA*→SmC* transition, the magnitude of the tilt is linear with the applied field amplitude. At higher fields and close to the transition, the induced tilt follows an $E^{1/3}$ trend. To show the magnitude of this effect the 50% mix was studied in the SmA* phase (121.5 – 72.5°C) at a range of field strengths; the results are shown in Figure 6.6.

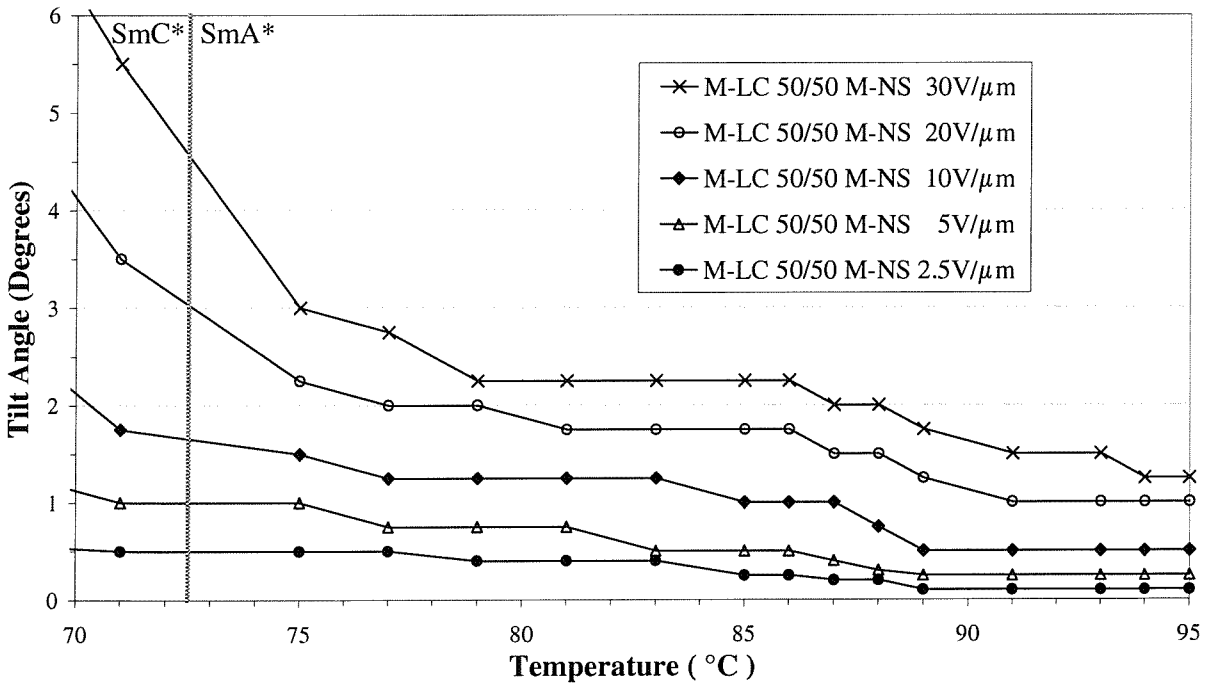

Figure 6.6 Electroclinic tilt in the SmA phase of a 50/50 M/M mix of NS11-Si_3 in Br11-Si_3.*

The angles measured are very small and are at the limit of measurement accuracy. The presence of an electroclinic tilt of up to ~3° in the SmA* phase is extremely beneficial to alignment. The ability to tilt the director allows the focal conic structure to be disrupted and surface alignment forces to prevail.

The electroclinic nature of the switch in the SmA* is confirmed by observing the switching hysteresis. In the SmC* phase the molecules respond spontaneously and the characteristic ferroelectric hysteresis loop described in §2.6.2 is seen. In the SmA* phase the electroclinic response is linear with the applied field and thus no hysteresis is observed and the loop is closed. Although it is not the main phase under investigation in this study, the smectic A phase does have DGH host applications. A suitably aligned mixture can be switched between a homeotropic texture, yielding a clear state, and a scattering mode, providing a dyed state. This mode of operation was seen in earlier organosiloxane work with the addition of non-liquid crystalline dyes similar to those discussed in the previous chapter[13].

6.3.2.4 Spontaneous Polarisation

The spontaneous polarisation of the SmC* phase is measured using the current pulse technique. With a triangular driving wave of 20 $V\mu m^{-1}$ at 80 Hz, the spontaneous polarisation reorientation peak is well defined in mixtures with up to 35% dye addition. However, dilution of the mesogenic host has an effect on the spontaneous polarisation. In order to observe fully saturated switching in the 50% mix the driving frequency is reduced, the oscilloscope trace begins to deteriorate and some baseline slope is seen. With 65% dye addition the trace becomes erratic and many runs are required to obtain a reasonable average. The 70% mix shows some spontaneous polarisation behaviour but this is not reproducible and cannot be measured against the background noise.

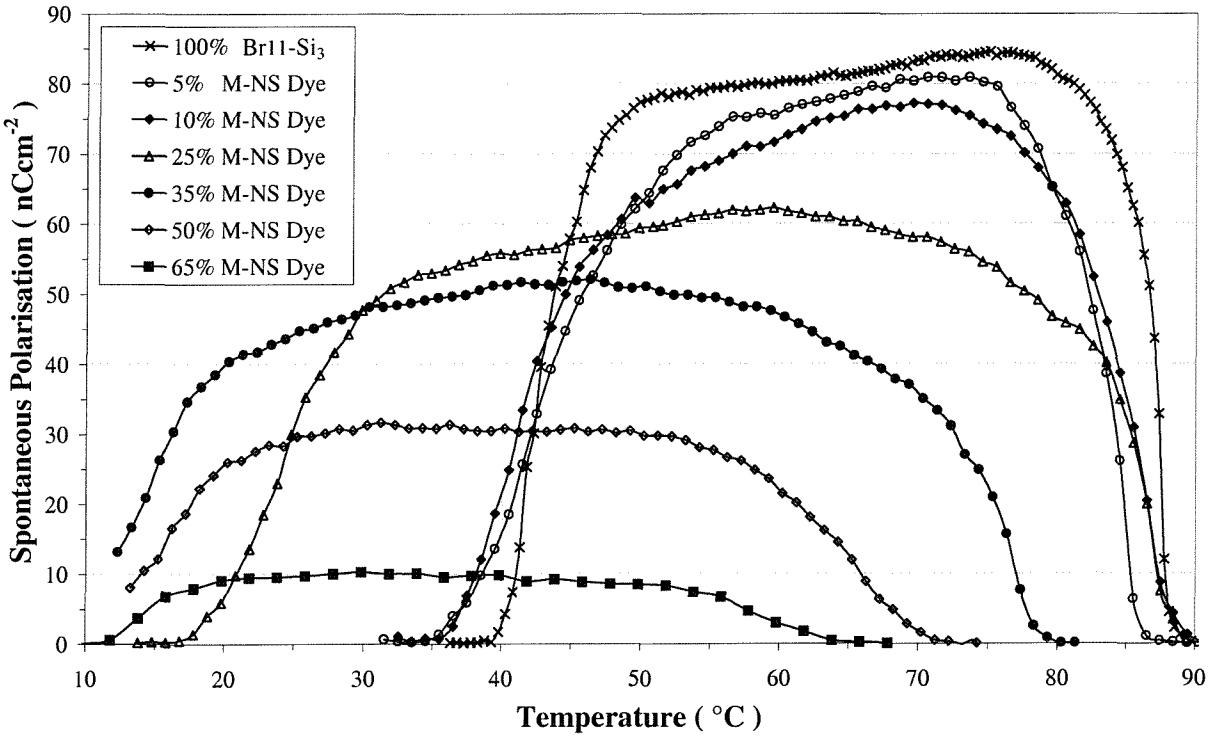

Figure 6.7 Spontaneous polarisation measurements of mixtures of NS11-Si3 in Br11-Si3.

The results in Figure 6.7 show that dilution effects reduce the magnitude of the spontaneous polarisation, as was seen with dye addition in the previous chapter. With up to 35% NS11-Si_3 addition, the spontaneous polarisation falls in direct proportion to the concentration of dye in the host. As the dye addition concentration is increased above 35%, the spontaneous polarisation falls-off more rapidly. One possible explanation for this behaviour is that the chiral interactions essential for the presence of ferroelectricity are sufficiently weakened that not all the chiral material responds spontaneously. As was observed in the measurements of tilt angle, at the higher NS11-Si_3 concentrations the second order nature of the SmA*→SmC* transition becomes apparent in the slope of the results.

6.3.2.5 Switching Time

The good quality alignment allowed all the switching time measurements to be made using the photodiode and oscilloscope method described in §3.4.3. The results are shown in Figure 6.8.

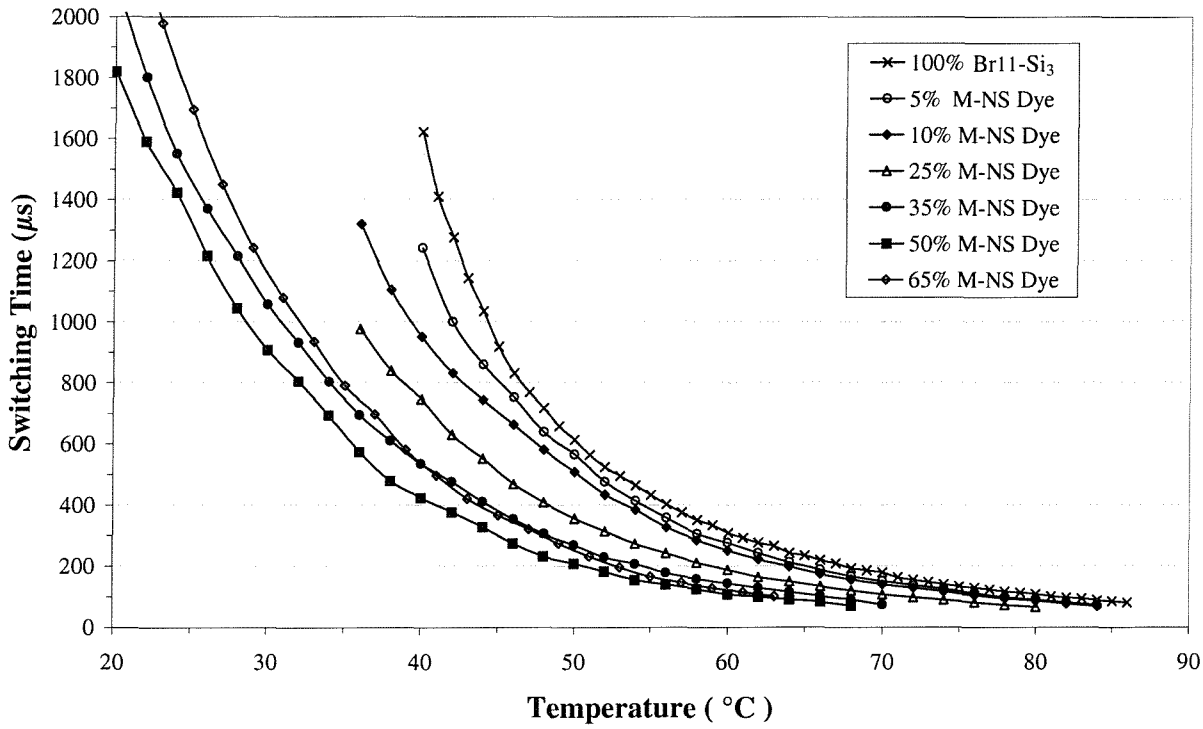

Figure 6.8 Optical switching time measurements of mixtures of NS11-Si_3 in Br11-Si_3.

In order to attempt to separate the results, they are replotted on a semi-log plot in Figure 6.9. The semi-log plot highlights the slight upward curve seen at lower temperatures in the pure Br11-Si_3 compound. As the percentage of NS11-Si_3 increases, the curve flattens. On the DSC traces the small bump (discussed in §4.4.2 of the organosiloxane chapter) observed at ~49.5°C in the pure host is no longer seen in samples containing the nitrostilbene dye. This phase anomaly, which was attributed to reconfigurations of the siloxane unit and chain, is no longer seen, and the switching times exhibit the exponential increase with temperature that is expected.

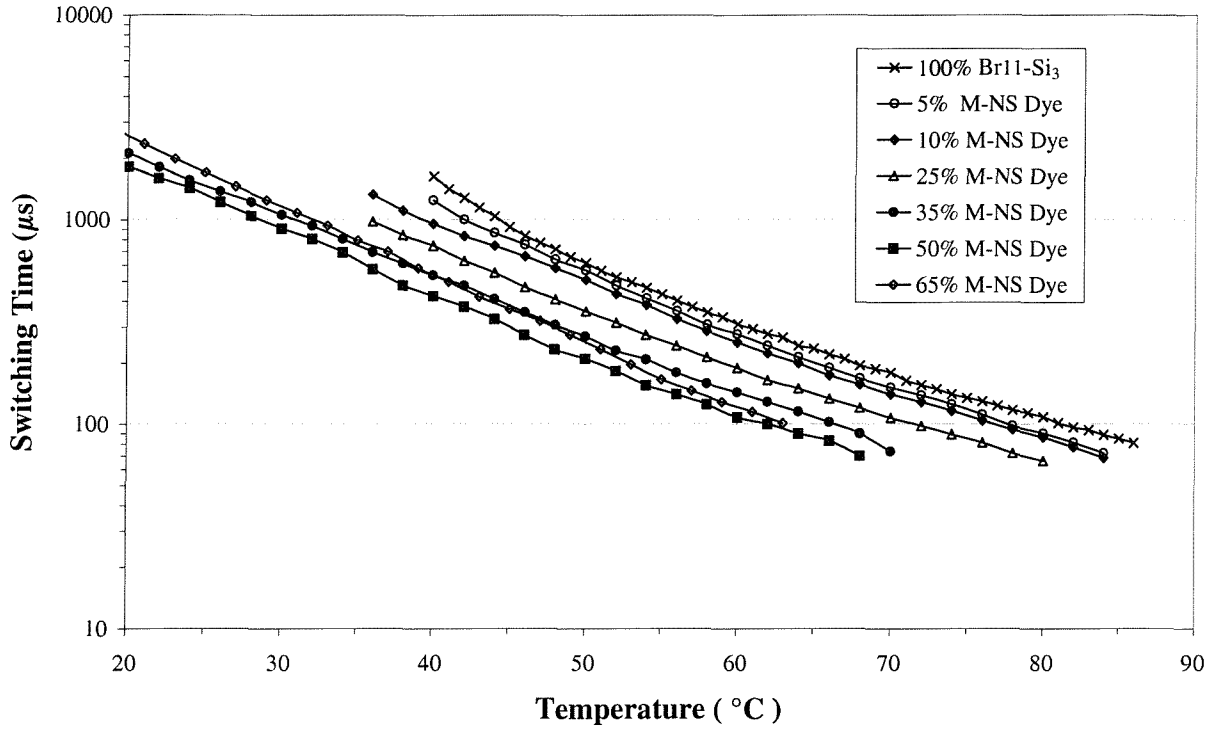

Figure 6.9 Switching time measurements of mixtures of NS11-Si3 in Br11-Si3 plotted on a semi-log scale.

The two switching time plots do not show a large change in the nature of the switch with increasing dye addition. If the graphs are replotted on a shifted temperature scale, the data overlaps.

6.3.2.6 Higher Ordered Smectic Phase

Although there are a number of higher ordered smectic phases possible below the SmC* phase, the electro-optic results help identify possible candidates. Using the 25% mix as an example, DSC and optical observations show a transition at around 18°C. Reviewing the tilt angle measurements in Figure 6.5, a sharp drop off is seen around 18°C, but electro-optic switching is still observed and hence a tilt angle is still measurable (down to 0°C). In order to examine the nature of the switch in the phase, the field and frequency are varied. Very little switching is seen below 25 $V\mu m^{-1}$, and above this level the switching is erratic, so the oscilloscope photodiode setup does not yield meaningful results. With the application of a 35 $V\mu m^{-1}$ field and a slow triangle wave, the tilt angle is visually observed to occur in a series of steps.

Below the SmC* phase the spontaneous polarisation measurements are also highly erratic, but by averaging a large number of current pulse peaks the response is resolved into a gradual curve such that the spontaneous polarisation realignment peak becomes measurable. The presence of a tilt angle and stepped switching points to the hexatic SmI* and SmF* phases as likely candidates for the phase[14]. Another consideration is the time required for complete formation of the phase. Work on more complex smectic systems suggests that the time required for the helical pitch to equilibrate in a

system undergoing a transition between some smectic phases can be of the order of days[15]. In the current work it was found that if the phase was allowed to form from a very slow cooling run with frequent long pauses over several days, the quality of the switching and electro-optic readings was initially superior. However, after several measurements the quality of the switch deteriorated once more. The lower smectic phase is not unambiguously identified at this time, so in order to investigate this phase further, samples are currently being studied by X-ray diffraction to determine the nature of the ordering[16].

6.4 MONO-MESOGEN Br11-Si_3 WITH BI-NITROSTILBENE NS11-Si_3-11NS

Having examined the influence of the monomeric nitrostilbene dye on the mono-mesogen Br11-Si_3-11Br, the focus moves to the dimeric dye. The dimeric dye NS11-Si_3-11NS is based on the Br11-Si_3-11Br template as shown in Figure 6.1. The dye exhibits only one liquid crystalline phase, the smectic A, with a phase range of

$$I \xrightarrow{149.8} SmA \xrightarrow{46.0} G .$$

6.4.1 Phase Diagram

The dimeric NS11-Si_3-11NS dye is added to the mono-mesogenic Br11-Si_3 and once more, the two compounds exhibit complete miscibility over the entire concentration range. The mixtures are studied by DSC and crossed polariser microscopy. Examining the results in Figure 6.10, the strong influence of the dye's SmA phase is clearly seen and exists as the only liquid crystal phase above 40% of dye concentration. The SmC* phase range of the host is broadly maintained with up to 25% of dye addition together with the presence of a higher temperature SmA* phase at 10% dye concentrations and above. Somewhat surprisingly with 30% and 35% addition of the NS11-Si_3-11NS dye, the SmC* phase exhibits antiferroelectric behaviour and this is discussed in §6.4.2.4.

The SmA* phase is first seen in the 10% mixture. Although the onset of the liquid crystalline phase is easily observed on the microscope and DSC traces, the transition from SmA*→SmC* is not. The transition from the isotropic phase is broadened by biphasic behaviour down to ~10° below the onset of the transition. Due to the narrowness of the SmA* range in the 10% mixture, any small peak due to the smectic/smectic transition is masked in the broad I→SmA* peak and cannot be discerned on the DSC trace. Even with slow cooling on the microscope the transition appears broad and the SmA*→SmC* transition temperature is difficult to assign. In order to clarify the position of the transition, the thermo-optic method is employed, as discussed in §3.6.2.1. The use of the microscope, photodiode and oscilloscope setup allows the transition to be resolved more easily. As with all the electro-optic readings in this chapter, the level of illumination is carefully controlled with a red-gel

filter. The assigned value for the transition is chosen from a match in the thermo-optic readings with the onset of ferroelectric switching after observing the switching nature of the mixture at low voltages. The broadening of the SmA* phase range in the mixtures with 25%-35% of dye addition allowed the smectic/smectic transition to be more easily identified. Once again the DSC traces exhibit a small diffuse peak at the transition. Examining unaligned samples between crossed polarisers on the microscope, the fans of the focal conics of the SmA* phase become distorted and breaks are seen at the transition temperature. Unlike the mixtures of the monomeric NS11-Si_3 in Br11-Si_3, no higher order phase is seen and with reducing temperature the highest order smectic phase (SmC*, SmC*$_A$ or SmA, as appropriate) freezes into a crystal/glass phase.

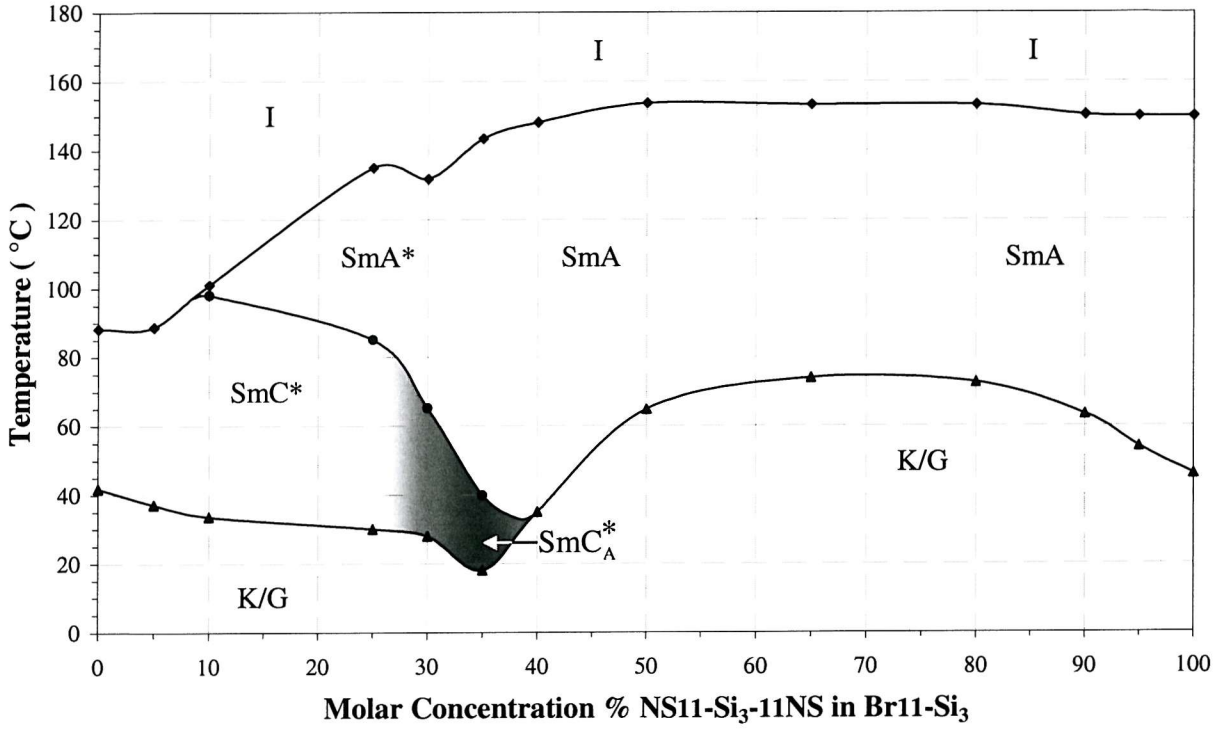

Figure 6.10 Phase diagram of molar concentration of NS11-Si_3-11NS in Br11-Si_3.

6.4.2 Electro-Optic Analysis

The lack of a SmA* phase in the mixtures with up to 10% dye addition meant the alignment quality in the SmC* phase was generally similar to that of the pure Br11-Si_3 compound. The mixtures were therefore aligned in the same manner as the host, as previously discussed in the organosiloxane chapter. The samples were annealed under the influence of a triangle-wave field at 100 Hz and 15-20 $V\mu m^{-1}$. The use of magnetic alignment allowed a slight improvement in the final alignment quality but took considerable time to set up and achieve. The mixture with 25% dye addition, with its SmA* phase, aligned relatively easily. In the antiferroelectric 30% and 35% mixtures, repeated cycling in the SmA* phase yielded some alignment, but this was difficult to reproduce and the alignment was easily lost with the application of high fields.

6.4.2.1 Tilt Angle

The alignment quality of mixtures containing up to 25% dye addition allowed the tilt angle measurements shown in Figure 6.11 to be made with the photodiode setup. The 30% and 35% curves are a combination of microscopy and rotating analyser observations[17] and the values quoted are for driven tilt, due to the antiferroelectric nature of the phase.

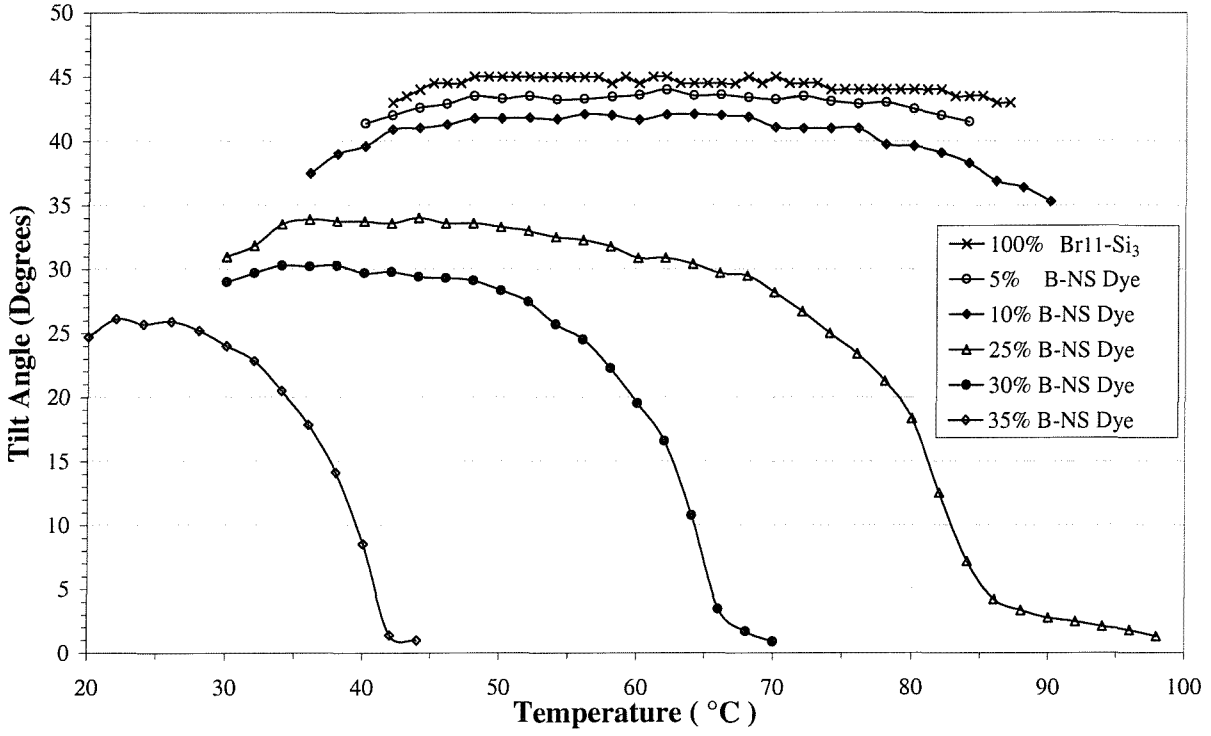

Figure 6.11 Optical tilt angle measurements of mixtures of NS11-Si3-11NS in Br11-Si3.

As was seen with the addition of the monomeric dye in Figure 6.5, the tilt angle is reduced with increasing dye addition and the shape of the curves becomes increasingly second order. Electroclinic behaviour is seen once more in the SmA* phase. The 25% mix exhibits measurable electroclinic behaviour in the 12°C before the transition to the SmC* phase. The antiferroelectric 30% and 35% mixtures also exhibited a small amount of electroclinic response, in the last 5°C before the transition. Although the tilt angles measured are less than 1° and at the limit of experimental accuracy, the electroclinic response is also seen in the thermo-optic measurements used to locate the phase transition temperature[18]. This small amount of electroclinic tilt was only observed with run speeds less than 0.2°Cmin^{-1}. At 40% of dye addition and above, no switching behaviour is identifiable.

6.4.2.2 Spontaneous Polarisation

The spontaneous polarisation results in Figure 6.12 follow a similar trend to that seen when the host is doped with the NS11-Si_3. The spontaneous polarisation reorientation peaks are well defined with mixtures up to 25%. In this region dilution effects can once again be held responsible for the majority of the decrease in spontaneous polarisation magnitude. The magnitude of the spontaneous polarisation in the 10% mixture is particularly depressed in the initial 10°C below the SmA*→SmC* transition and this behaviour is attributed to the biphasic nature of the transition.

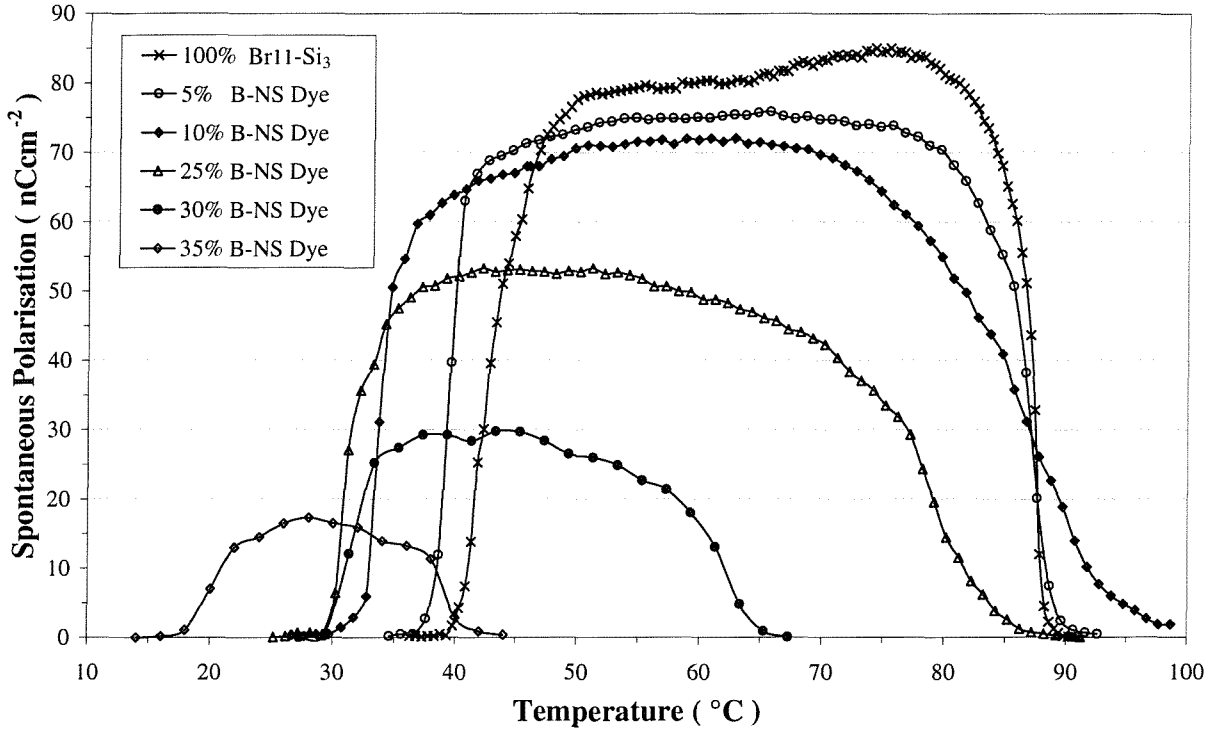

Figure 6.12 Spontaneous polarisation measurements of mixtures of NS11-Si_3-11NS in Br11-Si_3.

The spontaneous polarisation of the antiferroelectric phase of the 30% and 35% mixtures required manual measurement. The driven peaks were ~15% larger than the relaxation peaks and a large amount of baseline slope was also observed, requiring considerable compensation. The spontaneous polarisation realignment peaks exhibited long tails, enlarging the error for these particular readings. Despite the problems encountered, the spontaneous polarisation measurements for the antiferroelectric mixtures were reproducible to within ~5%. The magnitude of the spontaneous polarisation is severely attenuated, by amounts far greater than can be explained by dilution. In the previous chapter §5.6.1.1, with a small amount of dye addition and an antiferroelectric mixture, the spontaneous polarisation magnitude was also reduced by a far greater extent than could be explained by dilution. Although the circumstances are somewhat different in this case, it would appear that in general the antiferroelectric mixtures are very susceptible to disruptions, and this lowers the effect of spontaneous polarisation realignment.

6.4.2.3 Switching Time

Measurements of the ferroelectric switching times were made using the photodiode and oscilloscope method with mixtures containing up to 25% of dye. The antiferroelectric compounds' switching times were measured using the current pulse technique, although the presence of a large amount of baseline slope and an irregular signal response hampered these measurements. These difficulties limited the reproducibly of the results for the antiferroelectric phases to between 5% and 10%, leading to some scatter on the switching time curves shown in Figure 6.13.

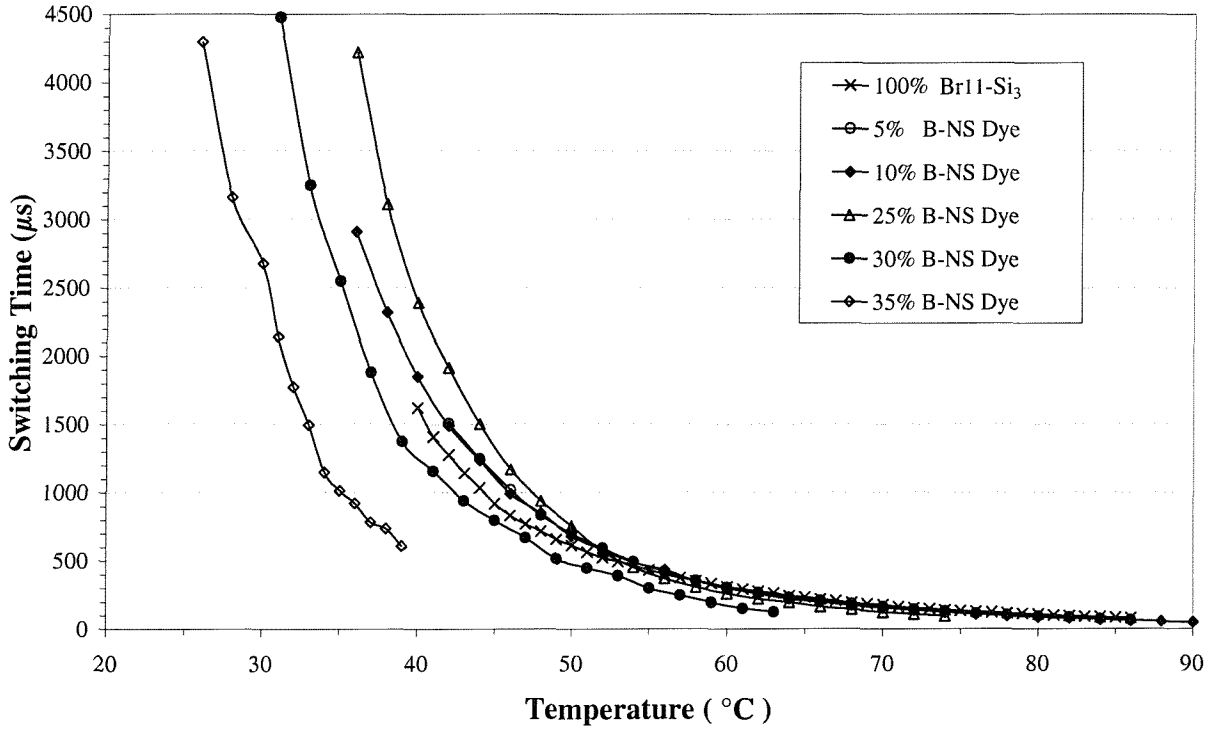

Figure 6.13 Switching time measurements of mixtures of NS11-Si3-11NS in Br11-Si3.

The ferroelectric mixtures follow the trend observed in the previous mixtures of NS11-Si_3 in Br11-Si_3, resulting in very little observable difference between the switching times at 5% and 10% of dye addition. At 25% dye concentration, and particularly in the antiferroelectric mixtures the switching time appears to increase. The large difference in the onset temperatures of the SmC* phase in the different mixtures makes a shifted temperature analysis less appropriate, however, it is clear that the general trend is towards a slower switch as the dye concentration is increased. This slowing of the switch is in line with typical results in the previous chapters for antiferroelectric compounds in comparison with ferroelectric switching.

6.4.2.4 Antiferroelectricity

Antiferroelectric behaviour is easily identified by the observation of twin spontaneous polarisation realignment peaks (driven and relaxed) on the oscilloscope trace. It is somewhat surprising that antiferroelectric behaviour is induced in the mono-mesogenic Br11-Si_3 ferroelectric host. Work within the group by C.Carboni looked at the possible effects on mesophase structure of mixtures of the mono-mesogenic Cl11-Si_3 and bi-mesogenic Cl11-Si_3-11Cl compounds[19]. His work suggests a phenomenological model for the energetic interactions between the two compounds driving ferroelectricity and antiferroelectricity. He proposes the use of an antiferroelectric liquid crystal to confer a bent conformation on the otherwise ferroelectric mono-mesogenic structures. In this chapter the antiferroelectricity has emerged from the interaction of a mono-mesogenic ferroelectric with a dimeric non-chiral compound. This result can also be considered alongside the three colour states of the antiferroelectric dye guest host device in §5.6.2. The antiferroelectric host acts as a template for the guest dye, causing the dye to adopt a herringbone structure. Combining the concepts of C.Carboni with the results of the dimeric nitrostilbene work, it is logical to suggest the antiferroelectricity observed is a consequence of a structural configuration imposed by a templating effect of the bent dimeric dye.

6.5 Bi-Mesogen Br11-Si_3-11Br with NS11-Si_3 and NS11-Si_3-11NS

In the final part of this chapter the mono-mesogenic host liquid crystal is replaced, and the two nitrostilbene dyes are mixed with the bi-mesogenic antiferroelectric organosiloxane Br11-Si_3-11Br. Mixing the non-chiral monomeric dye with the chiral bi-mesogenic host allows further investigation into the effect of templating. In this study, however, the bent dimeric compound is the already antiferroelectric organosiloxane, which is mixed with the monomeric nitrostilbene dye. Mixing the dimeric dye with the bi-mesogenic host completes the investigation.

6.5.1 Phase Diagrams

Once again the ranges and phase identifications, shown in Figure 6.14 and Figure 6.15, are the results of differential scanning calorimetry and optical microscopy. Both dyes were completely miscible with the host over the entire concentration range. With the addition of the monomeric dye, the antiferroelectric nature of the Br11-Si_3-11Br host is maintained in mixtures with up to 50% of dye addition. The alignment quality was similar to that of the pure host with up to 10% dye addition, as the effect of disrupting the antiferroelectric structure is offset by a weakened chirality, allowing easier alignment. On increasing dye addition up to 50%, the alignment deteriorates as the antiferroelectric structure is further disrupted. The 65% and 75% mixtures exhibited no alignment, and although they

appeared to show some switching effects with very high fields, the cells short-circuited and the mixture denatured under these conditions. At 90% of dye addition the alignment was greatly improved and of similar quality to the pure dye, being almost monodomain. The samples containing a large dye concentration exhibited reasonable alignment on slow cooling under a small field of ~2-3 $V\mu m^{-1}$ at ~50 Hz. The use of the magnet with a similar small electric field, produced good quality monodomain samples for the 90% and pure dye samples after one slow cooling run, from the isotropic phase, at $0.2°Cmin^{-1}$.

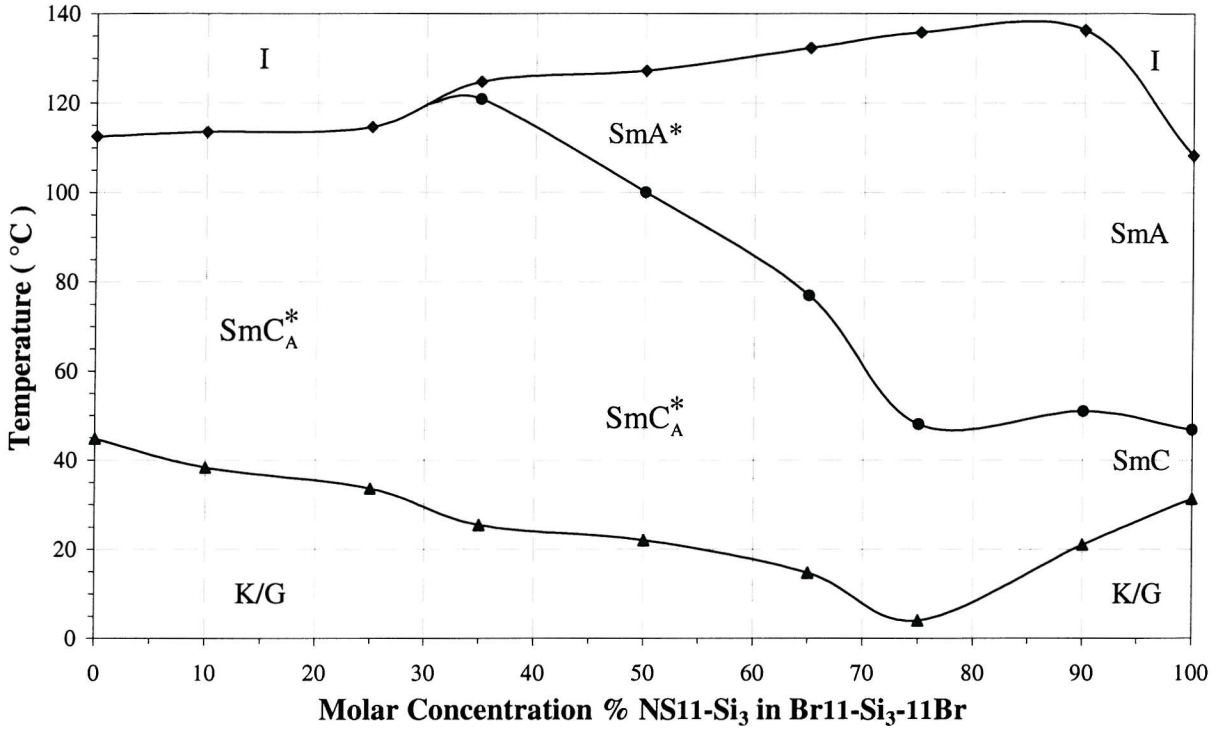

Figure 6.14 Phase diagram of molar concentration of NS11-Si$_3$ in Br11-Si$_3$-11Br.

In comparison with Figure 6.3, showing the effect on phase behaviour with the addition of the monomeric dye to the mono-mesogen (§6.3.1), it can be seen that the SmA* phase does not emerge until higher dye concentrations with the addition of the dye to the bi-mesogen (Figure 6.14). Previously, the monomeric dye was able to strongly influence and overcome the tilting tendency of the mono-mesogenic host. However, in this case, although the presence of dye molecules clearly disrupts the antiferroelectric order, it does not easily negate the tilt of the host. No higher ordered liquid crystal phase is seen at temperatures below the SmC* phase. The last electro-optic switching measurements were possible at 50% dye concentration.

The phase diagram of the mixtures between the dimeric nitrostilbene dye and the bi-mesogenic host, as shown in Figure 6.15, bears many similarities to the phase diagram of the mixtures between this dye and the mono-mesogenic host as shown in Figure 6.10. In the mixtures exhibiting the smectic C* phase, the antiferroelectricity of the host is maintained. With the addition of up to 10% of the dye, the alignment quality was similar to that of the host. The host and 10% mixture were aligned as

described in the organosiloxane chapter: the samples are heated into the isotropic phase and then cooled at 0.5-0.1°Cmin^{-1} to ~2° below the I→SmC*$_A$ transition. A triangular A.C. field is applied at ~100 Hz and high field strengths are used; 20-35 Vμm^{-1}. In the 25%→50% mixes it was hoped that the presence of the SmA* phase and the weakened chirality of the mixtures would make alignment easier. Unfortunately this was not the case, although a wide variety of field strengths, frequencies and waveforms were tested and some initial alignment was achieved, during electro-optic study any alignment achieved deteriorated rapidly. Despite the compatibility expected between the host and dye, it proved very difficult to maintain a monodomain sample in any of these mixtures.

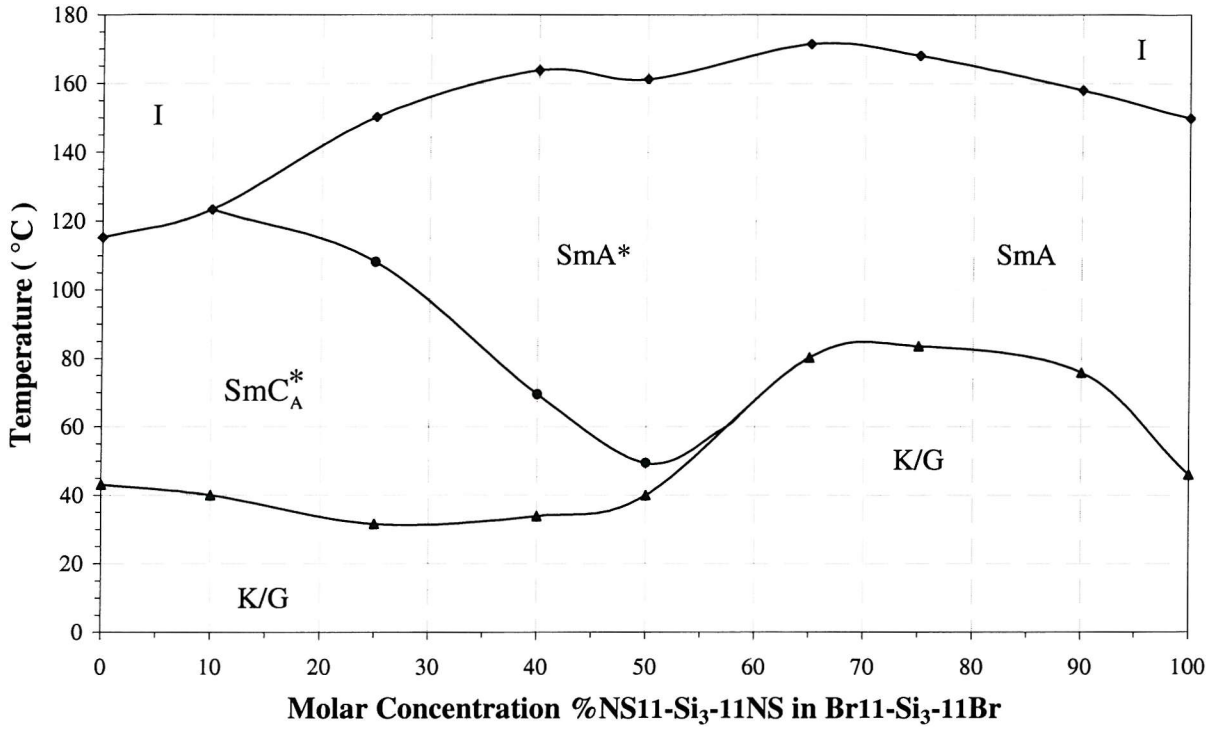

Figure 6.15 Phase diagram of molar concentration of NS11- Si$_3$-11NS in Br11-Si$_3$-11Br.

In general, the bi-mesogenic antiferroelectric host has maintained its phase characteristics at higher dye concentrations than was observed with the ferroelectric mono-mesogen. This behaviour may be a consequence of the sharply defined layer structure and ordering typical of the antiferroelectric phase.

6.5.2 Electro-Optic Analysis

6.5.2.1 Tilt Angle

Measuring the tilt in the antiferroelectric phase is typically more difficult than the normal ferroelectric measurement. The primary problem is one of alignment, as the antiferroelectric samples are generally harder to align than their ferroelectric equivalents. The high field strengths required to ensure complete switching in the antiferroelectric materials were found to lead to sample degradation after prolonged periods of switching, particularly with high amounts of dye addition.

Initially considering the addition of NS11-Si_3 in Br11-Si_3-11Br, induced tilt angle measurements were made in the mixtures up to 50% concentration of dye. With 10% addition a sufficient amount of alignment was available for microscopy to yield tilt measurements. At 25% and above, insufficient alignment was attainable to facilitate tilt angle evaluation using microscopy. The samples that did not align well were investigated by Chris Noot[17] using the rotating analyser rig. The use of automation and the different optical geometry allows the rotating analyser rig to yield results in samples with only a small degree of alignment (described in §3.4.1.2). At 50% addition, measurements become particularly difficult and hence a larger error is assigned as shown in Figure 6.16.

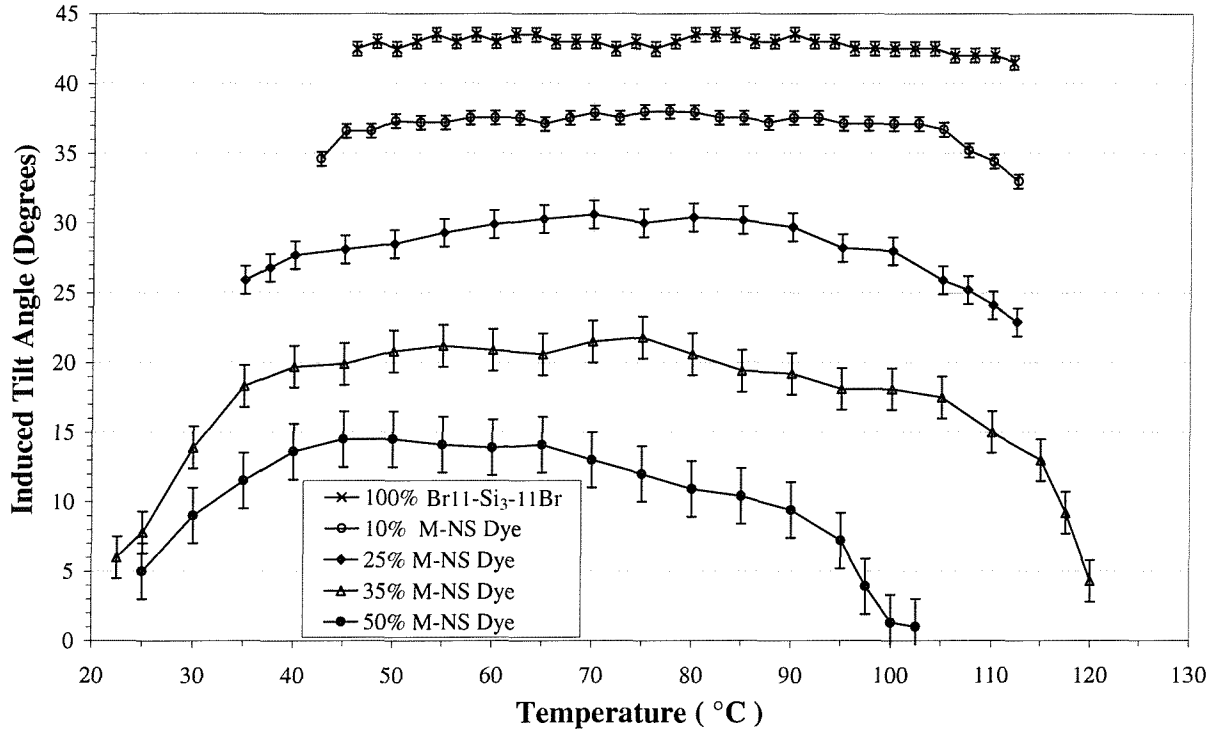

Figure 6.16 Induced optical tilt angle measurements of mixtures of NS11-Si_3 in Br11-Si_3-11Br.

The addition of the dimeric dye to the bi-mesogenic host showed the least alignment of any of the mixtures examined in the nitrostilbene work, with hardly any sustainable good quality alignment possible above 10% of dye addition. However, the use of the rotating analyser rig with many repeated runs and the maximum amount of averaging available, did yield some results. As it can be seen in Figure 6.17, the data for 25% and 40% dye addition show some scatter and also have a high associated error.

The results in Figure 6.16 and Figure 6.17 show that the magnitude of the induced tilt is greatly reduced by the addition of increasing quantities of dye. However, this result is not totally unexpected in light of the results discussed in §5.6.1.1, where the addition of as little as 2% w/w of dye to the antiferroelectric compounds caused a reduction in the director tilt by ~15%. The stability of the antiferroelectric phase appears to be strong, as is evident when considering its greater sustainability

(in comparison with the ferroelectric phase) across the concentration gradient. The tilt angle of the antiferroelectric phase is stable over a wider range of angles; as once again the addition of a dye has greatly reduced the magnitude of measurable tilt angle.

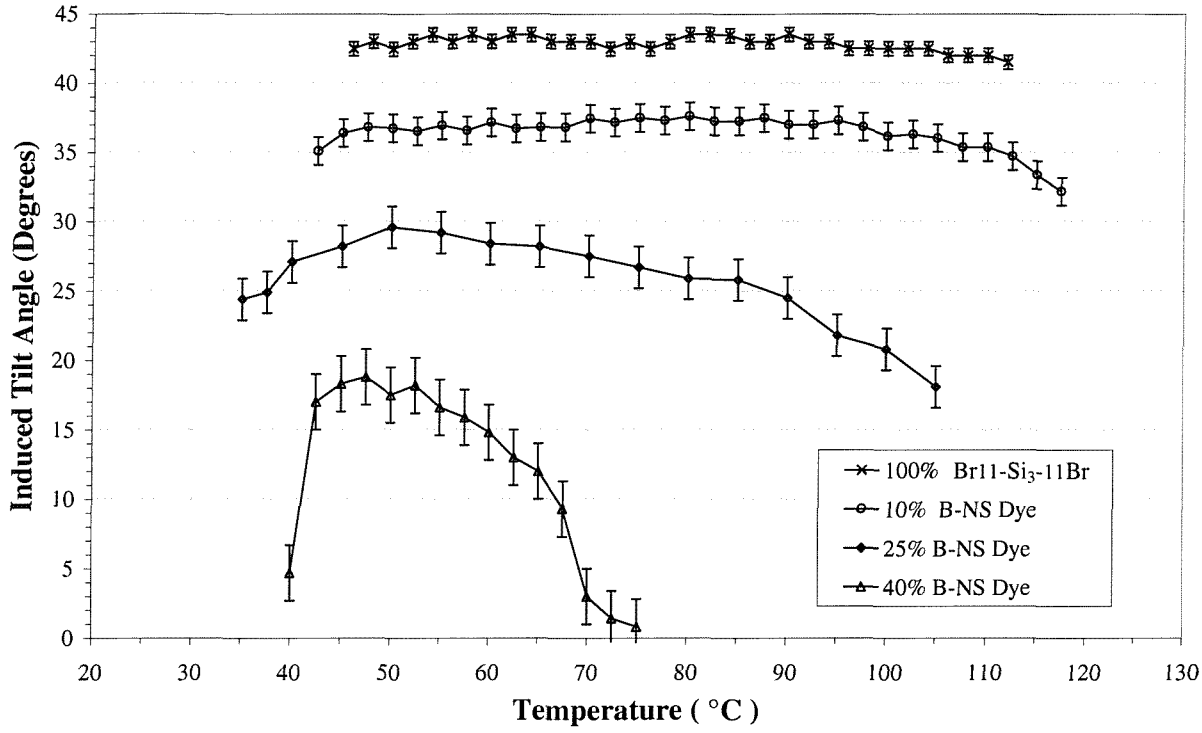

Figure 6.17 Induced optical tilt angle measurements of mixtures of NS11-Si$_3$-11NS in Br11-Si$_3$-11Br.

6.5.2.2 Spontaneous Polarisation

The spontaneous polarisation measurements discussed in this section were all carried out on the antiferroelectric phase. The results quoted are a sum of the spontaneous polarisations obtained by measuring both the driven and relaxed current pulse peaks. Although some automation is possible with 10% addition of either dye, the value of spontaneous polarisation (again by the current pulse technique) is calculated manually in the samples containing larger dye concentrations. Measurements were difficult because the spontaneous polarisation realignment peaks fluctuated greatly in amplitude and position and signal noise caused triggering problems on the oscilloscope.

Once more all the spontaneous polarisation results follow the previous general trends. With up to 10% dye addition, the drop in the magnitude of the spontaneous polarisation is largely due to dilution effects. Mixtures exhibiting an overlying SmA* phase also demonstrate temperature dependent behaviour in their results curves. Although the dilution effects can account for some of the reduction in spontaneous polarisation magnitude displayed in Figure 6.18 and Figure 6.19, for increasing dye concentrations the nature of the antiferroelectric switch is clearly being disrupted. Switching time measurements were made in the 10% mixtures, with some measurements possible in the 25% mixtures. These yielded almost identical switching times to that of the host and are not shown here.

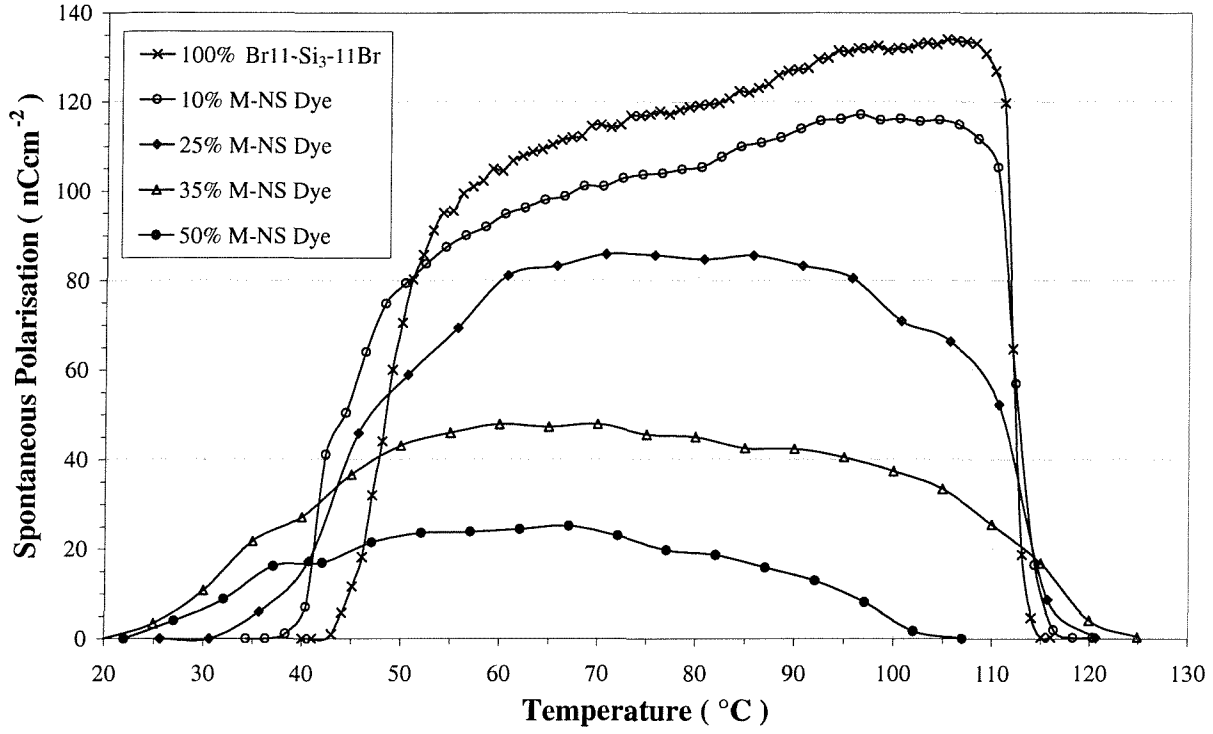

Figure 6.18 Spontaneous polarisation measurements of mixtures of NS11-Si3 in Br11-Si3-11Br.

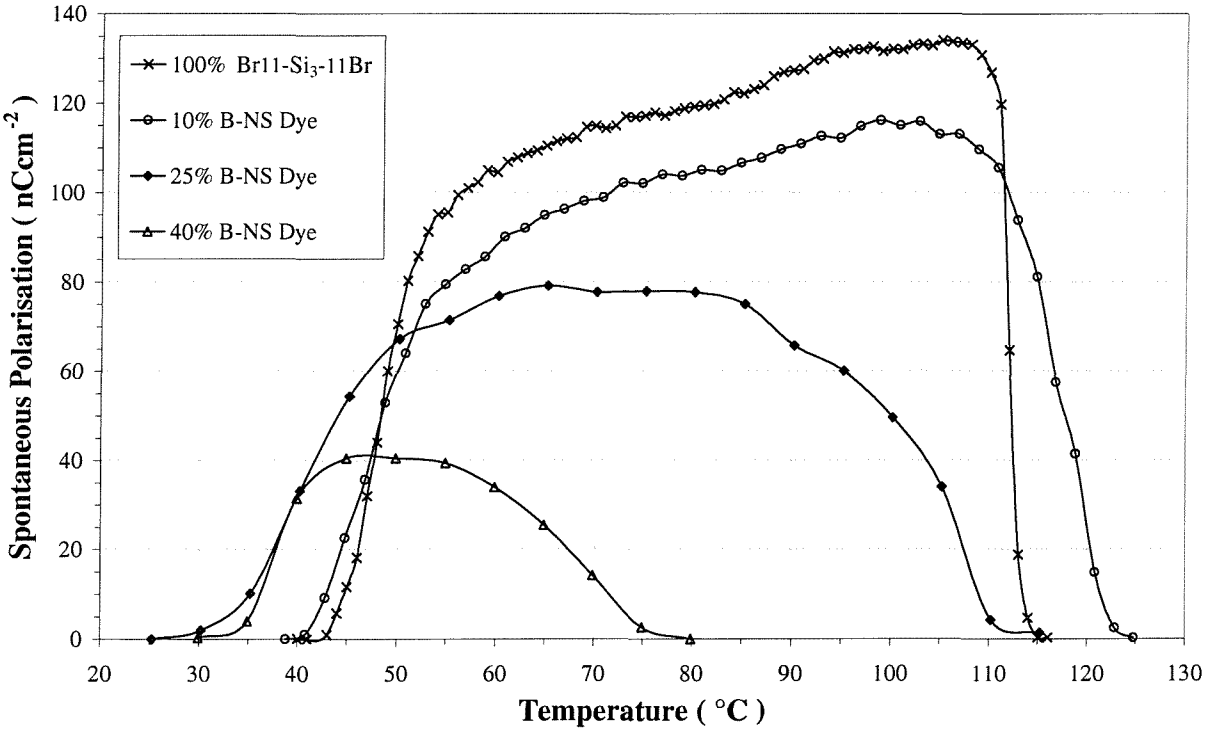

Figure 6.19 Spontaneous polarisation measurements of mixtures of NS11-Si3-11NS in Br11-Si3-11Br.

6.6 SUMMARY

The initial purpose of this chapter was to investigate the effect of organosiloxane dye doping in the biphenyl-benzoate hosts. The use of the nitrostilbene dye with its smectic properties allowed the study of dyed liquid crystal – host interactions.

The addition of the mono-mesogenic dye had the least adverse effect on the host's phase behaviour and electro-optic characteristics, particularly in the mixtures with Br11-Si_3. The results have shown that by simple mixing, the tilt angle and spontaneous polarisation of the host material can be altered. Room temperature ferroelectric phases have been created with broad, often largely temperature invariant properties i.e. spontaneous polarisation and tilt angle. These materials were easily aligned in the SmA* phase which was induced by the addition of the dye and showed electroclinic switching over a 10-20°C temperature range. The addition of the bi-mesogenic dye at particular concentrations yielded antiferroelectric behaviour in a ferroelectric. The fact that this antiferroelectricity was induced by dye possessing only a SmA phase demonstrates the strength of the templating effect.

The results presented in this chapter confirm that the *effective* or *virtual backbone effect* in low molar mass organosiloxane liquid crystals can be used to increase (by up to 100% in some cases) the solubility of a dye guest moiety in a liquid-crystalline host. The grafting of the siloxane group on the guest dye moiety does not affect, in most cases, the functionality of the guest and may induce mesomorphic phases in some non-mesogenic guests. The ferroelectric / antiferroelectric characteristics of the liquid-crystal host can be retained or advantageously controlled by the guest. This opens a new avenue for the design of dichroic, fluorescent or light-emitting materials with switching times in the microsecond range.

6.7 REFERENCES

[1] H.J.Coles, *Faraday Discuss. Chem. Soc.*, **79**, 201 (1985).
[2] H.J.Coles, H.F.Gleeson, G.Scherowsky, A.Schliwa, *Mol. Cryst. Liq. Cryst. Lett.*, **7**(4), 125 (1990); G.Scherowsky, A.Beer, H.J.Coles, *Liq. Cryst.*, **10**(6), 809 (1991).
[3] J.Newton, H.Walton, H.Coles, P.Hodge, *Mol. Cryst. Liq Cryst.*, **260**, 107 (1995).
[4] M.Kašpar, M.Glogarová, V.Hamplová, H.Sverenyák, S.A.Pakhomov, *Ferroelectrics,* **148**, 103 (1993).
[5] S.Perkins, (Personal Communication).
[6] D.Shoosmith, C.Carboni, S.Perkins, S.Meyer, H.J.Coles, *Mol. Cryst. Liq. Cryst.*, **331**, 181 (1999).
[7] J.W.Goodby, *Mol. Cryst. Liq. Cryst. Lett.*, **92**, 171 (1983).
[8] S.Imazeki, A.Mukoh, T.Yoneyama, M.Kaneko, *Mol. Cryst. Liq. Cryst.*, **145**, 79 (1987).
[9] D.E.Shoosmith, A.Remnant, S.P.Perkins, H.J.Coles, *Ferroelectrics,***243**, 75 (2000).
[10] K.Kondo, F.Kobayashi, A.Fukuda, E.Kuze, *Jpn. J. Appl. Phys.*, **20**(10), 1773 (1981).
[11] M. Ibn-Elhaj, H.J.Coles, D.Guillon, A.Skoulios, H.J.Coles, *J. de Phys. II (Paris),* **3**, 1807, (1993);
[12] M. Ibn-Elhaj, A.Skoulios, D.Guillon, J.Newton, P.Hodge, H.J.Coles, *Liq. Cryst.*, **19**(3), 373 (1995); *J. de Phys. II (Paris),* **6**, 271 (1996);
[13] H.J.Coles, I.Butler, K.Raina, J.Newton, *SPIE,* **2408** 14 (1995).
[14] A.M.Biradar, W.Haase, *Liq. Cryst.*, **7**(1), 143 (1990).
[15] J.Budai, R.Pindak, S.C.Davey, J.W.Goodby, *J. de Phys. Lett. (Paris)* **45**, L1053 (1984).
[16] Currently under study by D.Guillon, IPCMS, 23 Rue du Loess, F-67037, Strasbourg, France.
[17] C.Noot, Ph.D. thesis (in preparation), Univ. Southampton, U.K., (2002).
[18] S.Sarala, A.Roy, N.V.Madhusudana, H.T.Nguyen, C.Destrade, P.Cluzeau, *Mol. Cryst. Liq. Cryst.*, **261**, 1 (1995).
[19] C.Carboni, H.J.Coles, *Mol. Cryst. Liq. Cryst.*, **328**, 349 (1999).

Chapter Seven

Conclusions

One never notices what has been done;
one can only see what remains to be done ...

Marie Curie 1867-1934

7.1 INTRODUCTION

The purpose of this chapter is twofold; firstly to outline some of the preliminary work that has come about as a direct result of the work undertaken in this thesis; and secondly to summarise the important results and discoveries discussed in the previous chapters.

7.2 PRELIMINARY WORK

This section outlines some of the work carried out at the end of the research project, that is continuing within the Southampton Liquid Crystal Group. The first part looks at the effects of fluorination. One of the main drawbacks of the organosiloxanes used throughout this work is the high temperature of their ferroelectric phases. It was hoped that fluorination of parts of the organosiloxane molecules may shift the phase ranges towards room temperature. To further develop the ferroelectric dye guest host device, the possibility of using fluorescent dyes is being investigated. Using the nitrostilbene model, a perylene dye has been grafted onto the siloxane core. Ultraviolet light is also used to sterically control optically active dyes via the photomechanical effect. Building once again on the success of the nitrostilbene work, azo dyes are grafted to siloxanes to allow complete miscibility with the host organosiloxanes.

7.2.1 Fluorination

In the hope of further improving the characteristics of the organosiloxane series, the effects of end chain fluorination were investigated by P.Lehmann and W.K.Robinson. The organosiloxanes in this work have three main features; a polar siloxane spacer, a rigid highly polarisable aromatic group, and flexible, apolar, alkyl end chains. The chemical incompatibility of the constituent units causes the segregation of the three moieties into sub-layers resulting in the formation of smectic phases. It was thought that the fluorination of these end chains would lead to even stronger phase separation. Indeed, the results of the work show that the fluorination strongly affected the mesophase behaviour[1]. An extensive electro-optic study of some of the bi-mesogenic fluorinated end chain materials by W.K.Robinson[2] revealed very high spontaneous polarisations (200-450 $nCcm^{-2}$) and a ~38° tilt angle. In general it was found that fluorination increased both the spontaneous polarisation, and the number of phases observed, by introducing a number of hexatic phases.

It was hoped to continue the end chain fluorination work in this thesis. In order to conduct a systematic study of the effects of fluorination, the amount of fluorine was systematically varied. Trial batches were studied, and the observations revealed that although the spontaneous polarisation was

still high (~300 $nCcm^{-2}$), the magnitude of the tilt angle was severely reduced in the fluorinated materials. The ferroelectric and antiferroelectric phases were narrow (~20°C) and only present in excess of 100°C. In most cases the ferroelectric and antiferroelectric phases were monotropic and higher ordered smectic phases were also observed. The synthesis of end chain fluorinated products was abandoned and synthetic efforts moved towards fluorination of the aromatic biphenyl core.

7.2.1.1 Full Fluorination of the Biphenyl Core

It is well known that lateral fluorination in the aromatic core of liquid crystalline materials dramatically reduces phase transition temperatures[3]. Therefore, in an attempt to reduce the transition temperatures of the organosiloxane mesogens, the fluorinated analogues were prepared with the fluorine present in the biphenyl moiety[4]. The work focuses on the mono-mesogenic compound Cl_{11}-Si_3. In the first iteration, the biphenyl unit was fully fluorinated. The resultant compound is denoted $Cl_{11}(F_8)$-Si_3 and the structure is shown schematically in Figure 7.1.

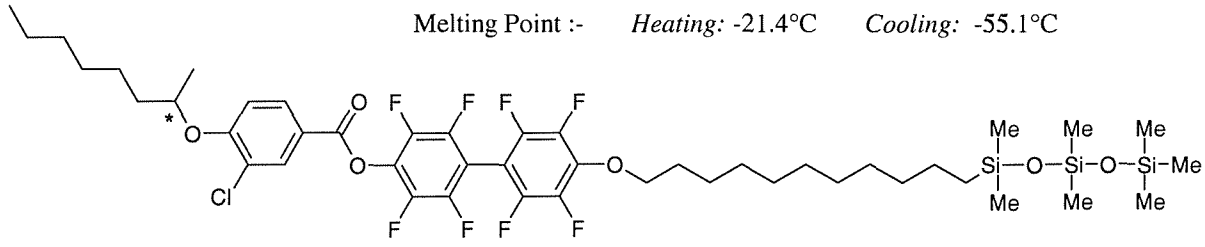

Figure 7.1 A schematic of the fully fluorinated biphenyl compound $Cl_{11}(F_8)$-Si_3.

The compound was characterised using a combination of differential scanning calorimetry and optical microscopy. No liquid crystal behaviour was observed, the compound undergoes a single transition from isotropic to crystal/glass with some supercooling. Although non-mesogenic, the melting point is substantially reduced when compared to the non-fluorinated analogue. Given the miscibility exhibited by the compounds of a similar structure, for example those described in the nitrostilbene chapter, and the concomitant reduction in transition temperatures the obvious next step was to create mixtures between the fluorinated and unfluorinated analogues.

The phase diagram obtained on cooling the mixtures is shown in Figure 7.2. As can be seen for mixtures containing up to ~50% of $Cl_{11}(F_8)$-Si_3, the freezing point remains almost constant. However, there is a steady reduction in the I→SmC* transition temperature, and thus a reduction in the mesophase range as the proportion of fluorinated analogue is increased. Biphasic behaviour is observed throughout the SmC* phase. For mixtures containing greater than 55% of the fluorinated compound the mesophase is completely extinguished. The DSC traces reveal some evidence of an intermediate crystal phase in the 45% - 75% mixtures which exists down to the freezing point of pure $Cl_{11}(F_8)$-Si_3 at approximately -55°C.

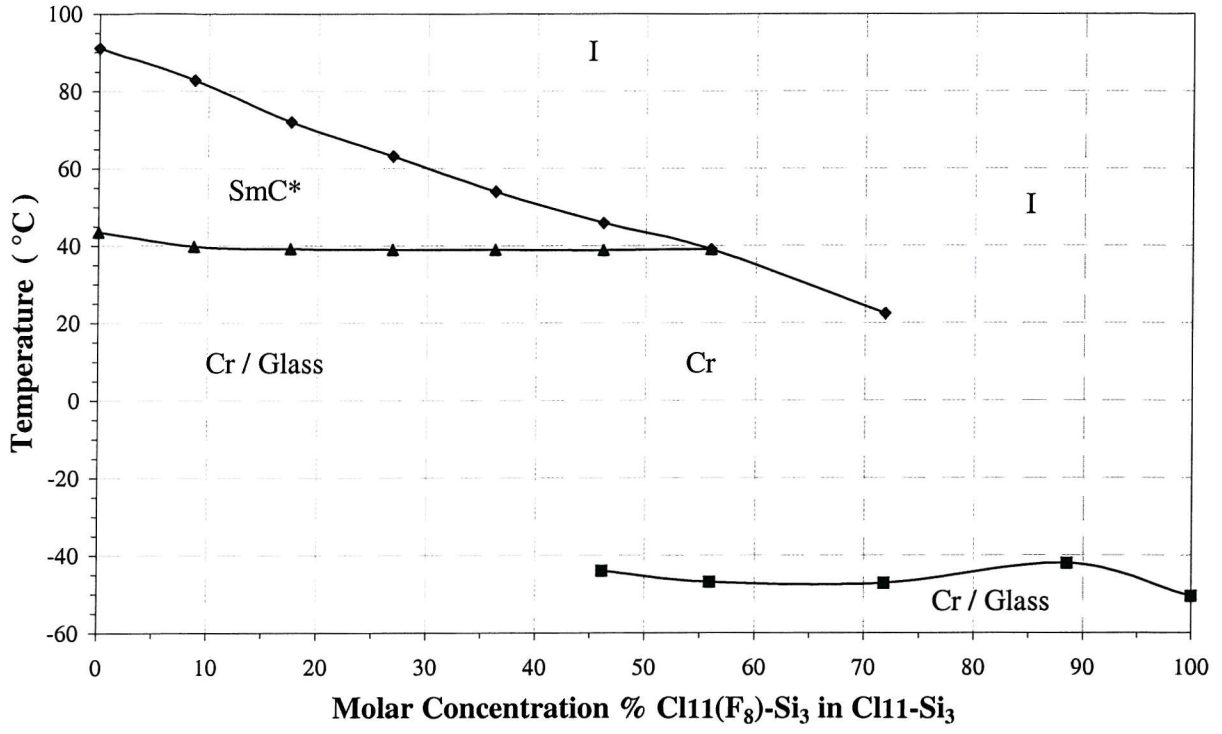

Figure 7.2 Phase diagram of molar concentration of mixtures of $Cl11(F_8)$-Si_3 in $Cl11$-Si_3.

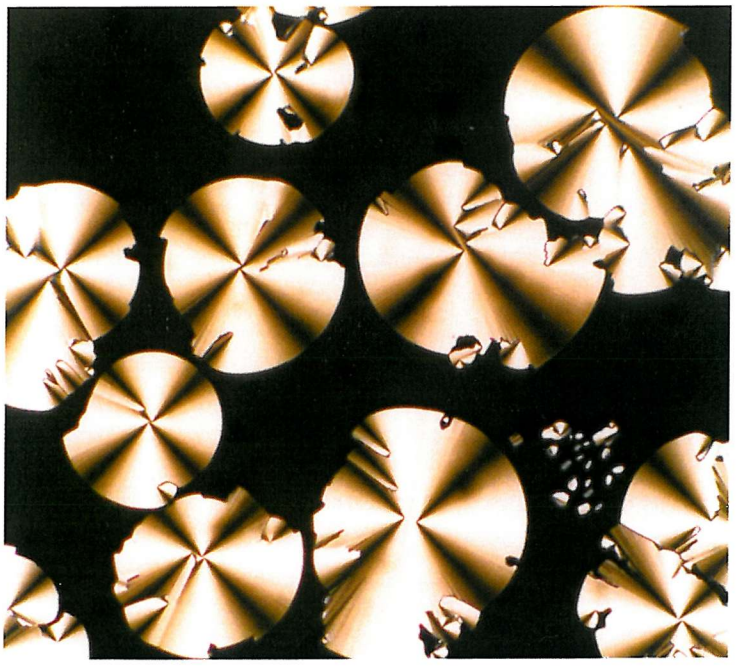

Figure 7.3 Crossed polariser photomicrograph of the texture in the mixture of 20% $Cl11(F_8)$-Si_3 in $Cl11$-Si_3. Taken at 100x magnification, at 75°C, with a field of 10 $V\mu m^{-1}$ in a 3.2 μm Lucid cell.

The gradual reduction in the I→SmC* transition temperature observed in Figure 7.2 demonstrates that the two components are miscible, as it would be expected that this transition would not change if the two components did not mix. However, Figure 7.3 shows the texture observed for the 20% mixture in which there is distinctly biphasic behaviour, with possible phase separation. This evidence suggests that the phase possesses a micellar structure with the siloxane units separating the fluorinated and non-fluorinated mesogenic units[4].

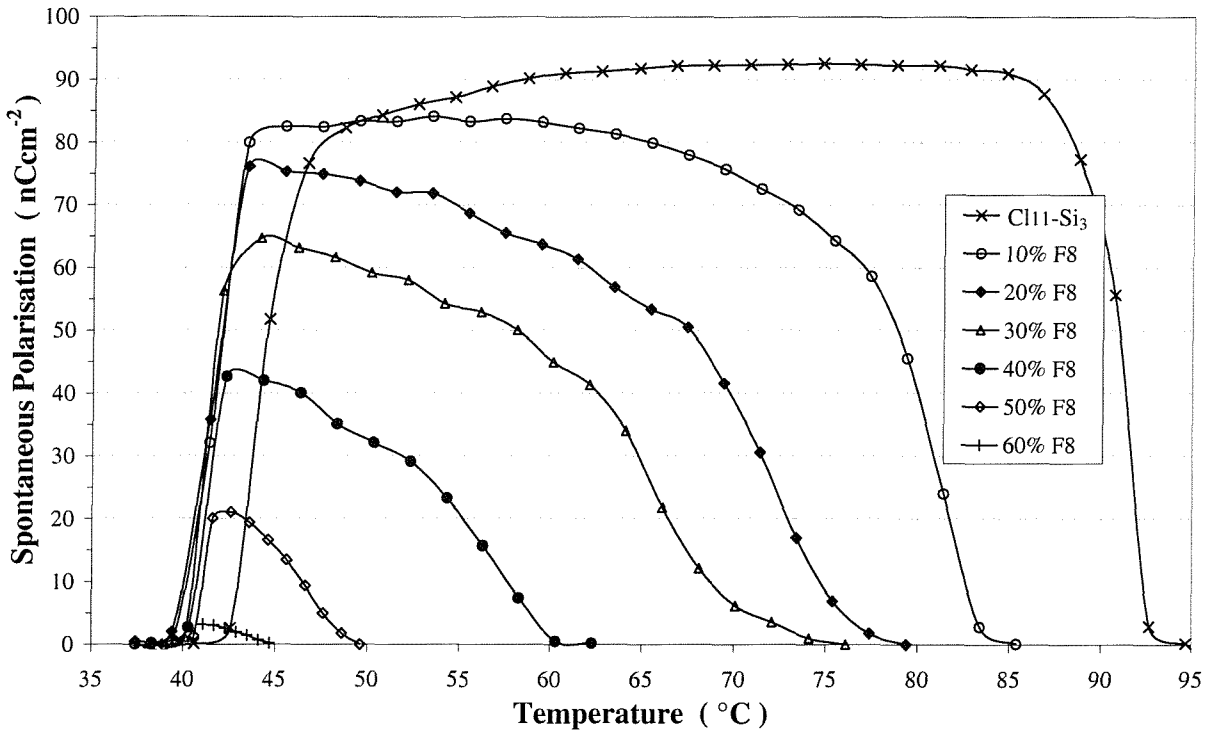

Figure 7.4 Spontaneous polarisation measurements of mixtures of Cl11(F_8)-Si_3 in Cl11-Si_3.

The measurement of spontaneous polarisation for the different mixtures is shown in Figure 7.4. The fully fluorinated organosiloxane does not appear to contribute towards the spontaneous polarisation which scales directly with the reduction of the amount of Cl11-Si_3.

7.2.1.2 Partial Fluorination of the Biphenyl Core

Although the fully fluorinated compound was not liquid crystalline, the large reduction it induced in the freezing temperature of the unfluorinated material was promising. Unfortunately, the mixtures of the fluorinated Cl11(F_8)-Si_3 with the non-fluorinated Cl11-Si_3 failed to promote a room temperature ferroelectric phase. The next step was to weaken the effect of the fluorination by separately fluorinating each of the rings in turn[5]. The two compounds synthesised are shown in Figure 7.5, each has one of the phenyl rings fluorinated to give compounds denoted ester and ether.

The Cl11(F_4ester)-Si_3 and Cl11(F_4ether)-Si_3 compounds are studied with differential calorimetry and optical microscopy. Once again no liquid crystal phases are seen. Although supercooling is still observed, the melting and freezing points are higher than the fully fluorinated biphenyl Cl11(F_8)-Si_3 compound. Reducing the amount of fluorination has weakened the effect of temperature suppression and it was hoped that this would prove more useful in mixtures.

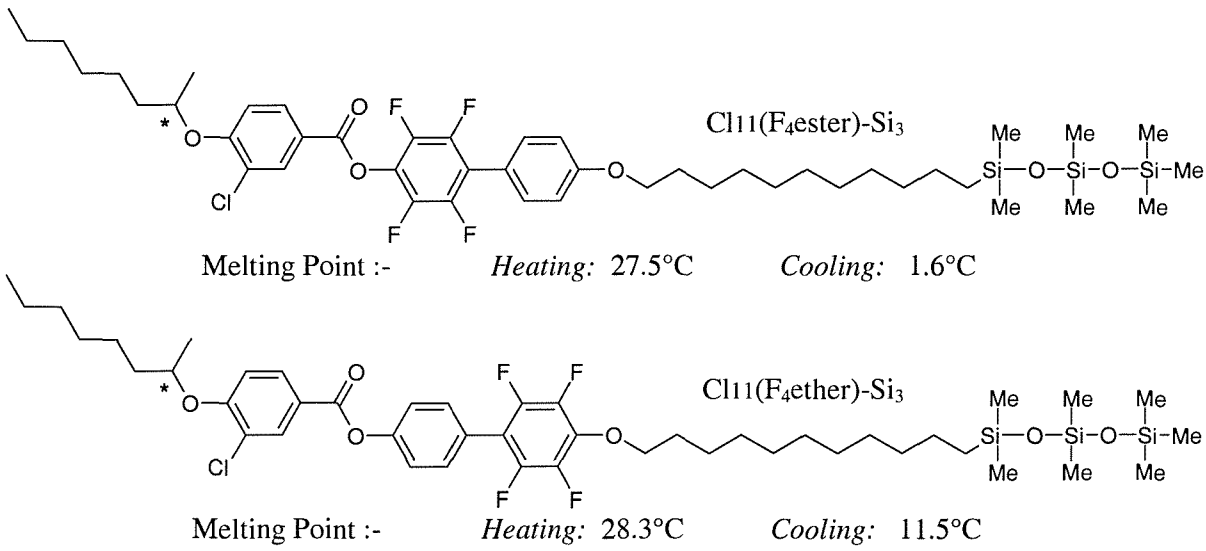

Figure 7.5 A schematic of the partially fluorinated compounds Cl11(F4 ester)-Si3 and Cl11(F4 ether)-Si3.

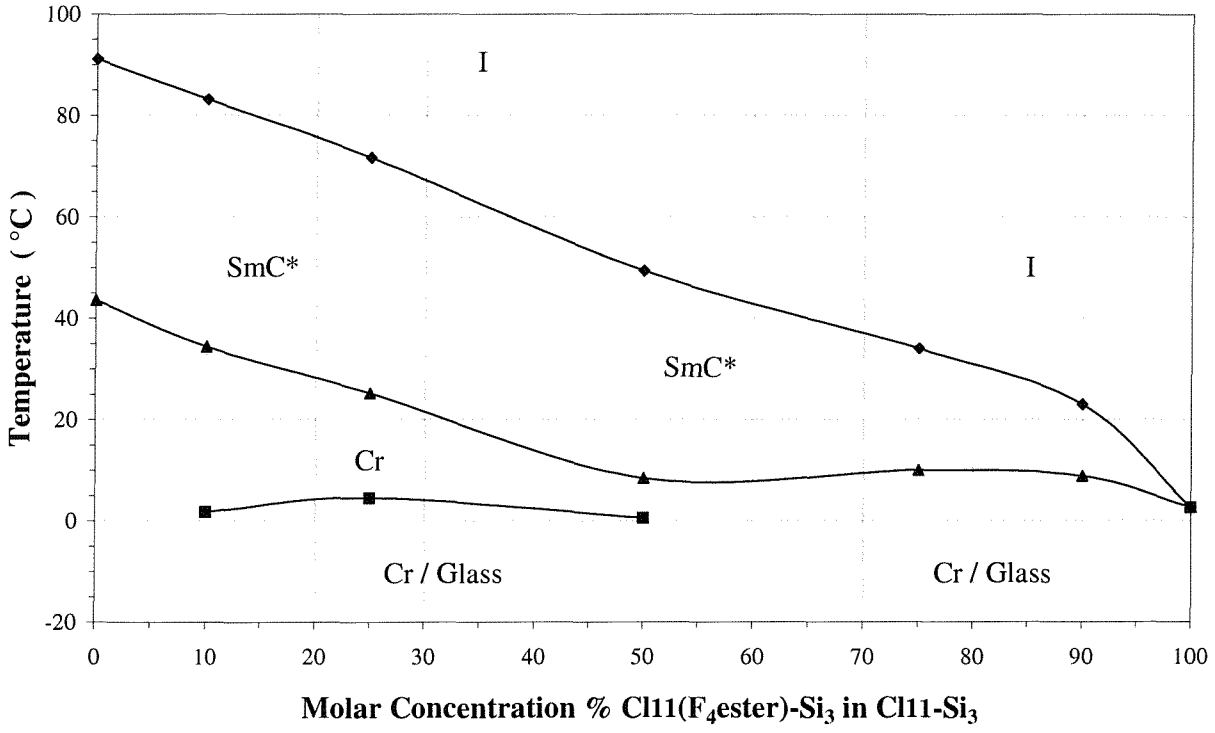

Figure 7.6 Phase diagram of molar concentration of mixtures of Cl11(F4 ester)-Si3 in Cl11-Si3.

The resultant phase diagram obtained on cooling mixtures between Cl11(F4ester)-Si3 and Cl11-Si3 is shown in Figure 7.6. As can be seen, the fluorinated material is completely miscible in the non-fluorinated host, with the I→SmC* transition temperature steadily decreasing as the amount of Cl11(F4ester)-Si3 is increased, until (for the pure fluorinated material) the mesophase is completely extinguished. However, unlike the fully fluorinated mixtures examined previously, the melting point

does not remain constant. An intermediate crystal phase is observed in the 10% - 50% mixtures. Although a small amount of biphasic nature is present in the SmC* phase of all the mixtures, the reduction of the liquid crystal transition temperatures has resulted in a room temperature SmC* phase.

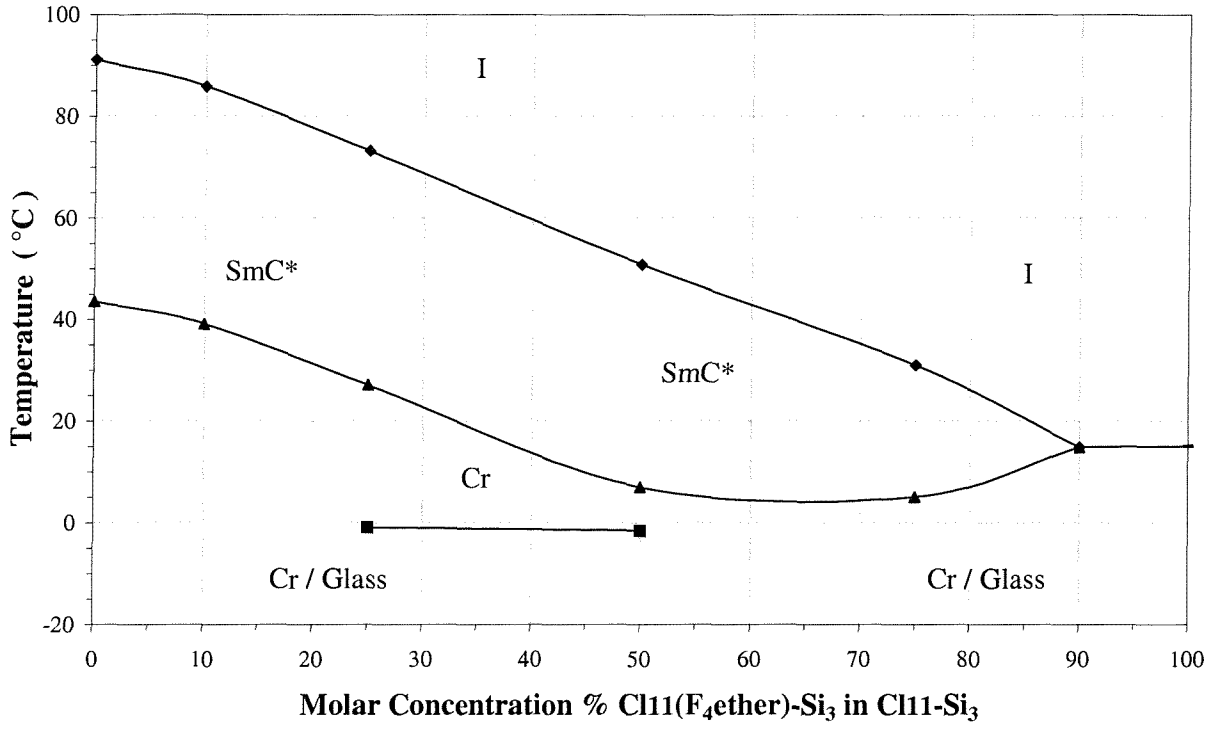

Figure 7.7 Phase diagram of molar concentration of mixtures of Cl11(F4ether)-Si3 in Cl11-Si3.

The final sequence of mixtures, Cl11(F_4ether)-Si_3 in Cl11-Si_3, yields the cooling phase diagram in Figure 7.7. The general phase trends are very similar to those of the mixtures between Cl11(F_4ester)-Si_3 and Cl11-Si_3. Once again the two components are fully miscible and the I→SmC* transition temperature steadily decreases until the liquid crystalline mesophase vanishes with around 90% M/M addition of Cl11(F_4ether)-Si_3.

The results of spontaneous polarisation measurements on the mixtures of Cl11(F_4ester)-Si_3 in Cl11-Si_3 are shown in Figure 7.8. The results are very different from those seen with the fully fluorinated Cl11(F_8)-Si_3 mixtures shown in Figure 7.4. The spontaneous polarisation of the unfluorinated compound does not appear to be diluted by the addition of the fluorinated material. The magnitude of the spontaneous polarisation remains above 90 $nCcm^{-2}$ in the mixtures containing up to 50% of the fluorinated compound and retains much of the temperature independence of the Cl11-Si_3 host. With increased fluorinated material addition some second order behaviour is seen, resulting in the reduction of the magnitude of the P_s exhibited by the 75% mix. The intermediate crystal phase observed in the 10% - 50% mixtures can yield a small amount of spontaneous polarisation although no optical switching is observed. The magnitude of the polarisation measured is highly dependent on the cooling speed; the measurements in Figure 7.8 were made at 0.2°$Cmin^{-1}$ where the largest P_s observed in this intermediate crystal phase is ~3 $nCcm^{-2}$. At a cooling rate of 1°$Cmin^{-1}$ the magnitude of the

spontaneous polarisation rises to ~15 $nCcm^{-2}$. Conversely at a cooling rate of 0.1°$Cmin^{-1}$ no spontaneous polarisation is observed. This behaviour is repeated in the mixtures of $Cl11(F_4ether)$-Si_3 in $Cl11$-Si_3, where the spontaneous polarisation curves are almost identical in shape and magnitude.

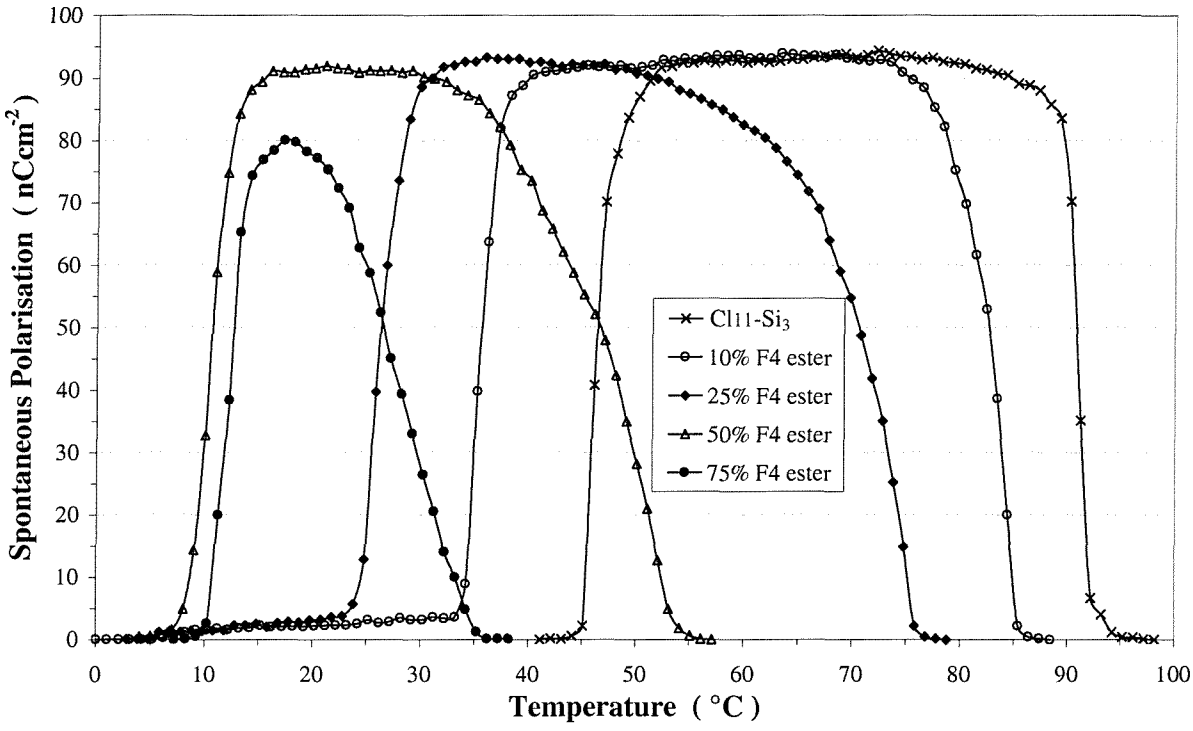

Figure 7.8 Spontaneous polarisation measurements of mixtures of $Cl11(F_4$ ester$)$-Si_3 in $Cl11$-Si_3.

The lack of mesogenicity in the three pure fluorinated compounds is disappointing. The compound $Cl11(F_8)$-Si_3 with its fully fluorinated biphenyl core did not yield promising mixtures as the SmC* phase of the unfluorinated host was suppressed along with its spontaneous polarisation. However, partially fluorinating the biphenyl core shows more potential. The SmC* phase of the host is maintained with up to 75% M/M addition of the partly fluorinated compounds and the phase range is shifted into the room temperature range. The spontaneous polarisation of the host does not appear to be reduced in mixtures with the partly fluorinated materials. Although neither the ester or the ether exhibit any liquid crystal behaviour, when mixed with the liquid crystalline host they appear to be able to respond ferroelectrically.

These initial results of the use of fluorination look promising. It is hoped that progress will be made, with future work concentrating on reducing the amount of ring fluorination. Although it is thought that this may be difficult from a synthetic viewpoint, the results thus far demonstrate the ability of ring fluorination to reduce the transition temperature of the organosiloxanes. By reducing the amount of fluorination further, it may be possible to synthesise room temperature ferroelectric and antiferroelectric organosiloxanes.

7.2.2 Fluorescent Dye Guest Host

Early fluorescent dye guest host work with nematic hosts was not greatly successful, mainly due to a lack of solubility of the dyes in the nematic hosts[6]. The use of fluorescence in ferroelectric dye guest host devices has been investigated previously[6], however, the creation of the 45° organosiloxanes has renewed interest in this field. Fluorescent dyes offer several advantages over normal dichroic dyes; up to 180° viewing angle, greater brightness, and a higher perceived contrast[7]. Because a fluorescent dye absorbs ultraviolet light and re-emits the light at a visible wavelength, the dye can appear bright at all angles.

A device with a fluorescent rather than dichroic dye can operate in several modes. The modes described here are based on the dichroic dye modes described in the dye guest host chapter (§5.2.6). Instead of illuminating the sample with polarised white light, polarised UV light is used. If the anisotropic fluorophores align with the host, they can be switched between a passive state and an active state where they absorb the polarised UV light and emit their characteristic colour. Thus an observer will see a switch from dark to the dyes emission colour. However, this method of operation requires the use of a UV polariser which can be expensive and inefficient. An alternative mode utilises the properties of polarised fluorescence[8]. When the fluorophores are illuminated with unpolarised UV light they will absorb the UV light and emit polarised visible light. The polarisation of the emitted light is dependent on the amount of freedom the fluorophore has; if it is free to rotate, the emitted light is depolarised, but if the fluorophore is well constrained, the system can produce a good contrast[6]. In this mode the polarised visible light emitted by the excited fluorophores is then incident on a visible light polariser. As the host is switched, the polarisation of the light emitted by the fluorophore is also switched and the polariser controls the amount of light transmitted by the device.

The success of the nitrostilbene work has led to the concept of grafting dye molecules to the organosiloxane core discussed in the previous chapter, being applied to fluorescent dyes. The nitrostilbene dye failed to show any significant fluorescence. The investigation has now turned to the perylene family of dyes. Some of the best exhibitors of strong fluorescence are the rigid aromatic systems. These qualities make perylene, a fused aromatic system an ideal choice as a fluorescent dye, but one major drawback with such large molecules is a lack of solubility (which tends to decrease with increasing molecular size[9]). In fact it has been found that a perylene dye is only soluble up to ~3% in our mono-mesogenic organosiloxanes[10]. In order to improve solubility a perylene dye unit has been grafted via an eleven unit alkyl chain onto the three unit siloxane core. Early results have shown that the resulting organosiloxane perylene dye may be highly soluble in the mesogenic Br11-Si_3 host[10]. A 20% M/M addition lowers the host transition temperatures by around 10°C whilst maintaining the SmC* phase range, as was found with the nitrostilbenes. Initial results look promising and this work is ongoing[11].

7.2.3 Cis-Trans Isomerising Dyes in Guest Host Work

A further line of investigation worth mentioning is the use of cis-trans isomerisation in dyes. The behaviour of such dyes has been investigated concurrently with the nitrostilbene work and takes advantage of the photomechanical effect. As discussed in the dye guest host chapter, a great deal of work has been done within the group on cis-trans isometric azobenzene dyes. With the addition of 5% w/w of an azo dye in a commercial smectic host, illumination with ultra-violet light causes a marked reduction in the spontaneous polarisation of the host[12]. The added disruption due to the bent conformation of the cis form of the azo dye can also reduce phase transition temperatures. These effects can be fully reversible upon removal of the UV (360nm) illumination[12]. The early success of the nitrostilbene work created the impetus to study the effect of grafting an azo group to the siloxane core and alkyl chain. The mixing of the monomeric and dimeric azo dyes with the mono-mesogen Br11-Si_3 yielded similar phase and electro-optic results[13] to those observed with the nitrostilbenes in this work. Antiferroelectricity was also induced in the Br11-Si_3 host by the dimeric azo dye as was observed when the dimeric nitrostilbene dye was added to the mono-mesogenic host. The azo dye has a slightly weaker effect on phase behaviour that the nitrostilbene dye and the SmC* and SmC^*_A phases are slightly more extended across the concentration range. Now that the azo dye has shown the same miscibility and potential as the nitrostilbenes, the effects of UV illumination and the possibilities of controlling the electro-optic parameters through the photomechanical effect are being assessed[14].

7.3 OVERVIEW

The following section contains an overview of the work presented in this thesis and the important results arising from it.

7.3.1 Introduction, Theory and Experimental Setup

In the first chapter, the contents of this thesis were set in the wider field of liquid crystals. The history and many other branches of the field were briefly discussed and the main phases of the liquid crystal family introduced. The nematic order parameter was established, leading to a derivation of the Landau – de Gennes theory of phase transitions. This overview established a basis for an in-depth discussion of the ideas used in this work. In the theory chapter it was shown that any chiral tilted phase can be ferroelectric. The helical nature of the ferroelectric SmC* phase can be unwound and utilised in a surface stabilised geometry. Equations are derived to allow the measurement of several physical parameters for the Goldstone mode (tilt angle, spontaneous polarisation, rotational viscosity and switching time) with an idea of their temperature dependence.

The setup chapter described the many components that make up the experimental apparatus. The backbone of liquid crystal analysis in this thesis was the test cell. Pre-fabricated and home-made cells were examined alongside the methods used to fill the cells and align the liquid crystal samples. The methods of sample analysis used throughout the results chapters were discussed in detail. Techniques used to measure tilt angle, spontaneous polarisation, switching time and rotational viscosity of switching liquid crystal phases were introduced. The first results from the apparatus were shown using the standard ferroelectric compound SCE13. This analysis served as a demonstration of the methods and also as a calibration and test of new techniques. Finally the topic of phase characterisation was covered. The differences between the liquid crystal phases encountered in this work were discussed in the context of optical polarising microscopy observations.

7.3.2 Organosiloxanes

In the first of the results chapters the organosiloxane materials used as host materials throughout the thesis were investigated. The mesogenic building block of the low molar mass materials was the laterally substituted biphenyl benzoate. The low molar mass organosiloxane compounds are the result of many years of synthetic development work within the group. The compounds used in this thesis consisted of a laterally halogen substituted biphenyl benzoate moiety joined to an organosiloxane core by an eleven length alkyl chain. These compounds were designed to exhibit the rugged nature of a polymer while retaining the wide phase range properties of the precursor. In the first results chapter, the experimental observations that led to the development of the current compounds was explained.

In the first part of the organosiloxane chapter the precursor mesogens are investigated. The biphenyl benzoate precursor was selected because of its tendency to form wide, temperature independent, high tilt angle SmC* phases. This tendency was confirmed with an investigation of the tilt angle, showing results of 20° to 45° for the three different lateral substitutions of bromine, chlorine and fluorine. The tilt angles were almost constant over the entire measurable SmC* liquid crystal temperature range of the compounds. The spontaneous polarisation ranged from around 70 $nCcm^{-2}$ to 130 $nCcm^{-2}$ with the magnitude of the spontaneous polarisation following the electronegativity of the laterally substituted halogen. In all cases the alignment was poor, yielding sandy textures.

When a single biphenyl benzoate is joined to the siloxane group, low molar mass mono-mesogenic compounds were formed. The increased ruggedness and polymer tendency to form layers resulted in the exclusive promotion of the SmC* phase as the only liquid crystal phase. The SmC* phase was around 50°C wide for all three halogens. Although it was not easy, alignment was now possible with lengthy field processing. The new layer geometry and steric forces imposed by the siloxane group resulted in 40-45° tilt angles for all three compounds. The addition of the siloxane group reduced the magnitude of the spontaneous polarisation by around 25%, and this corresponded to the reduction in the number of dipoles per unit volume. Measurements of switching time revealed the typical exponential behaviour with switching times increasing as the temperature was reduced for all three compounds. Switching times were sub-millisecond at temperatures as low as 40°C below the I→SmC* transition. A study of the rotational viscosity allowed an assessment of the activation energy of the ferroelectric switch. This study showed that the activation energy required for the switch increased in line with the size of the lateral substituent. Small anomalies were seen in the DSC traces of the three compounds which corresponded with a change in shape of the switching time plots and small changes in spontaneous polarisation. However, no textural change was observed and the electro-optic responses were smooth and continuous. The effect is attributed to a conformational change similar to that often seen with polymer backbone rearrangements[15].

Grafting a biphenyl benzoate mesogen to each end of a siloxane core formed the series of bi-mesogenic organosiloxane materials. These compounds exclusively exhibited a SmC* antiferroelectric phase. The antiferroelectric nature of the phase was confirmed by examination of the electro-optic responses, which show twin spontaneous polarisation realignment peaks and typical antiferroelectric hysteresis figures. The increased stability of the antiferroelectric phase resulted in a 60°C wide phase range. However, the lack of an overlying, less ordered phase made aligning the antiferroelectric phase very difficult. The near 45° tilt angle seen in the mono-mesogens was retained with only around 2° variation over the entire phase range. The spontaneous polarisation of the bi-mesogenic compounds was higher than that seen with the mono-mesogens. $Cl11\text{-}Si_3$ has P_s values ~95 $nCcm^{-2}$ over most of its phase range in comparison with ~130 $nCcm^{-2}$ for $Cl11\text{-}Si_3\text{-}11Cl$ at 10°C below the I→SmC^*_A transition. The spontaneous polarisation of the bi-mesogens was more

temperature dependent, and fell to ~100 $nCcm^{-2}$ at -55°C of shifted temperature. The bi-siloxane switching times were similar to those of the mono-siloxanes and this was attributed to the similar nature of the switch. A switching mechanism was hypothesised with the siloxane unit remaining fairly stationary and the biphenyl benzoate unit undergoing a Goldstone mode switch. The alternating structure of the antiferroelectric phase means that only half of the molecule is reoriented by changing the direction of the applied field and thus the actual switch mechanism is similar to that of the mono-mesogenic compounds. The viscosity measurements once again yielded a trend in activation energy that followed the atomic size of the lateral substituent. The idea of a bent molecular conformation is the result of work with varying siloxane core lengths and chemical modelling[16,17]. The concept of an in-built antiferroelectric nature, which was examined in the work of P. Kloess[17], fits the results seen in the antiferroelectric compounds throughout this work.

7.3.3 Dye Guest Host

The dye guest host chapter focused on the potential of dyes to replace the conventional polarisers and filters of a traditional twisted nematic display. The work was placed in the context of the established field of dye guest host using nematic materials as the host media, and the basic concepts behind these devices explained. The properties of anisotropic light absorption essential for a DGH dye were discussed, in terms of absorbance and contrast ratio. The many properties of a suitable dye were outlined, such as chemical stability, high solubility and dichroic ratio. Previous nematic dye guest host devices were described along with some of the problems that halted the development of a widely commercial device. This led to the development of a ferroelectric DGH device based on the operation of the surface stabilised mode discussed in the organosiloxane chapter. The mode used in this work requires a ferroelectric compound with a 45° tilt angle, and has only been possible very recently with the development of the organosiloxane compounds investigated here.

The synthesis of 45° tilt compounds has opened up the possibility of new avenues of research. In order to test the possibility of a single polariser dye guest host ferroelectric device, three dye types were tested. The dyes were typical commercial dyes from the anthraquinone and azo family chosen because of their previous success in DGH nematic work. The most extensive work was carried out with Cl_{11}-Si_3 as the host material. The addition of the dyes at 4% weight/weight concentration lowered the I→SmC* transition by up to 2.5°C and the SmC*→Crystal transition by up to 6°C. The alignment process was very successful, yielding mono-domain samples. The addition of the dyes had a small enhancement effect on the magnitude of the optical tilt angle (to a maximum of 1.5°) which was attributed to the interaction of the dye with the siloxane virtual backbone effect. The importance of layer spacing and ordering in these smectic compounds was seen with the addition of the siloxane unit to the biphenyl benzoate precursor in the organosiloxane chapter, causing an enhancement of the tilt angle from 37° to 42°. All three dyes reduced the magnitude of the spontaneous polarisation over the entire smectic range; the spontaneous polarisation scaled for each mixture in line with the

molecular mass of the dye. This is explained by considering the non-ferroelectric nature of the dyes which therefore do not contribute towards the spontaneous polarisation of the mixture and reduce the number of dipoles per unit volume. The addition of the dye caused a small increase in the switching times. This was not unexpected given a slightly increased tilt angle and reduced spontaneous polarisation.

An examination of the contrast ratios of the three dye mixtures with Cl11-Si_3 showed the effect of increasing the amount of dye addition on the light and dark states. In general, as the concentration of dye was increased, the contrast ratio increased: the dark state was enhanced, up to a point when further addition caused the light state to deteriorate and at this point the contrast ratio levelled off. The point at which further dye addition no longer enhanced the contrast level was around 4% w/w for the M777 and ICI black mixes. Thus the 4% w/w level chosen for study represented near optimal conditions for these dyes, with some potential for improvement with D102. Mixtures were also made with Br11-Si_3 and F11-Si_3 as host media. The results showed the same trends as the Cl11-Si_3 mixtures. With Br11-Si_3 as the host, although the tilt angle was unchanged at 44.5°, the addition of the dyes reduced the transition temperatures and spontaneous polarisation and increased the switching times, as was observed with the Cl11-Si_3 host. Alignment was harder to achieve and both ends of the smectic range exhibited a small amount of biphasic behaviour. The use of F11-Si_3 as the host yielded biphasic regions ranging from 3° wide with the M777 mixture, to 10° wide with the ICI mixture. These biphasic regions spread the DSC peaks, decreasing the accuracy of the measurement of onset temperatures and the electro-optic readings. The measurement of the F11-Si_3 mixes was hampered by the poorest alignment of all the mono-mesogenic mixtures and signal degradation in the electro-optic readings. However, once again the F11-Si_3 mixes followed the same general trends seen in the Cl11-Si_3 mixtures of lower transition temperatures, diluted spontaneous polarisation and slightly increased switching time.

With all three hosts the tilt angle was maintained across most of the smectic range. The small reduction in spontaneous polarisation caused by the dilution effect of the dye will not significantly affect a display application. Although dye addition has increased the switching time from that of the pure host, the mixtures were still capable of switching times in the 100 μs regime. The cells used in this work have been stored in the laboratory at room temperature and in a range of lighting conditions from darkness to ambient. On examining the electro-optic cells a few years on, the M777 mauve-dyed mixtures have generally faded slightly but still retain their alignment. The blue colour of the D102 mixtures faded to yellow and the ICI black dye mixtures have separated out from the host medium.

Having observed favourable results with the addition of the three dyes to the ferroelectric mono-mesogenic organosiloxanes, it was a natural progression to examine the dye guest host effect in the antiferroelectric bi-mesogenic organosiloxanes. Using Cl11-Si_3-11Cl as the host it was found that the

M777 and ICI dyes' solubilities were halved to 2% w/w. Although the only liquid crystal phase observed was the SmC^*_A phase, the phase range was greatly reduced with up to 10°C wide biphasic regions at each of the transitions. The alignment quality was generally poor and the electro-optic signals were noisy, hampering measurement. The 41.5° induced tilt angle of the host was reduced by between 4°-7° by the addition of any of the three dyes. When compared to the slight enhancement in tilt angle seen with the ferroelectric dye mixtures, it was clear that the antiferroelectric structure did not accommodate the dye as favourably. The addition of the dyes reduced the spontaneous polarisation by around 20% from the 115 $nCcm^{-2}$ peak of the host. This large reduction could not be explained by a dilution of the dipoles per unit volume as was seen in the ferroelectric measurements. The presence of the dye in the antiferroelectric herringbone structure disrupted the dipole alignment and weakened the spontaneous polarisation. The combination of the disruption of the dye with a reduced spontaneous polarisation leads to increased switching times.

In the final part of the dye guest host work, the possibility of a tri-state device was investigated. Although M777 and the ICI black compounds had reached their saturation limits at 2% w/w, the blue D102 dye was soluble up to 8% w/w in Cl_{11}-Si_3-$_{11}Cl$. The addition of the high level of D102 dye dramatically reduced the smectic phase range to around 10°C and made alignment difficult. However, with the polariser aligned along the effective optic axis of one of the switched states, the cell could be switched between three distinct states. If the switching mechanism proposed for the bi-mesogenic organosiloxane compounds is considered, the dye can be thought of as aligning in one of two orientations with each of the pendent biphenyl benzoate moieties. As the liquid crystal is switched, the dye follows the rotation of the pendent moieties and one, two or none of the dye molecules aligning with the host molecule can be realigned with the polariser. This schematically proposed switching mechanism yielded a clear state, a 50% dyed state and a 100% dyed state. This single polariser tri-state dye guest host device was only made possible by the near 45° tilt angle of the bi-mesogenic organosiloxane compounds.

7.3.4 Nitrostilbenes

In order to continue the work of the dye guest host chapter, several problems needed to be addressed. One of the criticisms of any dye guest host device is poor contrast. The contrast can be improved by adding larger amounts of high order parameter dyes. However, the limit of solution is typically around 4%, before dye aggregation occurs. The organosiloxanes used as the host material are difficult to align and only operate above room temperature. An ideal host would exhibit a room temperature ferroelectric phase with an overlying, less ordered phase (useful for alignment purposes). The motivation for the nitrostilbene chapter was to increase dye addition by grafting a dye molecule onto a siloxane core. It was then hoped that the dyed organosiloxane molecules would become part of the 'virtual backbone' and that engineering a dye to fit into this backbone would allow greater dye addition without the loss of the host properties.

A nitrostilbene dye was chosen for study and it was found that once grafted onto the usual three unit siloxane group via an eleven length alkyl chain, the resultant molecule was itself liquid crystalline. The organosiloxane nitrostilbene dye exhibited an isotropic transition at 108°C with a 60°C wide SmA range and a 15.5°C wide SmC range; once more the grafting onto the siloxane had promoted exclusively smectic phases. The spectra of both the mono- and bi-substituted nitrostilbene organosiloxane compounds were compared with the ungrafted dye precursor. The results showed that the grafting of the dye had caused a small (8 nm) red shift in the dye spectra, but otherwise the spectrum of the dye was unchanged.

An initial study of the new mono-nitrostilbene dye (NS11-Si_3) with Br11-Si_3 found that the two compounds were miscible over the entire concentration range. A range of concentration mixtures were made and a phase diagram established. In general, the mixing of the NS11-Si_3 with the organosiloxane host promoted a SmA phase over most of the concentration range and lowered the temperature of the host's SmC* range. A more ordered phase was observed at a lower temperature than the SmC* phase and although it has not been unambiguously identified, this phase appears to be a hexatic SmI* or SmF* phase. The addition of the dye to the organosiloxane host proved particularly beneficial to the alignment process. The mixtures were aligned with less treatment and yielded a higher quality final state than was seen in the pure host. The improved alignment was a consequence of the existence of a higher temperature, less ordered (SmA) phase and the weaker chirality of the mixtures in comparison with the host. Measurements of the tilt angle showed that as the percentage of dye in the mixture was increased beyond ~10%, the tilt angle was greatly reduced. In the synthesis of the organosiloxane hosts described in the organosiloxane chapter, large jumps in the tilt angle were seen when grafting the siloxane units on to the mesogenic precursors. The virtual backbone played a key role in the layer spacing and tilt angle of the compounds. It was therefore not surprising to find a large amount of tilt angle variability when attempting to interpose the dye into the structure. As a consequence of the SmA*→SmC* transition, the SmC* phase properties became more temperature dependent and second order in nature. The results of spontaneous polarisation measurements followed a similar trend to the dye addition in the mono-mesogens described in the dye guest host chapter: the magnitude of the spontaneous polarisation was reduced in-line with the dilution of the chiral host by the non-chiral dye. As the percentage of dye in the mixture was increased and the SmA* phase became more prominent, the spontaneous polarisation curves became sloped and lost their temperature independence. The measurements of switching times did not reveal any significant trends, and when plotted against shifted temperature, the curves overlapped.

The grafting of two nitrostilbene dyes to the siloxane core via alkyl chains formed the dimeric organosiloxane dye NS11-Si_3-11NS which was liquid crystalline with one mesophase, the SmA. The mixtures of the dye with the mono-mesogenic Br11-Si_3 host were also miscible over the entire concentration range. The influence of the SmA dye was strong giving only a SmA phase over most of

the concentration range. Somewhat surprisingly, as the SmC* phase of the host was suppressed, the ferroelectric behaviour became antiferroelectric with 30% and 35% addition of the dye. The antiferroelectric behaviour was thought to occur as a consequence of a templating effect of the dimeric dye. If the dye favours a bent conformation, as was suggested for the bi-mesogenic organosiloxanes described in the other results chapters, the influence of the siloxane virtual backbone may favour a herringbone alignment of the mono-mesogenic host. As was observed with the addition of the NS11-Si_3 dye, the magnitude of the tilt angle was greatly reduced as the amount of dye addition was increased. A small amount of electroclinic switching was observed in the three mixtures with a SmA* phase. The spontaneous polarisation of the antiferroelectric mixtures were even more seriously attenuated than simple dilution could explain. This result was similar to that seen with the measurements of dye addition in an antiferroelectric mix in the dye guest host chapter and was not unexpected given the unique nature of the antiferroelectricity in this particular case. The switching time measurements are generally similar for the ferroelectric mixtures, whilst the switching time of the two antiferroelectric mixtures were longer.

In the final part of the nitrostilbene work, the two dyes are mixed with the bi-mesogenic antiferroelectric organosiloxane Br11-Si_3-11Br. Once again the dyes were fully miscible with the host over the entire concentration range. Unlike the mixtures in the ferroelectric mono-mesogenic host, the influence of the dyes on the antiferroelectric phase range was not as strong. The smectic A phase does not extend as far across the concentration range and the SmC^*_A phase of the host was observed in mixtures with up to 50% dye addition. Although the antiferroelectric phase was maintained, with dye addition in excess of 10% the order was disrupted and alignment became increasingly difficult. This disruption was also observed in the electro-optic measurements, and the magnitudes of the tilt angle and spontaneous polarisation were once again greatly reduced. Again, this was not unexpected when the results are compared with the effects of dye addition to the antiferroelectric host described in the dye guest host chapter. The addition of 2% of dye reduced the tilt by ~15% and the spontaneous polarisation by ~20%.

The results of the nitrostilbene chapter have shown that the *effective backbone* or *virtual backbone effect* in low molar mass organosiloxane liquid crystals can be used to increase the solubility of a dye guest moiety. The ferroelectric / antiferroelectric characteristics of the liquid-crystal host can be retained and room temperature ferroelectric phases have been created with broad, temperature invariant properties i.e. spontaneous polarisation and tilt angle. Some of these mixtures exhibited a SmA* phase with significant electroclinic switching, and this phase allowed easy alignment of the underlying ferroelectric phases. The presence of antiferroelectricity induced by a SmA dye demonstrates the strength of the templating effect.

7.4 FUTURE APPLICATIONS

Although the field of liquid crystals is continually evolving, large scale devices such as hang on the wall televisions are not yet a part of everyday life. The early promise shown by the nematic display has reached maturity in the field of laptop and desktop computing applications, however, the problems experienced in scaling up this technology have meant that other, large scale devices have filled the gap. Field emission displays are just one example of technologies that have exploited this opening in the displays marketplace[18].

Fast switching, multiplexibilty and large viewing angles give ferroelectrics huge promise, but due to difficulties in exploitation of these devices they have remained largely a research topic and the number of commercial ferroelectric display devices is still limited to specialist products. Antiferroelectrics have also struggled to find full commercial applications, partly due to lower contrast levels than achieved in nematic devices and the difficulties of obtaining good alignment[19]. One area in which ferroelectric displays have shown real commercial promise is the small scale micro-displays. Mobile phones, head–up displays and projection systems are just some of the applications being investigated[20]. At the very small scale end of the spectrum, ferroelectric liquid crystals are finding uses in spatial light modulators with fibre optic applications. The field of optical communication and optical waveguides holds many possible applications[21]. The knock-on effects are potentially enormous, and applications for ferroelectrics in the field of optical computing could eclipse the already massive displays market[22].

It is hoped that the work presented in this thesis has shown that no area of liquid crystal research is ever dead. Undreamt of applications and the fast pace of development mean that previously dormant work can yield many possibilities. The results of this work have been highly encouraging in pointing the way to new avenues of development and possible applications.

7.5 REFERENCES

[1] P.Lehmann, W.K.Robinson, H.J.Coles, *Mol. Cryst. Liq. Cryst.*, **328**, 221 (1999).
[2] W.K.Robinson, P.Lehmann H.J.Coles, *Mol. Cryst. Liq. Cryst.*, **328**, 229 (1999).
[3] K.J.Toyne, *Thermotropic Liquid Crystals*, (ed. G.W.Gray) (Wiley, 1987); D.J.Byron, A.S.Matharu, R.C.Wilson, J.W.Brown, *Mol. Cryst. Liq. Cryst.*, **258**, 95 (1995).
[4] S.P.Perkins, D.E.Shoosmith, H.J.Coles, *Ferroelectrics,* **243**, 67 (2000).
[5] S.P.Perkins, D.E.Shoosmith, H.J.Coles, *Mol. Cryst. Liq. Cryst.*, **364**, 943 (2001).
[6] H.J.Coles, G.A.Lester, H.Owen, *Liq. Cryst.,* **14**(4) 1039 (1993).
[7] H.J.Coles, H.F.Gleeson, J.S.Kang, *Liq. Cryst.,* **5**(4) 1243 (1989).
[8] G.Baur, A.Stieb, G.Meier, *Mol. Cryst. Liq. Cryst.*, **22**, 261 (1973).
[9] R.J.Cox, *Mol. Cryst. Liq. Cryst* **55**, 1 (1979).
[10] P.DeHont, S.P.Perkins, H.J.Coles, *Mol. Cryst. Liq. Cryst.*, **366**, 263 (2001).
[11] P.DeHont, (Personal Communication).
[12] H.J.Coles, H.G.Walton, D.Guillon, G.Poetti, *Liq. Cryst.,* **15**(4) 551 (1993); *ibid.,* **17**(3) 333 (1994).
[13] D.E.Shoosmith, A.Remnant, S.P.Perkins, H.J.Coles, *Ferroelectrics,***243**, 75 (2000).
[14] A.M.Remnant, S.P.Perkins, H.J.Coles, *Mol. Cryst. Liq. Cryst.*, **366**, 751 (2001).
[15] J.Newton, *Ph.D. Thesis,* The University of Manchester (1994).
[16] W.K.Robinson, P.S.Kloess, C.Carboni, H.J.Coles, *Liq. Cryst.,* **23**(2), 309 (1997).
[17] P.Kloess, *Ph.D. Thesis,* The University of Southampton (1997).
[18] R.A.Tuck, *Information Display,* **16**(6), 15 (June 2000).
[19] D.C.Ulrich, S.J.Elston, *The Optics of Thermotropic Liquid Crystals*, (ed. Steve Elston, Roy Sambles), Chpt. **9**, (Taylor & Francis, London, 1998).
[20] P.D.Semenza, *Information Display,* **16**(7), 14 (July 2000).
[21] F.Yang, J.R.Sambles, G.W.Bradberry, *The Optics of Thermotropic Liquid Crystals*, (ed. Steve Elston, Roy Sambles), Chpt. **5**, (Taylor & Francis, London, 1998).
[22] K.M.Johnson, M.A.Handschy, L.A.Pagano-Stauffer, *Optical Engineering,* **26**(5), 385 (1987); M.A.Handschy, K.M.Johnson, G.Moddel, L.A.Pagano-Stauffer, *Ferroelectrics,* **85**, 279 (1988).

But Eeyore was saying to himself, "This writing business. Pencils and what-not.
Over-rated if you ask me. Silly stuff. Nothing in it."

A.A.Milne 1882-1956